Universidade Federal do Rio Grande do Sul

Instituto de Química

PREPARAÇÃO E CARACTERIZAÇÃO DE CARVÕES ATIVOS PARA REMOÇÃO DE COMPOSTOS ORGÂNICOS DE EFLUENTES AQUOSOS

Doutoranda: ***Caroline Saucier***

Novembro 2017

Porto Alegre, RS

Universidade Federal do Rio Grande do Sul

Instituto de Química

PREPARAÇÃO E CARACTERIZAÇÃO DE CARVÕES ATIVOS PARA REMOÇÃO DE COMPOSTOS ORGÂNICOS DE EFLUENTES AQUOSOS

Tese de Doutorado submetida ao Programa de Pós-graduação em Química da UFRGS como parte dos requisitos para a obtenção do Título de Doutor em Química

Doutoranda: ***Caroline Saucier***

Orientador: Prof. Dr. Éder Cláudio Lima

Novembro 2017

Porto Alegre, RS

DECLARAÇÃO DE AUTORIA

Esta tese foi desenvolvida inteiramente pela autora, exceto as colaborações, as quais foram devidamente citadas nos agradecimentos. O trabalho foi realizado no período entre novembro de 2013 e novembro de 2017, no Instituto de Química da Universidade Federal do Rio Grande do Sul, sob a orientação do Professor Doutor Éder Cláudio Lima.

À minha família.

AGRADECIMENTOS

Ao prof. Éder Lima, pela orientação, paciência e dedicação. Agradeço por todo o amadurecimento profissional proporcionado ao longo deste trabalho.

Ao prof. Silvio Dias, por compartilhar seu laboratório.

Aos profs. Andreia Fernandes, Caciano Noreña e Leliz Arenas pelas importantes contribuições na ocasião do meu exame de qualificação.

Aos colegas de laboratório Anderson Leite, Cibele Umpierres, Johana Puchana, Liziê Prola, Matthew Adebayo e Pascal Thue, pelo apoio técnico, encorajamento e agradáveis momentos de descontração.

Aos alunos de Iniciação Científica Beatris Mello e Diego Kunzler, pela valiosa colaboração na execução deste trabalho.

Ao Dr. Júlio Vaghetti e aos bolsistas premmium do LAMAT, pelo auxílio na realização das análises de FTIR e TGA/DTG.

Aos demais professores e funcionários do Instituto de Química da UFRGS, pelo apoio técnico.

Ao prof. Ranjithkumar (Kongunadu Arts and Science College, Coimbatore, Índia), por fornecer e caracterizar os nanocompósitos magnéticos utilizados em parte desta tese.

À minha família, pelo amor e incentivo.

A todos que de alguma forma contribuíram para a realização deste trabalho.

À Coordenação de Aperfeiçoamento de Pessoal de Nível Superior (CAPES) e ao Conselho Nacional de Desenvolvimento Científico e Tecnológico (CNPq), pelo apoio financeiro.

PRODUÇÃO BIBLIOGRÁFICA

ARTIGOS PUBLICADOS A PARTIR DESTA TESE

1) Saucier, C.; Adebayo, M.A.; Lima, E.C.; Prola, L.D.T.; Thue, P.S.; Umpierres, C.S.; Puchana-Rosero, M.J.; Machado, F.M. Comparison of a Homemade Bacuri Shell Activated Carbon With Carbon Nanotubes for Food Dye Removal. *Clean* **2015**, 43, 1389-1400.

2) Saucier, C.; Adebayo, M.A.; Lima, E.C.; Cataluña, R.; Thue, P.S.; Prola, L.D.T.; Puchana-Rosero, M.J.; Machado, F.M.; Pavan, F.A.; Dotto, G.L. Microwave-assisted activated carbon from cocoa shell as adsorbent for removal of sodium diclofenac and nimesulide from aqueous effluents. *J. Hazard. Mater.* **2015**, 289, 18-27.

3) Saucier, C.; Karthickeyan, P.; Ranjithkumar, V.; Lima, E.C.; Dos Reis, G.S.; De Brum, I.A.S. Efficient removal of amoxicillin and paracetamol from aqueous solutions using magnetic activated carbon. *Environ. Sci. Pollut. Res*. **2017**, 24, 5918-5932.

OUTROS ARTIGOS PUBLICADOS

4) Jauris, I.M.; Matos, C.F.; Saucier, C.; Lima, E.C.; Zarbin, A.J.G.; Fagan, S.B.; Machado, F.M.; Zanella, I. Adsorption of sodium diclofenac on graphene: a combined experimental and theoretical study. *Phys. Chem. Chem. Phys.* **2016**, 18, 1526-1536.

5) Machado, F.M.; Carmalin, S.A.; Lima, E.C.; Dias, S.L.P.; Prola, L.D.T.; Saucier, C.; Jauris, I.M.; Zanella, I.; Fagan, S.B. Adsorption of Alizarin Red S dye by carbon nanotubes: an experimental and theoretical investigation. *J. Phys. Chem. C* **2016**, 120, 18296-18306.

6) Jauris, I.; De Matos, C. F.; Zarbin, A. J.G.; Umpierres, C. S.; Saucier, C.; Lima, E.; Fagan, S. B.; Zanella, I.; Machado, F. M. Adsorption of anti-inflammatory nimesulide by graphene materials: a combined theoretical and experimental study. *Phys. Chem. Chem. Phys.* **2017**, 19, 22099-22110.

7) Thue, P.S.; Lima, E.C.; Sieliechi, J.M.; Saucier, C.; Dias, S.L.P.; Vaghetti, J.C.P.; Rodembusch, F.S.; Pavan, F.A. Effects of first-row transition metals and impregnation ratios on the physicochemical properties of microwave-assisted activated carbons from wood biomass. *J. Colloid Interface Sci.* **2017**, 486, 163-175.

8) Leite, A.J.B.; Lima, E.C. ; Dos Reis, G.S.; Thue, P.S.; Saucier, C.; Rodembusch, F.S.; Dias, S.L.P.; Umpierres, C.S. Hybrid adsorbents of tannin and APTES (3-aminopropyltriethoxysilane) and their application for the highly efficient removal of Acid Red 1 dye from aqueous solutions. *J. Environ. Chem. Eng.* **2017**, 5, 4307-4318.

SUMÁRIO

LISTA DE FIGURAS

LISTA DE TABELAS

LISTA DE ABREVIATURAS E SÍMBOLOS

q_e	Quantidade de adsorvato adsorvida no equilíbrio (mg g^{-1})
C_e	Concentração de adsorvato restante no equilíbrio (mg L^{-1})
K_L	Constante de equilíbrio de Langmuir (L mg^{-1})
Q_{max}	Capacidade máxima de adsorção (mg g^{-1})
K_F	Constante de equilíbrio de Freundlich [mg g^{-1}(mg L^{-1})$^{-1/nF}$]
n_F	Expoente de Freundlich (adimensional)
K_g	Constante de equilíbrio de Liu (L mg^{-1})
n_L	Expoente de Liu (adimensional)
θ_t	Número de sítios ativos disponíveis na superfície do adsorvente
SEM	Microscopia eletrônica de varredura (do inglês *scanning electron microscopy*)
FTIR	Espectroscopia vibracional na região do infravermelho com transformada de Fourier (do inglês *Fourier transform infrared spectroscopy*)
BET	Brunauer, Emmett e Teller
BJH	Barret, Joyner e Halenda
TGA	Análise termogravimétrica (do inglês *thermogravimetric analysis*)
DTG	Análise termogravimátrica derivativa (do inglês *derivative thermogravimetric analysis*)
XRD	Difração de raios X (do inglês *X-ray diffraction*)
pH_{pzc}	ponto de carga zero (do inglês *point of zero charge*)
q	Quantidade de adsorvato adsorvida (mg g^{-1})
C_o	Concentração inicial de DCF ou NM em contato com o adsorvente (mg L^{-1})
C_f	Concentração de fármaco depois do processo de adsorção (mg L^{-1})
R^2	Coeficiente de determinação
R^2_{adj}	Coeficiente de determinação ajustado
SD	Desvio padrão (do inglês *standard deviation*)
$q_{i,model}$	Valor de q teórico individual predito por um dado modelo
$q_{i,exp}$	Valor de q experimental individual
$\bar{q}_{exp}$	Média dos valores experimentais de q
VSM	Magnetômetro de amostra vibrante (do inglês *vibrating sample magnetometer*)

RESUMO

Esta tese consiste em três artigos científicos sobre a preparação, caracterização e aplicação de diferentes carvões ativos no tratamento de soluções aquosas contaminadas com compostos orgânicos. No primeiro artigo, foi produzido um carvão ativo usando casca de bacuri junto com componentes inorgânicos através de pirólise em um forno tubular convencional. O carvão ativo ABC-1.5 apresentou altos valores de área superficial e volume de poros, apropriados para a adsorção do corante Azul Brilhante (BB-FCF). A capacidade de adsorção do ABC-1.5 foi comparada com a de nanotubos de carbono de parede múltipla (MWCNT). As quantidades máximas removidas de BB-FCF a 50 ºC foram 647,9 e 231,5 mg g^{-1} para ABC-1.5 e MWCNT, respectivamente. ABC-1.5 e MWCNT foram aplicados ao tratamento de dois efluentes simulados, apresentando porcentagem de remoção de até 95,88% e 79,84%, respectivamente. O segundo estudo foi sobre a utilização de ativação química induzida por micro-ondas para preparar um carvão ativo de casca de cacau para remoção de diclofenaco de sódio (DFC) e nimesulida (NM). Foi possível realizar a pirólise em menos de 10 min. As quantidades máximas adsorvidas de DCF e NM pelo carvão ativo MWCS-1.0 a 25 ◦C foram 63,47 e 74,81 mg g^{-1}, respectivamente. Nos testes com efluentes hospitalares simulados, o MWCS-1.0 apresentou porcentagem de remoção de até 95,58%. Na terceira publicação, nanocompósitos magnéticos de carvão ativo (MAC-1 e MAC-2) foram preparados através de um método pirolítico simples usando uma mistura de benzoatos de ferro(III)/cobalto(II) e oxalatos de ferro(III)/cobalto(II), respectivamente, e foram utilizados como eficientes adsorventes para remoção de amoxicilina (AMX) e paracetamol (PCT). MAC-2 apresentou melhores propriedades magnéticas para separação do carvão ativo após a remoção dos fármacos. As capacidades máximas de adsorção obtidas para MAC-2 foram 444,2 mg g^{-1} (AMX) e 399,9 mg g^{-1} (PCT).

ABSTRACT

This thesis consists of three scientific papers on the preparation, characterization and application of different activated carbons in the treatment of aqueous solutions contaminated with organic compounds. In the first paper it was produced an activated carbon using bacuri shell together with inorganic components through pyrolysis in a conventional tubular furnace. ABC-1.5 showed high surface area and pore volume, suitable for the Brilliant Blue dye (BB-FCF) adsorption. The adsorption capacity of ABC-1.5 was compared with that of multi-walled carbon nanotubes (MWCNT). The maximum amounts removed of BB-FCF at 50 ºC were 647.9 and 231.5 mg g^{-1} for ABC-1.5 and MWCNT, respectively. ABC-1.5 and MWCNT were applied for the treatment of two simulated effluents, showing percentages of removal of up to 95.88% and 79.84%, respectively. The second study was about the use of microwave-induced chemical activation to prepare an activated carbon from cocoa shell for removal of sodium diclofenac (DFC) and nimesulide (NM). It was possible to perform the pyrolisis in less than 10 min. The maximum amounts adsorbed of DCF and NM onto MWCS-1.0 at 25 ◦C were 63.47 and 74.81 mg g^{-1}, respectively. In the tests with simulated hospital effluents, MWCS-1.0 presented a percentage of removal of up to 95.58%. In the third publication, magnetic activated carbon nanocomposites (MAC-1 and MAC-2) were prepared by a simple pyrolytic method using a mixture of iron(III)/cobalt(II) benzoates and iron(III)/cobalt(II) oxalates, respectively, and were used as efficient adsorbents for the removal of amoxicillin (AMX) and paracetamol (PCT). MAC-2 presented better magnetic properties for the separation of the activated carbon after the removal of the drugs. The maximum adsorption capacities obtained for MAC-2 were 444.2 mg g^{-1} (AMX) and 399.9 mg g^{-1} (PCT).

1. INTRODUÇÃO

O conhecimento atual sobre os níveis de contaminação dos recursos hídricos com compostos orgânicos alerta para a necessidade de desenvolvimento de métodos de remediação economicamente e ambientalmente sustentáveis[1]. Entre os contaminantes orgânicos, corantes e fármacos são amplas classes de compostos com grande impacto no meio ambiente.

Diversas indústrias, tais como alimentícia, têxtil, de papel e celulose, de cosméticos, de couro e de borracha aplicam corantes aos seus produtos[2]. A produção e o consumo desses produtos resultam em efluentes aquosos carregados de cor[3]. A presença de corantes no meio ambiente afeta todo tipo de organismo vivo[4] por causa da sua toxicidade e natureza carcinogênica[5]. Os corantes impedem a penetração da luz nas plantas aquáticas e reduzem a sua taxa de fotossíntese[6]. O tratamento de efluentes contendo corantes sintéticos é difícil[7], pois as suas moléculas possuem estruturas aromáticas complexas, as quais os tornam altamente estáveis[8].

Fármacos e seus metabólitos podem ser excretados por pacientes ou dispostos de forma imprópria por usuários, sendo encontrados nos efluentes aquosos municipais[9]. Hospitais e indústrias farmacêuticas também têm sido identificados como fontes desses contaminantes[10]. Como são resistentes à inativação e altamente solúveis em água, muitos medicamentos não são completamente removidos pelas estações de tratamento de efluentes[11–13]. Consequentemente, essas substâncias têm sido detectadas em água superficial, água subterrânea e água potável em todo o mundo[9,10,14]. Embora os fármacos estejam presentes no ambiente aquático em concentrações baixas (ng L^{-1} até µg L^{-1}), ainda assim oferecem riscos ecológicos e à saúde humana, pois são recalcitrantes e biologicamente ativos[9,12,14,15].

Diversos métodos têm sido estudados em busca do melhor tratamento para remoção de corantes e fármacos presentes em efluentes aquosos, como adsorção, oxidação eletroquímica, biodegradação, fotocatálise e ozonização[16–22]. A adsorção é um dos métodos mais promissores por causa da sua simplicidade, eficiência e economia[23,24]. Além disso, não gera produtos de degradação tóxicos[23]. Durante a operação unitária de adsorção, os contaminantes são transferidos do efluente para uma fase sólida, diminuindo a exposição dos seres vivos a essas substâncias[25,26]. Após, o efluente tratado pode ser liberado nos corpos receptores ou utilizado em algum processo industrial. Os adsorventes também podem ser regenerados e reutilizados[26,27].

Carvões ativos estão entre os materiais mais utilizados na adsorção de compostos orgânicos[28–31]. Possuem uma estrutura de poros complexa com grande área superficial, alta

estabilidade físico-química e vários grupos funcionais oxigenados na superfície[32–34]. Estas características estão associadas à sua capacidade de adsorção. A habilidade dos carvões ativos na remoção de contaminantes de soluções aquosas depende das condições experimentais do processo de ativação e da natureza do material orgânico empregado na sua preparação[29,30,34,35]. Resíduos da agroindústria têm sido utilizados como precursores, pois, além de seu baixo custo, estão disponíveis em grande quantidade e são ambientalmente amigáveis[10,36,37].

A produção de carvão ativo costuma ser feita em fornos elétricos convencionais[30,33,38]. Recentemente, fornos de micro-ondas também têm sido utilizados com esta finalidade[33,39–41]. O aquecimento por micro-ondas oferece vantagens em relação ao método convencional, como o aumento rápido de temperatura, que leva a tempos mais curtos de pirólise (menores do que 15 min), e uma diminuição considerável no consumo de energia[37,39]. A maior diferença entre o aquecimento por micro-ondas e o aquecimeto convencional é o modo como o calor é fornecido ao precursor orgânico a ser carbonizado. No aquecimento convencional, energia na forma de calor é transferida de uma fonte externa ao material precursor por condução, convecção e irradiação. No aquecimento por micro-ondas, energia eletromagnética é transferida diretamente em nível molecular ao material pecursor e então convertida em calor por rotação de dipolos e condução iônica[33,37,41,42].

Embora os carvões ativos sejam amplamente utilizados no tratamento de efluentes, é difícil separá-los quando suspensos em soluções aquosas. Assim, estudos têm sido realizados para investigar a incorporação de propriedades magnéticas a esses adsorventes para facilitar a sua separação após a adsorção.[43] Ranjithkumar *et al.*[44,45] e Do *et al*.[46] sintetizaram carvões ativos impregnados com α-Fe_2O_3 e Fe_3O_4, respectivamente, para remoção de corantes de soluções aquosas. Também têm sido desenvolvidas misturas de óxidos metálicos, tais como $MnFe_2O_4$[47] e $CoFe_2O_4$[48] para aplicação em adsorção de metais pesados. $CoFe_2O_4$ é um material promissor devido à sua saturação magnética moderada e estabilidades química e térmica.[49]

Nesse contexto, o objetivo geral deste trabalho foi explorar novas estratégias de produção e utilização de carvões ativos na adsorção de contaminates orgânicos de efluentes. Para tanto, teve-se em vista os seguintes objetivos específicos: (1) a valorização dos resíduos agroindustriais de casca de bacuri e casca de cacau na preparação de carvões ativos; (2) a produção de carvões ativos via forno elétrico convencional e via forno de micro-ondas; (3) produção de adsorventes magnéticos a partir de um carvão ativo comercial e (4) estudo da eficiência destes adsorventes no tratamento de soluções aquosas.

2. REVISÃO BIBLIOGRÁFICA

2.1. CONTAMINANTES ORGÂNICOS E IMPACTO NO MEIO AMBIENTE

Globalmente, grandes aumentos da demanda de água são previstos para a indústria e produção de energia. A urbanização acelerada e a expansão dos sistemas municipais de abastecimento de água e saneamento também contribuem para a crescente demanda.

Dois terços da população mundial atualmente vivem em áreas que passam pela escassez de água por, pelo menos, um mês ao ano. Cerca de 500 milhões de pessoas vivem em áreas onde o consumo de água excede os recursos hídricos localmente renováveis[50].

O aumento do despejo de efluentes inadequadamente tratados tem contribuído para degradar ainda mais a qualidade das águas superficiais e subterrâneas. Uma vez que a poluição hídrica afeta gravemente a disponibilidade da água, tal fenômeno deve ser gerenciado de forma apropriada para reduzir os impactos na crescente escassez de água[50].

Entre os compostos orgânicos mais encontrados em efluentes aquosos estão corantes e fármacos.

2.1.1. Corantes

A humanidade tem utilizado corantes por milhares de anos. A primeira aplicação de corante orgânico conhecida foi há aproximadamente 4.000 anos atrás, quando o azul índigo foi encontrado em envoltórios de múmias em tumbas no Egito. Até o fim do século XIX, os corantes eram naturais, feitos a partir de plantas, insetos e moluscos, e eram geralmente preparados em pequena escala. Foi somente depois de 1856, com a descoberta de Perkin do primeiro corante orgânico sintético, a mauveína, que os corantes começaram a ser produzidos sinteticamente em grande escala[51].

Os corantes sintéticos podem ser utilizados nas indústrias de couro, papel, alimentos, cosméticos, etc. Mais de 100.000 corantes comerciais estão disponíveis atualmente e mais de 700.000 ton de corantes são produzidas anualmente no mundo[52]. Estima-se que 10-15% dos corantes são perdidos em efluentes durante os processos de fabricação e aplicação[53].

Corantes são substâncias que possuem afinidade pelo substrato ao qual estão sendo aplicadas. São coloridos porque absorvem luz na faixa do visível em determinados comprimentos de onda. São basicamente compostos orgânicos ionizantes e aromáticos com

diferentes moléculas de cromóforos, que são responsáveis pela sua cor. Os cromóforos possuem ligações conjugadas com elétrons deslocalizados[53]. Também estão presentes nos corantes os auxocromos, grupos ionizáveis que intensificam a cor, tormam a molécula solúvel em água e aumentam a sua afinidade com o substrato. As configurações dos grupos cromóforos inclui azo (-N=N-), carbonila (-C=O), ligações π C-C (-C=C-, =C=C=), nitroso (-NO, -N-OH) e nitro ($-NO_2$). Os grupos auxocromos usuais são: amino ($-NH_2$), carboxila (-COOH), hidroxila (-OH) e ácido sulfônico ($-SO_3H$)[54].

Existem vários modos de classificar os corantes comerciais. Eles podem ser classificados em termo de estrutura, cor e método de aplicação. A classificação baseada na estrutura química para as classes mais comuns de corantes está apresentada na **Tabela I**.

A contaminação em efluentes devido aos corantes pode ser facilmente vista em concentrações menores do que 1 mg L^{-1}, afetando o aspecto e a transparência da água. Podem interferir na atividade fotossintética de organismos aquáticos por diminuir a penetração da luz na água e também podem ser tóxicos devido à presença de metais, compostos aromáticos, etc[55–57]. Além disso, são carcinogênicos, mutagênicos e teratogênicos a várias espécies de micróbios e peixes. Também podem causar sérios danos aos seres humanos, como problemas respiratórios, alergias, disfunções dos rins, do sistema reprodutivo, do fígado e do sistema nervoso central[58,59]. A presença de corantes em efluentes aquosos também contribui para altos valores de demanda química de oxigênio (DQO), causando mau cheiro[60]. Devido aos seus efeitos tóxicos, o uso de corantes tem gerado muita preocupação. Assim, diversas pesquisas têm sido direcionadas a encontrar métodos específicos para remover corantes de diferentes tipos de efluentes aquosos e garantir a descarga segura do efluente tratado nos cursos d'água[59].

A Resolução n°357 do Conselho Nacional do Meio Ambiente (CONAMA), de 17 de março de 2005, estabelece os padrões e condições de lançamento de efluentes. Segundo essa Resolução, uma das condições de qualidade da água é a ausência de corantes provenientes de fontes antrópicas que não sejam removíveis por processo de coagulação, sedimentação e filtração convencionais[61]. A Resolução n° 128/2006 do Conselho Estadual do Meio Ambiente (CONSEMA) dispõe sobre a fixação de padrões de emissão de efluentes líquidos para fontes de emissão que lancem seus efluentes em águas superficiais no Estado do Rio Grande do Sul. Este documento estabelece que os efluentes líquidos industriais não devem conferir mudança de coloração ao corpo hídrico receptor[62].

Tabela I. Classificação dos corantes de acordo com a sua estrutura química[59].

Classe	Cromóforo	Exemplo
Azo	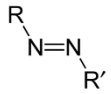	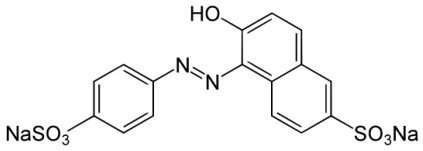 Amarelo Crepúsculo FCF
Antraquinona	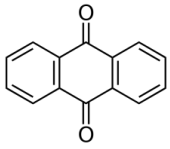	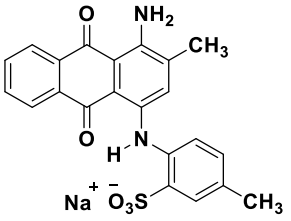 Azul Ácido 47
Indigoide	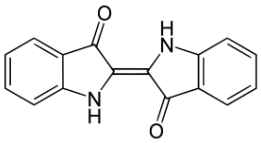	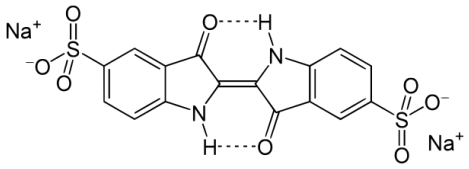 Índigo-Carmim
Nitroso	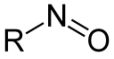	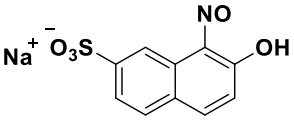 Azul Ácido 71
Nitro	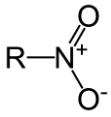	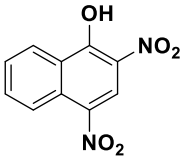 Verde Ácido 1
Triarilmetano	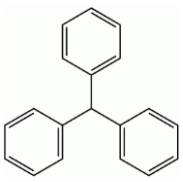	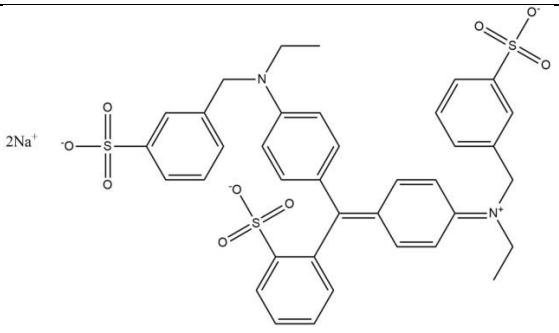 Azul Brilhante FCF

Diversos tipos de tratamento de efluentes contendo corantes tem sido desenvolvidos. Estes tratamentos podem ser classificados em três grupos: biológicos, químicos e físicos[59].

A biodegradação de corantes sintéticos por microrganismos é um método comum e simples em termos de operação, mas o processo envolvido na degradação biológica pode ser complexo. Diversos microrganismos têm sido utilizados para descoloração de corantes, como fungos e bactérias, em condições aeróbias, anaeróbias ou ambas[63–65]. Contudo, a maioria dos corantes é muito estável e resistente à biodegradação[66].

Os tratamentos químicos incluem precipitação, floculação, coagulação, flotação e filtração, oxidação, irradiação e tratamento eletroquímico[21]. Os reagentes tratam os efluentes assistindo o processo de separação ou ajudando a degradar e neutralizar alguns dos efeitos prejudiciais causados pelos contaminantes[67]. Estes tratamentos são eficazes, mas também são caros e possuem a desvantagem de gerar muito lodo, causando um problema de disposição deste lodo[22]. Além disso, um problema de poluição secundária pode surgir por causa da quantidade de reagente utilizada. Processos de oxidação geram poderosos agentes oxidantes, assim como radicais hidroxila, que tem sido utilizados com sucesso na degradação de contaminantes. Entretanto, esses processos são muito caros por causa do alto consumo de reagentes e energia elétrica[54].

Os métodos físicos incluem adsorção, osmose reversa, eletrodiálise, filtração por membranas e nanofiltração[68,69]. O principal inconveniente dos processos com membrana é que o tempo de vida útil das membranas, que precisam ser constante mente substituídas, gerando vários custos[70]. De acordo com a literatura, a adsorção é um dos métodos mais utilizados e tem se mostrado eficaz na remoção de contaminantes de águas[70–73]. Se uma planta de tratamento tiver um projeto apropriado, produz um efluente tratado de alta qualidade. A adsorção é uma alternativa eficiente de tratamento, particularmente nos casos em que o adsorvente é de baixo custo, disponível, abundante e requeira poucas etapas de pré-tratamento antes do uso[19].

A cor de um produto frequentemente determina o quão atrativo ele pode ser ao consumidor. Contudo, corantes naturais são instáveis e facilmente se degradam durante seu processamento[74]. Por isso os corantes alimentícios sintéticos são tão utilizados tanto em alimentos quanto em cosméticos. Alguns exemplos de aplicações são: bebidas alcoólicas e não alcoólicas, doces, geleias, sorvetes, perfumes, xampus, etc. Também são empregados na indústria farmacêutica. Em geral são utilizados corantes azo, antraquinona e triarilmetano[75,76].

O Azul Brilhante FCF é um corante muito comum. Devido à sua estrutura com múltiplas ligações π, ele apresenta uma cor intensa. É um corante aniônico devido à presença de grupos sulfônicos na sua estrutura e é altamente solúvel em água[77]. Embora sua aplicação seja permitida, pode provocar tumores e reações alérgicas[78,79]. Apesar de a remoção de Azul

Brilhante FCF de efluentes ser motivo de preocupação, ainda existem poucos estudos sobre este tema[3,77,80–86].

2.1.2. Fármacos

De acordo com a Agência de Proteção Ambiental Norte Americana (EPA, do inglês *Environmental Protection Agency*), contaminantes emergentes são substâncias químicas que estão sendo descobertas em água e que não haviam sido detectadas, ou que têm sido detectadas em níveis que podem ser significativamente diferentes do esperado[87]. Os riscos à saúde humana e ao meio ambiente associados com a sua presença, frequência de ocorrência ou fonte podem não ser conhecidos. Entre essas substâncias, estão fármacos, drogas ilícitas e produtos de higiene pessoal[87].

O uso do termo "emergente" não significa que a presença desses compostos no meio ambiente seja recente. Esses contaminantes têm sido liberados no meio ambiente desde que começaram a ser produzidos. O que é emergente é o interesse da comunidade científica a respeito deles, da sua presença no meio ambiente e dos efeitos que concentrações muito baixas parecem ter na biota aquática[88].

Os fármacos são um grupo amplo e diversificado de compostos orgânicos utilizados em grandes quantidades em todo o mundo.[89] Atualmente existem aproximadamente 3.000 substâncias utilizadas em medicament os, como analgésicos, antibióticos, antidepressivos, contraceptivos, entre outros.[90] Entre os contaminantes emergentes, os fármacos são o grupo mais relevante por causa do impacto que podem causar nos ecossistemas aquáticos devido à sua ampla utilização, das suas propriedades físico-químicas e da sua remoção incompleta nas estações de tratamento de efluentes[91]. Além disso, essas substâncias não são rotineiramente monitoradas, porque não foram incluídas na legislação ambiental[92]. Os danos ecológicos mais documentados incluem disfunção endócrina[93], aumento da resistência a medicamentos antimicrobianos[94–96], absorção pelas plantas[97] e bioacumulação na cadeia alimentar[98]. Esses riscos estão associados com a diminuição da biodiversidade[93,99], surgimento de superbactérias[95], infertilidade humana e câncer[100,101].

Cientistas já estavam cientes da presença de fármacos no meio ambiente há décadas. Em 1965, Stumm-Zollinger e Fair, da Universidade de Harvard, publicaram o primeiro estudo indicando que hormônios esteroides não eram completamente eliminados por tratamentos de efluentes[102]. Em 1977, pesquisadores da Universidade do Kansas relataram pela primeira vez a liberação de fármacos por plantas de tratamento de efluentes[103]. No final dos anos 1990 e

início dos anos 2000, estudos envolvendo a presença de fármacos em fontes de água, efluentes aquosos e água potável se tornaram um tema de destaque[104,105]. Uma das razões para que a comunidade científica considerasse essa contaminação motivo de preocupação foi o desenvolvimento das técnicas analíticas. A utilização de técnicas cromatográficas hifenadas poderosas, como, por exemplo, a cromatografia líquida acoplada à espectrometria de massas em *tandem* (LC-MS/MS, do inglês *liquid chromatography tandem mass spectrometry*), têm permitido a detecção e quantificação de concentrações extremamente baixas (μg L^{-1}, ng L^{-1}) desses compostos e seus metabólitos em matrizes líquidas e sólidas muito complexas, em efluentes aquosos, água superficial e água subterrânea[104,105].

Os fármacos se diferenciam dos contaminantes convencionais pelas seguintes caracterísiticas: (1) eles podem ser formados por uma diversidade de moléculas complexas quimicamente, que variam muito em massa molecular, estrutura, funcionalidade e forma; (2) eles são moléculas polares com mais de um grupo ionizável, e o grau de ionização e suas propriedades dependem do pH do meio; eles são lipofílicos e alguns deles são moderadamente solúveis em água; (3) medicamentos como eritromicina, ciclofosfamida, naproxeno e sulfametoxazol podem persistir no meio ambiente por mais de um ano, e outros, como, por exemplo, o ácido clofíbrico, podem persistir por vários anos e tornarem-se biologicamente ativos por acumulação; e (4) após a administração, as moléculas são absorvidas, distribuídas e sujeitas a reações metabólicas que podem modificar sua estrutura química[106,107].

A principal forma de entrada dos fármacos no meio ambiente é via excreção em urina e fezes. As outras formas incluem o suor (que libera os fármacos aplicados na pele ou os que foram excretados pela pele), a disposição inapropriada de produtos não utilizados ou parcialmente utilizados, efluentes de fábricas de medicamentos e efluentes de hospitais[108]. Os fármacos utilizados na medicina veterinária são excretados no solo ou diretamente em águas superficiais sem passar por uma estação de tratamento de efluentes, o que torna mais difícil seu controle[109]. Na pecuária intensiva, os fármacos entram diretamente no meio ambiente por meio da aplicação de estrume e purina como fertilizantes. Fármacos utilizados na piscicultura são diretamente liberados na água superficial[110].

A **Figura 1** ilustra as diferentes rotas possíveis através das quais os fármacos entram em contato com a água. Após a sua liberação no sistema de esgoto, eles passam pelas estações de tratamento de efluentes. Como não são completamente removidos, entram na rede de distribuição de água, onde uma grande variedade desses compostos e seus metabólitos tem sido detectada, produzindo uma complexa mistura de substâncias que pode ter efeitos

sinérgicos[111,112]. Muitos desses compostos metabólitos são mais bioativos do que seu precursor[88].

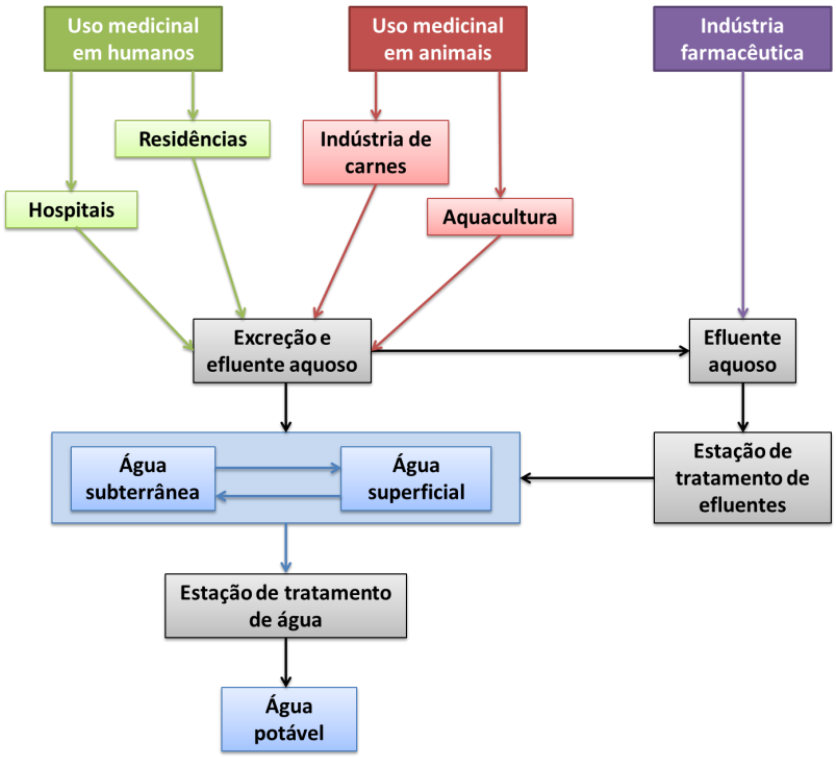

Figura 1. Rotas de entrada de fármacos na água[105].

Um grande número de fármacos tem sido detectado em plantas de tratamento de efluentes em todo o mundo. Por exemplo, na Coreia, Han *et al.*[113] detectaram diclofenaco (1,97 μg L^{-1}), ibuprofeno (0,07 μg L^{-1}), ácido clofíbrico (0,31 μg L^{-1}), carbamazepina (0,16 μg L^{-1}), ácido salicílico (2,43 μg L^{-1}) e paracetamol (0,06 μg L^{-1}). No Reino Unido, Ashton *et al.*[114] relataram a frequência de detecção e a concentração média propanolol (100%, 76 ng L^{-1}), diclofenaco (86%, 424 ng L^{-1}), ibuprofeno (84%; 3086 ng L^{-1}), ácido mefenâmico (81%, 133 ng L^{-1}), dextropropoxifeno (74%, 195 ng L^{-1}), trimetoprima (65%, 70 ng L^{-1}), eritromicina (44%, <10 ng L^{-1}) e acetil sulfametoxazol (38%, <50 ng L^{-1}). Na Suíça, Kahle *et al.*[115] detectaram fluconazol (28 até 83 ng L^{-1}). Nos Estados Unidos, o Instituto de Pesquisa Geológica dos Estados Unidos (USGS, do inglês *United States Geological Survey*)[116] identificou múltiplos fármacos em diversas estações de tratamento de efluentes em todo o país.

Estudos recentes demonstraram que as plantas de tratamento de efluentes convencionais, baseadas principalmente no uso de microrganismos, são inadequadas para

destruir efetivamente esse tipo de composto orgânico devido à sua estrutura molecular complexa e baixas concentrações na água[88]. Além disso, a maioria dos compostos não pode ser metabolizada por microrganismos e pode até mesmo inibir a sua atividade[106]. Gracia-Lor *et al.*[117] investigaram a ocorrência de fármacos em influentes (água superficial) e efluentes de três estações de tratamento de água na província de Castellón, Espanha. A **Tabela II** apresenta os resultados do monitoramento, exemplificando que muitas dessas substâncias não são removidas de forma eficaz pelos tratamentos convencionais.

Tabela II. Resultados do monitoramento de fármacos em influentes e efluentes de três estações de tratamento da província de Castellón, Espanha[117].

Fármacos	**Influente (*n*=42)**		**Efluente (*n*=42)**	
	Máx. (μg L^{-1})	**Positivos (%)**	**Máx. (μg L^{-1})**	**Positivos (%)**
Analgésicos/ anti-inflamatórios				
Paracetamol	201,3	100	n.d.	0
4-Aminoantipirina (metabólito do metamizol)	6,45	100	1,68	100
Diclofenaco	1,49	100	0,74	100
Ibuprofeno	39,8	98	<LOQ	33
Cetoprofeno	1,17	100	0,62	100
Naproxeno	3,58	100	0,72	100
Ácido salicílico	276,7	76	236,1	26
Estatinas/reguladores de lipídios				
Atorvastatina	0,45	100	0,16	76
Pravastatina	0,24	26	0,17	30
Benzafibrato	0,46	100	0,39	100
Genfibrozil	2,12	100	1,24	100
Antidepressivos				
Paroxetina	n.d.	0	n.d.	0
Venlafaxina	0,52	100	0,30	100

A existência de traços de fármacos em água potável é um problema de saúde pública, uma vez que pouco se sabe sobre os potenciais efeitos da ingestão de misturas de medicamentos a longo prazo[118,119]. Portanto, a remoção efetiva de fármacos de efluentes aquosos antes da sua descarga é uma questão prioritária.

Tratamentos mais eficazes e específicos são necessários para reduzir o impacto ambiental dos efluentes. Tratamentos terciários de água incluem: sistemas biológicos para remoção de nitrogênio, troca iônica para remoção de íons, precipitação química para remoção de fósforo, destilação para remoção de compostos orgânicos voláteis, adsorção com carvão ativo para remoção de contaminantes orgânicos e inorgânicos, e processos avançados de oxidação para remoção de compostos orgânicos tóxicos refratários, baseados na geração de radicais, principalmente o radical OH, que é altamente oxidante. Muitos desses sistemas estão sendo estudados e ainda precisam ser aplicados em escala industrial, pois são necessários dados de qualidade acerca dos mecanismos envolvidos, da influência das variáveis operacionais, da cinética das reações e do *design* de reatores[106].

Entre os grupos de medicamentos mais encontrados em água estão anti-inflamatórios, antibióticos e analgésicos[108,120,121].

O diclofenaco é um anti-inflamatório pertencente à classe dos derivados do ácido fenilacético. Cerca de 940 ton desse medicamento são consumidas anualmente no mundo[122]. As plantas convencionais de tratamento de efluentes são pouco eficientes na remoção de diclofenaco, e a porcentagem de remoção muitas vezes é menor do que 20%[123]. Consequentemente, esse contaminante tem sido detectado em efluentes aquosos na Alemanha, na Espanha, na Canadá, no Brasil, nos Estados Unidos, entre outros[120,122,124–126]. Devido à sua toxicidade e à baixa porcentagem de remoção nas estações de tratamento de efluentes, o diclofenaco foi incluído nas Lista de Contaminantes Prioritários regulada pela Diretiva 2013/39/EU do Parlamento Europeu[127].

A nimesulida é um anti-inflamatório e pertence à classe das sulfonanilidas. É comercializada em todo o mundo[128], sendo um dos anti-inflamatórios mais prescritos no Brasil[129]. Apesar de ser um fármaco relativamente novo[130], alguns estudos documentaram a sua presença em água do mar, em Portugal, em água superficial e potável, no Brasil, e em estações de tratamento de efluentes, na Irlanda[130–132]. Recentemente Miranda *et. al.*[129] detectaram sua presença em efluentes na região do Lago de Itaipu, em Foz do Iguaçu, Paraná. Estudos que indicam que a nimesulida pode causar danos ao fígado e aos rins.[128]

A amoxicilina é um antibiótico da classe das penicilinas e é utilizada para tratar diversos tipos de infecções bacterianas tanto na medicina humana como na veterinária. O consumo de amoxicilina é maior do que o de outros tipos de antibióticos da família das penicilinas por causa da sua facilidade de absorção oral[133]. Na França, por exemplo, o consumo de amoxicilina chegou a 333,22 ton em 2008[134]. Contudo, como ela não é biodegradável, inibe a fotossíntese de algas e pode afetar outros organismos menores[135]. Além

disso, quando acumulada por bactérias patogênicas, a amoxicilina pode aumentar sua resistência, levando à utilização de altas doses para o tratamento de doenças convencionais ou impossibilitando o seu tratamento[136]. Estudos relataram a presença de amoxicilina na faixa de ng a mg.L^{-1} em efluentes domésticos e industriais[137].

O paracetamol é um analgésico e antipirético usado comumente para alívio de dor e febre. É muito popular devido à sua alta tolerância quando utilizado em doses terapêuticas. Contudo, altas doses e uso crônico desse medicamento podem causar danos ao fígado e aos rins[138,139]. Na Espanha, por exemplo, o consumo de paracetamol no ano de 2010 foi 1065,84 ton[134]. É um dos medicamentos mais encontrados em efluentes e água superficial mundialmente[140]. Paracetamol foi detectado em água superficial na Baía de Santos em concentrações de até 34,6 ng L^{-1} e na Baía da Jamaica (concentrações de até 156 ng L^{-1})[141].

2.2. ADSORÇÃO

Muitos pesquisadores têm procurado o melhor modo para remoção de contaminantes orgânicos existentes no meio aquático ou em efluentes aquosos. A adsorção tem se mostrado um dos métodos mais competitivos, uma vez que pode ser aplicado aos processos de tratamento de água utilizados atualmente e não requer altas temperaturas de operação[10,142].

Adsorção é a acumulação de substâncias na interface entre duas fases (líquida-líquida, gasosa-líquida, gasosa-sólida ou líquida-sólida). A substância que se acumula na interface é chamada de adsorvato e o material em que a adsorção ocorre é o adsorvente[143].

Dependendo da natureza das forças envolvidas, a adsorção pode ser de dois tipos: fisissorção (ou adsorção física) ou quimissorção (ou adsorção química). No caso da fisissorção, o adsorvato está ligado à superfície do adsorvente por forças de van der Waals, relativamente fracas. A quimissorção, por outro lado, envolve troca ou compartilhamento de elétrons entre as moléculas de adsorvato e a superfície do adsorvente, resultando em reação química[143,144]. Como é uma ligação química, é mais forte do que a fisissorção.

Os dois tipos de adsorção diferem de várias maneiras. A diferença mais importante é a magnitude da entalpia de adsorção. Na fisissorção, a entalpia de adsorção é da mesma ordem que o calor de liquefação e usualmente não excede 10 ou 20 kJ mol^{-1}. Na quimissorção, a mudança de entalpia é geralmente da ordem de 80 a 400 kJ mol^{-1}. A fisissorção não é específica e ocorre entre qualquer sistema adsorvato-adsorvente, enquanto a quimissorção é específica[143,144]. Outro ponto importante é a espessura da fase adsorvida. Na fisissorção, ela pode ser monomolecular ou multimolecular e, na quimissorção, é unimolecular. O tipo de

adsorção que ocorre em um dado sistema depende da natureza do adsorvato e do adsorvente, da reatividade da superfície, da área superficial do adsorvato e das condições de temperatura e pressão da operação unitária de adsorção[143,144].

O mecanismo de adsorção de um adsorvato em fase líquida geralmente envolve quatro etapas[143,145,146] (**Figura 2**): **(1) Transporte do interior da solução:** transporte do adsorvato do interior da solução para a camada externa do filme líquido que envolve a partícula do adsorvente (via difusão ou advecção). **(2) Difusão externa:** difusão do adsorvato para a superfície do adsorvente através do filme líquido. **(3) Difusão intrapartícula:** transferência do adsorvato da superfície da partícula do adsorvente para os sítios no interior da partícula. Pode ocorrer por difusão de poro, que é a difusão molecular do soluto em poros preenchidos com um fluido. Adicionalmente, há outro tipo de difusão intrapartícula, chamada de difusão de superfície. É a difusão de um soluto ao longo da superfície do adsorvente depois da adsorção e ocorre somente se as forças de atração da superfície não são suficientemente fortes para evitar a mobilidade das moléculas. **(4) Adsorção:** ocorre nos poros menores até atingir o equilíbrio.

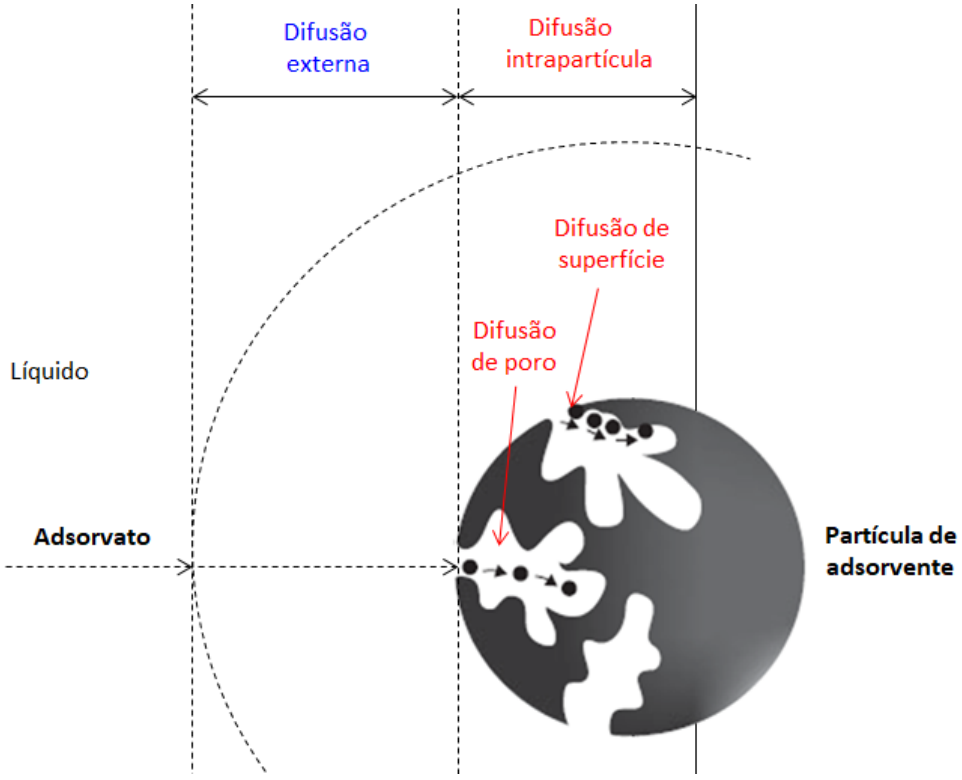

Figura 2. Transporte por difusão externa e difusão intrapartícula de um adsorvato em uma partícula de adsorvente.[143]

2.3. CARVÃO ATIVO

Os carvões ativos são materiais porosos à base de carbono. São formados por espaços moleculares (isto é, espaços ocupados por uma molécula normalmente no estado líquido) contidos dentro de uma rede tridimensional de camadas de grafeno defeituosas, ou seja, arranjos defeituosos de anéis de carbono de seis membros acomodados por anéis de outros tamanhos[32]. Essa rede é tridimensional, com algumas camadas empilhadas quase paralelamente umas às outras, em grupos de duas ou três, dificilmente mais, conforme ilustrado na **Figura 3A**[32].

A superfície dos carvões possui uma estrutura de poros que determina sua capacidade de adsorção e uma estrutura química que influencia sua interação com adsorvatos polares e não polares[144] (**Figura 3B**). Possui sítios ativos nas suas bordas, deslocamentos e descontinuidades que determinam sua reatividade em relação a outras substâncias. Assim, o comportamento dos carvões ativos na adsorção não pode ser interpretado somente com base na sua área superficial e distribuição de tamanho de poros[144].

Os carvões ativos possuem heteroátomos como oxigênio, enxofre, nitrogênio e outros elementos na forma de grupos funcionais e/ou átomos ligados quimicamente à sua estrutura (**Figura 3B**). Oxigênio é o elemento predominante, presente em grupos funcionais como carboxila, carbonila, éter, fenol, lactona e outros[147]. Os grupos oxigenados são os mais importantes, pois influenciam as características da superfície do material, como polaridade, acidez e molhabilidade[144]. Além disso, são essenciais para que o material tenha boas propriedades de adsorção[143,144].

Por serem adsorventes excelentes e versáteis, há diversos estudos sobre a aplicação de carvões ativos na remoção de contaminantes orgânicos de efluentes aquosos. De acordo com a literatura, os carvões ativos geralmente demonstram alta capacidade de adsorver fármacos e corantes[59,148]. A principal vantagem da utilização dos carvões ativos é que não são gerados produtos farmacologicamente ativos ou tóxicos durante a adsorção[106]. Além disso, carvões ativos produzidos a partir de resídos agroindustriais são uma alternativa de baixo custo em relação aos carvões ativos comerciais, apresentando capacidade de adsorção similar ou melhor que estes.[59] Entre esses materiais alternativos, podem ser citados cascas de sementes[30,142] e frutas[149,150], caroços de frutas[151,152] e caules de plantas[39]. Além disso, o aproveitamento desses resíduos para produção de carvão ativo é uma alternativa sustentável para evitar os problemas ambientais oriundos da sua disposição inadequada.

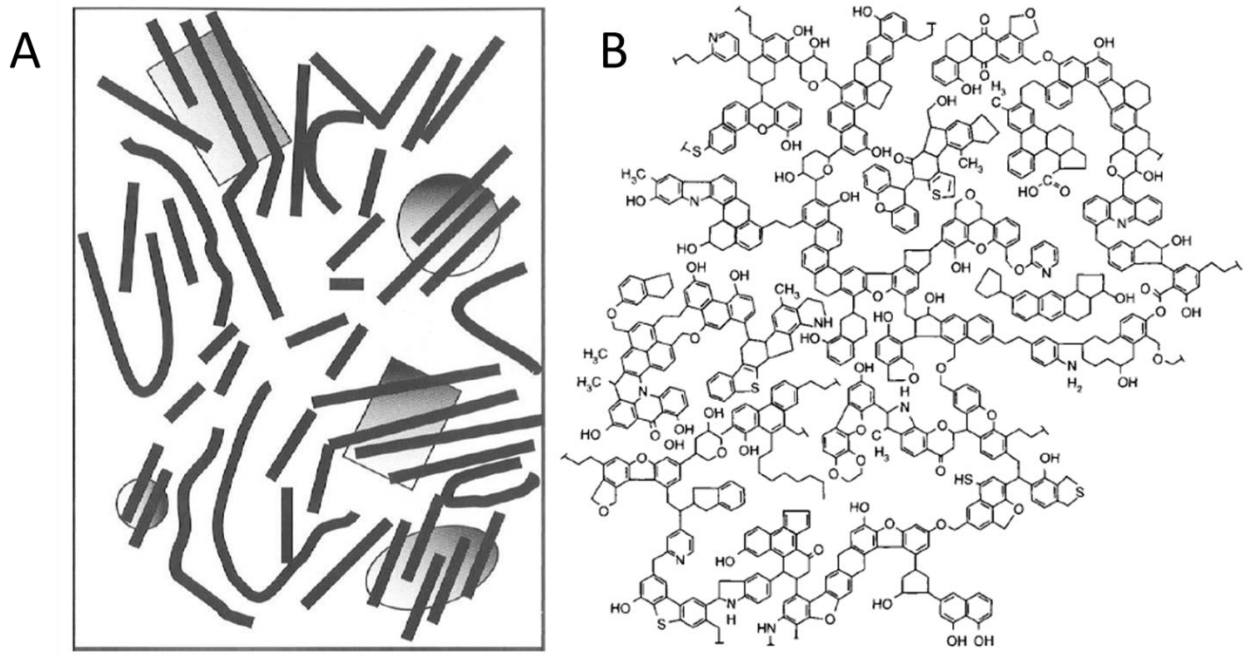

Figura 3. (A) Ilustração da estrutura de um carvão ativo, formada por camadas de átomos de carbono (camadas defeituosas de grafeno) dispostas de forma desordenada, mas com certo paralelismo. (B) Ilustração bidimensional das funcionalidades na superfície de um carvão ativo[32].

2.4. PRODUÇAO DE CARVÃO ATIVO

A preparação de carvões ativos geralmente envolve dois processos: a carbonização do material precursor e a ativação, que podem ser realizados em uma ou duas etapas, dependendo do método de ativação[147,153]. Quando a carbonização é realizada sob atmosfera inerte, o processo é chamado de pirólise. Durante a pirólise, ocorre a decomposição térmica dos materiais brutos, eliminando a maior parte dos elementos que não contêm carbono, como hidrogênio, oxigênio e nitrogênio, e produzindo uma massa rígida de carvão com uma estrutura rudimentar de poros (poros muito pequenos e fechados)[147,153]. O propósito da ativação é aumentar o diâmetro dos poros pequenos e criar novos poros. Há dois tipos de ativação para produção de carvão ativo: física (ou térmica) e química[153].

Na ativação física, o material precursor primeiro é carbonizado sob atmosfera inerte e a seguir o carvão resultante é submetido à gaseificação com vapor d'água, gás carbônico ou ar a temperaturas entre 800 e 1100 ºC. Também têm sido utilizados como agentes oxidantes $(NH_4)_2S_2O_8$, HNO_3 e H_2O_2[153,154].

Durante a ativação química, a etapa da carbonização e a etapa da ativação ocorrem simultaneamente. O material precursor é impregnado com $ZnCl_2$, H_3PO_4, HNO_3, H_2SO4, NaOH, KOH, sais de ferro, etc. Então o material é submetido à pirólise a temperaturas entre

400 e 800 ºC e lavado para eliminação do reagente ativante. A função do agente desidratante é inibir a formação de alcatrão e outros produtos indesejados durante a carbonização[41,153]. Após essa etapa, os reagentes inorgânicos devem ser lixiviados do materal carbonado, com lavagem com água, extração em sistema Soxlet ou ainda em refluxo com soluções ácidas.

A carbonização pode ser realizada utilizando-se fornos elétricos tubulares, reatores, muflas e, mais recentemente, reatores colocados em fornos de micro-ondas modificados[153].

2.4.1. Ativação em forno de micro-ondas

A radiação de micro-ondas está associada a qualquer radiação eletromagnética no intervalo de frequência de microondas de 300 MHz a 300 GHz (λ = 1 mm a 100 cm), que se encontra no segmento do espectro eletromagnético entre infravermelho e ondas de rádio[155,156]. Micro-ondas são uma forma de energia eletromagnética em que a energia aplicada é convertida em calor por meio de dois mecanismos principais[155,156]. O primeiro deles é chamado de rotação de dipolos e está relacionado com o alinhamento das moléculas (que têm dipolos permanentes ou induzidos) com o campo elétrico oscilante aplicado. Quando o campo oscila, as moléculas mudam de direção, e a energia que foi absorvida para a orientação dos dipolos é dissipada na forma de calor. O segundo mecanismo é chamado de condução iônica. O calor é gerado por meio de perdas por fricção, que acontecem pela migração de íons dissolvidos quando sob a ação de um campo eletromagnético[155,156].

O método de preparação afeta significativamente a qualidade e o custo dos carvões ativos. No método de aquecimento em forno convencional, o calor gerado é transferido para as partículas por convecção, condução e irradiação[155]. A superfície da amostra é aquecida antes da parte interna. Assim, há um gradiente de temperatura da superfície para o interior de cada partícula. Esse gradiente térmico impede a remoção eficaz dos produtos gasosos e, consequentemente, alguns compostos mais leves à base de carbono podem permanecer dentro das amostras, formando depósitos. Esse material depositado obstrui os poros do carvão, resultando em baixos valores de área superficial e volume de poros[154]. O gradiente térmico também leva a obtenção de carvões ativos com microestruturas heterogêneas. Para evitar esse gradiente térmico, uma taxa de aquecimento lenta é utilizada. Isso aumenta a duração do processo, resultando em um grande consumo de energia[154].

Utilizando-se forno de micro-ondas, é possível resolver o problema do gradiente térmico e do alto custo da preparação de carvões ativos. As micro-ondas interagem diretamente com o interior das partículas do material compactado, proporcionando um

aquecimento rápido. O uso de micro-ondas permite o alcance de altas temperaturas, curtos tempos de processamento e, portanto, grande economia de energia[33,154].

Nos últimos anos, resultados promissores tem sido obtidos pelo uso de micro-ondas para a preparação de carvões ativos de baixo custo, altos valores de área superficial e significativa capacidade de adsorção[154,156].

2.4.2. Nanocompósitos magnéticos de carvão ativo

Os carvões ativos são adsorventes bem conhecidos e amplamente utilizados comercialmente. Contudo, depois da sua utilização para remoção de contaminantes de soluções aquosas, o material fica saturado e precisa ser separado e regenerado, um processo que tipicamente envolve filtração ou centrifugação[43]. Por outro lado, muitos dos novos adsorventes desenvolvidos são nanopartículas, mas a sua remoção de soluções aquosas também consome tempo e a sua toxicidade é motivo de preocupação[157,158]. Um adsorvente ideal deveria ter as seguintes carctarísticas: (1) alta performance, (2) adsorção rápida, (3) baixo custo, (4) ambientalmente amigável, (5) reutilizável e (6) de fácil separação. Em relação à adsorção em batelada, o mais difícil desses desafios tem sido a separação eficiente do adsorvente após a adsorção em meio aquoso. A recuperação do adsorvente é essencial para que sejam evitados problemas de poluição secundária[159].

As nanopartículas magnéticas têm atraído considerável atenção na área de tratamento de efluentes devido à sua versatilidade (tamanho, forma, superfície), grande área superficial e facilidade de separação de soluções aquosas através da aplicação de um campo magnético externo[160]. Em particular, óxidos de metais de transição com estruturas de espinélio, ou ferritas (MFe_2O_4, onde M = Mn, Fe, Co, Ni, Co, Zn, etc.)[161], conforme ilustrado na **Figura 4**.

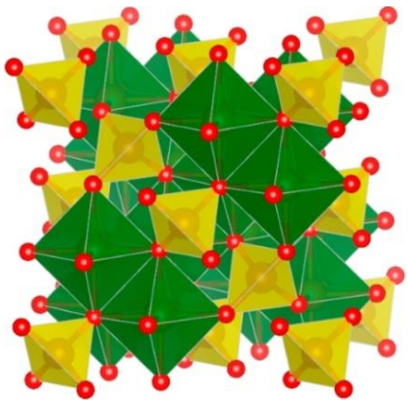

Figura 4. Representação esquemática da estrutura de uma ferrita, com átomos de oxigênio em vermelho, tetraedros em amarelo e octaedros em verde[161].

Estes materiais também possuem a vantagem de serem compostos por minerais naturalmente abundantes, o que viabiliza sua aplicação em escala industrial[161].

Existem poucos estudos na literatura sobre a utilização de nanocompósitos de carvões ativos e ferritas como adsorventes de contaminantes orgânicos. A **Tabela III** apresenta o desempenho desses materiais na remoção de corantes e de tetraciclina (fármaco).

Tabela III. Características e desempenho de nanocompósitos de carvão ativo e ferritas para remoção de compostos orgânicos de soluções aquosas.

Adsorvente[a]	**Tamanho (nm)**	**Área superficial ($m^2\ g^{-1}$)**	**Ms**[b] **($emu\ g^{-1}$)**	**Adsorvato**	**q_e**[c] **($mg\ g^{-1}$)**	**Referência**
$CA/CoFe_2O_4$	14-20	463	7,6	Verde Malaquita	89	Ai *et al.*[162]
$CA/NiFe_2O_4$	23	157	18,6	Alaranjado de Metila	183	Jiang *et al.*[163]
$CA/SnFe_2O_4$	25	110	1,9	Violeta Cristal	159	Rai *et al.*[164]
$CA/CoFe_2O_4$	24	347	-	Vermelho Direto 80	333	Yavari *et al.*[165]
				Verde Direto 6	385	
				Azul Ácido 92	625	
$CA/CoFe_2O_4$	-	1097	5,1	Azul de Metileno	99	Xu *et al.*[166]
$CA/MnFe_2O_4$	-	512	10,5	Tetraciclina	262	Shao *et. al*[167]

[a]CA=carvão ativo, [b]saturação magnética e [c]quantidade de adsorvato adsorvida no equilíbrio.

2.6. MODELOS DE ISOTERMAS DE ADSORÇÃO

Uma isoterma de adsorção descreve a distribuição do adsorvato entre a fase adsorvida e a fase em solução depois que o equilíbrio é atingido. Uma isoterma é característica de um sistema específico em uma temperatura particular[143]. Os parâmetros dos modelos de equilíbrio de adsorção fornecem informações úteis sobre as propriedades da superfície do adsorvente, o mecanismo de adsorção e as interações entre o adsorvato e o adsorvente. As isotermas podem ser utilizadas para selecionar o tipo de adsorvente mais apropriado, estimar a vida útil do adsorvente e testar a capacidade de adsorção de um material em uma operação em fluxo contínuo[143]. Há diversas equações para descrever o equilíbrio de adsorção de um adsorvato por um adsorvente. A mais empregada e discutida é a de Langmuir. Outros modelos de isotermas como o de Freundlich e o de Liu também têm sido estudados[168].

2.6.1. Langmuir

O modelo de Langmuir[169] é baseado nas seguintes hipóteses[168,170,171]:

- Os adsorvatos são quimicamente adsorvidos em um número fixo de sítios bem definidos.
- Uma monocamada de adsorvato é formada sobre a superfície do adsorvente quando ele fica saturado.
- Cada sítio pode conter somente uma espécie de adsorvato.
- Todos os sítios são energeticamente equivalentes.
- Não há interações entre as espécies de adsorvato.

A isoterma de Langmuir está descrita na **Equação 1**:

$$q_e = \frac{Q_{\max} \cdot K_L \cdot C_e}{1 + K_L \cdot C_e} \quad (1)$$

onde q_e é a quantidade de adsorvato adsorvida no equilíbrio (mg g^{-1}), C_e é a concentração de adsorvato restante no equilíbrio (mg L^{-1}), K_L é a constante de equilíbrio de Langmuir (L mg^{-1}) e Q_{max} é a capacidade máxima de adsorção do adsorvente (mg g^{-1}).

2.6.2. Freundlich

O modelo de Freundlich[172] é uma equação exponencial e assume que a concentração de adsorvato na superfície do adsorvente aumenta com o aumento da concentração. Assim, em princípio, a adsorção ocorre infinitamente. O modelo também assume que a adsorção poderia acontecer em múltiplas camadas. A equação tem uma ampla aplicação em sistemas heterogêneos[168,170]. A **Equação 2** mostra a isoterma de Freundlich:

$$q_e = K_F \cdot C_e^{1/n_F} \quad (2)$$

onde K_F é a constante de equilíbrio de Freundlich [mg g^{-1}(mg L^{-1})$^{-1/nF}$] e n_F é o expoente de Freundlich (adimensional).

2.6.3. Liu

O modelo de Liu[173] é uma combinação das isotermas de Langmuir e de Freundlich, mas a hipótese de monocamada do modelo de Langmuir e a hipótese da adsorção infinita do modelo de Freundlich foram desconsideradas. O modelo de Liu prevê que os sítios ativos do adsorvente não possuem a mesma energia. Portanto, o adsorvente pode apresentar sítios ativos preferenciais para ocupação pelas moléculas de adsorvato[168]. A **Equação 3** define a isoterma de Liu:

$$q_e = \frac{Q_{\max} \cdot (K_g \cdot C_e)^{n_L}}{1 + (K_g \cdot C_e)^{n_L}} \quad (3)$$

onde K_g é a constante de equilíbrio de Liu (L mg^{-1}); n_L é o expoente de Liu (adimensional) e Q_{max} é a capacidade máxima de adsorção do adsorvente (mg g^{-1}).

2.7. MODELOS DE CINÉTICA DE ADSORÇÃO

Estudos de cinética são importantes no tratamento de efluentes aquosos porque fornecem informações sobre o mecanismo de adsorção[168]. A cinética permite que seja determinada a taxa com que um determinado contaminate é removido de uma solução aquosa[174]. Muitos modelos de cinética foram desenvolvidos com o objetivo de encontrar as constantes intrínsecas da cinética de adsorção[168].

2.7.1. Ordem geral

Os expoentes de leis de velocidade de reações químicas normalmente não dependem dos coeficientes das equações químicas. Isso significa que a ordem da reação química deve ser determinada experimentalmente[175,176]. Com o objetivo de estabelecer uma lei geral de velocidade, a adsorção na superfície do adsorvente será tomado como a etapa determinante da velocidade. Assim, será considerada a mudança do número de sítios ativos efetivos na superfície do adsorvente durante a adsorção e não a concentração do adsorvato na solução[177]. Quando a lei universal de velocidade de reação é aplicada à **Equação 4**, a expressão da velocidade de adsorção é obtida[175–177].

$$\frac{dq}{dt} = k_N (q_e - q_t)^n \tag{4}$$

onde k_N é a constante de velocidade, q_e é a quantidade de adsorvato adsorvida no equilíbrio, q_t é a quantidade de adsorvato adsorvida no tempo t e n é a ordem da adsorção em relação à concentração dos sítios ativos presentes na superfície do adsorvente. O expoente n pode ser um número inteiro ou racional. A **Equação 5** descreve o número de sítios ativos (θ_t) disponíveis na superfície do adsorvente:

$$\theta_t = 1 - \frac{q_t}{q_e} \tag{5}$$

A **Equação 6** descreve a relação entre a variável θ_t e a velocidade de adsorção:

$$\frac{d\theta_t}{dt} = -k\theta_t^n \tag{6}$$

onde $k = k_N(q_e)^{n-1}$. Para o adsorvente puro, $\theta_t = 1$. O valor de θ_t diminui durante a adsorção. Quando o equilíbrio é atingido, θ_t se aproxima de um valor fixo. Para um adsorvente saturado, $\theta_t = 0$. A **Equação 6** leva à **Equação 7** após integração:

$$\int_1^{\theta} \frac{d\theta_t}{\theta_t^n} = -k \int_0^t dt \tag{7}$$

A **Equação 7** leva à **Equação 8**:

$$\frac{1}{1-n} \cdot \left[\theta_t^{1-n} - 1\right] = -kt \tag{8}$$

Rearranjando a **Equação 8**, é obtida a **Equação 9**:

$$\theta_t = \left[1 - k\left(1-n\right) \cdot t\right]^{1/1-n} \tag{9}$$

Substituindo a **Equação 5** na **Equação 9** e considerando $k = kN(qe)^{n-1}$, obtém-se a **Equação 10**:

$$q_t = q_e - \frac{q_e}{\left[k_N (q_e)^{n-1} \cdot t \cdot (n-1) + 1\right]^{1/1-n}} \tag{10}$$

A **Equação 10** é a equação de cinética de ordem geral de adsorção, sendo válida para $n \neq 1$[175–177].

2.7.2. Pseudo-primeira ordem

O modelo de cinética de pseudo-primeira ordem é um caso particular do modelo de ordem geral[175–177]. Considerando a **Equação 6** quando *n* = 1:

$$\frac{d\theta_t}{dt} = -k \cdot \theta_t^1 \tag{11}$$

Pela integração da **Equação 11**, é obtida a **Equação 12**:

$$\theta_t = \exp(-k_1 \cdot t) \tag{12}$$

Quando a **Equação 5** é substituída na **Equação 12** e *k* é substituída por k_1, é obtida a **Equação 13** ou modelo de cinética de pseudo-primeira ordem.

$$q_t = q_e \left[1 - \exp(-k_1 \cdot t)\right] \tag{13}$$

2.7.3. Pseudo-segunda ordem

O modelo de cinética de pseudo-segunda ordem é outro caso particular do modelo de ordem geral[175–177]. Será considerada agora a **Equação 10** quando *n* = 2:

$$q_t = q_e - \frac{q_e}{\left[k_2(q_e) \cdot t + 1\right]} \tag{14}$$

Rearranjando a **Equação 14**, é possível obter a **Equação 15**:

$$q_t = \frac{q_e^2 k_2 t}{\left[k_2(q_e) \cdot t + 1\right]} \tag{15}$$

2.7.4. Difusão intrapartícula

A adsorção ocorre em quatro etapas básicas, e a terceira etapa é a difusão intrapartícula, conforme explicado no **item 2.2**.

A possibilidade de a resistência à difusão intrapartícula afetar a adsorção pode ser explorada através do modelo de difusão intrapartícula, de acordo com a **Equação 16**:

$$q_t = k_{id}\sqrt{t} + C \tag{16}$$

onde *qt* é a quantidade de adsorvato adsorvia no tempo *t* (min), k_{id} é a constante de difusão intrapartícula (mg g^{-1} $min^{-0,5}$) e C é uma constante relacionada com a espessura da camada de difusão (mg g^{-1})[168].

2.8. ESTUDOS TERMODINÂMICOS

Estudos termodinâmicos possibilitam a obtenção de importantes informações sobre a operação unitária de adsorção com a variação da temperatura. A mudança de energia livre de Gibbs (ΔG°, kJ mol^{-1}) é o critério fundamental para a espontaneidade do sistema. Geralmente ΔG° para a fisissorção é menor do que para quimissorção. A variação de entalpia (ΔH°, kJ mol^{-1}) indica se a adsorção é endotérmica ou exotérmica, além de fornecer informações sobre a magnitude da interação entre o adsorvente e o adsorvato. A variação de entropia (ΔS°, J mol^{-1} K^{-1}) permite a obtenção de informações sobre a desordem do sistema. Essa avaliação pode ser feita através das **Equações 17, 18 e 19**[29]:

$$\Delta G^o = \Delta H^o - T\Delta S^o \tag{17}$$

$$\Delta G^o = -RT \cdot Ln(K) \tag{18}$$

Combinando-se as **Equações 17 e 18**, obtém-se a **Equação 19**:

$$Ln(K) = \frac{\Delta S^\circ}{R} - \frac{\Delta H^\circ}{R} \cdot \frac{1}{T} \tag{19}$$

onde R é a constante universal dos gases (8,314 J K^{-1} mol^{-1}), T é a temperatura absoluta (Kelvin), e K representa a constante de equilíbrio de adsorção dos modelos de isoterma. Os parâmetros termodinâmicos de adsorção podem ser estimados a partir da constante de

equilíbrio (K) do modelo de isoterma que melhor descreve os dados experimentais. O aumento no valor de K com o aumento da temperatura caracteriza um processo endotérmico. Os valores de ΔS e ΔH podem ser calculados a partir da inclinação e do intercepto da reta Ln (K) versus 1/T.

3. PARTE EXPERIMENTAL

3.1. REAGENTES E SOLUÇÕES

Todas as soluções foram preparadas com água deionizada. O corante Azul Brilhante FCF **(Apêndice 1, Supporting Information, Fig. S1)** foi fornecido pela empresa Plury Chemicals. Os fármacos diclofenaco **(Apêndice 2, Supplementary Material, Supplementary Fig. 1)**, nimesulida **(Apêndice 2, Supplementary Material, Supplementary Fig. 2)**, amoxicilina **(Apêndice 3, Supplementary Material, Supplementary Fig. 1)** e paracetamol **(Apêndice 3, Supplementary Material, Supplementary Fig. 2)** foram fornecidos pela empresa MedChem Express (Princeton, EUA) e utilizados sem tratamento adicional.

O pH das soluções foi ajustado com o auxílio de um pHmetro (Schott Lab 850, Mainz, Alemanha), sendo utilizadas soluções de NaOH 0,1 mol L^{-1} e/ou HCl 0,1 mol L^{-1}.

Para a ativação química dos carvões produzidos, foram empregados os reagentes sulfato duplo de alumínio e potássio $KAl(SO_4)_2$, hidróxido de potássio (KOH), hidróxido de alumínio $Al(OH)_3$, cloreto de zinco ($ZnCl_2$), e cloreto de ferro ($FeCl_3$) da marca Vetec (Duque de Caxias, Brasil), e cal [$CaCO_3$, CaO e $Ca(OH)_2$], obtida em uma loja de materiais de construção.

3.2. PREPARAÇÃO DOS ADSORVENTES

3.2.1. Carvão ativo de casca de bacuri em forno convencional

A casca de bacuri moída (75 g) foi misturada a 50 g de componentes inorgânicos [30% lama vermelha, 20% cal, 10% KOH, 20% $KAl(SO_4)_2$ e 20% $Al(OH)_3$] e 35 mL de água deionizada, na proporção inorgânicos:orgânicos de 1,5 (BC-1.5), gerando uma pasta homogênea. A pasta foi transferida para oito moldes em forma de disco (0,06 m de diâmetro e

0,007 m de espessura) e seca em estufa a 120 ºC durante 10 h. Os discos foram colocados em um reator de aço com suportes para os discos, o que permitiu uma distribuição simétrica de argônio com fluxo de 200 mL min^{-1}. A seguir o material foi colocado em um forno de pirólise tubular, que foi aquecido até 800 ºC e permaneceu nesta temperatura por 30 min. A taxa de aquecimento foi de 20 ºC min^{-1}. O reator foi então deixado esfriar a temperatura ambiente sob atmosfera de argônio (30 mL min^{-1}). Os discos carbonizados foram moídos e peneirados (tamanho de partícula < 106 µm). Este material foi identificado como BC-1.5. De modo similar, outros carvões foram preparados nas proporções inorgânicos:orgânicos de 1,0 (BC-1.0) e 2.0 (BC-2.0). Também foi preparado um material de referência sem componentess inorgânicos (BC-0). O procedimento para a preparação do carvão ativo está ilustrado na **Figura 4**.

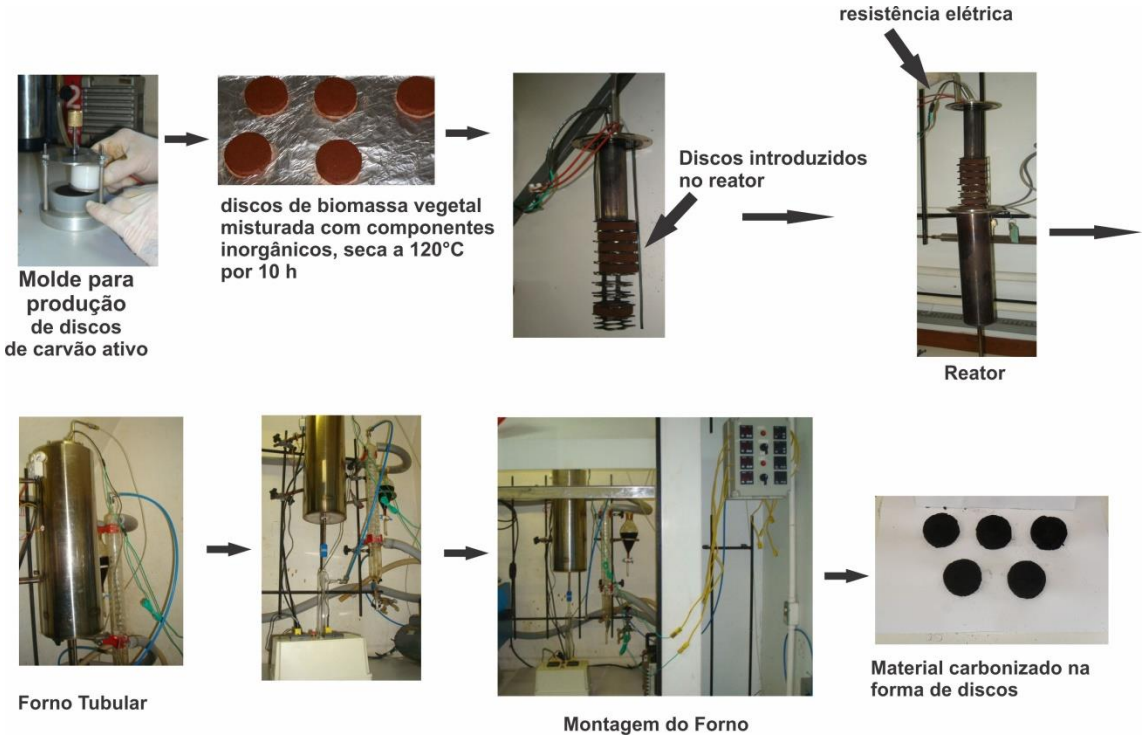

Figura 4. Produção dos adsorventes de carvão de casca de bacuri.

Para completar o processo de ativação química, 10 g de BC-1.5 e 200 mL de HCl 6 M foram adicionados a um balão de fundo chato de 500 mL. A mistura foi refluxada a 70 °C sob agitação magnética durante 12 h. O material sólido foi decantado, lavado com solução aquosa pH 2 e filtrado a vácuo. Após, foi seco em estufa (110 ºC, 5 h) e peneirado (tamanho de partícula < 106 µm). O mesmo procedimento foi realizado com os materiais (BC-1.0) e 2.0 (BC-2.0). Assim, os componentes inorgânicos foram lixiviados da matriz carbonada, originando os carvões ativos ABC-1.0, ABC-1.5 e ABC-2.0.

Os carvões ativos preparados em forno convencional foram utilizados para adsorção do corante Azul Brilhante FCF (BB-FCF).

3.2.2. Carvão ativo de casca de cacau em forno de micro-ondas

A ativação química induzida por micro-ondas foi utilizada para preparar um carvão ativo de casca de cacau para remoção de dois anti-inflamatórios, diclofenaco de sódio (DFC) e nimesulida (NM), de soluções aquosas. Este procedimento está ilustrado no **Apêndice 2 (Fig. 1)**. Inicialmente foram obtidas diferentes pastas homogêneas misturando-se 100 g de casca de cacau moída (previamente secos a 105 ºC durante 4 h), 100 g de componentes inorgânicos (20% cal, 40% $ZnCl_2$ e 40% $FeCl_3$) e 40 mL de água deionizada com proporções de inorgânicos:orgânicos de 1,0 (CSC-1.0); 1,5 (CSC-1.5) e 2,0 (CSC-2.0). As pastas foram secas em estufa a 100 ºC durante 6 h e quebradas em pedaços menores para que pudessem ser colocadas dentro de um reator de quartzo (30 g). O reator foi inserido em um forno de micro-ondas adaptado (Marca Philco, modelo PME22, 22 L, potência nominal:1200 W) com duas aberturas, uma na parte superior e outra na parte inferior. O reator foi posicionado verticalmente para que o óleo proveniente da pirólise fosse depositado no recipiente coletor por gravidade. Esta configuração impede que o óleo bloqueie os poros do adsorvente.

A programação de aquecimento do sistema foi: 360 W (80 s), 480 W (80 s), 600 W (80 s), 960 W (160 s) e 1200 W (160 s). Foi utilizada uma vazão de N_2 de 200 mL min^{-1}. Após a pirólise, o sistema foi resfriado sob 60 mL min^{-1} de nitrogênio durante 10 min. O tempo total de um ciclo de pirólise foi de somente 560 s (9,33 min), e um ciclo de pirólise completo pode ser obtido em menos de 20 min, sendo considerados os 10 min de resfriamento. Após, outros ciclos de pirólise podem ser realizados. O material obtido após a pirólise foi identificado como CSC-1.0. Procedimentos similares foram seguidos para a preparação de outros adsorventes com proporções inorgânicos:orgânicos de 0,0:1,0 (CSC-0); 1,0:1,5 (CSC-1.5) e 1,0:2,0 (CSC-2.0). O carvão CSC-0, carbonizado sem a presença de compostos inorgânicos, foi utilizado como material de referência. A preparação do CSC-0 possibilitou a investigação da influência da inclusão de componentes inorgânicos nos adsorventes e o efeito desses componentes na carbonização do precursor orgânico através de pirólise assistida por micro-ondas.

Para completar o processo de ativação química, os compostos inorgânicos foram lixiviados da matriz com HCl 6 mol L^{-1}. Para tanto, 10,0 g do adsorvente CSC-1.0 e 200 mL de HCl 6 mol L^{-1} foram adicionados a um balão de fundo chato de 500 mL. A mistura

permaneceu sob agitação magnética e refluxo a 90 ºC durante 8 h. Após o resfriamento da amostra, foi realizada a sua filtração à vácuo. O material sólido foi lavado exaustivamente com água deionizada. O pH final da suspensão foi ajustado para valores entre 6,0-7,0 com solução de carbonato de sódio 0,1 mol L^{-1}. Após, o carvão ativo foi seco em estufa a 70 ºC durante a noite. O adsorvente de casca de cacau obtido após a lixiviação dos compostos inorgânicos foi identificado como MWCS-1.0. O mesmo procedimento de acidificação foi seguido para a obtenção de outros adsorventes com proporção inorgânicos:orgânicos de 0,0:1,0 (MWCS-0); 1,0:1,5 (MWCS-1.5) e 1,0:2,0 (MWCS-2.0). O rendimento final dos carvões MWCS foi de aproximadamente 20%.

3.2.3. Nanocompósitos magnéticos de carvão ativo

Para a preparação dos nanocompósitos magnéticos, primeiro foi necessário realizar a síntese dos carboxilatos metálicos. Benzoato de ferro(III), benzoato de cobalto(II), oxalato de ferro(III) e oxalato de cobalto(II) foram preparados misturando-se os ácidos carboxílicos correspondentes aos sais dos metais de transição ferro e cobalto. Por exemplo, o benzoato de ferro(III) foi preparado através da mistura de nitrato de ferro(III) (8,08 g em 80 mL de água deionizada) e solução de ácido benzoico (7,32 g em 60 mL de água quente), seguida de agitação magnética durante 20 min.[178] O pó cristalino amarelo formado foi filtrado, lavado cuidadosamente com água destilada quente e seco. O mesmo procedimento foi realizado para os outros carboxilatos, conforme a tabela encontrada no **Anexo 3 (Supplementary Table 1)**.

Para a preparação do nanocompósito de carvão ativo e ferrita de cobalto ($AC/CoFe_2O_4$) MAC-1, inicialmente foram adicionados 10 g de carvão ativo comercial (AC) a uma mistura de 50 ml de solução aquosa de benzoato de cobalto(II) e benzoato de ferro(III). O material foi filtrado e seco (AC-1). A seguir, AC-1 foi aquecido a 600 ºC (temperatura de decomposição dos benzoatos)[45] por 15 min para facilitar a inserção das nanopartículas de ferrita de cobalto na matriz carbonada, originando o compósito MAC-1. O rendimento foi de 35%. Analogamente foi preparado o nanocompósito MAC-2: foram adicionados 10 g de AC a uma mistura de 50 ml de solução aquosa de oxalato de cobalto(II) e oxalato de ferro(III). O material foi filtrado e seco (AC-2). A seguir, AC-2 foi aquecido a 260 ºC (temperatura de decomposição dos oxalatos)[179] por 15 min, originando o compósito MAC-2. O rendimento foi de 45% depois da calcinação.

3.3. CARACTERIZAÇÃO DOS ADSORVENTES

O carvão ativo ABC-1.5 mostrou a maior capacidade de adsorção de BB-FCF de soluções aquosas. Assim, o material BC-1.5 e o carvão ativo ABC-1.5 foram selecionados para caracterização para que fossem investigados os efeitos da ativação química no carvão ativo de casca de bacuri. Da mesma forma, o carvão ativo MWCS-1.0 foi o que apresentou maior capacidade de adsorção de DCF e NM de soluções aquosas. Assim, o material CSC-1.0 e o carvão ativo MWCS-1.0 foram caracterizados.

Os carvões ativos de bacuri e cacau foram caracterizados quanto à morfologia, tipos de grupos funcionais, propriedades texturais, estabilidade térmica, presença de compostos inorgâncios e ponto de carga zero (pH_{pzc}, do inglês *point of zero charge*).

A morfologia da superfície dos adsorventes foi verificada através de microscopia eletrônica de varredura (SEM, do inglês *scanning electron microscopy*), em um microscópio JEOL, modelo JSM 6060 (Tóquio, Japão). A voltagem de aceleração empregada foi de 10 kV. As magnificação foi variável entre 1500 e 2500 vezes[31].

Os materiais também foram caracterizados por espectroscopia na região do infravermelho com transformada de Fourier (FTIR, do inglês *Fourier transform infrared spectroscopy*) em um equipamento Shimadzu, modelo IR Prestige 21 (Quioto, Japão). Os adsorventes e o KBr foram secos em estufa a 120 ºC durante 8 h, armazenados em frascos fechados e mantidos em um dessecador até o momento da análise. Os espectros foram obtidos com resolução de 4 cm^{-1} com 100 varreduras[180].

As isotermas de adsorção-dessorção de N_2 foram obtidas no ponto de ebulição do nitrogênio líquido (-196 °C) sendo utilizado um analizador de superfície Micromeritics, modelo TriStar II 3020 (Norcross, EUA). Os adsorventes foram desgaseificados a 180 °C durante 12 h sob vácuo antes das análises. As propriedades texturais dos adsorventes foram avaliadas através dos métodos de BET (Brunauer, Emmett e Teller) e de BJH (Barret, Joyner e Halenda), respectivamente[31].

As análises termogravimétrica (TGA, do inglês *thermogravimetric analysis*) e termogravimátrica derivativa (DTG, do inglês *derivative thermogravimetric analysis*) foram realizadas em um equipamento TA Instruments, modelo SDT Q600 (New Castle, EUA) com taxa de aquecimento de 10 ºC min^{-1} e fluxo de ar sintético de 100 mL min^{-1} (White Martins, Canoas, Brasil). A temperatura foi variada de 20 ºC a 1000 ºC (tempo de aquisição de 1 ponto a cada 5 s) com uma massa de amostra de 10,00-15,00 mg[31].

Para a verificação da presença de compostos inorgânicos, as análises de difração de raios X (XRD, do inglês *X-ray diffraction*) dos adsorventes foram realizadas em um difratômetro Philips X'pert MPD (PANanalytical, Almelo, Holanda), operado a 40 kV e 40 mA, com radiação Cu Kα (λ = 1.5406 Å).[26]

O pH_{pzc} dos carvões foi determinado através do seguinte procedimento: 20,00 mL de solução de NaCl 0,050 mol L^{-1} foram adicionados a vários tubos Falcon de 50 mL contendo 50,0 mg de adsorvente. O pH das soluções foi ajustado para valores de 2,00 a 10,00 com soluções de HCl 0,10 mol L^{-1} e de NaOH 0,10 mol L^{-1}. As suspensões foram colocadas em uma câmara climatizada com agitação reciprocante (Oxylab, São Leopoldo, Brasil) de 150 rpm, a 25 °C, durante 24 h. A seguir, as amostras foram centrifugadas a 3500 rpm durante 5 min em uma centrífuga Excelsa II 206-BL (Fanem, São Paulo, Brasil). O procedimento de centrifugação foi repetido quando necessário. O pH_i (pH das soluções sem contato com o adsorvente) e o pH_f (pH do sobrenadante depois do contato com o adsorvente) foi registrado. O valor do pH_{pzc} é o ponto onde a curva de ΔpH (pH_f - pH_i) *versus* pH_i cruza a linha do zero[180].

Os adsorventes magnéticos foram caracterizados por FTIR (Avatar 370, Termo Nicolet), XRD (40 kV e 40 mA, com radiação Cu Kα λ = 1.5418 Å), SEM (JEOL, modelo JSM 6390LV), espectroscopia de raios-X por dispersão de energia (EDX, do inglês *energy dispersive X-ray spectroscopy*) (JEOL, modelo JED 2300), microscopia eletrônica de transmissão (TEM, do inglês *Transmission Electron Microscopy*) (Philips, modelo CM-200, 20-200 kV, resolução 2,4 Å) e quanto às suas propriedades magnéticas utilizando-se um magnetômetro de amostra vibrante (VSM, do inglês *vibrating sample magnetometer*) (Lakeshore VSM 7410).

3.4. ESTUDOS DE ADSORÇÃO

3.4.1. Azul Brilhante

Para os experimentos de adsorção, 20 mL de soluções do corante alimentício Azul Brilhante (BB-FCF) (150-1800 mg L^{-1}) foram adicionados a 50 mg de adsorvente em tubos falcon de 50 mL (pH 2-10). As misturas foram agitadas por um período entre 5 e 480 min dentro de uma câmara climatizada com agitação reciprocante (150 rpm). A temperatura foi variada de 25 ºC a 40 ºC. As misturas foram centrifugadas durante 5 min para separar o adsorvente do adsorvato. O procedimento de centrifugação foi repetido quando necessário. A

quantidade de BB-FCF remanescente nas soluções após o processo de adsorção foi medida no comprimento de onda máximo de 629 nm em um espectrofotômetro T90+ UV-VIS, PG Instruments (Londres, Inglaterra). Alíquotas do sobrenadante foram diluídas com água deionizada pH 2 antes das medidas espectroscópicas quando as amostras apresentaram valores de absorbância superiores a 2,00. A quantidade de BB-FCF removida pelos adsorventes e a porcentagem de remoção foram calculadas através das **Equações 20** e **21.**

$$q = \frac{(C_o - C_f)}{m} . V \quad (20)$$

$$\%Rem = 100 . \frac{(C_o - C_f)}{C_o} \quad (21)$$

onde q é a quantidade de adsorvato adsorvida pelo adsorvente (mg g^{-1}), C_o é a concentração inicial de adsorvato (mg L^{-1}), C_f é a concentração de adsorvato depois da adsorção (mg L^{-1}), m é a massa de adsorvente (g), e V é o volume de solução de adsorvato (L).

A capacidade de adsorção do carvão ativo ABC-1.5 também foi comparada com a de nanotubos de carbono de parede múltipla (MWCNT, do inglês *multi-walled carbon nanotubes*) para remoção do corante BB-FCF de soluções aquosas.

Para elucidar a cinética de adsorção do corante BB-FCF pelos adsorventes ABC-1.5 e MWCNT, formas não lineares dos modelos de cinética de pseudo-primeira ordem, pseudo-segunda ordem, ordem geral e difusão intrapartícula foram empregadas.

Os modelos de equilíbrio de adsorção de Langmuir, Freundlich e Liu foram utilizados para análise dos dados das isotermas.

Estudos de dessorção foram realizados para determinar a eficiência de regeneração e o potencial de reutilização dos adsorventes. Os adsorventes carregados de corantes foram lavados com água deionizada para remover o corante BB-FCF não adsorvido e secos. Após, 20 mL dos seguintes eluentes foram adicionados aos adsorventes: água, NaOH (0,050-0,50 mol L^{-1}), acetona (10-50%) + água (90-50%), acetona (10-50%) + NaOH 0,05 mol L^{-1} (90-50%). As suspensões foram agitadas durante 1 h. O corante BB-FCF não adsorvido foi separado do adsorvente e quantificado conforme descrito acima. O adsorvente reciclado foi testado novamente em três ciclos de adsorção-dessorção.

Também foram realizadas simulações de efluentes da indústria de refrigerantes. A composição e concentrações dos componentes do efluente sintético estão descritas no **Apêndice 1 (Table 1).**

3.4.2. Diclofenaco e nimesulida

Para avaliar a habilidade do adsorvente MWCS-1.0 na remoção dos fármacos DCF e NM de soluções aquosas; 20,00 mL de solução de DCF ou NM (10,00-300,0 mg L^{-1}) foram adicionados a 50,0 mg de MWCS-1.0 em vários tubos Falcon de 50,0 mL. O pH das soluções foi variado de 7,0 a 10,0. As misturas foram agitadas por um período entre 5 e 480 min dentro de uma câmara climatizada com agitação reciprocante (150 rpm). A temperatura foi variada de 25 ºC a 50 ºC. As misturas foram centrifugadas durante 5 min para separar o adsorvente da solução de fármaco. O procedimento de centrifugação foi repetido quando necessário. A quantidade de DCF e NM remanescente nas soluções após a adsorção foi medida nos comprimentos de onda máximos de 275 nm para DCF e 392 nm para NM. Alíquotas do sobrenadante foram diluídas com soluções aquosas de pH 7,0 para DCF e 8,0 para NM quando as amostras apresentaram valores de absorbância superiores a 2,00. A quantidade de DCF ou NM removida pelo MWCS-1.0 e a porcentagem de remoção foram calculadas através das **Equações 20** e **21**, respectivamente.

Também foram realizados estudos de cinética de adsorção (com aplicação dos modelos de cinética de pseudo-primeira ordem, pseudo-segunda ordem e ordem geral) e isotermas de adsorção (modelos de Langmuir, Freundlich e Liu).

O adsorvente MWCS-1.0 foi utilizado no tratamento de dois efluentes hospitalares simulados. Acomposição e as concentrações do efluente A e do efluente B estão no **Apêndice 2 (Supplementary Table 1)**.

3.4.3. Amoxicilina e paracetamol

Para os estudos de adsorção do fármacos amoxicilina (AMX) e paracetamol (PCT) com os adsorventes magnéticos, 20 mL de solução de AMX ou PCT (70,00 - 2000,00 mg L^{-1}) foram adicionados a 30,0 mg de carvão ativo em tubos Falcon de 50 mL em diferentes valores de pH (4,00-10,0). As misturas foram agitadas entre 1 e 300 min a 150 rpm e a temperatura foi variada de 25 a 50 ºC. Após as misturas foram centrifugadas a 10.000 rpm durante 5 min. As quantidades de AMX e PCT remanescentes nas soluções foram medidas em comprimentos

de onda de 228 e 245 nm, respectivamente. A quantidade de AMX ou PCT removida e a porcentagem de remoção foram calculadas através das **Equações 20** e **21**, respectivamente.

Estudos de cinética de adsorção e isotermas de adsorção foram realizados conforme o **item 3.4.2**.

Dois efluentes hospitalares simulados foram tratados com os carvões ativos magnéticos para testar a sua capacidade de adsorção desses materiais em meios contendo outros fármacos, sais e compostos orgânicos. A composição e as concentrações do efluente A e do efluente B estão no **Apêndice 3 (Table 1)**.

3.5. AVALIAÇÃO ESTATÍSTICA DOS PARÂMETROS DE CINÉTICA E DAS ISOTERMAS DE ADSORÇÃO

O ajuste não linear para os dados de cinética e de equilíbrio de adsorção foram realizados utilizando-se Simplex e o método de aproximação sucessivas pelo algoritmo de Levenberg-Marquardt. Essas ferramentas estatísticas estão disponíveis no recurso *nonlinear fitting* do *software* Microcal Origin 9.0.

O coeficiente de determinação (R^2), o coeficiente de determinação ajustado (R^2_{adj}) e o desvio padrão dos resíduos (*SD*, do inglês *standard deviation*) foram utilizados para avaliar a adequação dos modelos[180,181]. O desvio padrão dos resíduos é uma medida da diferença entre as quantidades teórica (obtida através do modelo ajustado) e experimental adsorvidas. As expressões matemáticas de R^2, R^2_{adj} e *SD* estão apresentadas nas **Equações 22**, **23** e **24**, respectivamente.

$$R^2 = \left(\frac{\sum_i^n \left(q_{i,exp} - \bar{q}_{i,exp} \right)^2 - \sum_i^n \left(q_{i,\,exp} - q_{i,\,model} \right)^2}{\sum_i^n \left(q_{i,exp} - \bar{q}_{i,exp} \right)^2} \right) \tag{22}$$

$$R^2_{adj} = 1 - \left(1 - R^2\right) . \left(\frac{n-1}{n-p-1} \right) \tag{23}$$

$$SD = \sqrt{\sum_i^n \left(\frac{q_{i,\,exp} - q_{i,\,model}}{n-p} \right)^2} \tag{24}$$

onde $q_{i,model}$ representa cada valor de q teórico individual predito por um dado modelo; $q_{i,exp}$ representa cada valor de q experimental individual; $\bar{q}_{exp}$ representa a média dos valores

experimentais de *q*; *n* representa o número de experimentos; *p* representa o número de parâmetros do modelo[180,181].

4. CONCLUSÕES

As três seções a seguir apresentam as as conclusões desta tese de acordo com cada artigo científico publicado.

4.1. CARVÃO ATIVO DE CASCA DE BACURI PARA REMOÇÃO DE AZUL BRILHANTE FCF

Nesta parte do trabalho, foi produzido um carvão ativo de casca de bacuri via pirólise em forno elétrico convencional para remoção do corante alimentício Azul Brilhante FCF (BB-FCF) de soluções aquosas e efluentes simulados. Casca de bacuri moída e componentes inorgânicos foram misturados à temperatura ambiente. A mistura foi aquecida a 800 ºC sob condições inertes. Os materiais obtidos BC-1.0, BC-1.5 e BC-2.0 (carvões) foram tratados com solução de HCl 6 M e refluxados por 12 h para a obtenção dos carvões ativos ABC-1.0, ABC-1.5 e ABC-2.0, respectivamente. A acidificação lixiviou os components inorgânicos da matriz carbonada, o que foi confirmado através das análises de BET, XRD, TGA, SEM e FTIR. A capacidade de adsorção de ABC-1.5 foi comparada com a de MWCNT. Em pH 2, os tempos de equilíbrio foram de 45 min (ABC-1.5) e 90 min (MWCNT) para a remoção de BB-FCF de soluções aquosas. O modelo de cinética de ordem geral foi o que melhor descreveu a adsorção. Fases lineares múltiplas foram obtidas a partir do modelo de difusão intrapartícula. Os dados das isotermas se ajustaram melhor ao modelo Liu. As capacidades máximas de adsorção de BB-FCF a 50 ºC foram 647,9 e 231,5 mg g^{-1} para ABC-1.5 e MWCNT, respectivamente. Os parâmetros termodinâmicos de adsorção foram calculados. Com base na magnitude da entalpia de adsorção, a interação entre o corante BB-FCF e os dois adsorventes foi adsorção física. Foi possível regenerar os adsorventes com uma mistura de 50% de acetona e 50% de solução de NaOH 0,050 mol L^{-1}. ABC-1.5 é um adsorvente promissor para o tratamento de efluentes da indústria de bebidas, pois removeu 95,88% de diferentes corantes e outros componentes.

4.2. CARVÃO ATIVO DE CASCA DE CACAU PARA REMOÇÃO DE DICLOFENACO E NIMESULIDA

Neste trabalho foi estudada a utilização de carvão ativo de casca de cacau produzido através de pirólise assistida por micro-ondas para remoção de fármacos de soluções aquosas e de efluentes hospitalares simulados. A casca de cacau moída e componentes inorgânicos foram misturados à temperatura ambiente. Esta mistura foi aquecida em um forno de micro-ondas adaptado. Foi possível realizar a pirólise em menos de 10 min de aquecimento. O carvão de casca de cacau foi obtido em um único estágio devido à presença dos sais inorgânicos, que são condutores de micro-ondas. Os materiais carbonados CSC-1.0, CSC-1.5 e CSC-2.0 foram tratados com HCl para serem obtidos os adsorventes MWCS-1.0, MWCS-1.5 e MWCS-2.0, respectivamente. A acidificação lixiviou os inorgânicos da matriz carbonada, melhorando a sua capacidade de adsorção. O carvão ativo MWCS-1.0 foi o que apresentou o melhor desempenho na remoção dos fármacos diclofenaco e nimesulida de soluções aquosas. A remoção dos fármacos de soluções aquosas em pH 7,0 (diclofenaco) e 8,0 (nimesulida) atingiu o equilíbrio em 223,14 min (diclofenaco) e 45,46 min (nimesulida), respectivamente. O modelo de cinética que melhor descreveu a adsorção foi o de ordem geral. As quantidades máximas adsorvidas de diclofenaco e nimesulida a 25 ºC foram 63,47 e 74,81 mg g^{-1}, respectivamente. O carvão ativo MWCS-1.0 constitui uma alternativa eficiente para a remoção de DCF e NM de efluentes hospitalares. Esse adsorvente removeu 95,58% do efluente simulado, uma mistura com diferentes compostos orgâncios em um meio com altas concentrações de açúcar e sal.

4.3. CARVÃO ATIVO MAGNÉTICO PARA REMOÇÃO DE AMOXICILINA E PARACETAMOL

Nanocompósitos de carvão ativo e ferrita de cobalto AC/$CoFe_2O_4$, MAC-1 e MAC-2, foram preparados através de um método de pirólise simples utilizando-se uma mistura de benzoatos de ferro(III)/cobalto(II) e oxalatos de ferro(III)/cobalto(II), respectivamente. Estes nanocompósitos foram utilizados como adsorventes para remoção de amoxicilina (AMX) e paracetamol (PCT) de soluções aquosas e efluentes hospitalares simulados. Os materiais foram caracterizados por FTIR, XRD, SEM, EDX, TEM e VSM. A cinética de adsorção foi avaliada através dos modelos de ordem geral, pseudo-primeira ordem e pseudo-segunda ordem. Para AMX, o modelo de ordem geral foi o que melhor descreveu os dados de cinética

e, para PCT, o modelo de pseudo-primeira ordem possibilitou o melhor ajuste. Os dados de equilíbrio foram avaliados utilizando-se os modelos de Langmuir, Freundlich e Liu. Para os dois fármacos e os dois adsorventes, o modelo que melhor descreveu os dados das isotermas de adsorção foi o de Liu. A entalpia, a entropia e a energia livre de Gibbs foram determinadas através dos dados das isotermas de Liu de 25 a 50 ºC. Também foi proposto um mecanismo de adsorção para AMX e PCT com base na estrutura dos adsorventes, nos dados de cinética, equilíbrio e termodinâmicos. A interação entre os adsorvatos com os nanocompósitos magnéticos devem ser majoritariamente por forças de van der Walls (interações hidrofóbicas, interações π–π), ligações de hidrogênio e interações polares do oxigênio e hidrogênio do adsorvato com os grupos polares do adsorvente. Os adsorventes magnéticos MAC-1 e MAC-2 foram utilizados com sucesso no tratamento de efluentes hospitalares simulados, removendo pelo menos 93,00% (MAC-1) e 96,77% (MAC-2) de um meio contendo nove fármacos, dois açúcares, dois compostos orgânicos e oito inorgânicos.

5. REFERÊNCIAS BIBLIOGRÁFICAS

(1) Calisto, V.; Ferreira, C. I.; Oliveira, J. B. P.; Otero, M.; Esteves, V. I. Adsorptive Removal of Pharmaceuticals from Water by Commercial and Waste-Based Carbons. *J. Environ. Manage.* **2015**, *152*, 83–90.

(2) Silveira, M. B.; Pavan, F. A.; Gelos, N. F.; Lima, E. C.; Dias, S. L. P.; Alegre, P. Punica Granatum Shell Preparation, Characterization, and Use for Crystal Violet Removal from Aqueous Solution. *Clean* **2014**, *42* (7), 939–946.

(3) Esquerdo, V. M.; Cadaval Jr., T. R. S.; Dotto, G. L.; Pinto, L. A. A. Chitosan Scaffold as an Alternative Adsorbent for the Removal of Hazardous Food Dyes from Aqueous Solutions. *J. Colloid Interface Sci.* **2014**, *424*, 7–15.

(4) Royer, B.; Cardoso, N. F.; Lima, E. C.; Macedo, T. R.; Airoldi, C. A Useful Organofunctionalized Layered Silicate for Textile Dye Removal. *J. Hazard. Mater.* **2010**, *181* (1–3), 366–374.

(5) Oplatowska, M.; Donnelly, R. F.; Majithiya, R. J.; Glenn Kennedy, D.; Elliott, C. T. The Potential for Human Exposure, Direct and Indirect, to the Suspected Carcinogenic Triphenylmethane Dye Brilliant Green from Green Paper Towels. *Food Chem. Toxicol.* **2011**, *49* (8), 1870–1876.

(6) Gonçalves, J. O.; Duarte, D.; Dotto, G. L.; Pinto, L. A. Use of Chitosan with Different Deacetylation Degrees for the Adsorption of Food Dyes in a Binary System. *Clean* **2014**, *42* (6), 767–774.

(7) Lang, W.; Sirisansaneeyakul, S.; Martins, L. O.; Ngiwsara, L.; Sakairi, N.; Pathom-aree, W.; Okuyama, M.; Mori, H.; Kimura, A. Biodecolorization of a Food Azo Dye by the Deep Sea Dermacoccus Abyssi MT1.1T Strain from the Mariana Trench. *J. Environ. Manage.* **2014**, *132*, 155–164.

(8) Pereira, R.; Pereira, M. F. R.; Alves, M. M.; Pereira, L. Carbon Based Materials as Novel Redox Mediators for Dye Wastewater Biodegradation. *Appl. Catal. B Environ.* **2014**, *144*, 713–720.

(9) Fernández, M.; Fernández, M.; Laca, A.; Laca, A.; Díaz, M. Seasonal Occurrence and Removal of Pharmaceutical Products in Municipal Wastewaters. *J. Environ. Chem. Eng.* **2014**, *2* (1), 495–502.

(10) Kyzas, G. Z.; Deliyanni, E. Modified Activated Carbons from Potato Peels as Green Environmental-Friendly Adsorbents for the Treatment of Pharmaceutical Effluents. *Chem. Eng. Res. Des.* **2015**, *97*, 135–144.

(11) Rigobello, E. S.; Dantas, A. D. B.; Di Bernardo, L.; Vieira, E. M. Removal of Diclofenac by Conventional Drinking Water Treatment Processes and Granular Activated Carbon Filtration. *Chemosphere* **2013**, *92* (2), 184–191.

(12) Secondes, M. F. N.; Naddeo, V.; Belgiorno, V.; Ballesteros, F. Removal of Emerging Contaminants by Simultaneous Application of Membrane Ultrafiltration, Activated Carbon Adsorption, and Ultrasound Irradiation. *J. Hazard. Mater.* **2014**, *264*, 342–349.

(13) Alidina, M.; Li, D.; Ouf, M.; Drewes, J. E. Role of Primary Substrate Composition and Concentration on Attenuation of Trace Organic Chemicals in Managed Aquifer Recharge Systems. *J. Environ. Manage.* **2014**, *144*, 58–66.

(14) Nam, S.-W.; Choi, D.-J.; Kim, S.-K.; Her, N.; Zoh, K.-D. Adsorption Characteristics of Selected Hydrophilic and Hydrophobic Micropollutants in Water Using Activated Carbon. *J. Hazard. Mater.* **2014**, *270*, 144–152.

(15) Dutta, K.; Lee, M.-Y.; Lai, W. W.-P.; Lee, C. H.; Lin, A. Y.-C.; Lin, C.-F.; Lin, J.-G. Removal of Pharmaceuticals and Organic Matter from Municipal Wastewater Using Two-Stage Anaerobic Fluidized Membrane Bioreactor. *Bioresour. Technol.* **2014**, *165*,

4–6.

(16) Doll, T. E.; Frimmel, F. H. Kinetic Study of Photocatalytic Degradation of Carbamazepine, Clofibric Acid, Iomeprol and Iopromide Assisted by Different TiO_2 Materials - Determination of Intermediates and Reaction Pathways. *Water Res.* **2004**, *38* (4), 955–964.

(17) Esplugas, S.; Bila, D. M.; Krause, L. G. T.; Dezotti, M. Ozonation and Advanced Oxidation Technologies to Remove Endocrine Disrupting Chemicals (EDCs) and Pharmaceuticals and Personal Care Products (PPCPs) in Water Effluents. *J. Hazard. Mater.* **2007**, *149* (3), 631–642.

(18) Klavarioti, M.; Mantzavinos, D.; Kassinos, D. Removal of Residual Pharmaceuticals from Aqueous Systems by Advanced Oxidation Processes. *Environ. Int.* **2009**, *35* (2), 402–417.

(19) Crini, G. Non-Conventional Low-Cost Adsorbents for Dye Removal: A Review. *Bioresour. Technol.* **2006**, *97* (9), 1061–1085.

(20) Oller, I.; Malato, S.; Sánchez-Pérez, J. A. Combination of Advanced Oxidation Processes and Biological Treatments for Wastewater Decontamination-A Review. *Sci. Total Environ.* **2011**, *409* (20), 4141–4166.

(21) Pajootan, E.; Arami, M.; Mahmoodi, N. M. Binary System Dye Removal by Electrocoagulation from Synthetic and Real Colored Wastewaters. *J. Taiwan Inst. Chem. Eng.* **2012**, *43* (2), 282–290.

(22) Kobya, M.; Bayramoglu, M.; Eyvaz, M. Techno-Economical Evaluation of Electrocoagulation for the Textile Wastewater Using Different Electrode Connections. *J. Hazard. Mater.* **2007**, *148* (1–2), 311–318.

(23) Ghosh, S.; Badruddoza, A. Z. M.; Hidajat, K.; Uddin, M. S. Adsorptive Removal of Emerging Contaminants from Water Using Superparamagnetic Fe_3O_4 Nanoparticles Bearing Aminated Beta-Cyclodextrin. *J. Environ. Chem. Eng.* **2013**, *1* (3), 122–130.

(24) Kyzas, G. Z.; Siafaka, P. I.; Bikiaris, D. N.; Koukaras, E. N.; Froudakis, G. E. Alternative Use of Cross-Linked Polyallylamine (Known as Sevelamer Pharmaceutical Compound) as Biosorbent. *J. Colloid Interface Sci.* **2015**, *442*, 49–59.

(25) da Silva, L. G.; Ruggiero, R.; Gontijo, P. D. M.; Pinto, R. B.; Royer, B.; Lima, E. C.; Fernandes, T. H. M.; Calvete, T. Adsorption of Brilliant Red 2BE Dye from Water

Solutions by a Chemically Modified Sugarcane Bagasse Lignin. *Chem. Eng. J.* **2011**, *168* (2), 620–628.

(26) dos Santos, D. C.; Adebayo, M. A.; de Fátima Pinheiro Pereira, S.; Prola, L. D. T.; Cataluña, R.; Lima, E. C.; Saucier, C.; Gally, C. R.; Machado, F. M. New Carbon Composite Adsorbents for the Removal of Textile Dyes from Aqueous Solutions: Kinetic, Equilibrium, and Thermodynamic Studies. *Korean J. Chem. Eng.* **2014**, *31* (8), 1470–1479.

(27) Adebayo, M. A.; Prola, L. D. T.; Lima, E. C.; Puchana-Rosero, M. J.; Cataluña, R.; Saucier, C.; Umpierres, C. S.; Vaghetti, J. C. P.; da Silva, L. G.; Ruggiero, R. Adsorption of Procion Blue MX-R Dye from Aqueous Solutions by Lignin Chemically Modified with Aluminium and Manganese. *J. Hazard. Mater.* **2014**, *268*, 43–50.

(28) Fisal, A.; Daud, W. M. A. W.; Ahmad, M. A.; Radzi, R. Using Cocoa (Theobroma Cacao) Shell-Based Activated Carbon to Remove 4-Nitrophenol from Aqueous Solution: Kinetics and Equilibrium Studies. *Chem. Eng. J.* **2011**, *178*, 461–467.

(29) Calvete, T.; Lima, E. C.; Cardoso, N. F.; Vaghetti, J. C. P.; Dias, S. L. P.; Pavan, F. A. Application of Carbon Adsorbents Prepared from Brazilian-Pine Fruit Shell for the Removal of Reactive Orange 16 from Aqueous Solution: Kinetic, Equilibrium, and Thermodynamic Studies. *J. Environ. Manage.* **2010**, *91* (8), 1695–1706.

(30) Cardoso, N. F.; Pinto, R. B.; Lima, E. C.; Calvete, T.; Amavisca, C. V.; Royer, B.; Cunha, M. L.; Fernandes, T. H. M.; Pinto, I. S. Removal of Remazol Black B Textile Dye from Aqueous Solution by Adsorption. *Desalination* **2011**, *269* (1–3), 92–103.

(31) Ribas, M. C.; Adebayo, M. A.; Prola, L. D. T.; Lima, E. C.; Cataluña, R.; Feris, L. A.; Puchana-Rosero, M. J.; Machado, F. M.; Pavan, F. A.; Calvete, T. Comparison of a Homemade Cocoa Shell Activated Carbon with Commercial Activated Carbon for the Removal of Reactive Violet 5 Dye from Aqueous Solutions. *Chem. Eng. J.* **2014**, *248*, 315–326.

(32) Marsh, H.; Rodríguez-Reinoso, F. *Activated Carbon*; Elsevier Science & Technology Books: Oxford, 2006.

(33) Zheng, Z. Q.; Xia, H. Y.; Srinivasakannan, C.; Peng, J. H.; Zhang, L. B. Utilization of Crofton Weed for Preparation of Activated Carbon by Microwave Induced CO2 Activation. *Chem. Eng. Process. Process Intensif.* **2014**, *82*, 1–8.

(34) Pereira, R. G.; Veloso, C. M.; da Silva, N. M.; de Sousa, L. F.; Bonomo, R. C. F.; de Souza, A. O.; da Guarda Souza, M. O.; da Costa Ilhéu Fontan, R. Preparation of Activated Carbons from Cocoa Shells and Siriguela Seeds Using H_3PO_4 and $ZnCl_2$ as Activating Agents for BSA and α-Lactalbumin Adsorption. *Fuel Process. Technol.* **2014**, *126*, 476–486.

(35) Torrellas, S. Á.; García Lovera, R.; Escalona, N.; Sepúlveda, C.; Sotelo, J. L.; García, J. Chemical-Activated Carbons from Peach Stones for the Adsorption of Emerging Contaminants in Aqueous Solutions. *Chem. Eng. J.* **2015**, *279*, 788–798.

(36) Njoku, V. O.; Islam, M. A.; Asif, M.; Hameed, B. H. Utilization of Sky Fruit Husk Agricultural Waste to Produce High Quality Activated Carbon for the Herbicide Bentazon Adsorption. *Chem. Eng. J.* **2014**, *251*, 183–191.

(37) Hesas, R. H.; Arami-Niya, A.; Wan Daud, W. M. A.; Sahu, J. N. Preparation of Granular Activated Carbon from Oil Palm Shell by Microwave-Induced Chemical Activation: Optimisation Using Surface Response Methodology. *Chem. Eng. Res. Des.* **2013**, *91* (12), 2447–2456.

(38) Marsh, H.; Rodríguez-Reinoso, F. *Characterization of Activated Carbon*; 2006.

(39) Deng, H.; Yang, L.; Tao, G.; Dai, J. Preparation and Characterization of Activated Carbon from Cotton Stalk by Microwave Assisted Chemical Activation-Application in Methylene Blue Adsorption from Aqueous Solution. *J. Hazard. Mater.* **2009**, *166* (2–3), 1514–1521.

(40) Ferrera-Lorenzo, N.; Fuente, E.; Suárez-Ruiz, I.; Ruiz, B. KOH Activated Carbon from Conventional and Microwave Heating System of a Macroalgae Waste from the Agar-Agar Industry. *Fuel Process. Technol.* **2014**, *121*, 25–31.

(41) Njoku, V. O.; Foo, K. Y.; Asif, M.; Hameed, B. H. Preparation of Activated Carbons from Rambutan (Nephelium Lappaceum) Peel by Microwave-Induced KOH Activation for Acid Yellow 17 Dye Adsorption. *Chem. Eng. J.* **2014**, *250*, 198–204.

(42) Li, W.; Yang, K.; Peng, J.; Zhang, L.; Guo, S.; Xia, H. Effects of Carbonization Temperatures on Characteristics of Porosity in Coconut Shell Chars and Activated Carbons Derived from Carbonized Coconut Shell Chars. *Ind. Crops Prod.* **2008**, *28* (2), 190–198.

(43) Mehta, D.; Mazumdar, S.; Singh, S. K. Magnetic Adsorbents for the Treatment of

Water/wastewater-A Review. *J. Water Process Eng.* **2015**, *7*, 244–265.

(44) Ranjithkumar, V.; Hazeen, A. N.; Thamilselvan, M.; Vairan, S. Magnetic Activated Carbon-Fe_3O_4 Nanocomposites-Synthesys and Applications in the Removal of Acid Yellow Dye 17 from Water. *J. Nanosci. Nanotechnol.* **2014**, No. 14, 4949–4959.

(45) Ranjithkumar, V.; Sangeetha, S.; Vairam, S. Synthesis of Magnetic Activated Carbon/α-Fe_2O_3 Nanocomposite and Its Application in the Removal of Acid Yellow 17 Dye from Water. *J. Hazard. Mater.* **2014**, *273*, 127–135.

(46) Do, M. H.; Phan, N. H.; Nguyen, T. D.; Pham, T. T. S.; Nguyen, V. K.; Vu, T. T. T.; Nguyen, T. K. P. Activated carbon/Fe3O4 Nanoparticle Composite: Fabrication, Methyl Orange Removal and Regeneration by Hydrogen Peroxide. *Chemosphere* **2011**, *85* (8), 1269–1276.

(47) Podder, M. S.; Majumder, C. B. Application of Granular Activated carbon/MnFe2O4 Composite Immobilized on C. Glutamicum MTCC 2745 to Remove As(III) and As(V): Kinetic, Mechanistic and Thermodynamic Studies. *Spectrochim. Acta - Part A Mol. Biomol. Spectrosc.* **2016**, *153*, 298–314.

(48) Qiu, W.; Yang, D.; Xu, J.; Hong, B.; Jin, H.; Jin, D.; Peng, X.; Li, J.; Ge, H.; Wang, X. Efficient Removal of Cr(VI) by Magnetically Separable $CoFe_2O_4$/Activated Carbon Composite. *J. Alloys Compd.* **2016**, *678*, 179–184.

(49) Tan, F.; Fan, X.; Zhang, G.; Zhang, F. Coating and Filling of Carbon Nanotubes with Homogeneous Magnetic Nanoparticles. *Mater. Lett.* **2007**, *61* (8–9), 1805–1808.

(50) World Water Assessment Program. *Relatório Mundial Das Nações Unidas Sobre O Desenvolvimento Dos Recursos Hídricos, 2017: Aguas Residuais: O Recurso Inexplorado, Resumo Executivo*; 2017.

(51) Gordon, P. F.; Gregory, P. The Development of Dyes. In *Organic Chemistry in Colour*; Springer: Berlin, 1987; pp 1–22.

(52) Ajmal, A.; Majeed, I.; Malik, R. N.; Idriss, H.; Nadeem, M. A. Principles and Mechanisms of Photocatalytic Dye Degradation on TiO_2 Based Photocatalysts: A Comparative Overview. *RSC Adv.* **2014**, *4* (70), 37003–37026.

(53) Natarajan, S.; Bajaj, H. C.; Tayade, R. J. Recent Advances Based on the Synergetic Effect of Adsorption for Removal of Dyes from Waste Water Using Photocatalytic Process. *J. Environ. Sci.* **2016**, 1–22.

(54) Ngulube, T.; Gumbo, J. R.; Masindi, V.; Maity, A. An Update on Synthetic Dyes Adsorption onto Clay Based Minerals: A State-of-Art Review. *J. Environ. Manage.* **2017**, *191*, 35–57.

(55) Banat, I. M.; Nigam, P.; Singh, D.; Marchant, R. Microbial Decolorization of Textile-Dye-Containing Effluents: A Review. *Bioresour. Technol.* **1996**, *58* (3), 217–227.

(56) Clarke, E. A.; Anliker, R. Organic Dyes and Pigments. In *Anthropogenic Compounds*; Springer: Berlin, 1980; pp 181–215.

(57) Fu, Y.; Viraraghavan, T. Fungal Decolorization of Dye Wastewaters: A Review. *Bioresour. Technol.* **2001**, *79* (3), 251–262.

(58) Pan, H.; Feng, J.; He, G.-X.; Cerniglia, C. E.; Chen, H. Evaluation of Impact of Exposure of Sudan Azo Dyes and Their Metabolites on Human Intestinal Bacteria. *Anaerobe* **2012**, *18* (4), 445–453.

(59) Yagub, M. T.; Sen, T. K.; Afroze, S.; Ang, H. M. Dye and Its Removal from Aqueous Solution by Adsorption: A Review. *Adv. Colloid Interface Sci.* **2014**, *209*, 172–184.

(60) Tan, K. B.; Vakili, M.; Horri, B. A.; Poh, P. E.; Abdullah, A. Z.; Salamatinia, B. Adsorption of Dyes by Nanomaterials: Recent Developments and Adsorption Mechanisms. *Sep. Purif. Technol.* **2015**, *150*, 229–242.

(61) Conselho Nacional do Meio Ambiente (CONAMA). *Resolução 357, 18 de Março de 2005*; 2005; pp 58–63.

(62) Conselho Estadual do Meio Ambiente (CONSEMA). *Resolução 128/2006*; 2006; p 9.

(63) Babarinde, A.; Ogundipe, K.; Sangosanya, K. T.; Akintola, B. D.; Hassan, A.-O. E. Comparative Study on the Biosorption of Pb(II), Cd(II) and Zn(II) Using Lemon Grass (Cymbopogon Citratus): Kinetics, Isotherms and Thermodynamics. *Chem. Int.* **2016**, *2* (2), 89–102.

(64) Babarinde, A.; Onyiaocha, G. Equilibrium Sorption of Divalent Metal Ions onto Groundnut (Arachis Hypogaea) Shell: Kinetics, Isotherm and Thermodynamics. *Chem. Int.* **2016**, *2* (1), 37–46.

(65) Tahir, M. A.; Bhatti, H. N.; Iqbal, M. Solar Red and Brittle Blue Direct Dyes Adsorption onto Eucalyptus Angophoroides Bark: Equilibrium, Kinetics and Thermodynamic Studies. *J. Environ. Chem. Eng.* **2016**, *4* (2), 2431–2439.

(66) Buthelezi, S. P.; Olaniran, A. O.; Pillay, B. Textile Dye Removal from Wastewater

Effluents Using Bioflocculants Produced by Indigenous Bacterial Isolates. *Molecules* **2012**, *17* (12), 14260–14274.

(67) Mohan, D.; P. Singh, K.; Singh, G.; Kumar, K. Removal of Dyes from Wastewater Using Flyash, a Low-Cost Adsorbent. *Ind.Eng.Chem.Res.* **2002**, *41*, 3688–3695.

(68) Khan, T. A.; Khan, E. A.; Shahjahan. Removal of Basic Dyes from Aqueous Solution by Adsorption onto Binary Iron-Manganese Oxide Coated Kaolinite: Non-Linear Isotherm and Kinetics Modeling. *Appl. Clay Sci.* **2015**, *107*, 70–77.

(69) Shon, H. K.; Phuntsho, S.; Chaudhary, D. S.; Vigneswaran, S.; Cho, J. Nanofiltration for Water and Wastewater Treatment - A Mini Review. *Drink. Water Eng. Sci.* **2013**, *6* (1), 47–53.

(70) Shamraiz, U.; Hussain, R. A.; Badshah, A.; Raza, B.; Saba, S. Functional Metal Sulfides and Selenides for the Removal of Hazardous Dyes from Water. *J. Photochem. Photobiol. B.* **2016**, *159*, 33–41.

(71) Gomes, R. F.; de Azevedo, A. C. N.; Pereira, A. G. B.; Muniz, E. C.; Fajardo, A. R.; Rodrigues, F. H. A. Fast Dye Removal from Water by Starch-Based Nanocomposites. *J. Colloid Interface Sci.* **2015**, *454*, 200–209.

(72) Mu, B.; Wang, A. Adsorption of Dyes onto Palygorskite and Its Composites: A Review. *J. Environ. Chem. Eng.* **2016**, *4* (1), 1274–1294.

(73) Saygili, H.; Güzel, F.; Önal, Y. Conversion of Grape Industrial Processing Waste to Activated Carbon Sorbent and Its Performance in Cationic and Anionic Dyes Adsorption. *J. Clean. Prod.* **2015**, *93*, 84–93.

(74) Kucharska, M.; Grabka, J. A Review of Chromatographic Methods for Determination of Synthetic Food Dyes. *Talanta* **2010**, *80* (3), 1045–1051.

(75) Guo, J.; Wu, H.; Du, L.; Fu, Y. Determination of Brilliant Blue FCF in Food and Cosmetic Samples by Ionic Liquid Independent Disperse Liquid–liquid Micro-Extraction. *Anal. Methods* **2013**, *5* (16), 4021.

(76) Tikhomirova, T. I.; Ramazanova, G. R.; Apyari, V. V. Adsorption Preconcentration of Synthetic Anionic Food Dyes. *J. Anal. Chem.* **2017**, *72* (9), 917–934.

(77) Abbas, A.; Rehman, R.; Murtza, S.; Ayub, R. Isothermal Evaluation of Chemical Modification of Ricinus Communis Stem Used for Adsorptive Removal of Brilliant Blue FCF Dye from Water. *Asian J. Chem.* **2013**, *25* (16), 9153–9158.

(78) Ramesh, M.; Muthuraman, A. Flavoring and Coloring Agents: Health Risks and Potential Problems. In *Natural and artificial flavoring agents and food dyes*; Grumezesco, A. M., Holban, A. M., Eds.; Elsevier Academic Press publications: Londres, 2018; p 18.

(79) Ferreira, L. G. B.; Faria, R. X.; Ferreira, N. C. D. S.; Soares-Bezerra, R. J. Brilliant Blue Dyes in Daily Food: How Could Purinergic System Be Affected? *Int. J. Food Sci.* **2016**, *2016*, 5–8.

(80) Wu, Z.; Joo, H.; Lee, K. Kinetics and Thermodynamics of the Organic Dye Adsorption on the Mesoporous Hybrid Xerogel. *Chem. Eng. J.* **2005**, *112* (1–3), 227–236.

(81) Pinedo-Hernández, S.; Díaz-Nava, C.; Solache-Ríos, M. Sorption Behavior of Brilliant Blue FCF by a Fe-Zeolitic Tuff. *Water. Air. Soil Pollut.* **2012**, *223* (1), 467–475.

(82) Pesoutová, R.; Hlavínek, P.; Matysíkova, J. Use of Advanced Oxidation Processes for Textile Wastewater Treatment – a Review. **2011**, *X* (3), 59–65.

(83) Parvin, T.; Keerthiraj, N.; Ibrahim, I. A.; Phanichphant, S.; Byrappa, K. Photocatalytic Degradation of Municipal Wastewater and Brilliant Blue Dye Using Hydrothermally Synthesized Surface-Modified Silver-Doped ZnO Designer Particles. *Int. J. Photoenergy* **2012**, *2012*.

(84) Khataee, A.; Vatanpour, V.; Farajzadeh, M. R. Remediation of the Textile Dye Brilliant Blue FCF from Contaminated Water via a Fenton-Like Reaction : Influence of Aromatic Additives. *Turkish J. Eng. Env. Sci.* **2008**, *32*, 367–376.

(85) Hernández-Hernández, K. A.; Solache-Ríos, M.; Díaz-Nava, M. C. Removal of Brilliant Blue FCF from Aqueous Solutions Using an Unmodified and Iron-Modified Bentonite and the Thermodynamic Parameters of the Process. *Water. Air. Soil Pollut.* **2013**, *224* (5).

(86) Gupta, V. K.; Mittal, A.; Krishnan, L.; Mittal, J. Adsorption Treatment and Recovery of the Hazardous Dye, Brilliant Blue FCF, over Bottom Ash and de-Oiled Soya. *J. Colloid Interface Sci.* **2006**, *293* (1), 16–26.

(87) United States Environmental Protection Agency (EPA). Contaminants of Emerging Concern including Pharmaceuticals and Personal Care Products https://www.epa.gov/wqc/contaminants-emerging-concern-including-pharmaceuticals-and-personal-care-products (accessado em 2 nov 2017).

(88) Aga, D. S. Fate of Pharmaceuticals in the Environment and in Water Treatment Systems. *CRC Press* **2008**.

(89) Redshaw, C. H.; Cooke, M. P.; Talbot, H. M.; McGrath, S.; Rowland, S. J. Low Biodegradability of Fluoxetine HCl, Diazepam and Their Human Metabolites in Sewage Sludge-Amended Soil. *J. Soils Sediments* **2008**, *8*, 217–230.

(90) Rodriguez-Narvaez, O. M.; Peralta-Hernandez, J. M.; Goonetilleke, A.; Bandala, E. R. Treatment Technologies for Emerging Contaminants in Water: A Review. *Chem. Eng. J.* **2017**, *323*, 361–380.

(91) Zenker, A.; Cicero, M. R.; Prestinaci, F.; Bottoni, P.; Carere, M. Bioaccumulation and Biomagnification Potential of Pharmaceuticals with a Focus to the Aquatic Environment. *J. Environ. Manage.* **2014**, *133*, 378–387.

(92) Petrie, B.; Barden, R.; Kasprzyk-Hordern, B. A Review on Emerging Contaminants in Wastewaters and the Environment: Current Knowledge, Understudied Areas and Recommendations for Future Monitoring. *Water Res.* **2014**, *72*, 3–27.

(93) Mills, L. J.; Chichester, C. Review of Evidence: Are Endocrine-Disrupting Chemicals in the Aquatic Environment Impacting Fish Populations? *Sci. Total Environ.* **2005**, *343*, 1–34.

(94) Le-Minh, N.; Khan, S. J.; Drewes, J. E.; Stuetz, R. M. Fate of Antibiotics during Municipal Water Recycling Treatment Processes. *Water Res.* **2010**, *44* (15), 4295–4323.

(95) Andersson, D. I.; Hughes, D. Evolution of Antibiotic Resistance at Non-Lethal Drug Concentrations. *Drug Resist. Updat.* **2012**, *15* (3), 162–172.

(96) Merlin, C.; Bonot, S.; Courtois, S.; Block, J. C. Persistence and Dissemination of the Multiple-Antibiotic-Resistance Plasmid pB10 in the Microbial Communities of Wastewater Sludge Microcosms. *Water Res.* **2011**, *45* (9), 2897–2905.

(97) Calderón-Preciado, D.; Matamoros, V.; Bayona, J. M. Occurrence and Potential Crop Uptake of Emerging Contaminants and Related Compounds in an Agricultural Irrigation Network. *Sci. Total Environ.* **2011**, *412–413*, 14–19.

(98) Jean, J.; Perrodin, Y.; Pivot, C.; Trepo, D.; Perraud, M.; Droguet, J.; Tissot-Guerraz, F.; Locher, F. Identification and Prioritization of Bioaccumulable Pharmaceutical Substances Discharged in Hospital Effluents. *J. Environ. Manage.* **2012**, *103*, 113–121.

(99) Oaks, J. L.; Gilbert, M.; Virani, M. Z.; Watson, R. T.; Meteyer, C. U.; Rideout, B.; Shivaprasad, H. L.; Ahmed, S.; Chaudhry, M. J. I.; Arshad, M.; Mahmood, S.; Ali, A.; Khan, A. A. Diclofenac Residues as the Cause of Vulture Population Decline in Pakistan. *Nature* **2004**, *427* (6975), 630–633.

(100) Fowler, P. a.; Bellingham, M.; Sinclair, K. D.; Evans, N. P.; Pocar, P.; Fischer, B.; Schaedlich, K.; Schmidt, J. S.; Amezaga, M. R.; Bhattacharya, S.; Rhind, S. M.; O'Shaughnessy, P. J. Impact of Endocrine-Disrupting Compounds (EDCs) on Female Reproductive Health. *Mol. Cell. Endocrinol.* **2012**, *355* (2), 231–239.

(101) Hess-Wilson, J. K.; Knudsen, K. E. Endocrine Disrupting Compounds and Prostate Cancer. *Cancer Lett.* **2006**, *241* (1), 1–12.

(102) Stumm-Zollinger, E.; Fair, G. M. Biodegradation of Steroid Hormones. *Water Pollut. Control Fed.* **1965**, 1506–1510.

(103) Higaite, C.; Azarnoff, D. L. Drugs and Drugs Metabolites as Environmental Contaminants: Chlorophenoxyisobutyrate and Salicylic Acid in Sewage Water Effluent. *Life Sci.* **1977**, *20* (2), 337–341.

(104) Petrovic, M.; Barcelo, D.; Pérez, S. *Analysis, Removal, Effects and Risk of Pharmaceuticals in the Water Cycle*; Elsevier B.V.: Oxford, 2013.

(105) Santos, L. H. M. L. M.; Araújo, A. N.; Fachini, A.; Pena, A.; Delerue-Matos, C.; Montenegro, M. C. B. S. M. Ecotoxicological Aspects Related to the Presence of Pharmaceuticals in the Aquatic Environment. *J. Hazard. Mater.* **2010**, *175* (1–3), 45–95.

(106) Rivera-Utrilla, J.; Sánchez-Polo, M.; Ferro-García, M. Á.; Prados-Joya, G.; Ocampo-Pérez, R. Pharmaceuticals as Emerging Contaminants and Their Removal from Water. A Review. *Chemosphere* **2013**, *93* (7), 1268–1287.

(107) Kümmerer, K. The Presence of Pharmaceuticals in the Environment due to Human Use - Present Knowledge and Future Challenges. *J. Environ. Manage.* **2009**, *90* (8), 2354–2366.

(108) Goldstein, W. E. *Pharmaceutical Accumulation in the Environment: Prevention, Control,Health Effects, and Economic Impact*; CRC Press-Taylor & Francis Group: Boca Raton, 2014.

(109) Whitacre, D. M. *Reviews of Environmental Contamination and Toxicology*; Springer:

New York, 2010; Vol. 202.

(110) Halling-Sorensen, B.; Nielsen, S. N.; Lanzky, P. F.; Ingerslev, F.; Holten Lutzhoft, H. C.; S.E., J. Occurence, Fate and Effects of Pharmaceuticals Substance in the Environment - A Review. *Chemosphere* **1998**, *36* (2), 357–393.

(111) Soulet, B.; Tauxe, A.; Tarradellas, J. Analysis of Acidic Drugs in Swiss Wastewaters. *Int. J. Environ. Anal. Chem.* **2002**, *82* (10), 659–667.

(112) Jones, O. A. H.; Voulvoulis, N.; Lester, J. N. Human Pharmaceuticals in Wastewater Treatment Processes. *Crit. Rev. Environ. Sci. Technol.* **2005**, *35*, 401–427.

(113) Han, G. H.; Hur, H. G.; Kim, S. D. Ecotoxicological Risk of Pharmaceuticals from Wastewater Treatment Plants in Korea: Occurrence and Toxicity to Daphnia Magna. *Environ. Toxicol. Chem.* **2006**, *25* (1), 265–271.

(114) Ashton, D.; Hilton, M.; Thomas, K. V. Investigating the Environmental Transport of Human Pharmaceuticals to Streams in the United Kingdom. *Sci. Total Environ.* **2004**, *333* (1–3), 167–184.

(115) Kahle, M.; Buerge, I. J.; Hauser, A.; Muller, M. D.; Poiger, T. Azole Fungicides: Occurrence and Fate in Wastewater and Surface Waters. *Environ. Sci. Technol.* **2008**, *42* (19), 7193–7200.

(116) United States Geological Survey (USGS). *Occurrence and Potential Transport of Selected Pharmaceuticals and Other Organic Wastewater Compounds from Wastewater-Treatment Plant Influent and Effluent to Groundwater and Canal Systems in Miami-Dade County, Florida*; 2012.

(117) Gracia-Lor, E.; Sancho, J. V.; Serrano, R.; Hernández, F. Occurrence and Removal of Pharmaceuticals in Wastewater Treatment Plants at the Spanish Mediterranean Area of Valencia. *Chemosphere* **2012**, *87* (5), 453–462.

(118) Petrović, M.; Hernando, M. D.; Díaz-Cruz, M. S.; Barceló, D. Liquid Chromatography-Tandem Mass Spectrometry for the Analysis of Pharmaceutical Residues in Environmental Samples: A Review. *J. Chromatogr. A* **2005**, *1067* (1–2), 1–14.

(119) Taylor, D.; Senac, T. Human Pharmaceutical Products in the Environment - The "problem" in Perspective. *Chemosphere* **2014**, *115*, 95–99.

(120) Dietrich, D. R.; Webb, S. F.; Petry, T. *Hot Spot Pollutants: Pharmaceuticals in the Environment*; Elsevier Academic Press publications: Burlington, 2005.

(121) Jjemba, P. K. *Pharma-Ecology: The Occurrence and Fate of Pharmaceuticals and Personal Care Products in the Environment*; John Wiley & Sons, Inc.: New Jersey, 2008.

(122) Zhang, Y.; Geißen, S. U.; Gal, C. Carbamazepine and Diclofenac: Removal in Wastewater Treatment Plants and Occurrence in Water Bodies. *Chemosphere* **2008**, *73* (8), 1151–1161.

(123) Sotelo, J. L.; Ovejero, G.; Rodríguez, A.; Álvarez, S.; Galán, J.; García, J. Competitive Adsorption Studies of Caffeine and Diclofenac Aqueous Solutions by Activated Carbon. *Chem. Eng. J.* **2014**, *240*, 443–453.

(124) Stülten, D.; Zühlke, S.; Lamshöft, M.; Spiteller, M. Occurrence of Diclofenac and Selected Metabolites in Sewage Effluents. *Sci. Total Environ.* **2008**, *405* (1–3), 310–316.

(125) Rosal, R.; Rodríguez, A.; Perdigón-Melón, J. A.; Petre, A.; García-Calvo, E.; Gómez, M. J.; Agüera, A.; Fernández-Alba, A. R. Occurrence of Emerging Pollutants in Urban Wastewater and Their Removal through Biological Treatment Followed by Ozonation. *Water Res.* **2010**, *44* (2), 578–588.

(126) Snyder, S. a.; Wert, E. C.; Lei, H. D.; Westerhoff, P.; Yoon, Y. *Removal of EDCs and Pharmaceuticals in Drinking and Reuse Treatment Processes*; 2007.

(127) Álvarez, S.; Ribeiro, R. S.; Gomes, H. T.; Sotelo, J. L.; García, J. Synthesis of Carbon Xerogels and Their Application in Adsorption Studies of Caffeine and Diclofenac as Emerging Contaminants. *Chem. Eng. Res. Des.* **2015**, *95*, 229–238.

(128) de Sousa, J. M.; Neto, M. F. A.; Partata, A. K. Ação Anti-Inflamatória Da Nimesulida E Seu Grau de Hepatotoxicidade. *Rev. Científica do ITPAC* **2016**, *9*.

(129) Miranda, L.; Pereira, V. C.; Machado, C. S.; Torres, Y. R.; Dos Anjos, V. E.; Quináia, S. P. Direct Determination of Nimesulide in Natural Waters and Wastewater by Cathodic Stripping Voltammetry. *Arch. Environ. Contam. Toxicol.* **2017**, 1–10.

(130) Silveira, M. A. K.; Caldas, S. S.; Guilherme, J. R.; Costa, F. P.; Guimarães, B. D. S.; Cerqueira, M. B. R.; Soares, B. M.; Primel, E. G. Quantification of Pharmaceuticals and Personal Care Product Residues in Surface and Drinking Water Samples by SPE and LC-ESI-MS/MS. *J. Braz. Chem. Soc.* **2013**, *24* (9), 1385–1395.

(131) Lolić, A.; Paíga, P.; Santos, L. H. M. L. M.; Ramos, S.; Correia, M.; Delerue-Matos, C.

Assessment of Non-Steroidal Anti-Inflammatory and Analgesic Pharmaceuticals in Seawaters of North of Portugal: Occurrence and Environmental Risk. *Sci. Total Environ.* **2015**, *508*, 240–250.

(132) Lacey, C.; Basha, S.; Morrissey, A.; Tobin, J. M. Occurrence of Pharmaceutical Compounds in Wastewater Process Streams in Dublin, Ireland. *Environ. Monit. Assess.* **2012**, *184* (2), 1049–1062.

(133) Den Berghe, H. Van; Garric, X.; Vert, M.; Coudane, J. New Amoxicillin-Poly(lactic Acid)-Based Conjugates: Synthesis and in Vitro Release of Amoxicillin. *Polym. Int.* **2011**, *60* (3), 398–404.

(134) Wilkinson, J.; Hooda, P. S.; Barker, J.; Barton, S.; Swinden, J. Occurrence, Fate and Transformation of Emerging Contaminants in Water: An Overarching Review of the Field. *Environ. Pollut.* **2017**, *231*, 954–970.

(135) Pan, X.; Deng, C.; Zhang, D.; Wang, J.; Mu, G.; Chen, Y. Toxic Effects of Amoxicillin on the Photosystem II of Synechocystis Sp. Characterized by a Variety of in Vivo Chlorophyll Fluorescence Tests. *Aquat. Toxicol.* **2008**, *89* (4), 207–213.

(136) Kadurina, M.; Bocheva, G.; Tonev, S. Penicillin and Semisynthetic Penicillins in Dermatology. *Disease-a-Month* **2004**, *50* (6), 291–314.

(137) de Franco, M. A. E.; de Carvalho, C. B.; Bonetto, M. M.; Soares, R. de P.; Féris, L. A. Removal of Amoxicillin from Water by Adsorption onto Activated Carbon in Batch Process and Fixed Bed Column: Kinetics, Isotherms, Experimental Design and Breakthrough Curves Modelling. *J. Clean. Prod.* **2017**, *161*, 947–956.

(138) Xu, J. J.; Hendriks, B. S.; Zhao, J.; de Graaf, D. Multiple Effects of Acetaminophen and p38 Inhibitors: Towards Pathway Toxicology. *FEBS Lett.* **2008**, *582* (8), 1276–1282.

(139) Bosch, M. E.; Sánchez, A. J. R.; Rojas, F. S.; Ojeda, C. B. Determination of Paracetamol: Historical Evolution. *J. Pharm. Biomed. Anal.* **2006**, *42* (3), 291–321.

(140) Ebele, A. J.; Abou-Elwafa Abdallah, M.; Harrad, S. Pharmaceuticals and Personal Care Products (PPCPs) in the Freshwater Aquatic Environment. *Emerg. Contam.* **2017**, *3* (1), 1–16.

(141) Pereira, C. D. S.; Maranho, L. A.; Cortez, F. S.; Pusceddu, F. H.; Santos, A. R.; Ribeiro, D. A.; Cesar, A.; Guimarães, L. L. Occurrence of Pharmaceuticals and

Cocaine in a Brazilian Coastal Zone. *Sci. Total Environ.* **2016**, *548–549*, 148–154.

(142) Hashemian, S.; Salari, K.; Yazdi, Z. A. Preparation of Activated Carbon from Agricultural Wastes (Almond Shell and Orange Peel) for Adsorption of 2-Pic from Aqueous Solution. *J. Ind. Eng. Chem.* **2013**, *20* (4), 1892–1900.

(143) Cecen, F.; Aktas, O. *Activated Carbon for Water and Wastewater Treatment: Integration of Adsorption and Biological Treatment*; Wiley-VCH Verlag & Co. KGaA: Weinheim, 2012.

(144) Bansal, R. C. R. C.; Goyal, M.; Roop, C. B.; Meenakshi, G.; Bansal, R. C. R. C.; Goyal, M. *Activated Carbon Adsorption*; Taylor & Francis Group: Boca Raton, 2005.

(145) Cheung, W. H.; Szeto, Y. S.; McKay, G. Intraparticle Diffusion Processes during Acid Dye Adsorption onto Chitosan. *Bioresour. Technol.* **2007**, *98* (15), 2897–2904.

(146) Plazinski, W.; Rudzinski, W. Kinetics of Adsorption at solid/Solution Interfaces Controlled by Intraparticle Diffusion: A Theoretical Analysis. *J. Phys. Chem. C* **2009**, *113* (28), 12495–12501.

(147) Yahya, M. A.; Al-Qodah, Z.; Ngah, C. W. Z. Agricultural Bio-Waste Materials as Potential Sustainable Precursors Used for Activated Carbon Production: A Review. *Renew. Sustain. Energy Rev.* **2015**, *46*, 218–235.

(148) Yang, Y.; Ok, Y. S.; Kim, K.-H.; Kwon, E. E.; Tsang, Y. F. Occurrences and Removal of Pharmaceuticals and Personal Care Products (PPCPs) in Drinking Water and Water/sewage Treatment Plants: A Review. *Sci. Total Environ.* **2017**, *596–597*, 303–320.

(149) Cardoso, N. F.; Lima, E. C.; Pinto, I. S.; Amavisca, C. V.; Royer, B.; Pinto, R. B.; Alencar, W. S.; Pereira, S. F. P. Application of Cupuassu Shell as Biosorbent for the Removal of Textile Dyes from Aqueous Solution. *J. Environ. Manage.* **2011**, *92* (4), 1237–1247.

(150) Köseoğlu, E.; Akmil-Başar, C. Preparation, Structural Evaluation and Adsorptive Properties of Activated Carbon from Agricultural Waste Biomass. *Adv. Powder Technol.* **2015**, *26*, 811–818.

(151) Attia, A. A.; Girgis, B. S.; Fathy, N. A. Removal of Methylene Blue by Carbons Derived from Peach Stones by H_3PO_4 Activation: Batch and Column Studies. *Dye. Pigment.* **2008**, *76* (1), 282–289.

(152) Olivares-Marín, M.; Del Prete, V.; Garcia-Moruno, E.; Fernández-González, C.; Macías-García, a.; Gómez-Serrano, V. The Development of an Activated Carbon from Cherry Stones and Its Use in the Removal of Ochratoxin A from Red Wine. *Food Control* **2009**, *20* (3), 298–303.

(153) Montoya, V. H.; Petriciolet, A. B. *Lignocellulosic Precursors Used in the Synthesis of Activated Carbon: Characterization Techniques and Applications in the Wastewater Treatment*; INTECH: Rijeka, 2012.

(154) Hesas, R. H.; Daud, W. M. A. W.; Sahu, J. N.; Arami-Niya, A. The Effects of a Microwave Heating Method on the Production of Activated Carbon from Agricultural Waste: A Review. *J. Anal. Appl. Pyrolysis* **2013**, *100*, 1–11.

(155) Sanseverino, A. M. Microondas Em Síntese Orgânica. *Quim. Nova* **2002**, *25* (4), 660–667.

(156) Yuen, F. K.; Hameed, B. H. Recent Developments in the Preparation and Regeneration of Activated Carbons by Microwaves. *Adv. Colloid Interface Sci.* **2009**, *149* (1–2), 19–27.

(157) Mueller, N. C.; Nowack, B. Nanoparticles for Remediation: Solving Big Problems with Little Particles. *Elements* **2010**, *6* (6), 395–400.

(158) Tesh, S. J.; Scott, T. B. Nano-Composites for Water Remediation: A Review. *Adv. Mater.* **2014**, *26* (35), 6056–6068.

(159) Gómez-Pastora, J.; Bringas, E.; Ortiz, I. Recent Progress and Future Challenges on the Use of High Performance Magnetic Nano-Adsorbents in Environmental Applications. *Chem. Eng. J.* **2014**, *256*, 187–204.

(160) Kefeni, K. K.; Mamba, B. B.; Msagati, T. A. M. Application of Spinel Ferrite Nanoparticles in Water and Wastewater Treatment: A Review. *Sep. Purif. Technol.* **2017**, *188*, 399–422.

(161) Reddy, D. H. K.; Yun, Y. S. Spinel Ferrite Magnetic Adsorbents: Alternative Future Materials for Water Purification? *Coord. Chem. Rev.* **2016**, *315*, 90–111.

(162) Ai, L.; Huang, H.; Chen, Z.; Wei, X.; Jiang, J. Activated Carbon/$CoFe_2O_4$ Composites: Facile Synthesis, Magnetic Performance and Their Potential Application for the Removal of Malachite Green from Water. *Chem. Eng. J.* **2010**, *156* (2), 243–249.

(163) Jiang, T.; Liang, Y. D.; He, Y. J.; Wang, Q. Activated Carbon/$NiFe_2O_4$ Magnetic

Composite: A Magnetic Adsorbent for the Adsorption of Methyl Orange. *J. Environ. Chem. Eng.* **2015**, *3* (3), 1740–1751.

(164) Rai, P.; Gautam, R. K.; Banerjee, S.; Rawat, V.; Chattopadhyaya, M. C. Synthesis and Characterization of a Novel $SnFe_2O_4$@Activated Carbon Magnetic Nanocomposite and Its Effectiveness in the Removal of Crystal Violet from Aqueous Solution. *J. Environ. Chem. Eng.* **2015**, *3* (4), 2281–2291.

(165) Yavari, S.; Mahmodi, N. M.; Teymouri, P.; Shahmoradi, B.; Maleki, A. Cobalt Ferrite Nanoparticles: Preparation, Characterization and Anionic Dye Removal Capability. *J. Taiwan Inst. Chem. Eng.* **2016**, *59*, 320–329.

(166) Xu, J.; Xin, P.; Gao, Y.; Hong, B.; Jin, H.; Jin, D.; Peng, X.; Li, J.; Gong, J.; Ge, H.; Wang, X. Magnetic Properties and Methylene Blue Adsorptive Performance of $CoFe_2O_4$/Activated Carbon Nanocomposites. *Mater. Chem. Phys.* **2014**, *147* (3), 915–919.

(167) Shao, L.; Ren, Z.; Zhang, G.; Chen, L. Facile Synthesis, Characterization of a $MnFe_2O_4$/Activated Carbon Magnetic Composite and Its Effectiveness in Tetracycline Removal. *Mater. Chem. Phys.* **2012**, *135* (1), 16–24.

(168) Bergmann, C. P.; Machado, F. M. *Carbon Nanomaterials as Adsorbents for Environmental and Biological Applications*; Springer: New York.

(169) Langmuir, I. The Adsorption of Gases on Plane Surfaces of Glass, Mica and Platinum. *J. Am. Chem. Soc.* **1918**, *40* (9), 1361–1403.

(170) Foo, K. Y.; Hameed, B. H. Mesoporous Activated Carbon from Wood Sawdust by K_2CO_3 Activation Using Microwave Heating. *Bioresour. Technol.* **2012**, *111*, 425–432.

(171) Vasanth Kumar, K.; Sivanesan, S. Isotherms for Malachite Green onto Rubber Wood (Hevea Brasiliensis) Sawdust: Comparison of Linear and Non-Linear Methods. *Dye. Pigment.* **2007**, *72* (1), 124–129.

(172) Freundlich, H. Adsorption in Solution. *Phys. Chem. Soc.* **1906**, *40*, 1361–1368.

(173) Liu, Y.; Xu, H.; Yang, S. F.; Tay, J. H. A General Model for Biosorption of Cd2+, Cu^{2+} and Zn^{2+} by Aerobic Granules. *J. Biotechnol.* **2003**, *102* (3), 233–239.

(174) Ho, Y. S.; McKay, G. Pseudo-Second Order Model for Sorption Processes. *Process Biochem.* **1999**, *34* (5), 451–465.

(175) Liu, Y.; Liu, Y. J. Biosorption Isotherms, Kinetics and Thermodynamics. *Sep. Purif.*

Technol. **2008**, *61* (3), 229–242.

(176) Liu, Y.; Shen, L. A General Rate Law Equation for Biosorption. *Biochem. Eng. J.* **2008**, *38* (3), 390–394.

(177) Alencar, W. S.; Lima, E. C.; Royer, B.; dos Santos, B. D.; Calvete, T.; da Silva, E.; Alves, C. N. Application of Aqai Stalks as Biosorbents for the Removal of the Dye Procion Blue MX-R from Aqueous Solution. *Sep. Sci. Technol.* **2012**, *47* (3), 513–526.

(178) Ranjithkumar, V.; Hazeen, A. N.; Thamilselvan, M.; Vairam, S. Magnetic Activated Carbon-Fe3O4 Nanocomposites-Synthesis and Applications in the Removal of Acid Yellow Dye 17 from Water. *J. Nanosci. Nanotechnol.* **2014**, *14* (7), 4949–4959.

(179) Hermanek, M.; Zboril, R.; Mashlan, M.; Machala, L.; Schneeweiss, O. Thermal Behaviour of iron(II) Oxalate Dihydrate in the Atmosphere of Its Conversion Gases. *J. Mater. Chem.* **2006**, *16* (13), 1273.

(180) Prola, L. D. T.; Acayanka, E.; Lima, E. C.; Umpierres, C. S.; Vaghetti, J. C. P.; Santos, W. O.; Laminsi, S.; Djifon, P. T. Comparison of Jatropha Curcas Shells in Natural Form and Treated by Non-Thermal Plasma as Biosorbents for Removal of Reactive Red 120 Textile Dye from Aqueous Solution. *Ind. Crops Prod.* **2013**, *46*, 328–340.

(181) Prola, L. D. T.; Acayanka, E.; Tarley, C. R. T. Application of Aqai Stalks as Biosorbent for the Removal of Evans Blue and Vilmafix Red RR-2B Dyes from Aqueous Solutions. *Desalin. Water Treat.* **2013**, *51*, 4582–4592.

APÊNDICE 1

CLEAN
Soil Air Water

Caroline Saucier[1]
Matthew A. Adebayo[2]
Eder C. Lima[1]
Lizie D. T. Prola[1]
Pascal S. Thue[1,3]
Cibele S. Umpierres[1]
Mayerly J. Puchana-Rosero[1]
Fernando M. Machado[4]

[1]Institute of Chemistry, Federal University of Rio Grande do Sul (UFRGS), Porto Alegre, Rio Grande do Sul, Brazil
[2]Department of Chemistry, Federal University of Agriculture, Ogun State, Nigeria
[3]Department of Applied Chemistry, University of Ngaoundere, Ngaoundere, Cameroon
[4]Center of Technological Development, Federal University of Pelotas, Pelotas, RS, Brazil

Research Article

Comparison of a Homemade Bacuri Shell Activated Carbon With Carbon Nanotubes for Food Dye Removal

The shell of bacuri together with inorganic components [red mud + lime + KOH + $KAl(SO_4)_2 + Al(OH)_3$] at different ratios of 1.0 (BC-1.0), 1.5 (BC-1.5), and 2.0 (BC-2.0) were pyrolized at 1073 K. To complete the chemical activation process, the inorganic components were leached from the carbonaceous matrix through acidification with 6 M HCl under reflux to obtain ABC-1.0, ABC-1.5 and ABC-2.0. ABC-1.5 showed the highest adsorption capacity among these adsorbents. Fourier transform IR spectroscopy, scanning electron microscopy, N_2 adsorption/desorption curves and X-ray diffraction were used to characterize BC-1.5 (precursor) and ABC-1.5 (activated carbon). The analyses indicate that the majority of the inorganic compounds were leached from the carbonaceous matrix, resulting in an activated carbon with a high surface area and pore volume, suitable for dye adsorption. The sorption capacity of ABC-1.5 was compared with multi-walled carbon nanotubes (MWCNT) for removal of Brilliant Blue food dye (BB-FCF) from aqueous solutions. The general order kinetic model described well the adsorption process. The maximum amounts of BB-FCF removed at 323 K were 647.9 and 231.5 mg g^{-1} for ABC-1.5 and MWCNT, respectively. In addition, ABC-1.5 and MWCNT were applied for the treatment of two simulated effluents.

Keywords: Adsorption; Carbonaceous matrix; General order kinetic; Nonlinear isotherms; Simulated beverage effluents

Received: September 12, 2014; *revised:* October 22, 2014; *accepted:* November 11, 2014

DOI: 10.1002/clen.201400669

1 Introduction

Population growth increases the demand for industrial products globally. A number of industries such as foodstuff and textile industry, paper and pulp mills, cosmetic, food, leather, and rubber industry, etc., apply dyes to their products [1, 2]. The production and consumption of these products result in dye-laden wastewater [3, 4].

Dye-loaded wastewater is unsafe for aquatic organisms. It impedes light penetration to aquatic plants and reduces the photosynthetic rate of plants [5]. Generally, the presence of dyes in the environment affects all living organisms [6] because dyes have toxic and carcinogenic properties [7]. The treatment of an effluent containing synthetic dyes is a difficult task [8–10] because these dyes have a complex aromatic molecular structure, which make them highly stable and non-biodegradable [10, 11]. Strict regulations imposed by the government of some countries have led to the treatment of industrial effluents before they are released into the environment [12–16]. The search for environmental friendly techniques for the removal of dyes from wastewater arises from the strict regulations imposed on these industries [17, 18].

Adsorption is a common and effective technique for purification of dye-laden wastewater [17, 18]. In addition, adsorption is a simple technique. Similarly, low cost adsorbents are available [2–4, 12, 13]. Adsorption is a process by which pollutants are transferred from the effluent to a solid phase thereby minimizing the bioavailability of the pollutants to the living organisms [19, 20]. After the effluents have been treated, they can be released into the environment [21, 22] or used for industrial processes that require water of low purity. Another advantage of the adsorption technology is that the adsorbents can be regenerated and reused [23, 24].

Activated carbons are known for their excellent adsorption characteristics because of their enhanced pore structures. This unique property makes activated carbons as one of the materials mostly used for the treatment of industrial wastewater [25, 26]. Major determinants of the ability of activated carbons to adsorb pollutants from aqueous solutions are: the nature of organic material used to prepare the activated carbon [27, 28] and the experimental conditions of the activation processes [29, 30]. Chemical activation of activated carbons utilizes H_3PO_4, $ZnCl_2$, KOH, NaOH, H_2SO_4, and K_2CO_3, etc. [27, 28, 31]. The chemical activation process requires that the raw materials and inorganic activating agents are mixed properly in an aqueous medium. The mixture is dried in the oven and carbonized (673–1073 K). The inorganic components can be leached from the activated carbon using water or acidic solutions [27, 28]. This

Correspondence: Prof. Eder C. Lima, Institute of Chemistry, Federal University of Rio Grande do Sul (UFRGS), Av. Bento Gonçalves 9500, Postal Box 15003, 91501-970 Porto Alegre, Rio Grande do Sul, Brazil
E-mail: eder.lima@ufrgs.br or profederlima@gmail.com

Abbreviations: **ABC**, acidified BC; **BB**, Brilliant Blue; **BC**, bacuri carbon adsorbent; **FCF**, food dye; **MWCNT**, multi-walled carbon nanotube; $\mathbf{pH_{pzc}}$, point of zero charge

CLEAN Soil Air Water

procedure, however, could not yield a homogeneous distribution of the inorganic components with the organic carbonaceous materials because of the problems associated with the drying of impregnated organic components [27, 28].

The bacuri shell is a residue of the bacuri fruit. Bacuri shell corresponds to 60–70% of the dried weight of the bacuri fruit [32]. The annual production of bacuri in Brazil is about 500 000–tons/year. Therefore, the ice-cream industry in Brazil generates large quantities of bacuri shells, most of which are discarded in aquifers and the environment [32]. The accumulation and decomposition of the bacuri residues lead to the generation of various chemicals and micro-organisms that can contaminate the environment. Therefore, it is important to find industrial applications for this waste to avoid environmental disasters.

This paper reports the chemical activation of activated carbons prepared from powdered bacuri shells and inorganic components [30% red mud + 20% lime + 10% KOH + 20% $KAl(SO_4)_2$ + 20% $Al(OH)_3$] with ratios of 1.0, 1.5, and 2.0 that were pyrolyzed at 1073 K under inert atmosphere. The carbonized materials (BC-1.0, BC-1.5, and BC-2.0) were acidified with 6 M HCl to obtain chemically activated bacuri carbons (ABC-1.0, ABC-1.5, ABC-2.0). According to preliminary adsorption experiments, ABC-1.5 exhibited the best adsorption capacity among the three adsorbents. The adsorption capacity of multi-walled carbon nanotubes (MWCNT), an efficient adsorbent [14, 23, 33–35] for the removal of toxic pollutants from aqueous solutions, was compared with the adsorption capacity of ABC-1.5. ABC-1.5 and MWCNT were used for the removal of Brilliant Blue food dye (BB-FCF) from aqueous solutions.

2 Materials and methods

2.1 Solutions and reagents

All solutions were prepared using deionized water. The food dye (C.I. Brilliant Blue FCF, BB-FCF; purity >85%; $C_{37}H_{34}N_2O_9S_3Na_2$; 792.84 g mol^{-1}; $\lambda_{max} = 629$ nm; Supporting Information Fig. S1) was supplied by Plury Chemicals and used without purification. BB-FCF was used in this study because it is largely used by the Brazilian Food industries.

A stock solution, 5 g L^{-1}, of BB-FCF was prepared and different working solutions were prepared by diluting the stock solution. 0.1 M NaOH and 0.1 M HCl were used to adjust the pH of the solutions using the Schott model Lab 850 set pH meter.

2.2 Adsorbents

Multi-walled carbon nanotubes (MWCNT) were supplied by Hwnano (China; outer diameter 8–20 nm; length 5–15 μm; carbon content >99%; amorphous carbon <2%). The adsorption capacity of MWNCT was compared with bacuri shell activated carbon.

The activated carbon adsorbent was prepared using the following steps: 75 g powdered bacuri shell, 50 g inorganic components (30% red mud + 20% lime + 10% KOH + 20% $KAl(SO_4)_2$ + 20% $Al(OH)_3$), and 35 mL water were mixed properly to yield a homogeneous paste with a ratio of 1.5 (BC-1.5). The homogenous paste was transferred into a mold disc (diameter, 0.06 m; thickness, 0.007 m). The resulting material was wet-shaped, dried at room temperature overnight and thereafter dried in an oven at 393 K for 10 h. Subsequently, eight dried discs were placed in a coiled stainless reactor that allows a symmetric gas distribution and ensures a homogeneous gas rate

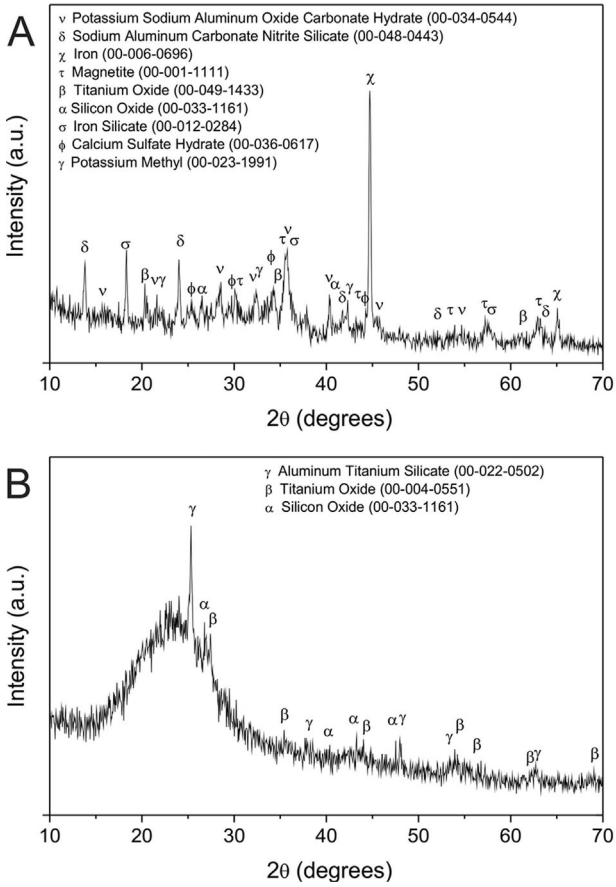

Figure 1. XRD patterns of (A) BC-1.5; (B) ABC-1.5.

(argon at 200 mL/min) [29]. This process prevented formation of unhomogenised carbonised materials. The reactor inside the tubular furnace was later heated at 293 K min^{-1} until 1073 K, and left at 1073 K for 30 min. Afterwards, the pyrolyzed carbon material was cooled down to room temperature under argon (30 mL/min). Thereafter, the carbonized discs were milled, sieved (particle size ≤106 μm) and stored until use. This carbon composite adsorbent was labeled BC-1.5. Similarly, other carbon materials with the ratio of 1.0 (BC-1.0) and 2.0 (BC-2.0) were prepared. A carbonized material that served as a reference (BC-0, without inorganic compounds) was also prepared.

To complete the chemical activation process of the carbon adsorbent, 10 g BC-1.5 were given into a 500 mL boiling flask and 200 mL of 6 M HCl were added. The mixture was stirred on a magnetic stirrer and refluxed at 343 K for 12 h. The slurry was cooled down and filtered under vacuum using a 0.45 μm membrane in a polycarbonate Sartorius system. The solid material was properly washed with water (pH 2), dried in an oven at 383 K for 5 h, milled to particle sizes ≤106 μm and stored until use. The acidification process leached the inorganic components from the carbon adsorbent. The bacuri activated carbon that was obtained after acidification was labeled as ABC-1.5.

2.3 Characterization of BC-1.5 and ABC-1.5

The textural properties, thermal stability and morphology of ABC-1.5 were compared with the precursor BC-1.5. The comparison

revealed the improvement in the characteristics of ABC-1.5 due to acidification.

Surface morphologies of BC-1.5 and ABC-1.5 were investigated using scanning electron microscopy (SEM) (JEOL microscope, model JSM 6060, Tokyo, Japan) [30].

BC-1.5 and ABC-1.5 were also characterized using Fourier transform IR spectroscopy (FTIR) (Shimadzu Spectrometer, IR Prestige 21, Kyoto, Japan). The adsorbents and KBr were dried in an oven at 393 K for 8 h, stored in capped flasks and then kept in a desiccator before FTIR analysis. The spectra were obtained with a resolution of 4 cm^{-1} with 100 cumulative scans [30].

The N_2 adsorption–desorption isotherms of BC-1.5 and ABC-1.5 were performed at liquid nitrogen boiling point (77 K) using a surface analyzer (Micrometrics Instrument, TriStar II 3020). The adsorbents were degassed at 453 K for 12 h under vacuum before analysis. The specific surface areas and pore size distributions of the adsorbents were evaluated using Brunauer-Emmett-Teller (BET) analysis, multipoint technique, and Barret-Joyner-Halenda analysis, respectively [34].

Thermogravimetric (TGA) and derivative thermogravimetric (DTG) curves of BC-1.5 and ABC-1.5 were obtained on a TA Instruments model SDT Q600 (New Castle, USA) with a heating rate of 283 K min^{-1} at 100 mL min^{-1} of synthetic air flow (White Martins, Canoas, RS, Brazil). The temperature of the analysis varied from 293 to 1273 K (acquisition time of 1 point/5 s) using an amount of 10–15 mg of solid per analysis [29].

X-ray diffraction (XRD) (Philips X'pert MPD diffractometer, Netherlands) was determined at 40 kV and 40 mA with Cu K_α radiation ($\lambda = 1.5406$ Å) of BC-1.5 and ABC-1.5. Measurements were done with a scanning step width of 0.05°/s over the 2θ range of 10–70° [30].

The determination of the point of zero charge (pH_{pzc}) is briefly described below. 20 mL 0.050 mol L^{-1} NaCl solution was added to 50 mL Falcon tubes containing 50 mg of the adsorbent and capped instantly. The pH values of the solutions were adjusted from 1 to 10 with 0.1 M HCl and/or 0.1 M NaOH. The suspensions were agitated and equilibrated in a thermostatic shaker at 298 K for 48 h. The suspensions were centrifuged at 10 000 rpm for 10 min. The pH_i of the solutions without adsorbent and pH_f of the supernatant after contact with the adsorbents were determined and recorded. The value of pHpzc describes the condition when the electrical net particle charge becomes zero [24].

2.4 Batch adsorption studies

The adsorption capacity of ABC-1.5 was compared with MWCNT. 20 mL of BB-FCF solution (150–1800 mg L^{-1}) was added to 50 mg adsorbent in 50 mL Falcon tubes at different pH values (2 to 10). The mixtures were agitated between 5 and 480 min inside a thermostatic shaker (Oxylab, São Leopoldo, Brazil) between 298 and 323 K. The mixtures were centrifuged at 10 000 rpm for 5 min (UniCen M, Herolab centrifuge, Stuttgart, Germany) to separate the adsorbents from the dye solutions. Aliquots of the supernatant were diluted with deionised water (pH 2) before spectroscopic measurement when necessary.

The residual BB-FCF in the solution after adsorption was quantified at a maximum wavelength of 629 nm using UV/Vis spectrophotometry (T90 + UV-Vis spectrophotometer, PG Instruments, London, UK).

The amount of BB-FCF removed by the activated carbon and the percentage of removal were calculated Eqs. (1) and (2), respectively

$$q = \frac{(C_o - C_f)}{m} V \tag{1}$$

$$\%\text{Removal} = 100 \times \frac{(C_o - C_f)}{C_o} \tag{2}$$

where q is the amount of dye adsorbed by the adsorbent in mg g^{-1}, C_o is the initial dye concentration (mg L^{-1}), C_f is the dye concentration (mg L^{-1}) after the batch adsorption process, m (g) is the mass of adsorbent, and V is the volume of the dye solution (L).

Desorption experiments were investigated using the following procedure: the dye-laden adsorbents were washed with water to remove any unadsorbed BB-FCF. Subsequently, 20 mL aqueous solutions (water; 0.05–0.5 mol L^{-1} NaOH; 10–50% acetone + 90–50% water; 10–50% acetone + 90–50% 0.05 M NaOH) was added to the dye-loaded adsorbents and agitated for 1 h. The desorbed BB-FCF was separated from the adsorbent and quantified as described above. The recycled adsorbent was again tested for three new adsorption–desorption cycles.

2.5 Quality assurance and statistical evaluation of models

All experiments were carried out in triplicate to ensure reproducibility, reliability, and accuracy of the experimental data. The relative standard deviations of all measurements were <5% [21]. Blanks were run in parallel and corrected when necessary [22].

The BB-FCF solutions were stored in glass bottles, which were cleaned by soaking in 1.4 mol L^{-1} HNO_3 for 24 h [23], rinsing with deionized water, drying, and storing them in a suitable cabinet.

Standard dye solutions (10–220 mg L^{-1}) were used for calibration in parallel with a blank. The linear analytical calibration curve was performed on the UV-Win software of the T90+ PG Instruments spectrophotometer. All analytical measurements were carried out in triplicate, and the precisions of the standards were < 3% ($n = 3$). The detection limit of BB-FCF was 0.14 mg L^{-1} with a signal/noise ratio of 3 [24]. A total of 80 mg L^{-1} of the BB-FCF standard solution was used as a quality control after every five measurements to ensure accuracy [25].

Nonlinear methods with successive interactions calculated by the Levenberg–Marquardt method were used to fit the kinetic and equilibrium data. Interactions were also evaluated using the Simplex method, based on the nonlinear fitting facilities of the Microcal Origin 9.0 software. A determination coefficient (R^2), an adjusted determination coefficient (R^2_{adj}) and the standard deviation (SD) were used to evaluate the suitability of the models [17, 18]. Standard deviation is a measure of the differences between the theoretical and experimental amounts of dye adsorbed. The R^2, R^2_{adj}, and SD are represented in Eqs. (3) to (5), respectively.

$$R^2 = \left(\frac{\sum_i^n \left(q_{i,exp} - \bar{q}_{i,exp}\right)^2 - \sum_i^n \left(q_{i,exp} - q_{i,model}\right)^2}{\sum_i^n \left(q_{i,exp} - \bar{q}_{i,exp}\right)^2} \right) \tag{3}$$

$$R^2_{adj} = 1 - (1 - R^2)\left(\frac{n-1}{n-p-1}\right) \tag{4}$$

$$SD = \sqrt{\left(\frac{1}{n-p}\right)\sum_{i}^{n}\left(q_{i,exp} - q_{i,model}\right)^2} \quad (5)$$

where $q_{i,model}$ represents the individual theoretical q value predicted by the model; $q_{i,exp}$ represents the individual experimental q value; $\bar{q}_{exp}$ is the average of the experimental q values; n represents the number of experiments; p represents the number of parameters in the fitting model [17, 18].

2.6 Kinetic models

Pseudo-first order [36], pseudo second-order [36], general order kinetic [37], and intra-particle diffusion [37] models were used to analyze the kinetic data. The respective mathematical expressions of these models are presented in Eqs. (6) to (9).

$$q_t = q_e(1 - \exp(-k_1 t)) \quad (6)$$

$$q_t = q_e - \frac{q_e}{(k_2(q_e)t + 1)} \quad (7)$$

$$q_t = q_e - \frac{q_e}{(k_N(q_e)^{n-1}t(n-1) + 1)^{1/1-n}} \quad (8)$$

$$q_t = k_{id}\sqrt{t} + C \quad (9)$$

2.7 Equilibrium models

Langmuir, Freundlich, and Liu models are represented in Eqs. (10) to (12), respectively [30]. These models were used for the analysis of equilibrium data in this work.

$$q_e = \frac{Q_{max}K_L C_e}{1 + K_L C_e} \quad (10)$$

$$q_e = K_F C_e^{1/n_F} \quad (11)$$

$$q_e = \frac{Q_{max}(K_g C_e)^{n_L}}{1 + (K_g C_e)^{n_L}} \quad (12)$$

2.8 Simulated soft-drink effluents

Two simulated effluents, similar to the industrial soft-drink effluents, were prepared with pH 3. Three dyes that are commonly used as food colorants, together with other chemicals that are regularly used in the production of soft-drinks, were included in the synthetic effluents. The compositions and concentrations of the effluents are shown in Table 1 [38–40].

Table 1. Chemical composition of the simulated soft-drink effluents [38–40]

	Concentration ($mg\,L^{-1}$)	
Dyes	Effluent A	Effluent B
Brilliant Blue–FCF ($\lambda = 629$ nm)	70	140
Tartrazine yellow ($\lambda = 420$ nm)	20	40
Red 40 ($\lambda = 533$ nm)	20	40
Acidulates and preservatives		
EDTA	10	15
Sodium sulphite	20	30
Sodium bicarbonate	100	100
Benzoic acid	70	100
Tartaric acid	100	150
Phosphoric acid	100	150
Ascorbic acid	200	300
Citric acid	200	300
Sucrose	5000	5000
pH[a)]	3	3

[a)] pH of most soft drinks.

3 Results and discussion

3.1 Preparation of bacuri shell activated carbon and preliminary experiments of adsorption

Lime ($CaCO_3 + Ca(OH)_2 + CaO$) was used as one of the inorganic components in the preparation of bacuri carbon adsorbents to avoid impregnation of the carbonaceous material with aqueous solution [19, 28]. Lime in the presence of water forms a paste that holds together all solid constituents [17, 30].

In this study, the inorganic components used as activating agents include lime, red mud, KOH, $Al(NO_3)_3$, and $KAl(SO_4)_2$ [19, 29, 30]. Red mud has been used as adsorbent for dye removal [12, 41] and also in the formulation of carbon composite materials [29]. Similarly, the use of KOH [19] and aluminium salts [42] as activating agents for the preparation of activated carbons has been reported. All inorganics contribute to catalyze the oxidation reactions of the organic matrix and they also helps on sintering of clay minerals to form high porosity materials [17, 29].

The dried discs were placed inside a stainless reactor and pyrolyzed at 1073 K under inert conditions. The stainless reactor was placed vertically for proper delivery of the tar (by gravity) into the recipient vessel [17, 30]. This arrangement prevented the tar from blocking the pores of the carbon adsorbent [30]. The bacuri carbon adsorbents produced after this step were labeled as BC-1.0, BC-1.5, and BC-2.0 with ratios of 1.0, 1.5, and 2.0, respectively. BC-0, a control adsorbent, without the presence of inorganics.

A total of 6 M HCl was used to leach the inorganics from the carbonized adsorbents (BC-1.0, BC-1.5, and BC-2.0). The inorganic components present on the carbon material have the tendency to hydrolyze the organic precursor (bacuri shell) during the pyrolysis stage, and subsequently enhance the release of some organic components that could weaken the expanding molecules of the carbon materials during the pyrolysis [28]. However, the inorganic components of the carbon material also occupy a volume in the carbonaceous matrix preventing the shrinkage of the particles during the pyrolysis [28]. After the pyrolysis, the carbonaceous material was treated with HCl, leaching out inorganic components and increasing the porosity and surface area of the activated carbon obtained [17, 29, 30].

BC-0, BC-1.0, BC-1.5, BC-2.0, ABC-0, ABC-1.0, ABC-1.5, and ABC-2.0 were utilized for adsorption studies of 400 $mg\,L^{-1}$ BB-FCF from aqueous solutions with an agitation time of 1 h. The percentages of removal are provided in Supporting Information Fig. S2. The percentages of removal of BB-FCF using BC-0 and ABC-0 are quite low. The carbonization of the powdered bacuri shells produced an enormous amount of tar-oil that blocked the pores of the synthesized carbon material [17, 29, 30]. It was necessary to leach

the inorganic constituents from the carbonaceous material to increase the percentage removal of BB-FCF because all ABC adsorbents exhibited higher sorption capacities compared to the corresponding BC adsorbents.

ABC-1.5 was used for all experiments because it showed the highest removal efficiency for BB-FCF during the preliminary experiments. The adsorptive capacity of MWCNT was compared with ABC-1.5.

3.2 Characterization of BC-1.5 and ABC-1.5

The precursor, BC-1.5, was used to investigate the effects of chemical activation on the bacuri shell activated carbon.

ABC-1.5 and BC-1.5 were chosen for characterization as ABC-1.5 showed the highest removal capacity for BB-FCF from aqueous solutions.

The textural properties obtained from N_2 adsorption–desorption curves for BC-1.5 and ABC-1.5 are as follows: superficial area (S_{BET}), 18.5 and 530.2 $m^2\ g^{-1}$; average pore diameter (Barret-Joyner-Halenda), 11.9 and 7.32 nm; and total pore volume, 0.057 and 0.696 $cm^3\ g^{-1}$. It could be observed that the pore size diameter distribution of ABC-1.5 is higher compared to BC-1.5. The maximum peak at 3.68 nm in BC-1.5 was shifted to two maximum peaks at 3.91 and 8.70 nm in ABC-1.5. However, considering just the value of the average pore diameter, BC-1.5 possesses a higher pore diameter than ABC-1.5. Similarly, it was noticed that BC-1.5 and ABC-1.5 show mesopores (pores with a diameter of 2–50 nm) to adsorb BB-FCF from aqueous solutions [1], and a minor fraction of macropores (pores with a diameter >50 nm). The textural properties of BC-1.5 and ABC-1.5 revealed that acidification of BC-1.5 yielded ABC-1.5 with better textural characteristics for dye adsorption [30]. Acidification of BC-1.5 increased the surface area and total pore volume of ABC-1.5 by 28.7-fold and 12.2-fold, respectively.

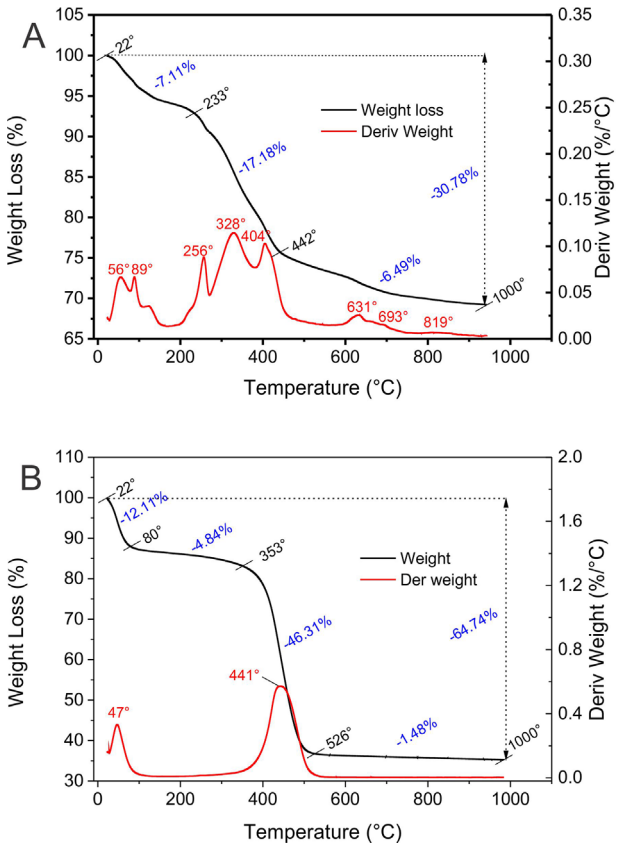

Figure 2. TGA and DTG curves of (A) BC-1.5; (B) ABC-1.5.

The XRD patterns of BC-1.5 and ABC-1.5 are presented in Fig. 1A and B, respectively. The peaks of BC-1.5 (Fig. 1A) are assigned to $KNa_{1.2}Al_2O_2(CO_3)_2 \cdot (H_2O)_{2.16}$, $Na_8[AlSiO_4]_6(NO_2)(CO_3)_{0.5}$, Fe, Fe_3O_4, TiO_2, SiO_2, Fe_2SiO_4, $CaSO_4 \cdot (H_2O)_{0.67}$, and CH_3K. The XRD patterns of BC-1.5 matched with the inorganic components in red mud [30] and activating agents used to prepare BC-1.5. On the other hand, the XRD patterns of ABC-1.5 (Fig. 1B) indicated an amorphous material with a wide band between 14 and 35° that corresponds to amorphous carbon, and small amounts of aluminium titanium silicate ($Al_4Ti_2SiO_{12}$), titanium oxide (TiO_2) and silicon oxide (SiO_2), shown in Fig. 3B, that remained in ABC-1.5 even after the leaching process. The peaks of ABC-1.5 are characterized by smaller intensities unlike the peaks of BC-1.5. This observation indicated that the acidification process removed the inorganic components from the bacuri carbon precursor. Similarly, the textural features discussed above are in agreement with the XRD data. In summary, a carbon material (ABC-1.5) characterized with higher pores volumes, higher superficial area and lower crystallinity was obtained when the inorganic components were leached from the precursor.

Figure 2 shows the thermogravimetric profiles of BC-1.5 and ABC-1.5. There peaks in the DTG curve of BC-1.5 reflect: the elimination of water at 56 and 89°C; 256°C, the decomposition of the organic contents of BC-1.5 at 328 and 404°C; a tiny peak at 631°C; and a shoulder at 693°C that corresponds to the decomposition of the carbon structure. The TG curves can be categorized into three parts. The first part from 22.0 to 233°C showing a mass loss of 7.11% assigned to the loss of water. The second part from 233 to 442°C reflecting a mass loss of 17.18% assigned to the decomposition of the carbonaceous matrix [25]. The third part from 442 to 1000°C with a mass loss of 6.49% (skeleton decomposition) assigned to residual carbon. A residual mass of ≈69.2% was obtained from 22 to 1000°C. This mass was allocated to the inorganic components of the precursor and undecomposed carbonaceous materials.

The thermogravimetric profiles of ABC-1.5 are different to BC-1.5 (Fig. 2). For ABC-1.5, the residual mass is 35.26% (from 22 to 1000°C), which means that the acidification leached most of the inorganic components from the precursor. This observation is in agreement with the XRD data discussed above. Two decomposition parts (47 and 441°C) were observed in the DTG curves for ABC-1.5. There are four regions in the TG curves of ABC-1.5 using DTG. From 22 to 80°C with a mass loss of 12.11% assigned to water. The humidity of ABC-1.5 was higher compared with BC-1.5 due to $HCl_{(aq)}$ treatment. Furthermore, from 80 to 353°C showing a mass loss of 4.84% assigned to water captured in the carbonaceous matrix. A mass loss of 46.31% was observed for 353 to 526°C, attributed to the decomposition of the carbon skeleton. Finally, an additional mass loss of 1.48% was observed for 526 to 1000°C.

The SEM images of ABC-1.5 and its precursor are presented in Fig. 3. The fibrous property of BC-1.5, a feature of lignin cellulosic materials [2, 4, 24], was lost during pyrolysis and the roughness of the carbon materials is visible (Fig. 3). The main difference between the SEM images of BC-1.5 and ABC-1.5 is that the granules of BC-1.5 are larger than those of ABC-1.5. This observation could be attributed to the acidic treatment of BC-1.5 that leached the majority of the inorganic components, leaving the granules with a spherical shape. Additionally, the surface of ABC-1.5 is rougher compared to BC-1.5.

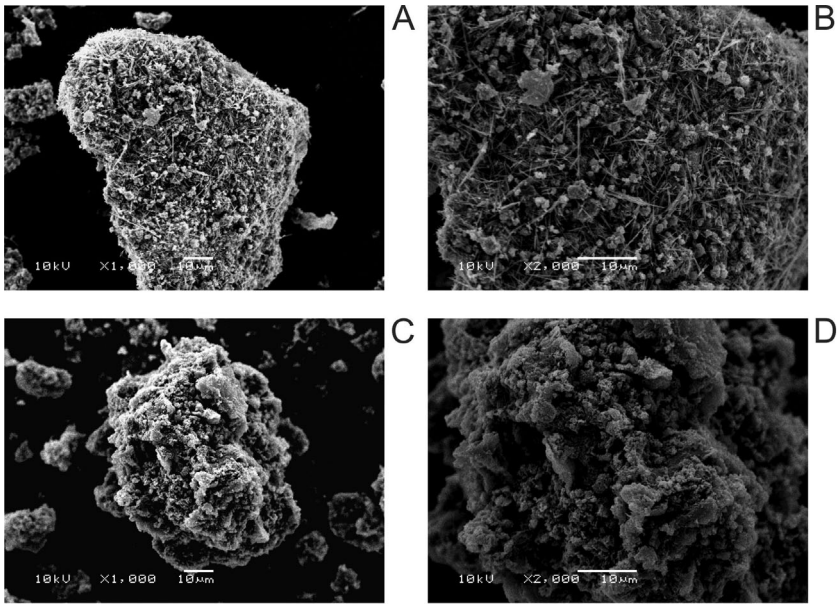

Figure 3. SEM images of (A) BC-1.5 magnification 1000×; (B) BC-1.5 magnification 2000×; (C) ABC-1.5 magnification 1000×; (D) ABC-1.5 magnification 2000×.

Fourier transform IR (FTIR) spectroscopy was used to identify the functional groups possessed by BC-1.5 and ABC-1.5, and the groups that were responsible for the adsorption of BB-FCF. The FTIR spectra of the adsorbents were recorded between 4000 and 400 cm^{-1} (Table 2). Table 2 shows the band assignments of the functional groups of BC-1.5 and ABC-1.5. [18, 20–25]. The FTIR spectra of BC-1.5 and ABC-1.5 are slightly different from each other (see Supporting Information Fig. S3). ABC-1.5 shows minor vibrational bands compared to BC-1.5. The Si-O stretch of silicates is obvious in BC-1.5 at 991 cm^{-1} unlike in ABC-1.5 (at 1105 cm^{-1}). The functional groups O-H (alcohols, phenols), aromatic rings, C−O (alcohols), Si−O (silicates), and C−H (aromatics, aliphatic chains) are present in BC-1.5 and ABC-1.5 carbon materials. The FTIR data are in agreement with those of XRD discussed in Fig. 1.

3.3 pH dependence studies

The optimum pH of a dye depends on the type of the adsorbent. Therefore, the pH of the solution is one of the influential factors affecting the adsorption of a dye on an adsorbent [1, 2, 4, 6, 18, 24]. pH values in the range of 2 and 10 were investigated for the removal of BB-FCF from aqueous solutions (300 mg L^{-1}) using ABC-1.5 and MWCNT (Supporting Information Fig. S4). For adsorption of BB-FCF by ABC-1.5, the percentage of removal decreased from 99.4% (pH 2) to 28.5% (pH 10). It was noted that from pH 2 to 3, the decrease of the removal of BB-FCF by ABC-1.5 was <0.9%. Therefore, the optimum pH values ranged from 2 to 3 for ABC-1.5. The percentage of removal of BB-FCF using MWCNT decreased from 86.0% (pH 2) to 74.3% (pH 10). The difference in the behavior of both adsorbents for the adsorption of BB-FCF with respect to the pH of the dye solution is quite remarkable. It can be noted that the percentage of removal of the food dye is higher for ABC-1.5 within the pH range of 2–3. However, for pH 3.5–10, a decrease in the percentage of removal of the adsorbate is evident (see Supporting Information Fig. S4). The percentage of removal of BB-FCF using MWCNT is lower compared with ABC-1.5 at lower pH values. This observation becomes contrariwise at higher pH values.

Table 2. FTIR vibrational bands of BC-1.5 and ABC-1.5. Assignments are based on literature [18, 20–25]

Band (cm^{-1})	Assignment
BC-1.5	
3330	O−H stretch
1541	Rings mode of aromatic
1404	CH_2 bending
991	C−O stretch of alcohols or Si−O stretch of silicates
868, 665	CH out of plane bends of aromatic rings
ABC-1.5	
3300	O−H stretch
1585	Rings mode of aromatic
1105	C−O stretch of alcohols or Si−O stretch of silicates
970 800	CH out of plane bends of aromatic rings

The pH_{pzc} values of ABC-1.5 and MWCNT were responsible for the remarkable behaviors of the adsorbents with respect to the pH of the dye solutions. The pH_{pzc} values of ABC-1.5 and MWCNT are 2.31 and 6.85, respectively, as shown in Supporting Information Fig. S4. If an adsorbent shows $pH < pH_{pzc}$, the surface of the adsorbent will be positively charged [24]. The BB-FCF possesses sulphonic groups that are negatively charged in aqueous solutions even in acidic media (Supporting Information Fig. S1). Hence, adsorption of BB-FCF will take place when the surface of the adsorbent is positively charged. For ABC-1.5 and MWCNT, the electrostatic interactions occurred at pH < 2.31 and <6.85, respectively. The lower the pH of the adsorbate solution in relation to pH_{pzc}, the more positively charged the surface of the adsorbent [18, 20, 24]. For the subsequent experiments, the pH of the BB-FCF solution was fixed at pH 2 for both adsorbents. This result is also in agreement with the literature for adsorption of different anionic dyes on different adsorbents [1, 6, 17, 18, 20–26].

The final pH values of BB-FCF solutions after adsorption were determined. These values varied from 2.1 to 2.3 for ABC-1.5 and from 4.5 to 5.0 for MWCNT. The ΔpH values ($pH_{final} - pH_{initial}$) of MWCNT with a neutral solid surface (pH_{pzc} 6.85) varied from 2.5 to 3.0 but the ΔpH values of ABC-1.5 with an acidic solid surface (pH_{pzc} 2.31) varied from 0.1 to 0.3. The smaller the difference of the initial pH of the adsorbate solution and the pHpzc of the adsorbent, the lower is the variation of the pH of the adsorbate solution during the adsorption process.

Table 3. Kinetic parameters of BB-FCF adsorption onto ABC-1.5 and MWCNT. Conditions: temperature, 298 K; pH, 2; mass of adsorbent, 50 mg

	ABC-1.5		MWCNT	
	400 mg L^{-1}	600 mg L^{-1}	400 mg L^{-1}	600 mg L^{-1}
Pseudo-first-order				
k_1 (min^{-1})	0.1896	0.1888	0.1094	0.1088
q_e (mg g^{-1})	152.8	231.9	112.8	122.2
$t_{1/2}$ (min)	3.66	3.67	6.34	6.37
R^2_{adj}	0.9918	0.9930	0.9947	0.9935
SD (mg g^{-1})	3.214	4.533	2.055	2.469
Pseudo-second-order				
k_2 (g mg^{-1} min^{-1})	0.002637	0.001731	0.001731	0.001579
q_e (mg g^{-1})	157.3	238.8	117.5	127.4
$t_{1/2}$ (min)	2.41	2.42	4.92	4.97
R^2_{adj}	0.9948	0.9946	0.9882	0.9907
SD (mg g^{-1})	2.564	3.960	3.074	2.957
General order				
k_N [h^{-1} (g mg^{-1})$^{n-1}$]	0.02369	0.02171	0.02972	0.02267
q_e (mg g^{-1})	154.6	234.5	113.8	123.6
n	1.484	1.458	1.319	1.376
$t_{1/2}$ (min)	3.04	3.08	5.76	5.70
R^2_{adj}	0.9995	0.9998	0.9992	0.9995
SD (mg g^{-1})	0.8128	0.7706	0.7811	0.6964
Intra-particle diffusion				
$k_{id,2}$ (mg g^{-1} $min^{-0.5}$)[a)]	4.631	10.15	4.197	4.523

[a)] Second phase.

3.4 Kinetic studies

To elucidate the kinetic of adsorption of BB-FCF onto ABC-1.5 and MWCNT, nonlinear forms of pseudo-first order, pseudo-second order, and general order kinetic models were employed. Supporting Information Fig. S5 and Table 3 show the kinetic plots and the fitting parameters of the kinetic models, respectively. Standard deviation (SD) values were used to explain the suitability of the nonlinear kinetic models. The smaller the difference between q_{theor} and q_{exp}, the lower the value of SD [17, 18, 20–26] (Eq. (5)). It is known that the number of parameters in nonlinear equations determines the best fit of data [43]. This observation (the number of fitting parameters, p term in Eq. (5)) was taken into consideration while evaluating SD. For comparison, SD of the minimum value was used to divide SD of each model (SD ratio). A general order kinetic model has the lowest SD ratio values. The SD ratio values of the pseudo-first order kinetic model varied from 3.95 to 5.88 and from 2.63 to 3.55 for ABC-1.5 and MWCNT, respectively. The SD ratio values of the pseudo-second order model varied from 3.15 to 5.14 (ABC-1.5) and from 3.94 to 4.25 (MWCNT). The general order kinetic model best described the adsorption process of BB-FCF onto ABC-1.5 and MWCNT, because it exhibited lowest SD ratio values.

The general order kinetic model assumed that the order of the adsorption process must follow the same pattern of a chemical reaction, where the order of reaction is experimentally determined [29, 30, 34, 37] and not being predicted by a given model.

Regarding the adsorption of BB-FCF, the kinetic of ABC-1.5 was faster compared with MWCNT. The half-life ($t_{1/2}$), the time required to attain 50% of q_e (amount adsorbed at equilibrium), was obtained by interpolation of the kinetic plots. The values of $t_{1/2}$ are given in Table 3. The $t_{1/2}$ values of the general kinetic model only have physical meaning because the model gave the best fit of the experimental data. The $t_{1/2}$ values of the adsorption of BB-FCF onto ABC-1.5 are 87.3% lower compared to MWCNT.

The intra-particle diffusion model [37] was used to investigate the influence of mass transfer resistance on the binding of BB-FCF onto ABC-1.5 and MWCNT (Table 3 and Supplementary Fig. S6). The intra-particle diffusion constant, k_{id} (mg g^{-1} $min^{-0.5}$), can be obtained from the slope of the plot of q_t vs. $\sqrt{t}$ (Supporting Information Fig. S6). Adsorption often requires more than one adsorption step [29, 30]. This observation explained the reason why the plots of q_t vs. $\sqrt{t}$ for the adsorption of BB-FCF onto ABC-1.5 and MWCNT exhibited three linear phases. There are three phases of the adsorption process for ABC-1.5 and MWCNT, where each one is allocated to each linear phase of the plots (Supporting Information Fig. S6). The first linear phase is the fastest. This phase describes the process by which dye molecules diffuse into the surface of the adsorbents [29, 30]. The second phase is a delayed process, which describes intra-particle diffusion [29, 30]. The third phase describes diffusion through smaller pores. This phase is obtained after equilibrium [29, 30]. Perusing through the first data point of the third phase, the minimum equilibrium contact time for ABC-1.5 to adsorb BB-FCF is 45 min, but the equilibrium time is 90 min for MWCNT. The difference between the equilibrium times is consistent with the $t_{1/2}$ values and initial sorption rates presented in Table 3.

The contact times of 75 and 120 min were used for adsorption experiments of BB-FCF on ABC-1.5 and MWCNT, respectively. To ensure that equilibrium is attained between the dye molecules (even at higher concentrations) and the adsorbents, the contact time was raised by 30 min [29, 30].

3.5 Equilibrium studies

The adsorption equilibrium models give the informative parameters that explain surface properties, adsorption mechanism and interaction between the adsorbent and adsorbate. In this work, Langmuir, Freundlich, and Liu [30] isotherm models were utilized for the analysis of isothermal data.

The isothermal experiments were carried out at 298–323 K using the optimum experimental conditions stated earlier (Table 4 and Supporting Information Fig. S7). Supporting Information Fig. S7 shows the adsorption isotherms for BB-FCF onto ABC-1.5 and

CLEAN Soil Air Water

Table 4. Isotherm parameters of BB-FCF adsorption using ABC-1.5 and MWCNT. Conditions: pH, 2; adsorbent mass, 50 mg; contact time, 75 min for ABC-1.5, and 120 min for MWCNT

	298 K	303 K	308 K	313 K	318 K	323 K
ABC-1.5						
Langmuir						
Q_{max} (mg g^{-1})	427.4	435.6	434.0	484.5	459.5	495.5
K_L (L mg^{-1})	0.2499	0.2737	0.3501	0.2478	0.3718	0.3257
R^2_{adj}	0.9955	0.9760	0.9601	0.9712	0.9475	0.9483
SD (mg g^{-1})	9.082	21.06	26.24	24.67	30.64	32.82
Freundlich						
K_F (mg g^{-1} (mg L^{-1})$^{-1/nF}$)	198.7	200.8	211.3	225.0	238.0	250.0
n_F	7.071	6.970	7.393	7.048	8.058	7.784
R^2_{adj}	0.9081	0.9524	0.9753	0.9683	0.9887	0.9883
SD (mg g^{-1})	40.88	29.71	20.65	25.89	14.20	15.63
Liu						
Q_{max} (mg g^{-1})	440.2	482.1	518.4	557.0	600.3	647.9
K_g (L mg^{-1})	0.2448	0.2155	0.1889	0.1669	0.1451	0.1271
n_L	0.8033	0.5823	0.4605	0.5312	0.3594	0.3698
R^2_{adj}	0.9993	0.9999	0.9999	0.9999	0.9999	0.9999
SD (mg g^{-1})	3.532	0.2472	0.4220	0.4289	0.3333	0.4682
MWCNT						
Langmuir						
Q_{max} (mg g^{-1})	124.5	130.9	136.6	142.8	149.6	149.6
K_L (L mg^{-1})	0.4732	0.4520	0.5579	0.7037	1.047	1.047
R^2_{adj}	0.9453	0.9350	0.9310	0.9376	0.9359	0.9359
SD (mg g^{-1})	8.400	9.533	10.17	9.944	10.44	10.44
Freundlich						
K_F (mg g^{-1} (mg L^{-1})$^{-1/nF}$)	68.26	74.34	80.93	89.14	98.89	98.89
n_F	9.667	10.22	10.96	12.12	13.56	13.56
R^2_{adj}	0.9863	0.9915	0.9948	0.9970	0.9981	0.9981
SD (mg g^{-1})	4.209	3.438	2.786	2.184	1.800	1.800
Liu						
Q_{max} (mg g^{-1})	156.1	172.1	190.7	209.6	231.5	231.5
K_g (L mg^{-1})	0.1932	0.1743	0.1500	0.1352	0.1199	0.1199
n_L	0.3406	0.2962	0.2491	0.2106	0.1774	0.1774
R^2_{adj}	0.9999	0.9999	0.9999	0.9999	0.9999	0.9999
SD (mg g^{-1})	0.3134	0.2600	0.3557	0.4262	0.5160	0.5160

MWCNT at 323 K. Considering the SD values (Table 4) between 298 and 323 K the Liu model best described adsorption equilibrium data of BB-FCF onto ABC-1.5 and MWCNT. The values of the SD ratio of the Langmuir model ranged from 2.57 to 91.93 (ABC-1.5) and from 20.23 to 36.67 (MWCNT) while those of the Freundlich model ranged from 11.57 to 120.2 (ABC-1.5) and from 3.49 to 13.43 (MWCNT).

The Q_{max} values, maximum amounts of BB-FCF adsorbed at 323 K, were 647.9 (ABC-1.5) and 231.5 mg g^{-1} (MWCNT). The values of Q_{max} of ABC-1.5 at all experimental temperatures were ca. 2.73 times higher than those of MWCNT. According to the literature, MWCNT is one of the best adsorbents for dye removal from aqueous solutions [14, 23, 33–35]. However, comparing the kinetic and equilibrium data of BB-FCF onto ABC-1.5 and MWCNT, ABC-1.5 shows higher adsorption capacities and faster kinetic rates than MWCNT. The adsorption characteristic of a low-priced ABC-1.5 would allow its large scale applications for industrial wastewater treatment compared to the expensive carbon nanotubes.

3.6 Thermodynamics studies

Equations (13) to (15) were used to evaluate the Gibb's free energy change (ΔG°, kJ mol^{-1}), enthalpy change (ΔH°, kJ mol^{-1}), and entropy change (ΔS°, J mol^{-1} K^{-1}), respectively.

$$\Delta G^\circ = \Delta H^\circ - T\Delta S^\circ \quad (13)$$

$$\Delta G^\circ = -RT\ln K \quad (14)$$

Equation (15) was derived from Eqs. (13) and (14).

$$\ln K = \frac{\Delta S^\circ}{R} - \frac{\Delta H^\circ}{R}\frac{1}{T} \quad (15)$$

where R is the universal gas constant (8.314 J K^{-1} mol^{-1}); T is the absolute temperature (K); K represents the adsorption constants of the isotherm fits (K_g – Liu equilibrium constant) obtained from the isotherm plots. Various adsorption equilibrium constants (K) can be obtained from different isotherm models [16, 18, 21–26, 29, 30, 34–37, 44, 45]. Similarly, thermodynamic parameters can be evaluated from Liu equilibrium constant (K_g) as reported earlier [18, 21, 22, 24, 29, 30, 34, 37].

Calculations from the slope and intercept of the linear plot of ln$K$ versus T^{-1} results in ΔH° and ΔS° values, respectively. The R^2_{adj} values of the plots are >0.99, an indication that the values of ΔH° and ΔS° are reliable. Table 5 shows the thermodynamic parameters. It can be noted that an increase in the temperature led to a decrease in K_g, which means that the process of adsorption is exothermic [18]. Although the Q_{max} value increased (see Table 4) as the temperature increased, the process of adsorption was exothermic. Several authors calculated K_D (distribution constant), and the value of this constant really increases as the Q_{max} value increases [46]. However, if K_D is calculated for all points of the isotherm, it is impossible to find a unique value for this

Table 5. Thermodynamic parameters of BB-FCF adsorption onto ABC-1.5 and MWCNT. Conditions: mass of adsorbent, 50 mg; pH, 2; contact time, 75 min for ABC-1.5, and 120 min for MWCNT

	Temperature (K)					
	298	303	308	313	318	323
ABC-1.5						
K_g ($L\,mol^{-1}$)	$1.941.10^5$	$1.709.10^5$	$1.498.10^5$	$1.323.10^5$	$1.150.10^5$	$1.008.10^5$
$\triangle G$ ($kJ\,mol^{-1}$)	−30.17	−30.35	−30.52	−30.69	−30.81	−30.94
$\triangle H^\circ$ ($kJ\,mol^{-1}$)	−20.97	–	–	–	–	–
$\triangle S^\circ$ ($J\,K^{-1}\,mol^{-1}$)	30.94	–	–	–	–	–
R^2_{adj}	0.9983					
MWCNT						
K_g ($L\,mol^{-1}$)	$6.048.10^4$	$5.455.10^4$	$4.696.10^4$	$4.232.10^4$	$3.753.10^4$	$3.318.10^4$
$\triangle G$ ($kJ\,mol^{-1}$)	−27.28	−27.48	−27.55	−27.72	−27.85	−27.95
$\triangle H^\circ$ ($kJ\,mol^{-1}$)	−19.33	–	–	–	–	–
$\triangle S^\circ$ ($J\,K^{-1}\,mol^{-1}$)	26.77	–	–	–	–	–
R^2_{adj}	0.9974					

constant, and it is necessary to make extrapolation to infinite dilution in order to evaluate the value of K_D. The extrapolated K_D value is applied to Eq. (15) to compute the thermodynamic parameters. However, a good linear relationship for K_D versus $1/T$ could not be obtained. Therefore, in the thermodynamic calculations, the Liu equilibrium constant [18, 21, 22, 24, 29, 30, 34, 37] with $R^2_{adj} > 0.99$ was used.

The magnitude of enthalpy can be used to classify the interaction between adsorbate and adsorbent as either chemical or physical adsorption. The physical adsorption is $<40\,kJ\,mol^{-1}$ [47]. The values of enthalpy of adsorption of BB-FCF using ABC-1.5 and MWCNT correspond to physical adsorption [47]. The values of enthalpy change (ΔH°) are negative, indicating that the interaction between BB-FCF and adsorbents is an exothermic process. The adsorption of BB-FCF onto ABC-1.5 as well as MWCNT is a spontaneous and a favourable process because the values of ΔG° are negative. The positive values of ΔS° indicate an increase in the randomness at the solid/liquid interface. The dye dissolved in water presents coordinated water molecules, which are displaced to the bulk solution when the dye is adsorbed in the solid phase. Therefore the enthropy of the system is increased [48, 49].

3.7 Desorption studies and mechanism of adsorption

Desorption experiments are usually carried out to determine the regeneration efficiency and reusability potential of adsorbents. Therefore, desorption experiments were carried out to regenerate ABC-1.5 and MWCNT. Water, NaOH (0.050–0.50 mol L^{-1}), acetone (10–50%) + water (90–50%), acetone (10–50%) + 0.05 mol L^{-1} NaOH (90–50%) were used as eluents to regenerate the adsorbents (Table 6). Desorption was not possible using water alone, because water could only desorb 1.4% BB-FCF. Similar, NaOH solutions could not impressively desorb BB-FCF (<15.2%) from ABC-1.5 and MWCNT. The mixture of acetone (10–50%) + water (90–50%) presented a reasonable desorption capability, 34.18–78.42% BB-FCF for ABC-1.5 and 39.36–77.83% for MWCNT. The mixture of 50% acetone and 50% 0.05 mol L^{-1} NaOH was an excellent eluent; the mixture desorbed up to 99.85 and 99.36% of BB-FCF from ABC-1.5 and MWCNT, respectively. These results were obtained for the first cycle of adsorption–desorption.

The results of desorption studies were supported by the data on pH studies and the magnitude of enthalpy changes. BB-FCF is bonded electrostatically in ABC-1.5 and MWCNT at pH 2. By addition of NaOH solution, the interaction between the adsorbate and adsorbents was perturbed. There are also other interactions, such as London forces, van der Waals interactions between the adsorbents and the aromatic groups of the dye as reported earlier [22, 24]. Acetone was added to disrupt the existing interactions, which exceptionally enhanced the elution efficiency. The regenerated adsorbents (ABC-1.5 and MWCNT) using the mixture of 50% acetone and 50% 0.05 mol L^{-1} NaOH were reused for the adsorption of the BB-FCF, which attained an adsorption efficiency of approximately 95.85 and 95.36% in the second adsorption–desorption cycle, 91.14 and 90.27% in the third and 88.38 and 87.63% in the fourth cycle for ABC-1.5 and MWCNT, respectively. It could be shown that ABC-1.5 can be easily regenerated, therefore, its usage for dye removal from solutions is practically economical.

Figure 4 shows the proposed mechanism of the adsorption–desorption of BB-FCF onto ABC-1.5. In the first step of the

Table 6. Desorption of dye-loaded ABC-1.5 and MWCNT. Conditions: initial BB-FCF concentration, 200 mg L^{-1}; mass of adsorbent, 50 mg; pH 2; time of contact for adsorption, 120 min; time of contact between the eluent solutions and dye-laden adsorbents during desorption stage, 60 min

	% Recovery	
Composition of eluent	ABC-1.5	MWCNT
Water	1.05	1.36
0.05 M NaOH	15.12	7.56
0.1 M NaOH	14.61	7.85
0.2 M NaOH	13.52	8.04
0.3 M NaOH	14.52	7.56
0.4 M NaOH	15.06	7.57
0.5 M NaOH	14.56	8.65
10% Acetone + 90% water	34.18	39.36
20% Acetone + 80% water	47.09	52.36
30% Acetone + 70% water	59.28	56.32
40% Acetone + 60% water	75.26	74.36
50% Acetone + 50% water	78.42	77.83
10% Acetone + 90% 0.05 M NaOH	58.95	45.25
20% Acetone + 80% 0.05 M NaOH	78.36	52.57
30% Acetone + 70% 0.05 M NaOH	95.25	77.02
40% Acetone + 60% 0.05 M NaOH	98.25	96.55
50% Acetone + 50% 0.05 M NaOH	99.85	98.36

CLEAN Soil Air Water

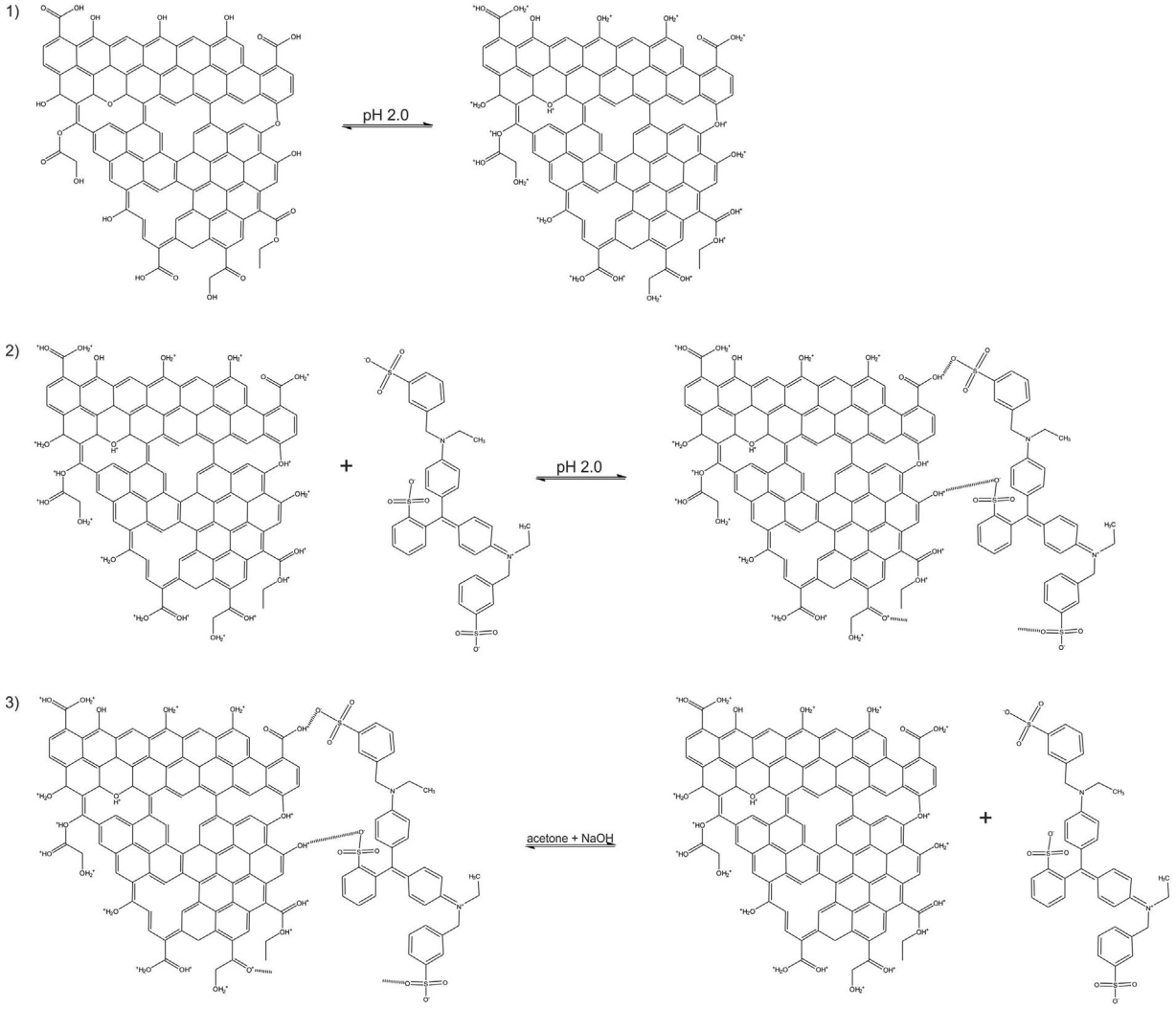

Figure 4. Mechanism of adsorption–desorption of BB-FCF using ABC-1.5.

mechanism, the fastest step, ABC-1.5 was submerged in aqueous solution, pH 2, to protonate OH, C=O, C−O−C functional groups of the adsorbent (Supporting Information Fig. S3). In the second step at pH 2, the electrostatic attraction of the negatively charged dye by the positively charged adsorbents occurred. This step is proposed to be the rate-determining step. The magnitude of the enthalpy of the adsorption is in agreement with the existing electrostatic attraction between the BB-FCF (negatively charged) and the adsorbent (positive superficial charge, if $pH < pH_{pzc}$). The third step is the desorption of BB-FCF from the adsorbents using a mixture of acetone and NaOH solution.

3.8 Simulated soft-drink effluents

To test the potentiality of ABC-1.5 and MWCNT for the treatment of industrial effluents, two simulated soft-drink effluents were used (Table 1). The spectra of the simulated effluents before and after the treatment with the adsorbents were recorded between 300 and 800 nm using UV–Vis spectrophotometry (Fig. 5). The percentage of the mixture of dyes removed from the effluents is a function of the areas under the absorption bands. In the treatment of simulated soft-drink effluents, ABC-1.5 was found to be more efficient and effective than MWCNT. The percentage of removal for ABC-1.5 was 95.88% (effluent A) and 90.49% (effluent B). The percentage of removal was 79.84% (effluent A) and 68.03% (effluent B) for MWCNT. These data showed that the usage of ABC-1.5 for the treatment of simulated dye effluents is satisfactory compared to other adsorbents that have been previously used [18, 21–24, 26, 29, 30, 34, 37]. However, MWCNT did not show an appreciable performance for the treatment of simulated soft-drink effluents.

4 Conclusion

Powdered bacuri shell and inorganic components (red mud + lime + KOH + $KAl(SO_4)_2$ + $Al(OH)_3$)) were mixed at room temperature. The mixture was heated at 1073 K under inert conditions. BC-1.0, BC-1.5, and BC-2.0 (carbon materials) were treated with 6 M HCl and refluxed for 12 h to obtain ABC-1.0, ABC-1.5, and ABC-2.0, respectively. The acidification process leached the inorganics from the carbonaceous matrix, which was confirmed by BET surface area, XRD, TGA, SEM, and FTIR spectroscopy. The adsorption capacity of ABC-1.5 was compared with that of MWCNT. At optimum pH 2, equilibrium

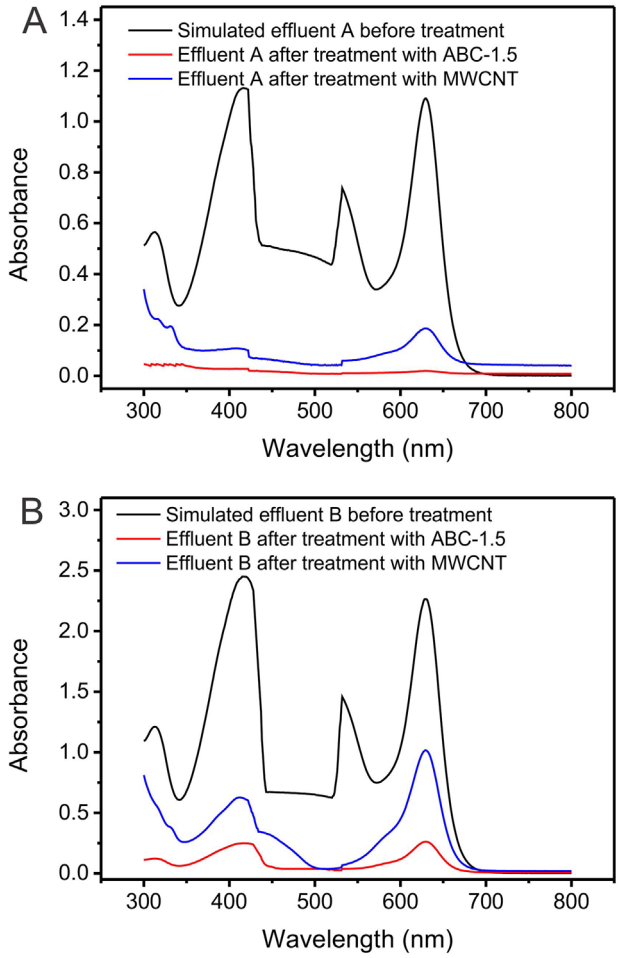

Figure 5. UV/Vis spectra of simulated beverage effluents before and after treatment with ABC-1.5 and MWCNT. (A) Effluent A, (B) effluent B. See Table 1 for the composition of the effluents.

times of 45 min (ABC-1.5) and 90 min (MWCNT) were obtained for the removal of the BB-FCF from aqueous solutions. The general order kinetic model best described the adsorption process. Multiple linear phases were obtained from the intra-particle diffusion model. The Liu isotherm model gave the best fit of isothermal data. Q_{max} of BB-FCF adsorbed at 323 K was 647.9 and 231.5 mg g^{-1} for ABC-1.5 and MWCNT, respectively. The thermodynamic parameters of the adsorption process were calculated. Based on the magnitude of enthalpy of adsorption, the interaction between BB-FCF and the two adsorbents was a physical interaction. Efficient regeneration of the adsorbents was possible with a mixture of 50% acetone and 50% 0.050 mol L^{-1} NaOH. ABC-1.5 is an efficient adsorbent for the treatment of simulated beverage effluents because it effectively removed 95.88% of a mixture of different dyes and other chemicals.

Acknowledgments

The authors are grateful to The National Council for Scientific and Technological Development (CNPq, Brazil), The Coordination of Improvement of Higher Education Personnel (CAPES, Brazil) and The Academy of Sciences for Developing World (TWAS, Italy) for financial support and sponsorship. We are grateful to Centre of Electron Microscopy (CME-UFRGS) for the use of the SEM microscope. We also thank Chemaxon for giving an Academic Research licence for the MarvinSketch software (Version 14.9.22.0), (www.chemaxon.com), 2014 that was used for comparisons of the dyes properties.

The authors have declared no conflict of interest.

References

[1] B. Royer, N. F. Cardoso, E. C. Lima, V. S. O. Ruiz, T. R. Macedo, C. Airoldi, Organofunctionalized Kenyaite for Dye Removal from Aqueous Solution, *J. Colloid Interface Sci.* **2009**, *336*, 398–405.

[2] M. B. Silveira, F. A. Pavan, N. F. Gelos, E. C. Lima, S. L. P. Dias, Punica Granatum Shell Preparation, Characterization, and Use for Crystal Violet Removal from Aqueous Solution, *Clean - Soil Air Water* **2014**, *42*, 939–946.

[3] V. M. Esquerdo, T. R. S. Cadaval Jr., G. L. Dotto, L. A. A. Pinto, Chitosan Scaffold as an Alternative Adsorbent for the Removal of Hazardous Food Dyes from Aqueous Solutions, *J. Colloid Interface Sci.* **2014**, *424*, 7–15.

[4] F. A. Pavan, E. S. Camacho, E. C. Lima, G. L. Dotto, V. T. A. Branco, S. L. P. Dias, Formosa Papaya Seed Powder (FPSP): Preparation, Characterization and Application as an Alternative Adsorbent for the Removal of Crystal Violet from Aqueous Phase, *J. Environ. Chem. Eng.* **2014**, *2*, 230–238.

[5] J. O. Gonçalves, D. A. Duarte, G. L. Dotto, L. A. A. Pinto, Use of Chitosan with Different Deacetylation Degrees for the Adsorption of Food Dyes in a Binary System, *Clean – Soil Air Water* **2014**, *42*, 767–774.

[6] B. Royer, N. F. Cardoso, E. C. Lima, T. R. Macedo, C. Airoldi, A Useful Organofunctionalized Layered Silicate for Textile Dye Removal, *J. Hazard. Mater.* **2010**, *181*, 366–374.

[7] M. Oplatowska, R. F. Donnelly, R. J. Majithiya, D. G. Kennedy, C. T. Elliott, The Potential for Human Exposure, Direct and Indirect, to the Suspected Carcinogenic Triphenylmethane Dye Brilliant Green from Green Paper Towels, *Food Chem. Toxicol.* **2011**, *49*, 1870–1876.

[8] W. Lang, S. Sirisansaneeyakul, L. O. Martins, L. Ngiwsara, N. Sakairi, W. Pathom-aree, M. Okuyama, et al., Biodecolorization of a Food Azo Dye by the Deep Sea *Dermacoccus abyssi* MT1. 1T Strain from the Mariana Trench, *J. Environ. Manage.* **2014**, *132*, 155–164.

[9] E. J. R. Almeida, C. R. Corso, Comparative Study of Toxicity of Azo Dye Procion Red MX-5B Following Biosorption and Biodegradation Treatments with the Fungi *Aspergillus niger* and *Aspergillus terreus*, *Chemosphere* **2014**, *112*, 317–322.

[10] K. Ullah, S. Ye, L. Zhu, Z. D. Meng, S. Oh, W. C. Sarkar, Microwave Assisted Synthesis of a Noble Metal-Graphene Hybrid Photocatalyst for High Efficient Decomposition of Organic Dyes Under Visible Light, *Mater. Sci. Eng., B* **2014**, *180*, 20–26.

[11] R. A. Pereira, M. F. R. Pereira, M. M. Alves, L. Pereira, Carbon Based Materials as Novel Redox Mediators for Dye Wastewater Biodegradation, *Appl. Catal., B* **2014**, *144*, 713–720.

[12] S. Wang, Y. Boyjoo, A. Choueib, Z. H. Zhu, Removal of Dyes from Aqueous Solution Using fly Ash and Red Mud, *Water Res.* **2005**, *39*, 129–138.

[13] S. Wang, L. Li, H. Wu, Z. H. Zhu, Unburned Carbon as a Low Cost Adsorbent for Dye Removal, *J. Colloid Interface Sci.* **2005**, *292*, 336–343.

[14] S. Wang, C. W. Ng, W. Wang, Q. Li, L. Li, A Comparative Study on Adsorption of Acid and Reactive Dyes on Multiwall Carbon Nanotubes in Single and Binary Dye Systems, *J. Chem. Eng. Data* **2012**, *57*, 1563–1569.

[15] N. M. Mahmoodi, O. Masrouri, A. M. Arabi, Synthesis of Porous Adsorbent Using Microwave Assisted Combustion Method and Dye Removal, *J. Alloys Compd.* **2014**, *602*, 210–220.

[16] G. L. Dotto, E. C. Lima, L. A. A. Pinto, Biosorption of Food Dyes onto *Spirulina platensis* Nanoparticles: Equilibrium Isotherm and Thermodynamic Analysis, *Bioresour. Technol.* **2012**, *103*, 123–130.

[17] S. Rovani, M. T. Censi, S. L. Pedrotti Jr., E. C. Lima, R. Cataluña, A. N. Fernandes, Development of a New Adsorbent from Agro-

industrial Waste and Its Potential Use in Endocrine Disruptor Compound Removal, *J. Hazard. Mater.* **2014**, *271*, 311–320.

[18] S. Rovani, A. N. Fernandes, L. D. T. Prola, E. C. Lima, W. O. Santos, M. A. Adebayo, Removal of Cibacron Brilliant Yellow 3G-P Dye from Aqueous Solutions by Brazilian Peats as Biosorbents, *Chem. Eng. Commun.* **2014**, *201*, 1431–1458.

[19] V. O. Njoku, K. Y. Foo, M. Asif, B. H. Hameed, Preparation of Activated Carbons from Rambutan (*Nephelium lappaceum*) Peel by Microwave-induced KOH Activation for Acid Yellow 17 Dye Adsorption, *Chem. Eng. J.* **2014**, *250*, 198–204.

[20] L. G. da Silva, R. Ruggiero, P. M. Gontijo, R. B. Pinto, B. Royer, E. C. Lima, T. H. M. Fernandes, et al., Adsorption of Brilliant Red 2BE Dye from Water Solutions by a Chemically Modified Sugarcane Bagasse Lignin, *Chem. Eng. J.* **2011**, *168*, 620–628.

[21] N. F. Cardoso, E. C. Lima, B. Royer, M. V. Bach, G. L. Dotto, L. A. A. Pinto, T. Calvete, Comparison of *Spirulina platensis* Microalgae and Commercial Activated Carbon as Adsorbents for the Removal of Reactive Red 120 Dye from Aqueous Effluents, *J. Hazard. Mater.* **2012**, *241–242*, 146–153.

[22] M. A. Adebayo, L. D. T. Prola, E. C. Lima, M. J. Puchana-Rosero, R. Cataluña, C. Saucier, C. S. Umpierres, et al., Adsorption of Procion Blue MX-R Dye from Aqueous Solutions by Lignin Chemically Modified with Aluminium and Manganese, *J. Hazard. Mater.* **2014**, *268*, 43–50.

[23] L. D. T. Prola, F. M. Machado, C. P. Bergmann, F. E. de Souza, C. R. Gally, E. C. Lima, M. A. Adebayo, et al., Adsorption of Direct Blue 53 Dye from Aqueous Solutions by Multi-walled Carbon Nanotubes and Activated Carbon, *J. Environ. Manage.* **2013**, *130*, 166–175.

[24] L. D. T. Prola, E. Acayanka, E. C. Lima, C. S. Umpierres, J. C. P. Vaghetti, W. O. Santos, S. Laminsi, et al., Comparison of *Jatropha curcas* Shells in Natural Form and Treated by Non-thermal Plasma as Biosorbents for Removal of Reactive Red 120 Textile Dye from Aqueous Solution, *Ind. Crop. Prod.* **2013**, *46*, 328–340.

[25] T. Calvete, E. C. Lima, N. F. Cardoso, J. C. P. Vaghetti, S. L. P. Dias, F. A. Pavan, Application of Carbon Adsorbents Prepared from Brazilian-pine Fruit Shell for the Removal of Reactive Orange 16 from Aqueous Solution: Kinetic, Equilibrium, and Thermodynamic Studies, *J. Environ. Manage.* **2010**, *91*, 1695–1706.

[26] N. F. Cardoso, R. B. Pinto, E. C. Lima, T. Calvete, C. V. Amavisca, B. Royer, M. L. Cunha, et al., Removal of Remazol Black B Textile Dye from Aqueous Solution by Adsorption, *Desalination* **2011**, *269*, 92–103.

[27] H. Marsh, F. R. Reinoso, *Activated Carbon*, Elsevier, Amsterdam **2006**.

[28] F. R. Reinoso, A. S. Escribano, Porous carbons in adsorption and catalysis, in *Handbook of Surfaces and Interfaces of Materials, Volume 5: Biomolecules, Biointerfaces, and Applications* (Ed.: H. S. Nalwa), Academic Press, Oxford **2001**.

[29] D. C. dos Santos, M. A. Adebayo, S. F. P. Pereira, L. D. T. Prola, R. Cataluña, E. C. Lima, C. Saucier, et al., New Carbon Composite Adsorbents for the Removal of Textile Dyes from Aqueous Solutions: Kinetic, Equilibrium, and Thermodynamic Studies, *Korean J. Chem. Eng.* **2014**, *31*, 1470–1479.

[30] M. C. Ribas, M. A. Adebayo, L. D. T. Prola, E. C. Lima, R. Cataluña, L. A. Feris, M. J. Puchana-Rosero, et al., Comparison of a Homemade Cocoa Shell Activated Carbon with Commercial Activated Carbon for the Removal of Reactive Violet 5 Dye from Aqueous Solutions, *Chem. Eng. J.* **2014**, *248*, 315–326.

[31] R. Pietrzak, P. Nowicki, J. Kaźmierczak, I. Kuszyńska, J. Goscianska, J. Przepiórsk, Comparison of the Effects of Different Chemical Activation Methods on Properties of Carbonaceous Adsorbents Obtained from Cherry Stones, *Chem. Eng. Res. Design* **2014**, *92*, 1187–1191.

[32] P. Shanley, G. Medina, S. Ferreira, Bacuri, *Platonia insignis* Mart., in *Frutíferas e Plantas Úteis na Vida Amazônica* (Eds.: P. Shanley, G. Medina), CIFOR & Imazon, Belem **2005**, pp. 55–64.

[33] V. K. Gupta, R. Kumar, A. Nayak, T. A. Saleh, M.A. Barakat, Adsorptive Removal of Dyes from Aqueous Solution onto Carbon Nanotubes: A Review, *Adv. Colloid Interface Sci.* **2013**, *193–194*, 24–34.

[34] F. M. Machado, C. P. Bergmann, E. C. Lima, B. Royer, F. E. de Souza, I. M. Jauris, T. Calvete, et al., Adsorption of Reactive Blue 4 Dye from Water Solutions by Carbon Nanotubes: Experiment and Theory, *Phys. Chem. Chem. Phys.* **2012**, *14*, 11139–11153.

[35] J. G. Yu, X. H. Zhao, H. Yang, X. H. Chen, Q. Yang, L. Y. Yu, J. H. Jiang, et al., Aqueous Adsorption and Removal of Organic Contaminants by Carbon Nanotubes, *Sci. Total Environ.* **2014**, *482–483*, 241–251.

[36] Y. Liu, Y. J. Liu, Review – Biosorption Isotherms, Kinetics and Thermodynamics, *Sep. Purif. Technol.* **2008**, *61*, 229–242.

[37] W. S. Alencar, E. C. Lima, B. Royer, B. D. dos Santos, T. Calvete, E. A. da Silva, C. N. Alves, Application of Aqai Stalks as Biosorbents for the Removal of the Dye Procion Blue MX-R from Aqueous Solution, *Sep. Sci. Technol.* **2012**, *47*, 513–526.

[38] O. O. Hart, B. R. Hammond, M. J. Steyn, P. Skivington, G. MacFarlaine, *Soft Drink Industry, Water Research Commission*, Binne & Partners Consulting Engineers, Pretoria **1987**.

[39] B Taylor, Other beverage ingredients, in *Chemistry and Technology of Soft Drinks and Fruit Juices* (Ed.: P. R. Ashurst), 2nd ed., Blackwell, Oxford, UK **2005**, pp. 90–128.

[40] B. Taylor, Ingredients and formulation of carbonated soft drinks, in *Carbonated Soft Drinks - Formulation and Manufacturer* (Eds.: D. P. Steen, P. R. Ashurst), Blackwell, Ames, Iowa, USA **2006**, pp. 48–86.

[41] M. S. Siboni, S. J. Jafari, O. Giahi, I. Kim, S. M. Lee, J. K. Yang, Removal of Acid Blue 113 and Reactive Black 5 Dye from Aqueous Solutions by Activated Red Mud, *J. Ind. Eng. Chem.* **2014**, *20*, 1432–1437.

[42] J. A. M. Agulló, B. C. Moore, D. C. Amorós, A. L. Solano, Activation of Coal Tar Pitch Carbon Fibres: Physical Activation vs. Chemical Activation, *Carbon* **2004**, *42*, 1367–1370.

[43] M. I. El-Khaiary, G. F. Malash, Common Data Analysis Errors in Batch Adsorption Studies, *Hydrometallurgy* **2011**, *105*, 314–320.

[44] V. K. Gupta, A. Nayak, Cadmium Removal and Recovery from Aqueous Solutions by Novel Adsorbents Prepared from Orange Peel and Fe_2O_3 Nanoparticles, *Chem. Eng. J.* **2012**, *180*, 81–90.

[45] J. Zhang, Q. Ping, M. Niu, H, Shi, N. Li, Kinetics and Equilibrium Studies from the Methylene Blue Adsorption on Diatomite Treated with Sodium Hydroxide, *Appl. Clay Sci.* **2013**, *83–84*, 12–16.

[46] M. G. Mahfouz, A. A. Galhoum, N. A. Gomaa, S. S. Abdel-Rehem, A. A. Atia, T. Vincent, E. Guibal, Uranium Extraction Using Magnetic Nano-based Particles of Diethylenetriamine-functionalized Chitosan: Equilibrium and Kinetic Studies, *Chem. Eng. J.* **2015**, *262*, 198–209.

[47] C. L. Sun, C. S. Wang, Estimation on the Intramolecular Hydrogen-bonding Energies in Proteins and Peptides by the Analytic Potential Energy Function, *J. Mol. Struct.* **2010**, *956*, 38–43.

[48] G. Z. Kyzas, N. K. Lazaridis, D. N. Bikiaris, Optimization of Chitosan and β-Cyclodextrin Molecularly Imprinted Polymer Synthesis for Dye Adsorption, *Carbohydr. Polym.* **2013**, *91*, 198–208.

[49] N. A. Travlou, G. Z. Kyzas, N. K. Lazaridis, E. A. Deliyanni, Graphite Oxide/Chitosan Composite for Reactive Dye Removal, *Chem. Eng. J.* **2013**, *217*, 256–265.

Supporting Information for

Comparison of a homemade bacuri shell activated carbon with carbon nanotubes for food dye removal

Caroline Saucier[1], Matthew A. Adebayo[2], Eder C. Lima[1,*], Lizie D. T. Prola[1], Pascal S. Thue[1,3], Cibele S. Umpierres[1], M. J. Puchana Rosero[1], and Fernando M. Machado[4]

[1] Institute of Chemistry, Federal University of Rio Grande do Sul (UFRGS), Porto Alegre, RS, Brazil

[2] Department of Chemical Sciences, Ajayi Crowther University, Oyo, Oyo State, Nigeria

[3] Department of Applied Chemistry, University of Ngaoundere, Ngaoundere, Cameroon

[4] Universitary Center Franciscano (UNIFRA), Santa Maria, RS, Brazil

Correspondence: Professor E. C. Lima, Institute of Chemistry, Federal University of Rio Grande do Sul (UFRGS), Av. Bento Gonçalves 9500, Postal Box 15003, ZIP 91501-970, Porto Alegre, RS, Brazil
e-mail: eder.lima@ufrgs.br or profederlima@gmail.com

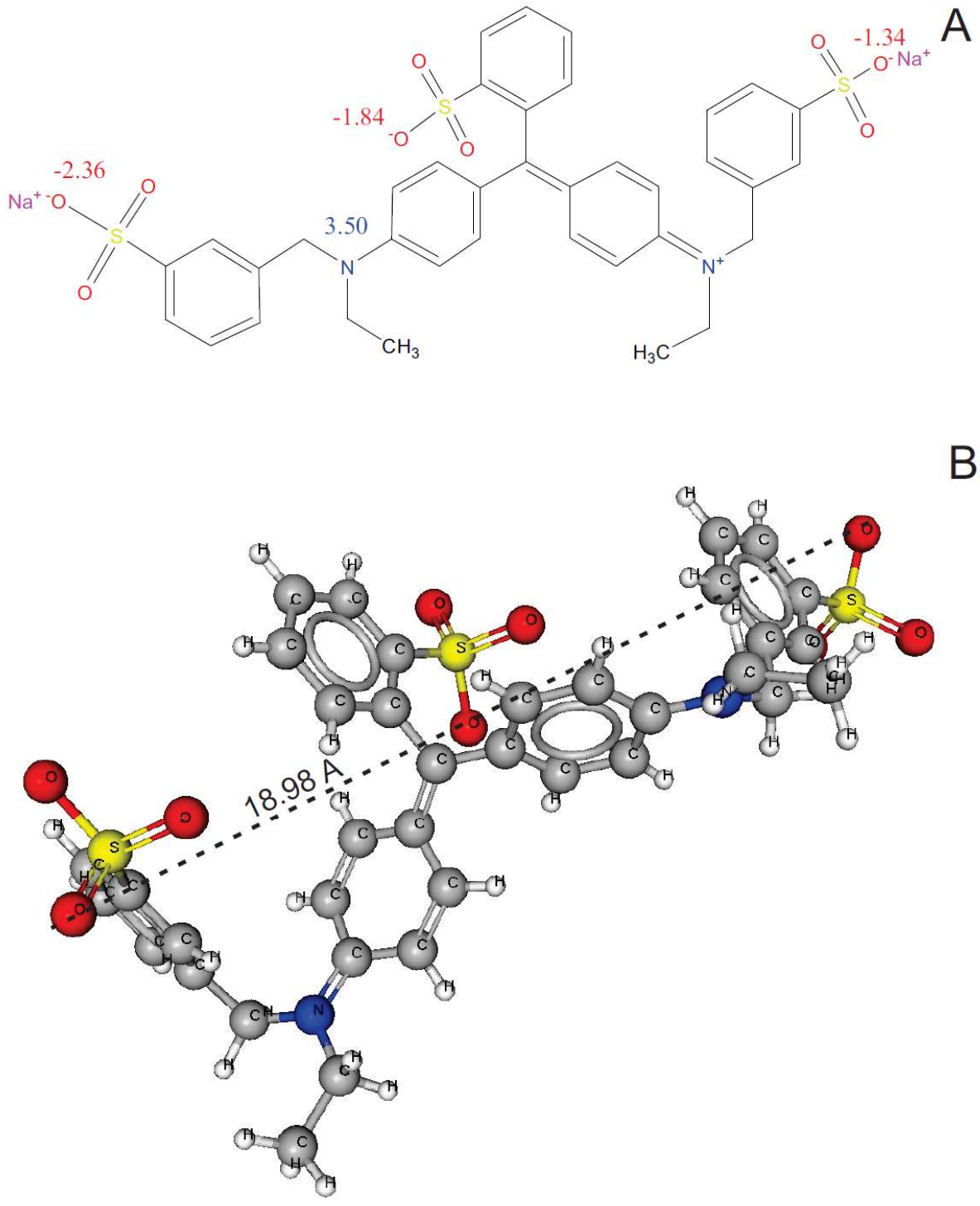

Supporting Information Fig S1. (A) Structural formula of BB-FCF and pK_a values of each acidic group. (B) Optimized 3D structural formula of BB-FCF. The physical-chemical properties of the chemical molecule were calculated using MarvinSketch version 14.9.22.0. Van der Waals surface area = 991.67 A^2 (pH 0--3); polar surface area 179.05 A^2 (pH 0--3); dipole moment 194.06 Debye.

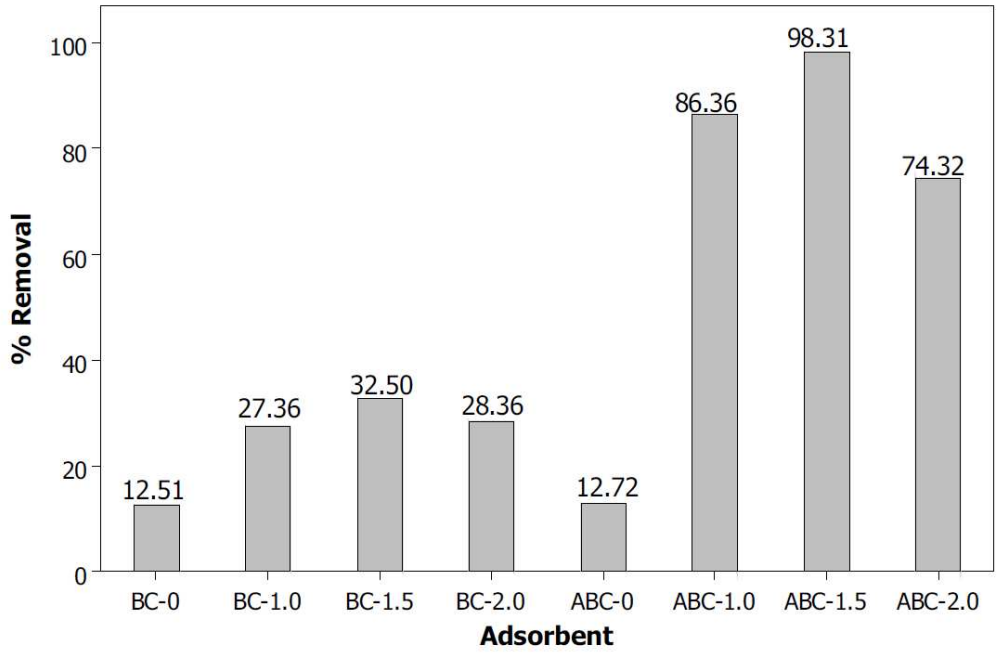

Supporting Information Fig S2. Comparison of different bacuri carbon adsorbents for the removal of BB-FCF. Conditions: C = 400 mg L^{-1} BB-FCF, adsorbent dosage 2.5 g L^{-1}, temperature 298 K, time of contact 60 min.

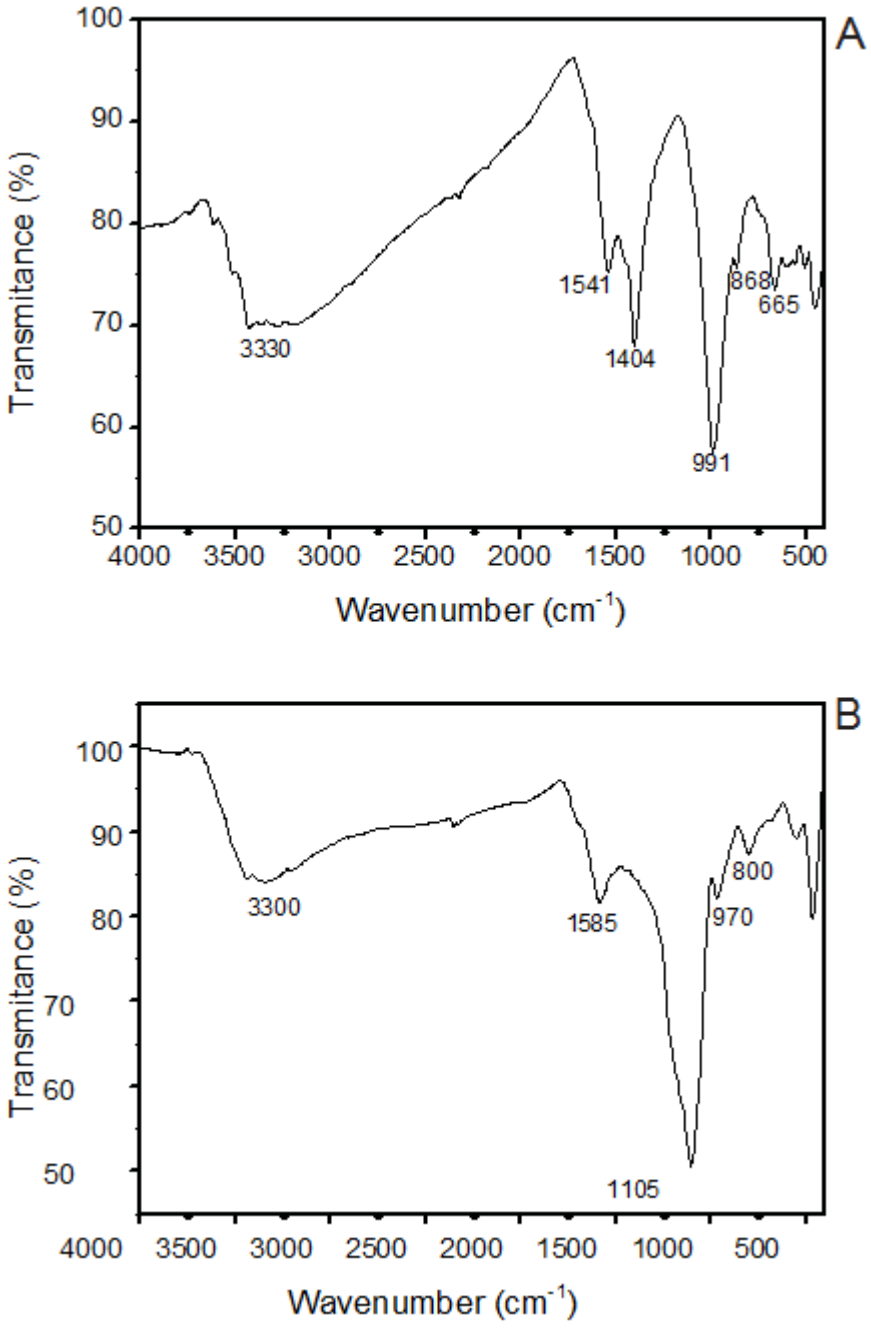

Supporting Information Fig S3: FTIR for (A) BC-1.5 and (B) ABC-1.5.The numbers are expressed in cm^{-1}.

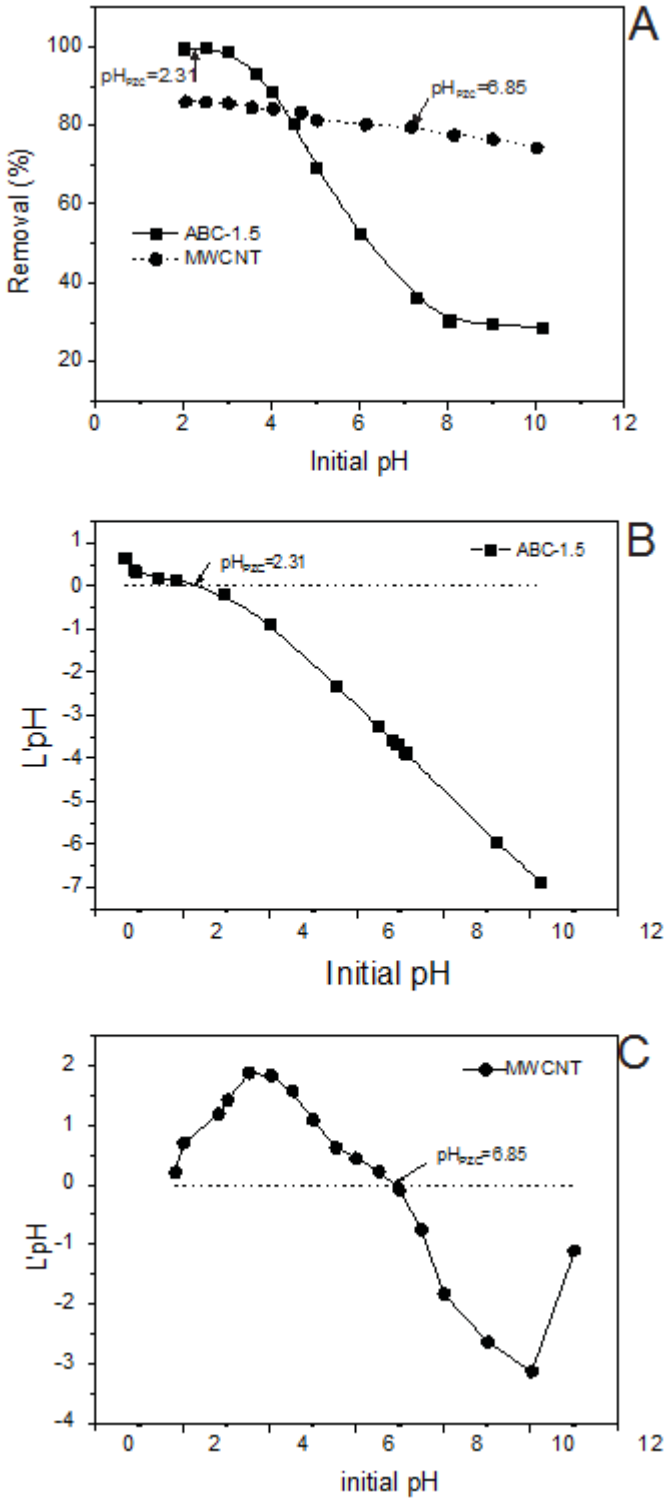

Supporting Information Fig S4. (A) Dependence of pH on the sorption capacity of BB-FCF on ABC-1.5 and MWCNT; (B) pH_{pzc} of ABC-1.5; (C) pH_{pzc} of MWCNT. Conditions: temperature 298 K; adsorbent mass 50 mg; dye concentration 300 mg L^{-1};

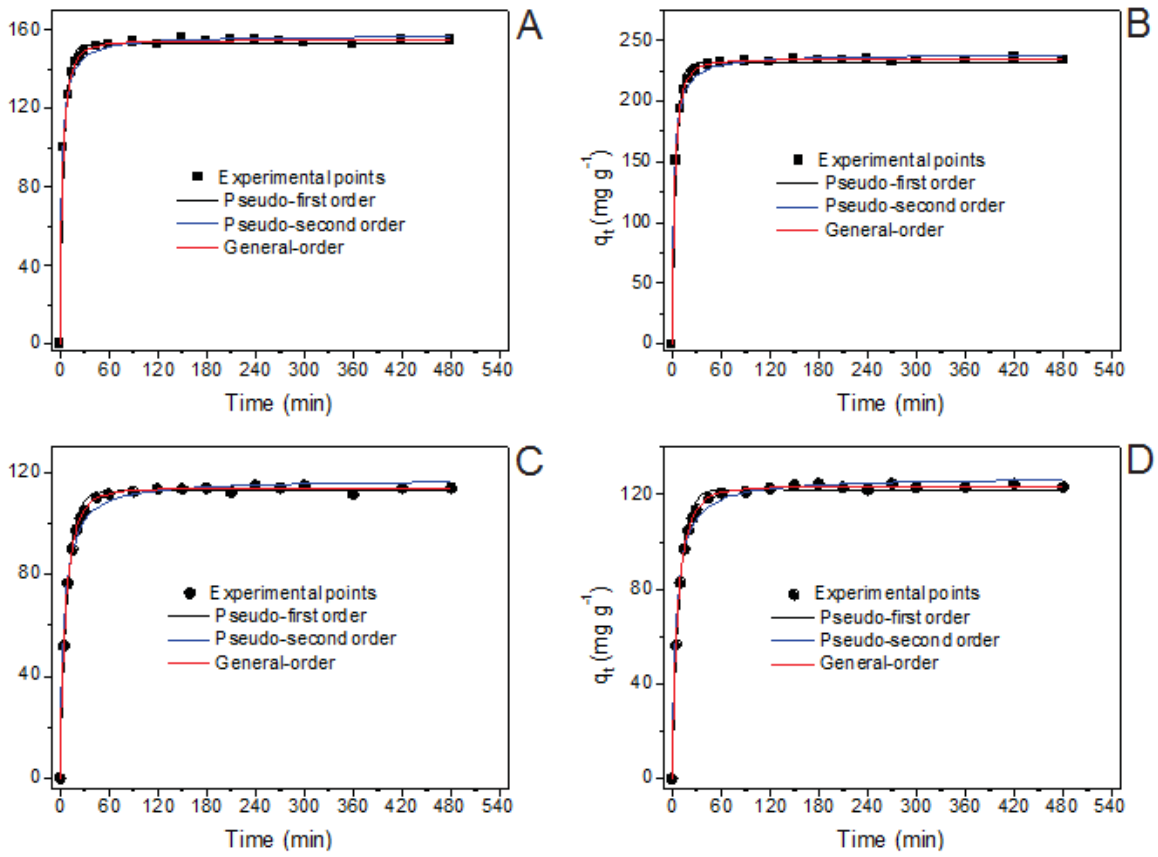

Supporting Information Fig S5. Kinetic curves of (A) ABC-1.5 and BB-FCF at 400 mg L^{-1}; (B) ABC-1.5 and BB-FCF at 600 mg L^{-1}; (C) MWCNT and BB-FCF at 400 mg L^{-1}; (D) MWCNT and BB-FCF at 600 mg L^{-1}. Conditions: initial pH, 2; temperature, 298 K; adsorbent mass, 50 mg.

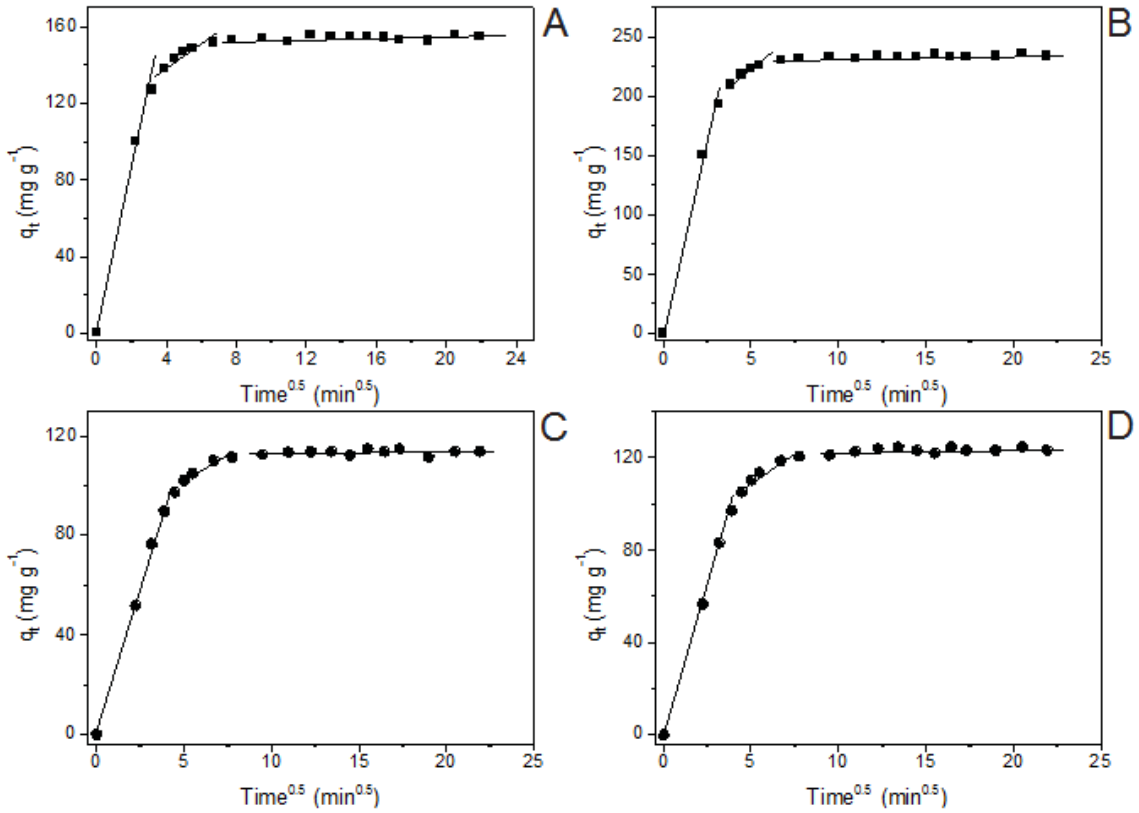

Supporting Information Fig S6. Intra-particle diffusion. (A) 400 mg L^{-1} of BB-FCF and ABC-1.5 adsorbent; (B) 600 mg L^{-1} of BB-FCF and ABC-1.5 adsorbent; (C) 400 mg L^{-1} of BB-FCF and MWCNT adsorbent; (D) 600 mg L of BB-FCF and MWCNT adsorbent.

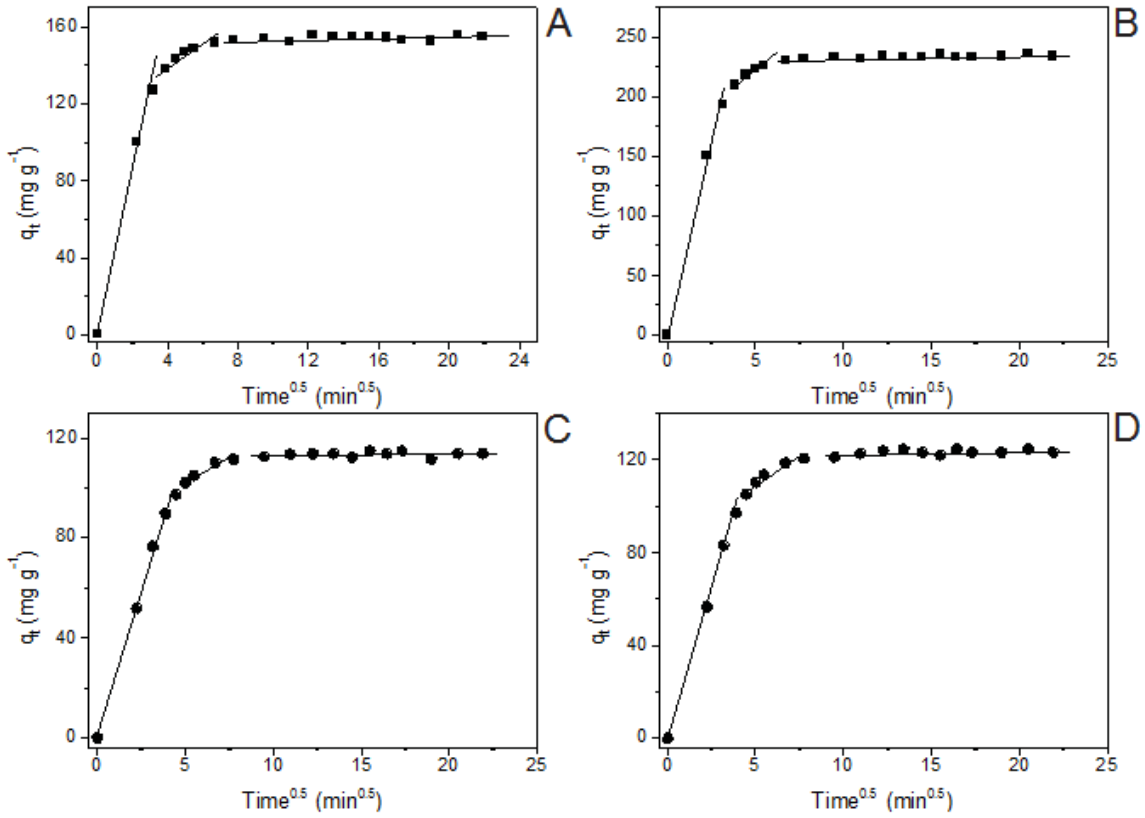

Supporting Information Fig. S7. Isothermal curves of BB-FCF on (A) ABC-1.5 and (B) MWCNT at 323 K. Conditions: initial pH, 2; adsorbent mass, 50 mg; contact time, 75 min for ABC-1.5 and 120 min for MWCNT.

APÊNDICE 2

Journal of Hazardous Materials 289 (2015) 18–27

Contents lists available at ScienceDirect

Journal of Hazardous Materials

journal homepage: www.elsevier.com/locate/jhazmat

Microwave-assisted activated carbon from cocoa shell as adsorbent for removal of sodium diclofenac and nimesulide from aqueous effluents

Caroline Saucier[a], Matthew A. Adebayo[b], Eder C. Lima[a,*], Renato Cataluña[a], Pascal S. Thue[a,c], Lizie D.T. Prola[a], M.J. Puchana-Rosero[a], Fernando M. Machado[d], Flavio A. Pavan[e], G.L. Dotto[f]

[a] Institute of Chemistry, Federal University of Rio Grande do Sul (UFRGS), Av. Bento Gonçalves 9500, P.O. Box 15003, 91501-970 Porto Alegre, RS, Brazil
[b] Department of Chemical Sciences, Ajayi Crowther University, Oyo, Oyo State, Nigeria
[c] Department of Applied Chemistry, University of Ngaoundere, P.O. Box 455, Ngaoundere, Cameroon
[d] Technology Development Center, Federal University of Pelotas (UFPEL), Pelotas, Brazil
[e] Institute of Chemistry, Federal University of Pampa (UNIPAMPA), Bagé, RS, Brazil
[f] Chemical Engineering Department, Federal University of Santa Maria (UFSM), Santa Maria, RS, Brazil

HIGHLIGHTS

- Microwave-assisted cocoa shell activated carbon was prepared and characterized.
- The anti-inflammatories, diclofenac and nimesulide, were adsorbed onto MWCS-1.0.
- Adsorption maximum values are 63.47 (diclofenac) and 74.81 mg g^{-1} (nimesulide).
- General order kinetic model suitably explained the adsorption process.
- MWCS-1.0 was effectively used for treatment of simulated hospital effluents.

ARTICLE INFO

Article history:
Received 11 November 2014
Received in revised form 4 February 2015
Accepted 8 February 2015
Available online 11 February 2015

Keywords:
Activated carbon
Anti-inflammatory
Effluents
Microwave-assisted activation

ABSTRACT

Microwave-induced chemical activation process was used to prepare an activated carbon from cocoa shell for efficient removal of two anti-inflammatories, sodium diclofenac (DFC) and nimesulide (NM), from aqueous solutions. A paste was obtained from a mixture of cocoa shell and inorganic components; with a ratio of inorganic: organic of 1 (CSC-1.0). The mixture was pyrolyzed in a microwave oven in less than 10 min. The CSC-1.0 was acidified with a 6 mol L^{-1} HCl under reflux to produce MWCS-1.0. The CSC-1.0 and MWCS-1.0 were characterized using FTIR, SEM, N_2 adsorption/desorption curves, X-ray diffraction, and point of zero charge (pH_{pzc}). Experimental variables such as initial pH of the adsorbate solutions and contact time were optimized for adsorptive characteristics of MWCS-1.0. The optimum pH for removal of anti-inflammatories ranged between 7.0 and 8.0. The kinetic of adsorption was investigated using general order, pseudo first-order and pseu do-second order kinetic models. The maximum amounts of DCF and NM adsorbed onto MWCS-1.0 at 25 °C are 63.47 and 74.81 mg g^{-1}, respectively. The adsorbent was tested on two simulated hospital effluents. MWCS-1.0 is capable of efficient removal of DCF and NM from a medium that contains high sugar and salt concentrations.

1. Introduction

The concern about the occurrence and fate of pharmaceutical compounds in the aquatic environment is on the increase [1,2]. The concern is heightened because there is no much information about the potential effects of pharmaceuticals on living organisms, though the pharmaceuticals are present at low concentrations (ng L^{-1} or μg L^{-1}) in natural waters [3]. The major problems are: most of pharmaceuticals are polar substances with high solubility in water [3], and are not completely removed by conventional wastewater treatment plants [4]. Therefore, a large number of the highly used prescription drugs have been globally detected in the

* Corresponding author. Tel.: +55 51 3308 7175; fax: +55 51 3308 7304.
E-mail addresses: eder.lima@ufrgs.br, profederlima@gmail.com (E.C. Lima).

http://dx.doi.org/10.1016/j.jhazmat.2015.02.026
0304-3894/

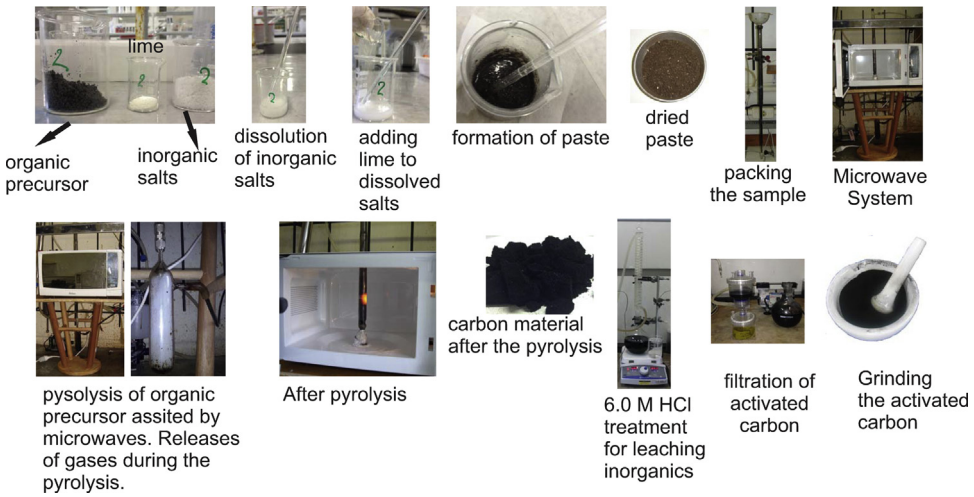

Fig. 1. Microwave-induced preparation of cocoa shell activated carbon.

aquatic environment [3]. In this context, there is an increasing demand for efficient methods to remove pharmaceuticals from wastewater [5–9].

A useful and reliable method for removal of organic compounds from wastewater is an adsorption technology [10–13]. It is a process in which pollutants are transferred from the effluent to a solid phase thereby alleviates exposure of living organisms to pollutants [14,15]. After effluent treatment through adsorption, it can be released into the environment [15,16] or used for some industrial processes. Adsorbents can also be regenerated after adsorption process and reutilized [15,16].

Activated carbons are famous because they possess outstanding adsorption characteristics due to their improved pore structures [17,18]. Therefore, activated carbon is one of the materials mostly used for the treatment of industrial wastewaters [19–23]. The ability of activated carbons to adsorb pollutants from aqueous solutions depends on two major factors: experimental conditions of the activation processes [17,18] and the nature of organic material utilized for the preparation of activated carbon [19,20]. Activated carbons can be prepared by physical and chemical activations [19]. Chemical activation utilizes H_3PO_4, $ZnCl_2$, KOH, NaOH, H_2SO_4, and K_2CO_3, among others [17,18,23,24]. In the chemical activation process, inorganic activating agent(s) and the raw materials are thoroughly mixed in an aqueous medium. The mixture is oven-dried (100–120 °C) and subsequently carbonized (400–800 °C) [17,18]. The inorganic components of activated carbon are removed using acid solutions or water [17,18]. This method does not allow homogeneous distribution of the inorganics with the organic carbonaceous materials because it is difficult to dry impregnated organic components [17,18]. To prevent nonhomogeneous distribution of the inorganic activating agent on the carbon precursor, the use of lime [1,21] mixed with the inorganic components was recently proposed. The inclusion of lime improves distribution of the inorganic component into the organic matrix during the pyrolysis step to obtain desirable adsorbents [1,21].

Conventional tubular furnace has been widely used for production of activated carbons *via* chemical and physical activation processes [17–21]. The application of microwave irradiation as a source of heating was recently reported [24–27]. The microwave heating offers some advantages over conventional heating methods. Some of these advantages are: rapid temperature rise that leads to shorter pyrolysis time for producing activated carbons (<15 min) [27], and a remarkable decrease in energy consumption [27]. The major difference between microwave heating and conventional heating is the mode in which the heat is generated. Heat transfer takes place by conduction in conventional furnace, but in microwave heating energy is supplied directly to the organic precursor at molecular level, and converted the energy into heat by dipole rotation and friction within the organic matrix [26,27].

In this work, powdered cocoa shell was mixed with inorganic components (20% lime + 40% $FeCl_3$ + 40% $ZnCl_2$) with inorganic: organic ratio of 0:1, 1:1, 1:1.5 and 1:2. Water was included in the preparation to form a paste [21]. The paste was dried at 100 °C for

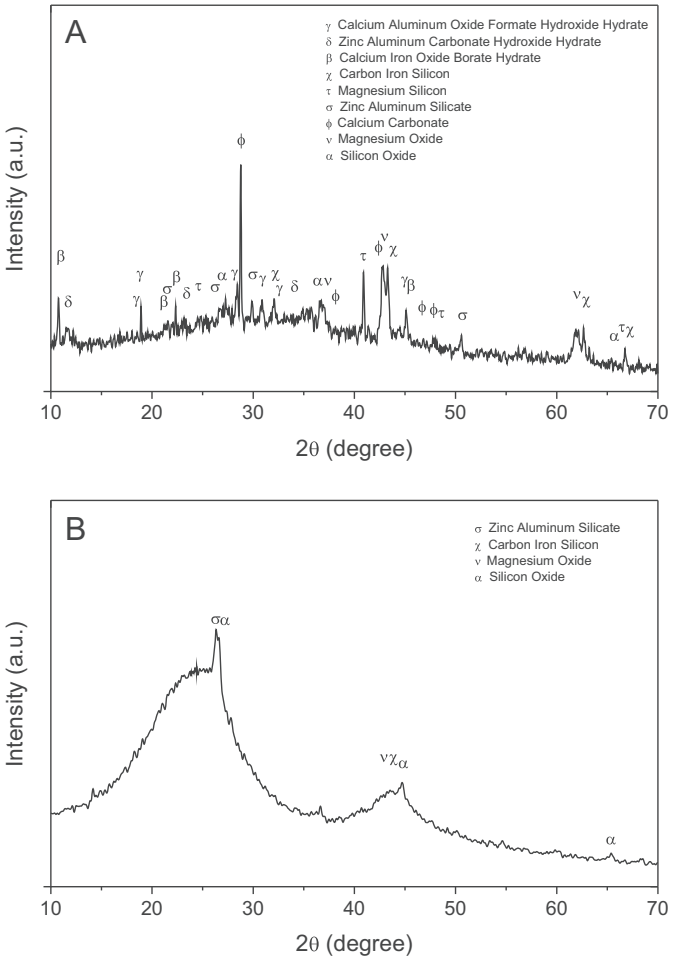

Fig. 2. XRD patterns of: (A) CSC-1.0; (B) MWCS-1.0.

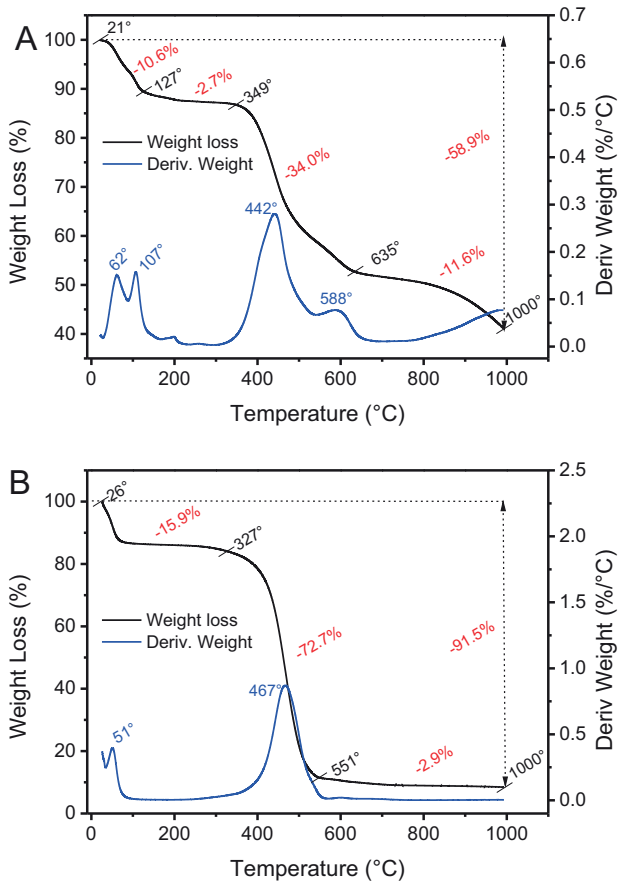

Fig. 3. TGA and DTG curves of: (A) CSC-1.0; (B) MWCS-1.0.

6 h and subsequently placed in a quartz reactor, which was disposed in a microwave oven and was heated using a heating program under inert atmosphere. A 6.0 mol L^{-1} HCl was used to acidified the carbonized materials (CSC-0, CSC-1.0, CSC-1.5, CSC-2.0) under reflux to obtain chemically activated cocoa-shell carbons induced by microwave (MWCS-0, MWCS-1.0, MWCS-1.5, MWCS-2.0). In this study, the preliminary experiments showed that MWCS-1.0 possessed the best adsorption capacity for removal of diclofenac (DCF) and nimesulide (NM) anti-inflammatories from aqueous solutions. Adsorption influencing factors such as initial pH of pharmaceutical solutions, time and temperature were investigated. The adsorbents were applied for treatment of simulated hospital wastewater effluents that are contaminated with pharmaceuticals.

2. Experimental

2.1. Chemicals, reagents and solutions

All solutions were prepared using deionized water. The diclofenac (DCF; see Supplementary Fig. 1) and nimesulide (NM; see Supplementary Fig. 2) were supplied by Medchemexpress and used without purification. $ZnCl_2$ and $FeCl_3$ were purchased from Vetec, and lime was obtained from a building material store. These reagents were used for chemical activation of cocoa shell. Solutions were prepared as described elsewhere [15,16].

2.2. Preparation and characterization of activated carbon adsorbent

The activated carbon adsorbent was prepared using the steps illustrated in Fig. 1: a 100.0 g of powdered cocoa shell (previously dried at 105 °C for 4 h), a 100.0 g of inorganic components (20% lime + 40% $ZnCl_2$ + 40% $FeCl_3$) and 40.0 mL of water were added and evenly mixed to yield a homogeneous paste. This prepared sample had inorganic:organic weight ratio of 1:1. The homogeneous paste was dried in an oven at 100 °C for 6 h. Subsequently, a 30.0 g of the sample was placed in a quartz reactor (see Fig. 1). The quartz reactor was inserted in a microwave oven as shown on Fig. 1. The atmosphere of the pyrolysis was kept constant at 200 mL min^{-1} of nitrogen. A collector flask was fitted in the lower part of the quartz reactor to collect the pyrolytic oil. For heating the system, the heating programs were: 360 W (80 s); 480 W (80 s); 600 W (80 s); 960 W (160 s); and 1200 W (160 s). After pyrolysis, the system was cooled down under 60 mL min^{-1} of nitrogen for 10 min. The total time for a cycle of pyrolysis is only 560 s (9.33 min), and a complete cycle of pyrolysis could be obtained in less than 20 min taking into consideration the 10 min of cooling down. After this time, other cycles of pyrolysis could be carried out. The material obtained after pyrolysis was named as CSC-1.0. Similar procedure was followed for preparation of other carbon adsorbents with inorganic: organic ratio 0:1 (CSC-0), 1:1.5 (CSC-1.5) and 1:2.0 (CSC-2.0). The CSC-0, carbonized material without inorganic compounds, served as a reference. To complete the chemical activation process, inorganics of CSC adsorbents were leached with a 6 mol L^{-1} HCl as earlier described [21]. The final yield of MWCS activated carbon was about 20% after treatment with a 6 mol L^{-1} HCl. Surface morphologies of CSC-1.0 and MWCS-1.0 were carried out using scanning electron microscopy (SEM) (JEOL microscope, model JSM 6060) [21]. The CSC-1.0 and MWCS-1.0 were also characterized using Fourier transform infra-red spectroscopy (FTIR) (Shimadzu Spectrometer, IR Prestige 21) [28]. The N_2 adsorption–desorption isotherms of CSC-1.0 and MWCS-1.0 were carried out using a surface analyzer (Micrometrics Instrument, TriStar II 3020) [21]. Thermogravimetric (TGA) and derivative thermogravimetric (DTG) curves of CSC-1.0 and MWCS-1.0 were obtained on a TA Instruments model SDT Q600 (New Castle, USA) with a heating rate of 10 °C min^{-1} at 100 mL min^{-1} of synthetic air flow (White Martins, Canoas, RS, Brazil). Temperature was varied from 20 °C to 1000 °C (acquisition time of 1 point per 5 s) using 10.00–15.00 mg of solid [21]. X-ray diffractions (XRD) (Philips X'pert MPD diffractometer) of CSC-1.0 and MWCS-1.0 were carried out at 40 kV and 40 mA with Cu Kα radiation (λ = 1.5406 Å) [15]. The point of zero charge (pH_{pzc}) was obtained as described elsewhere [28].

2.3. Adsorption studies

A 20.00 mL of DCF or NM solution (10.00–300.0 mg L^{-1}) was added to a 50.0 mg of MWCS-1.0 adsorbent in various 50.0 mL Falcon tubes at different pH values (7.0–10.0). The mixtures were agitated between 5 and 480 min inside a thermostatic shaker (150 rpm) between 25 °C and 50 °C. The mixtures were centrifuged for 5 min to separate the adsorbents from the pharmaceutical solutions. The DCF and NM left in solution after adsorption were quantified at maximum wavelengths of 275 and 392 nm, respectively, using UV/Visible spectrophotometer. The amount of DCF or NM removed by the MWCS-1.0 activated carbon and the percentage of removal were calculated using of Eqs. (1) and (2), respectively:

$$q = \frac{(C_o - C_f)}{m} \times V \quad (1)$$

$$\%\text{Removal} = 100 \times \frac{(C_o - C_f)}{C_o} \quad (2)$$

q is the amount of pharmaceutical adsorbed by the adsorbent (mg g^{-1}); C_o is the initial DCF or NM concentration in contact with the adsorbent (mg L^{-1}); C_f is the pharmaceutical concentration after the batch adsorption process (mg L^{-1}); m is the mass of

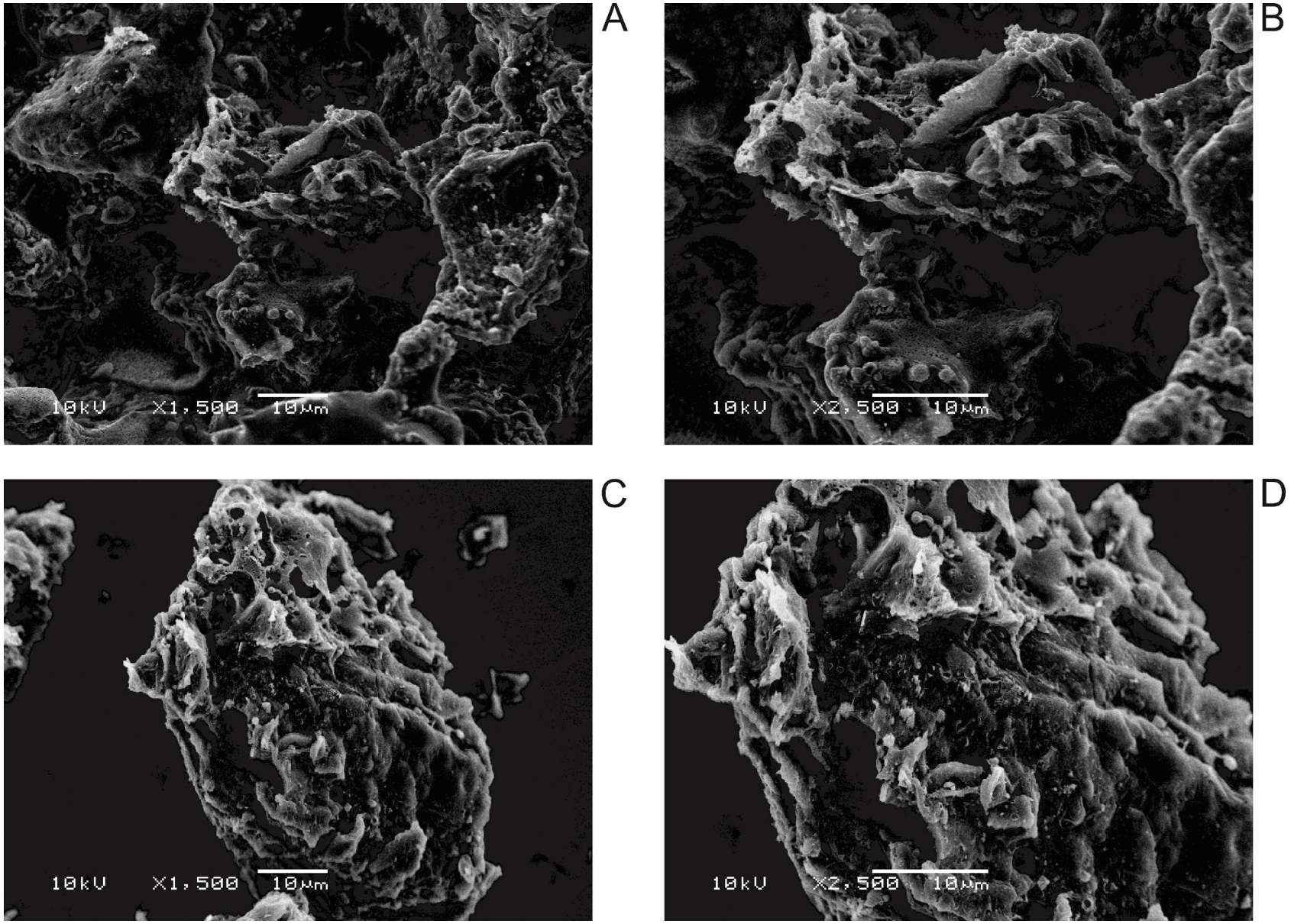

Fig. 4. SEM images of (A): CSC-1.0 magnification 1500×; (B) CSC-1.0 magnification 2500×; (C) MWCS-1.0 magnification 1500×; (D) MWCS-1.0 magnification 2500×.

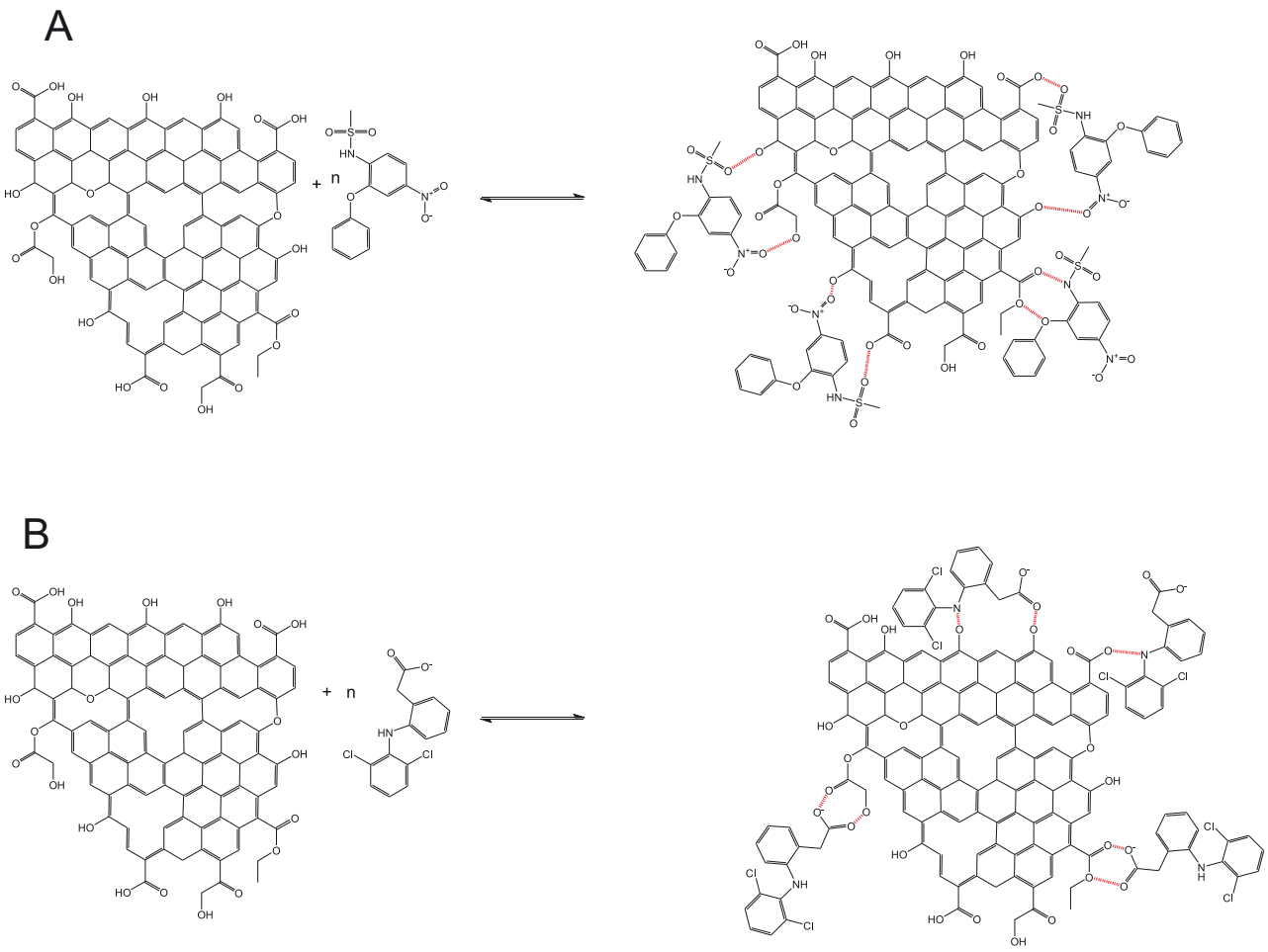

Fig. 5. Mechanisms of adsorption of (A) NM and (B) DCF using MWCS-1.0 activated carbon.

adsorbent (g); and V is the volume of the pharmaceutical solution (L).

2.4. Kinetic models

Pseudo-first order, pseudo second-order and general order kinetic models [29–31] were used to analyze the kinetic data. The respective mathematical expressions of these models are presented in Eqs. ((3)–(5)).

$$q_t = q_e \times [1 - \exp(-k_1 \times t)] \quad (3)$$

$$q_t = q_e - \frac{q_e}{[k_2(q_e) \times t + 1]} \quad (4)$$

$$q_t = q_e - \frac{q_e}{[k_N(q_e)^{n-1} \times t \times (n-1) + 1]^{1/1-n}} \quad (5)$$

where t is the time of contact (min); q_t is the amount of adsorbate adsorbed at time t ($mg\,g^{-1}$); q_e is the amount adsorbate adsorbed at the equilibrium ($mg\,g^{-1}$); k_1 is the pseudo-first order rate constant (min^{-1}); k_2 is the pseudo-second order rate constant ($g\,mg^{-1}\,min^{-1}$); k_N is the general order constant rate [$min^{-1} \times (g\,mg^{-1})^{n-1}$], n is the order of kinetic adsorption (n could be an integral or a fractional number).

2.5. Equilibrium models

Langmuir, Freundlich and Liu models are represented in Eqs. ((6)–(8)), respectively [29,31]. These models were used for analysis of equilibrium data in this work.

$$q_e = \frac{Q_{max} \times K_L \times C_e}{1 + K_L \times C_e} \quad (6)$$

$$q_e = K_F \times {C_e}^{1/n_F} \quad (7)$$

$$q_e = \frac{Q_{max} \times (K_g \times C_e)^{n_L}}{1 + (K_g \times C_e)^{n_L}} \quad (8)$$

where q_e is the amount adsorbate adsorbed at equilibrium ($mg\,g^{-1}$); C_e is the pharmaceutical concentration at equilibrium ($mg\,L^{-1}$); Q_{max} is the maximum sorption capacity of the adsorbent ($mg\,g^{-1}$); K_L is the Langmuir equilibrium constant ($L\,mg^{-1}$); K_F is the Freundlich equilibrium constant [$mg\,g^{-1} \times (mg\,L^{-1})^{-1/n_F}$]; K_g is the Liu equilibrium constant ($L\,mg^{-1}$); n_F and n_L are the exponents of Freundlich and Liu model, respectively (dimensionless).

2.6. Simulated effluents

Two simulated effluents, which comprised four pharmaceuticals, two sugars, urea and other inorganic components usually found in wastewater, were prepared at pH 8.0. The compositions and concentrations of these effluents are shown in Supplementary

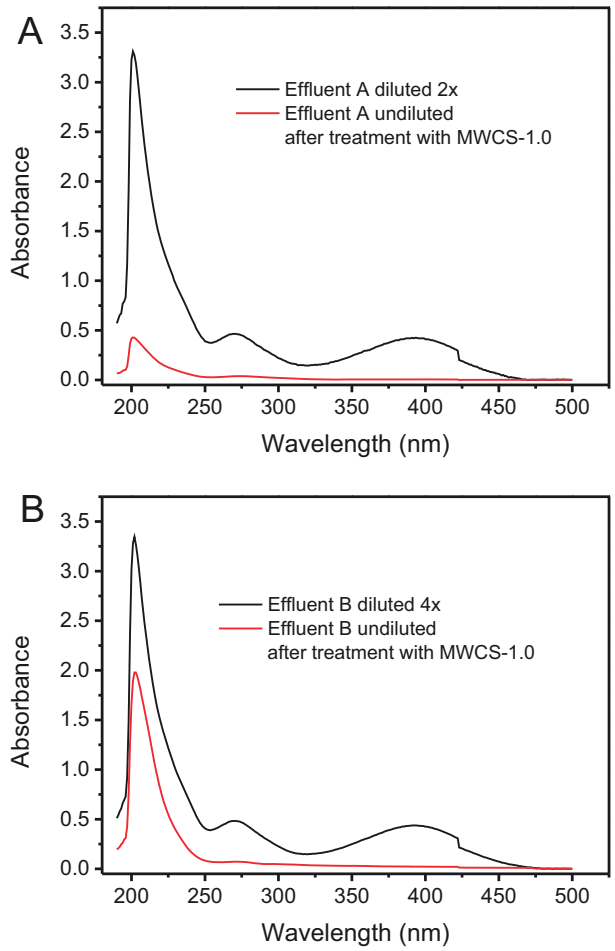

Fig. 6. UV–vis spectra of simulated hospital effluents before and after treatment with MWCS-1.0 (A) Effluent A; (B) Effluent B. See Table 1 for composition of effluents.

Table 1. The aim of this simulated effluents is to test the sorption capacity of the proposed MWCS-1.0 activated carbon for removal of pharmaceuticals in a medium of high salt, sugar and organic concentrations.

3. Results and discussion

3.1. Preparation of cocoa shell activated carbon induced by microwave and preliminary experiments of adsorption

In the preparation of cocoa carbon adsorbents, lime ($CaCO_3 + Ca(OH)_2 + CaO$) was included as one of the inorganic components to prevent impregnation of the carbonaceous material with aqueous solution [22,24]. After the paste being dried, part of calcium compounds could be separated from the organic matrix, however this did not bring any impairment to the pore structure, surface area and pore volume, since calcium compounds detected in the XRD diffraction pattern were eliminated by the HCl treatment (see subsequent discussions below). Also, it is important to point out that the MWCS-1.0 was made several times in the laboratory and tested for the removal of DCF and NM with the same performance (%removal and maximum sorption capacity). There were not significantly differences observed among the activated carbons made at different times.

Apart from lime, other inorganic components (activating agents) used in this study are $ZnCl_2$ and $FeCl_3$. The activating agent commonly used for preparation of activated carbon is $ZnCl_2$ [32]. Similarly, iron salts have been used as activating agents [15,21]. The paste formed was broken and inserted in the quartz reactor and pyrolyzed using a convenient heating program under inert conditions (see Fig. 1). The quartz reactor was placed vertically in the microwave oven for delivering the tar into the recipient vessel by gravity. This arrangement did not allow the tar to block the pores of the adsorbent [15,21]. Similarly, it is noteworthy to say that $ZnCl_2$ and $FeCl_3$ allowed transmission of the microwaves to the carbonaceous matrix that is inert to microwaves. Therefore, the use of paste with lime and inorganics enabled better disperse of the inorganics in the organic matrix and facilitated the transmission of microwave energy in the organic precursor.

The cocoa shell carbon adsorbents produced after treatment with microwaves were labeled as CSC-1.0, CSC-1.5 and CSC-2.0 for inorganic: organic ratios of 1.0, 1.5 and 2.0, respectively. An adsorbent without the inorganic portion was also prepared and labeled as CSC-0. The preparation of CSC-1.0 allowed us to investigate the influence of the inclusion of inorganic components in the carbon adsorbents and the effect on the inorganics on the carbonization of the organic precursor by microwave-assisted pyrolysis.

The inorganics were leached from the carbonized adsorbents (CSC-1.0, CSC-1.5 and CSC-2.0) using a 6 mol L^{-1} HCl. The inorganics can hydrolyze the organic precursor and enhance the release of some organic components that could weaken the expanding molecules of the carbon materials during the pyrolysis [21]. The inorganic portion of the carbon material, on the contrary, prevents the shrinkage of the particles during the pyrolysis [21]. As the inorganics are leached during acidification, the porosity of the carbon material is improved [17,18,21].

The CSC-0, CSC-1.0, CSC-1.5, CSC-2.0, MWCS-0, MWCS-1.0, MWCS-1.5 and MWCS-2.0 were used to adsorb a 50.0 mg L^{-1} of DCF and NM pharmaceuticals from aqueous solutions at agitation time of 120 min. Table 1 presents the percentages of adsorption of the carbon adsorbents. The percentages of removal of DCF and NM using CSC-0 and MWCS-0 are very low. In the absence of inorganics, the cocoa shell was not carbonized by microwaves. This should be one of the reasons why several authors [24–27] first carbonize the organic precursors in a conventional oven to produce carbonized material that is microwave-conductor, and then activate through microwave induction [24–27]. For all other materials the percentages of removal of DCF and NM were much higher than those of uncarbonized CSC-0. To increase the sorption capacity of the adsorbent, the inorganics were leached from the carbonaceous materials. All MWCS adsorbents show higher adsorption capacities than CSC adsorbents. MWCS-1.0, the best adsorbent from preliminary experiment, was used for the rest of our experiments.

One of the achievements of this work is the ability to produce activated carbon via microwave-induced pyrolysis in a single stage of pyrolysis. Another achievement is that the total time of pyrolysis, which includes the time for cooling down the quartz reactor, was less than 20 min. This procedure has advantages over already published methods [21,24–27].

3.2. Characterization of CSC-1.0 and MWCS-1.0

In order to verify the effects of the chemical activation of the cocoa shell activated carbon, the CSC-1.0 precursor was used to check the improvements in the textural properties, the thermal stability and morphology.

Taking into account that MWCS-1.0 presented the best adsorption capacity for removal of DCF and NM from aqueous solutions, just CSC-1.0 (precursor of MWCS-1.0) and MWCS-1.0 activated carbons were chosen for characterization purpose. The unique properties that are relevant and informative are the surface area, the average pore radius and total pore volume. These properties are presented in Table 1 for all the adsorbents. It is observed that higher surface area and higher total pore volume of adsor-

bent increase the percentage of removal of pharmaceuticals from aqueous solution. Comparison of the textural properties of CSC-1.0, CSC-1.5 and CSC-2.0 (carbon materials that were not acidified to leach inorganics) with MWCS-1.0, MWCS-1.5 and MWCS-2.0 (adsorbents that were acidified to leach inorganics) showed that acidification produced adsorbents with better textural characteristics for adsorption of pharmaceuticals, as already reported for adsorption of dyes [15,21]. The surface area and total pore volume of MWCS-1.0, MWCS-1.5 and MWCS-2.0 increased by 9.3-fold and 10.5-fold (MWCS-1.0), 9.2-fold and 10.2-fold (MWCS-1.5) and 9.5-fold and 10.8-fold (MWCS-2.0) after acidification of CSC-1.0, CSC-1.5 and CSC-2.0, respectively.

Fig. 2A and B present the XRD patterns of CSC-1.0 and MWCS-1.0, respectively. The CSC-1.0 sample (Fig. 2A) has the following peaks: calcium carbonate ($CaCO_3$; JCPDS Card 00-003-0569); zinc aluminum silicate ($Zn_2Al_4Si_5O_{18}$; JCPDS Card 00-032-1456); magnesium silicon (Mg_2Si; JCPDS Card 00-035-0773); silicon oxide (SiO_2; JCPDS Card 00-033-1161); calcium iron oxide borate hydrate ($B_{0.5}Ca_4Fe_2H_{21.5}O_{18.5}$; JCPDS Card 00-049-0012); zinc aluminum carbonate hydroxide hydrate ($Zn_{0.61}Al_{0.39}(OH)_2(CO_3)_{0.195}.H_2O$; JCPDS Card 00-048-1025); calcium aluminum oxide formate hydroxide hydrate ($C_{0.66}H_{20}Al_2Ca_4O_{17.67}$; JCPDS Card 00-041-0724); carbon iron silicon ($C_{0.124}Fe_{0.787}Si_{0.089}$; JCPDS Card 00-047-1293); magnesium oxide (MgO; JCPDS Card 00-004-0829). The XRD patterns of CSC-1.0 reflect the inorganics utilized as activating agents for the preparation of the carbon material [33]. Contrarily, the XRD patterns of MWCS-1.0 (Fig. 2B) reflect those of amorphous materials with a wide band (between 13° and 35°) that corresponds to amorphous carbon, and also 4 crystalline phases that were left in the activated carbon after the leaching procedure with a 6.0 mol L^{-1} HCl. The mineralogical phases are: silicon oxide, zinc aluminum silicate, carbon iron silicon and magnesium oxide. After treatment, the peak intensities of MWCS-1.0 are lesser than those of CSC-1.0, indicating that the inorganics were leached through acidification. In addition, the XRD data are consistent with the textural properties described above. The leaching of the inorganic components produced carbon material (MWCS-1.0) with low crystallinity, and higher pore volume and superficial area as found in the literature [21].

Fig. 3 shows the thermogravimetric profiles of CSC-1.0 and MWCS-1.0. There are ample peaks in the DTG curve of CSC-1.0: 62 °C and 107 °C, the elimination of solvent; 442 °C and 588 °C, decomposition of the organic contents of CSC-1.0. The TG curves can be classified into four regions. The first region, from 21 °C to 127 °C, a mass loss of 10.6% is ascribed to the loss of adsorbed water [10,11]. The second region, from 127 °C to 349 °C, a slight mass loss of 2.7% is assigned to disappearance of water of crystallization of the inorganic components present in the CSC-1.0 (see Fig. 2A) [10,11]. The third and main weight loss (34.0%), from 349 °C to 635 °C, is ascribed to the decomposition of carbonaceous matrix [15,19]. The last part, from 635 °C to 1000 °C – a mass loss of 11.6% (skeleton decomposition), is assigned to residual carbon [15,19]. From 21 °C to 1000 °C, a residual mass of approximately 41.1%, which could be allocated to the undecomposed carbonaceous materials and inorganic components of CSC-1.0, is observed [15,21].

The thermogravimetric profiles of MWCS-1.0 and CSC-1.0 differ (see Fig. 3B). For MWCS-1.0, the weight loss is 91.5% (26–1000 °C), an indication that acidification leached most of the inorganics from the precursor. This remark concurred with the XRD data (see Fig. 2B). Two decomposition peaks at 51 °C and 467 °C are observable on DTG curves of MWCS-1.0. There are three segments of weight loss in the TG curves of MWCS-1.0. A mass loss of 15.9% (26–327 °C) is assigned to water molecules (adsorbed and interstitials) [10,11]. The humidity of CSC-1.0 is somewhat lower than that of MWCS-1.0 because of acid treatment. A mass loss of 72.7% (327–551 °C) is ascribed to the decomposition of carbonaceous matrix. Lastly, additional mass loss of 2.9% (551–1000 °C), which could be assigned to skeleton decomposition, is observed. The residual mass observed at 1000 °C (8.5%) could be linked to the ash content of the residue of decomposed MWCS-1.0 since the TGA/DTG curves were obtained with synthetic air.

Fig. 4 shows the SEM images of MWCS-1.0 and CSC-1.0. A characteristic of lignin cellulosic materials, a fibrous appearance of cocoa shell [28], disappeared during pyrolysis. As shown in the figure, the roughness of the carbon materials is obvious. However, the granules of MWCS-1.0 are smaller than those of CSC-1.0. This could be attributed to the acidic treatment of CSC-1.0 that leached most of the inorganic components, leaving MWCS-1.0 with granules of more spherical appearance. Macro-cavities are observed in both materials, but the cavities of CSC-1.0 are higher than those of MWCS-1.0. Probably, these large cavities of the precursor allow its breakage to form small carbon particles, after the acid treatment.

Fourier transform infra-red spectroscopy (FTIR) is a useful tool for identification of functional groups possessed by adsorbents, and the groups that are responsible for adsorption of adsorbates. The FTIR spectra of the adsorbents were recorded between 4000 and 400 cm^{-1} (see Supplementary Fig. 3 and Table 2).

Supplementary Table 2 shows the band assignments of the functional groups possessed by CSC-1.0 and MWCS-1.0. [1,13–16,19–21]. The FTIR spectra of CSC-1.0 and MWCS-1.0 slightly differ (see Supplementary Fig. 3). The MWCS-1.0 spectrum shows lesser vibrational bands than the spectrum of CSC-1.0. The Si—O stretch of silicates is noticeable in CSC-1.0 at 995 cm^{-1} unlike in MWCS-1.0 (at 1099 cm^{-1}). The major functional groups present in CSC-1.0 are O—H (alcohols, phenols), aromatic rings, C—O (alcohols), Si—O (silicates) and C—H (aromatics, aliphatic chains) while the conspicuous groups in MWCS-1.0 are O—H (alcohols, phenols), aromatic rings, C—O (phenols, alcohols, carboxylic), and

Table 1
Textural properties and comparison of different cocoa carbon adsorbents for the removal of DCF and NM pharmaceuticals. Conditions: C_o, 100.0 mg L^{-1} of pharmaceutical; adsorbent dosage, 2.5 g L^{-1}; temperature, 25 °C; contact time, 120 min.

Sample	BET surface area (m^2 g^{-1})	Average pore radius (nm)	total pore volume (cm^3 g^{-1})	%Removal DCF	NM
CSC-0[a]	1.1	1.8	0.001	0.17	0.21
CSC-1.0	67	7.6	0.030	45.23	40.25
CSC-1.5	61	8.4	0.028	40.25	39.25
CSC-2.0	57	10.6	0.025	36.54	38.25
MWCS-0	2.6	1.7	0.003	4.62	3.89
MWCS-1.0	619	4.8	0.315	97.05	98.75
MWCS-1.5	562	5.2	0.286	90.25	89.52
MWCS-2.0	541	5.5	0.270	88.56	85.23

[a] CSC-0 (in the absence of inorganics) was not carbonized using microwave.

C—H (aromatics, aliphatic chains). The FTIR data agreed with those of XRD discussed in Fig. 2.

3.3. pH dependence studies

The pH of the solution is a pronounced factor affecting removal of a pharmaceutical on an adsorbent [1,14–16,28,29]. The optimum pH of an organic compound is a function of the type of adsorbent being used during adsorption experiments while the solubility of an organic compound depends on the pH of the solution. It was observed that both DCF and NM solutions (150.0 mg L^{-1}) precipitated at pH ranging from 2.0 to 6.0. The precipitation of NM was immediate while that of DCF occurred after 48 h. Therefore, the pH range for pH dependence studies are from 7.0 to 10.0 for both pharmaceuticals (see Supplementary Fig. 4). The optimum pH values for adsorption of DCF and NM onto MWCS-1.0 are pH 7.0 and 8.0, respectively.

The pH_{pzc} value of MWCS-1.0 is 6.7. At pH 7.0 (DCF) and 8.0 (NM), the surface of the MWCS-1.0 is expected to be negative. The estimated p*K*a values of DCF and NM using Marvin Sketch 14.9.22.0 software are 4.0 and 6.7, respectively. Considering conditions such as solubility of the pharmaceuticals, the pH studies, and the pH_{pzc} of the adsorbent, it is expected that the mechanism of adsorption of DCF and NM on MWCS-1.0 should not be an electrostatic attraction that is generally admitted for adsorption of dyes [13–16]. Alternatively, the interaction of the pharmaceuticals with the activated carbon should be π–π stacking [1], hydrogen bonding, and van der Waals forces [1].

3.4. Kinetic studies

Nonlinear pseudo-first order, pseudo-second order and general order kinetic models were utilized to explain the kinetic of adsorption of DCF and NM onto CSC-1.0 and MWCS-1.0. Supplementary Fig. 5 shows the kinetic curves while Supplementary Table 3 presents the fitting parameters of the kinetic models. Standard deviation (SD) values explain the suitability of each nonlinear kinetic model. The bigger the deviation of the theoretical q value from the experimental q value, the higher the SD value [1,10,11,14–16]. The SD of the minimum value was used to divide SD of each model (SD ratio) to compare the fitness of each model. General order kinetic model has the lowest SDratio values. The *SD* ratio values of the pseudo-first order kinetic model vary from 11.5 to 13.0 (DCF), and 8.2 (NM). The *SD* ratio values of the pseudo-second order model vary from 1.8 to 2.3 (DCF) and from 2.4 to 2.5 (NM). Therefore, the adsorption of both pharmaceuticals onto MWCS-1.0 is best described by the general order kinetic model that has SD ratio value of 1.0.

In the adsorption of DCF and NM, the kinetic of adsorption of NM onto MWCS-1.0 was faster than that of DCF. The half-life ($t_{1/2}$), the time taken to attain 50% of q_e (amount adsorbed at the equilibrium), was obtained by interpolation of the kinetic curves. Supplementary Table 3 presents the $t_{1/2}$ values. Since the general kinetic model is the best model that explains kinetic data, its $t_{1/2}$ values are meaningful. The $t_{1/2}$ values of the adsorption DCF onto MWCS-1.0 are between 4.1–fold and 19.7–fold higher than the values obtained for NM. With the aids of Marvin Sketch 14.9.22.0[1] software, the dipole moments of DCF and NM were calculated. These values are 19.21 and 11.52 Debye for DCF and NM, respectively. The bigger the dipole moment, the higher the polarity of the molecule [34]. On the account that the adsorption of an organic molecule onto active surface of carbon involves dehydration of the organic molecule before being adsorbed on the solid surface, the more polar molecule will possess a higher energy barrier to be surpassed so as to release the water to the bulk of the solution, and the adsorption of the adsorbate takes place onto the adsorbent surface. Therefore, the difference in polarity of the pharmaceuticals explains why the kinetic of adsorption of NM onto MWCS-1.0 is faster than that of DCF.

To verify the time it takes to attain the equilibrium, an interpolation was made on the general order kinetic model plot for both pharmaceuticals. In this calculation, the value of q_t that was 95% of the maximum value of experimental q_t was used. For DCF pharmaceutical, the $t_{0.95}$ is 223.14 min, and for NM the $t_{0.95}$ is 45.46 min. The difference between the equilibrium times for adsorption of DCF and NM in the MWCS-1.0 adsorbent agrees with the $t_{1/2}$ values and initial sorption rates shown in Supplementary Table 3.

For other experiments on adsorption of DCF and NM onto MWCS-1.0, the contact times of 240 min and 60 min, respectively, were used. The contact time was increased to ensure that equilibrium is attained between the pharmaceuticals and the adsorbent at higher concentrations of pharmaceuticals [19,20].

3.5. Equilibrium studies

In this work Langmuir, Freundlich and Liu [31] isotherm models were utilized to analyze the isothermal data.

The isothermal experiments were investigated between 25 °C and 50 °C using the optimum experimental conditions (see Supplementary Table 4 and Fig. 6). The adsorption isotherm plots of DCF and NM onto MWCS-1.0 at 25 °C are presented in Supplementary Fig. 6. Between 25 °C and 50 °C, the Liu model gives the best description of adsorption equilibrium data of DCF and NM onto MWCS-1.0 based on the SD values (Supplementary Table 4). The SD ratio values of the Langmuir model range from 10.87 to 14.57 (DCF), and 6.68 and 17.00 (NM) while those of Freundlich model range from 11.08 to 14.02 (DCF) and from 5.18 to 11.98 (NM).

The maximum amounts (Q_{max} values) of NM and DCF removed at 25 °C are 63.47 and 74.81 mg g^{-1} for DCF and NM, respectively. Q_{max} values of NM (25–50 °C) are between 17.87% and 20.88% higher than those of DCF. The rate of adsorption of NM is also faster than that of DCF. The chemical behaviors of the pharmaceuticals could be linked to their differences in the adsorptive characteristics. The van der Waals surface area of DCF (pH 4.0–14.0) and NM (pH 7.0–14.0) are 359.64 A^2 and 406.46 A^2, respectively, while the polar surface area of DCF (pH 4.0–14.0) and NM (pH 7.0–14.0) are 52.16 and 104.12 A^2, respectively [35]. Taking into account that the polar parts of the pharmaceutical molecule interact intensely with the polar part of the activated carbon (OH groups of phenols and alcohols, carboxylic groups), it is expected that NM would show a higher affinity for the polar groups present on the surface of activated carbon. This fact explains higher amount of NM adsorbed. Therefore, the difference in sorption capacity of NM and DCF on MWCS-1.0 is attributed to higher polar surface area that leads to higher sorption capacity of NM compared to DCF.

3.6. Thermodynamics studies and mechanism of adsorption

The values of ΔH° and ΔS° were evaluated from the slope and intercept, respectively, of the linear plot of Ln(K) versus $1/T$ as extensively described in the literature [13,15,16,19–21,28,31]. The R^2_{adj} values of the plots are *ca* 0.99, an indication that the ΔH° and ΔS° values are accurate. Supplementary Table 5 presents the thermodynamic parameters.

The adsorbent-adsorbate interaction can be classified into either chemical or physical adsorption using the magnitude of enthalpy. The physical adsorption is <40 kJ mol^{-1} [36]. The enthalpy values of adsorption of DCF and NM pharmaceuticals using MWCS-1.0

[1] Calculator Plugins of the MarvinSketch Version 14.9.22.0 software, ChemAxon (http://www.chemaxon.com), 2014, were used for structure property prediction and calculation of physical properties of the pharmaceuticals.

activated carbon correspond to physical adsorption [36]. ΔH° has negative values–an indication that the interactions of both pharmaceuticals with the adsorbent are exothermic. The adsorption of DCF and NM onto MWCS-1.0 is spontaneous, and a favorable process because ΔG° has negative values. The negative values of ΔS° imply a decrease in the randomness at the solid/liquid interface, which should be a higher order of the interaction of the pharmaceuticals with the activated carbon.

Based on the combined data of characterization of MWCS-1.0 as well as the kinetic, equilibrium and thermodynamic studies, it is possible to suggest mechanisms for adsorption of DCF and NM onto MWCS-1.0 adsorbent. The polar parts of pharmaceuticals interact with the main functional groups of the adsorbent (OH, C=O, COOH) as depicted in Fig. 5. In addition to this, there exist other interactions between the adsorbent and the aromatic groups of the pharmaceuticals as previously stated [21,28,29]. The magnitude of adsorption enthalpy concurs with the physical forces of attractions that exist between the adsorbent and pharmaceuticals.

3.7. Simulated hospital effluents

MWCS-1.0 was utilized for treatment of two simulated hospital effluents (see Supplementary Table 1). The spectra of the simulated effluents before and after treatment with MWCS-1.0 were recorded between 190 and 500 nm on UV–vis spectrophotometer (Fig. 6). The percentage of the mixture of pharmaceuticals removed from the effluent depends on the area under the absorption band. MWCS-1.0 impressively removed 95.58% of effluent A and 91.14% of effluent B. These results indicate that MWCS-1.0 is a very good adsorbent for removal of pharmaceuticals from hospital effluents.

4. Conclusion

Powdered cocoa shell, inorganic components were mixed at a room temperature. The mixture was heated in a microwave oven using a pyrolysis time lower than 10 min of heating. The microwave-assisted pyrolysis was obtained in a single stage because the inorganic components are microwave conductors. The CSC-1.0, CSC-1.5 and CSC-2.0 (carbon materials) were treated with HCl to obtain MWCS-1.0, MWCS-1.5 and MWCS-2.0, respectively. The acidification process leached the inorganics from the carbonaceous matrix. MWCS-1.0 showed highest adsorption capacity for the removal of DCF and NM pharmaceuticals from aqueous solutions. At optimum pH 7.0 (DCF) and 8.0 (NM), the removal of the pharmaceuticals from aqueous solutions attained equilibrium at 223.14 min (DCF) and 45.46 min (NM). The general order kinetic model best described the adsorption process. The maximum amounts (Q_{max}) of DCF and NM pharmaceuticals adsorbed at 25 °C are 63.47 and 74.81 mg g^{-1} for DCF and NM, respectively. The MWCS-1.0 showed reliable outcome in the treatment of simulated hospital effluents; it effectively removed 95.58% of a mixture of different organic compounds in a medium with high salinity and sugar contents.

Acknowledgments

The authors are grateful to the National Council for Scientific and Technological Development (CNPq, Brazil), the Coordination of Improvement of Higher Education Personnel (CAPES, Brazil) and the Academy of Sciences for Developing World (TWAS, Italy) for financial support and sponsorship. We are also grateful to Center of Electron Microscopy (CME-UFRGS) for the use of the SEM microscope. We thank Chemaxon for giving an Academic Research license for the software MarvinSketch Version 14.9.22.0, (http://www.chemaxon.com), 2014 used for comparisons of the pharmaceuticals properties.

Appendix A. Supplementary data

Supplementary data associated with this article can be found, in the online version, at http://dx.doi.org/10.1016/j.jhazmat.2015.02.026.

References

[1] S. Rovani, M.T. Censi, S.L. Pedrotti Jr., E.C. Lima, R. Cataluña, A.N. Fernandes, Development of a new adsorbent from agro-industrial waste and its potential use in endocrine disruptor compound removal, J. Hazard. Mater. 271 (2014) 311–320.
[2] E.S. Rigobello, A.D.B. Dantas, L.D. Bernardo, E.M. Vieira, Removal of diclofenac by conventional drinking water treatment processes and granular activated carbon filtration, Chemosphere 92 (2013) 184–191.
[3] K. Dutta, M.Y. Lee, W.W.P. Lai, C.H. Lee, A.Y.C. Lin, C.F. Lin, J.G. Lin, Removal of pharmaceuticals and organic matter from municipal wastewater using two-stage anaerobic fluidized membrane bioreactor, Bioresour. Technol. 165 (2014) 42–49.
[4] M. Alidina, D. Li, M. Ouf, J.E. Drewes, Role of primary substrate composition and concentration on attenuation of trace organic chemicals in managed aquifer recharge systems, J. Environ. Manage. 144 (2014) 58–66.
[5] S.W. Nam, D.J. Choi, S.K. Kim, N. Her, K.D. Zoh, Adsorption characteristics of selected hydrophilic and hydrophobic micropollutants in water using activated carbon, J. Hazard. Mater. 270 (2014) 144–152.
[6] J.L. Sotelo, G. Ovejero, A. Rodríguez, S. Álvarez, J. Galán, J. García, Competitive adsorption studies of caffeine and diclofenac aqueous solutions by activated carbon, Chem. Eng. J. 240 (2014) 443–453.
[7] M.F.N. Secondes, V. Naddeo, V. Belgiorno, F. Ballesteros Jr., Removal of emerging contaminants by simultaneous application of membrane ultrafiltration, activated carbon adsorption, and ultrasound irradiation, J. Hazard. Mater. 264 (2014) 342–349.
[8] D. Krajišnik, A. Daković, A. Malenović, M. Milojević-Rakić, V. Dondur, Ž. Radulović, J. Milić, Investigation of adsorption and release of diclofenac sodium by modified zeolites composites, Appl. Clay Sci. 83–84 (2013) 322–326.
[9] N. Suriyanon, P. Punyapalakul, C. Ngamcharussrivichai, Mechanistic study of diclofenac and carbamazepine adsorption on functionalized silica-based porous materials, Chem. Eng. J. 214 (2013) 208–218.
[10] B. Royer, N.F. Cardoso, E.C. Lima, V.S.O. Ruiz, T.R. Macedo, C. Airoldi, Organofunctionalized kenyaite for dye removal from aqueous solution, J.Colloid Interface Sci. 336 (2009) 398–405.
[11] B. Royer, N.F. Cardoso, E.C. Lima, T.R. Macedo, C. Airoldi, A useful organofunctionalized layered silicate for textile dye removal, J. Hazard. Mater. 181 (2010) 366–374.
[12] C. Jung, J. Park, K.H. Lim, S. Park, J. Heo, N. Her, J. Oh, S. Yun, Y. Yoon, Adsorption of selected endocrine disrupting compounds and pharmaceuticals on activated biochars, J. Hazard. Mater. 263 (2013) 702–710.
[13] G.L. Dotto, E.C. Lima, L.A.A. Pinto, Biosorption of food dyes onto *Spirulina platensis* nanoparticles: equilibrium isotherm and thermodynamic analysis, Bioresour. Technol. 103 (2012) 123–130.
[14] L.G. da Silva, R. Ruggiero, P.M. Gontijo, R.B. Pinto, B. Royer, E.C. Lima, T.H.M. Fernandes, T. Calvete, Adsorption of Brilliant Red 2BE dye from water solutions by a chemically modified sugarcane bagasse lignin, Chem. Eng. J. 168 (2011) 620–628.
[15] D.C. dos Santos, M.A. Adebayo, S.F.P. Pereira, L.D.T. Prola, R. Cataluña, E.C. Lima, C. Saucier, C.R. Gally, F.M. Machado, New carbon composite adsorbents for the removal of textile dyes from aqueous solutions: kinetic, equilibrium, and thermodynamic studies, Kor. J. Chem. Eng. 31 (2014) 1470–1479.
[16] M.A. Adebayo, L.D.T. Prola, E.C. Lima, M.J. Puchana-Rosero, R. Cataluña, C. Saucier, C.S. Umpierres, J.C.P. Vaghetti, L.G. da Silva, R. Ruggiero, Adsorption of procion blue MX-R dye from aqueous solutions by lignin chemically modified with aluminum and manganese, J. Hazard. Mater. 268 (2014) 43–50.
[17] H. Marsh, F.R. Reinoso, Activated Carbon, Elsevier, Amsterdam, 2006.
[18] F.R. Reinoso, A.S. Escribano, Porous carbons in adsorption and catalysis, in: H.S. Nalwa (Ed.), Handbook of Surfaces and Interfaces of Materials, vol. 5, Biomolecules, Biointerfaces, and Applications, Academic Press, Oxford, 2001.
[19] T. Calvete, E.C. Lima, N.F. Cardoso, J.C.P. Vaghetti, S.L.P. Dias, F.A. Pavan, Application of carbon adsorbents prepared from Brazilian-pine fruit shell for the removal of reactive orange 16 from aqueous solution: kinetic, equilibrium, and thermodynamic studies, J. Environ. Manage. 91 (2010) 1695–1706.
[20] N.F. Cardoso, R.B. Pinto, E.C. Lima, T. Calvete, C.V. Amavisca, B. Royer, M.L. Cunha, T.H.M. Fernandes, I.S. Pinto, Removal of Remazol black B textile dye from aqueous solution by adsorption, Desalination 269 (2011) 92–103.
[21] M.C. Ribas, M.A. Adebayo, L.D.T. Prola, E.C. Lima, R. Cataluña, L.A. Feris, M.J. Puchana-Rosero, F.M. Machado, F.A. Pavan, T. Calvete, Comparison of a homemade cocoa shell activated carbon with commercial activated carbon for the removal of reactive violet 5 dye from aqueous solutions, Chem. Eng. J. 248 (2014) 315–326.

[22] R.G. Pereira, C.M. Veloso, N.M. da Silva, L.F. de Sousa, R.C.F. Bonomo, A.O. de Souza, M.O.G. Souza, R.C.I. Fontan, Preparation of activated carbons from cocoa shells and siriguela seeds using H_3PO_4 and $ZnCl_2$ as activating agents for BSA and α-lactalbumin adsorption, Fuel Process. Technol. 126 (2014) 476–486.
[23] A. Fisal, W.M.A.W. Daud, M.A. Ahmad, R. Radzi, Using cocoa (*Theobroma cacao*) shell-based activated carbon to remove 4-nitrophenol from aqueous solution: kinetics and equilibrium studies, Chem. Eng. J 178 (2011) 461–467.
[24] V.O. Njoku, K.Y. Foo, M. Asif, B.H. Hameed, Preparation of activated carbons from rambutan (*Nephelium lappaceum*) peel by microwave-induced KOH activation for acid yellow 17 dye adsorption, Chem. Eng. J. 250 (2014) 198–204.
[25] Z.Z. Qiang, X.H. Ying, C. Srinivasakannan, P.J. Hui, Z.L. Bo, Utilization of Crofton weed for preparation of activated carbon by microwave induced CO_2 activation, Chem. Eng. Process. 82 (2014) 1–8.
[26] N. Ferrera-Lorenzo, E. Fuente, I. Suárez-Ruiz, B. Ruiz, KOH activated carbon from conventional and microwave heating system of a macroalgae waste from the agar–agar industry, Fuel Process. Technol. 121 (2014) 25–31.
[27] R.H. Hesas, W.M.A.W. Daud, J.N. Sahu, A.A. Niya, The effects of a microwave heating method on the production of activated carbon from agricultural waste: a review, J. Anal. Appl. Pyrol. 100 (2013) 1–11.
[28] L.D.T. Prola, E. Acayanka, E.C. Lima, C.S. Umpierres, J.C.P. Vaghetti, W.O. Santos, S. Laminsi, P.T. Njifon, Comparison of *Jatropha curcas* shells in natural form and treated by non-thermal plasma as biosorbents for removal of Reactive Red 120 textile dye from aqueous solution, Ind. Crop. Prod. 46 (2013) 328–340.
[29] L.D.T. Prola, E. Acayanka, E.C. Lima, C. Bestetti, W.O. Santos, F.A. Pavan, S.L.P. Dias, C.R.T. Tarley, Application of aqai stalks as biosorbent for the removal of Evans Blue and Vilmafix Red RR-2B dyes from aqueous solutions, Desalin. Water Treat. 51 (2013) 4582–4592.
[30] Y. Liu, L. Shen, A general rate law equation for biosorption, Biochem. Eng. J. 38 (2008) 390–394.
[31] W.S. Alencar, E.C. Lima, B. Royer, B.D. dos Santos, T. Calvete, E.A. da Silva, C.N. Alves, Application of aqai stalks as biosorbents for the removal of the dye Procion Blue MX-R from aqueous solution, Sep. Sci. Technol. 47 (2012) 513–526.
[32] D. Angin, Production and characterization of activated carbon from sour cherry stones by zinc chloride, Fuel 115 (2014) 804–811.
[33] R.G. Newton, J.H. Sharp, The chemical composition of lime plasters, Cem. Concr. Res. 17 (1987) 77–80.
[34] R. Chang, General Chemistry: The Essential Concepts, 6th ed., McGraw-Hill, New York, 2011.
[35] Calculator Plugins of the software MarvinSketch Version 14.9.22.0, ChemAxon (http://www.chemaxon.com), 2014, were used for structure property prediction and calculation of physical properties of the pharmaceuticals.
[36] C.L. Sun, C.S. Wang, Estimation on the intramolecular hydrogen-bonding energies in proteins and peptides by the analytic potential energy function, J. Mol. Struct. 956 (2010) 38–43.

Supplementary Material

Supplementary Table 1. Chemical composition of simulated hospital effluents.

	Concentration (mg L^{-1})	
Pharmaceuticals	Effluent A	Effluent B
Diclofenac	20.0	40.0
Nimesulide	20.0	40.0
Amoxicillin	10.0	20.0
Acetyl salicylic acid	10.0	20.0
Sugars		
Saccharose	50.0	70.0
Glucose	30.0	40.0
Other Organic component		
Urea	20.0	40.0
Inorganic components		
Ammonium phosphate	20.0	30.0
Ammonium chloride	20.0	30.0
Sodium sulfate	50.0	70.0
Sodium chloride	50.0	70.0
Sodium carbonate	50.0	70.0
Sodium acetate	20.0	30.0
Magnesium carbonate	50.0	70.0
Potassium nitrate	10.0	20.0
pH*	8.0	8.0

*pH of hospital effluents.

Supplementary Table 2. FTIR vibrational bands of CSC-1.0 and MWCS-1.0. Assignments are based on literature [1,13-16,19-21].

Band (cm^{-1})	
CSC-1.0	**Assignments**
3515	O-H stretch
1547	Rings mode of aromatic
1406	CH_2 bending
995	C-O stretch of alcohols or Si-O stretch of silicates
665	CH out of plane bends of aromatic rings
MWCS-1.0	
3451	O-H stretch
1632	Rings mode of aromatic, carboxyl groups
1099	C-O stretch of alcohols, phenols
799	CH out of plane bends of aromatic rings

Supplementary Table 3. Kinetic parameters of DCF and NM pharmaceuticals adsorption onto MWCS-1.0. Conditions: temperature, 298 K; pH, 7.0 for DCF and pH 8.0 for NM; mass of adsorbent, 50.0 mg.

	Diclofenac		**Nimesulide**	
	100.0 mg L^{-1}	150.0 mg L^{-1}	100.0 mg L^{-1}	150.0 mg L^{-1}
Pseudo-first-order				
k_1 (min^{-1})	0.1357	0.04465	0.3121	0.3136
q_e (mg g^{-1})	37.33	45.72	38.07	54.78
$t_{1/2}$ (min)	5.11	15.52	2.22	2.21
R^2_{adj}	0.9617	0.9711	0.9787	0.9780
SD (mg g^{-1})	1.806	2.344	1.292	1.888
Pseudo-second-order				
k_2 (g mg^{-1} min^{-1})	$6.495.10^{-3}$	$1.272.10^{-3}$	0.01881	0.01310
q_e (mg g^{-1})	38.96	49.66	39.03	56.16
$t_{1/2}$ (min)	3.95	15.84	1.36	1.36
R^2_{adj}	0.9991	0.9991	0.9982	0.9979
SD (mg g^{-1})	0.2792	0.4087	0.3757	0.5814
General order				
k_N [min^{-1}.(g $mg^{-1})^{n-1}$]	$3.043.10^{-3}$	$3.489.10^{-4}$	$3.508.10^{-3}$	$1.505.10^{-3}$
q_e (mg g^{-1})	39.52	51.63	39.84	57.49
n	2.240	2.335	2.628	2.710
$t_{1/2}$ (min)	3.77	16.90	0.91	0.86
R^2_{adj}	0.9997	0.9998	0.9997	0.9997
SD (mg g^{-1})	0.1574	0.1808	0.1576	0.2295

Supplementary Table 4. Isotherm parameters of DCF and NM adsorption using MWCS-1.0. Conditions: pH, 7.0 and 8.0 for DCF and NM, respectively; adsorbent mass, 50.0 mg; contact time, 240 min for DCF and 60 min for NM.

	25°C	30°C	35°C	40°C	45°C	50°C
Diclofenac						
Langmuir						
Q_{max} (mg g^{-1})	56.30	54.10	50.90	48.73	46.45	44.22
K_L (L mg^{-1})	1.310	0.9406	0.8696	0.7595	0.6317	0.5443
R^2_{adj}	0.9780	0.9830	0.9762	0.9778	0.9775	0.9808
SD (mg g^{-1})	2.406	1.967	2.231	2.130	2.089	1.838
Freudlich						
K_F (mg g^{-1} (mg $L^{-1})^{-1/n_F}$)	34.70	33.04	30.14	26.92	24.25	22.21
n_F	8.576	8.602	8.019	7.246	6.689	6.339
R^2_{adj}	0.9797	0.9823	0.9772	0.9755	0.9704	0.9706
SD (mg g^{-1})	2.315	2.004	2.180	2.239	2.394	2.273
Liu						
Q_{max} (mg g^{-1})	63.47	60.77	57.87	55.01	52.25	49.61
K_g (L mg^{-1})	1.131	0.8961	0.7231	0.5881	0.4779	0.4117
n_L	0.4926	0.5098	0.5185	0.5435	0.5712	0.5917
R^2_{adj}	0.9999	0.9999	0.9998	0.9998	0.9998	0.9999
SD (mg g^{-1})	0.1651	0.1809	0.1793	0.1800	0.1889	0.1280
Nimesulide						
Langmuir						
Q_{max} (mg g^{-1})	68.53	64.49	62.32	60.51	47.44	45.37
K_L (L mg^{-1})	1.084	1.134	1.034	0.7942	1.368	1.057
R^2_{adj}	0.9902	0.9821	0.9827	0.9849	0.9534	0.9569
SD(mg g^{-1})	1.765	2.326	2.301	2.076	2.853	2.602
Freudlich						
K_F (mg g^{-1} (mg $L^{-1})^{-1/n_F}$)	47.72	42.75	38.28	35.99	30.47	28.35
n_F	11.22	9.732	8.403	8.027	9.044	8.616
R^2_{adj}	0.9883	0.9813	0.9756	0.9720	0.9939	0.9934
SD (mg g^{-1})	1.927	2.376	2.733	2.827	1.032	1.015
Liu						
Q_{max} (mg g^{-1})	74.81	71.68	68.71	65.89	62.68	59.97
K_g (L mg^{-1})	1.518	1.215	0.9700	0.7735	0.6497	0.5072
n_L	0.5291	0.5243	0.5584	0.6058	0.3223	0.3406
R^2_{adj}	0.9998	0.9998	0.9998	0.9998	0.9998	0.9999
SD (mg g^{-1})	0.2641	0.2522	0.2539	0.2359	0.1991	0.1531

Supplementary Table 5. Thermodynamic parameters of DCF and NM adsorption onto MWCS-1.0. Conditions: pH, 7.0 and 8.0 for DCF and NM, respectively; adsorbent mass, 50.0 mg; contact time, 240 min for DCF and 60 min for NM. The values of K_g were converted to S.I. units using the molecular weight of the pharmaceuticals.

	Temperature (K)					
	298	303	308	313	318	323
DFC						
K_g (L mol^{-1})	$3.60.10^5$	$2.85.10^5$	$2.30.10^5$	$1.87.10^5$	$1.52.10^5$	$1.31.10^5$
ΔG (kJ mol^{-1})	-31.70	-31.64	-31.61	-31.59	-31.55	-31.64
$\Delta H°$ (kJ mol^{-1})	-32.71	-	-	-	-	-
$\Delta S°$ (J K^{-1} mol^{-1})	-3.49	-	-	-	-	-
R^2_{adj}	0.9980					
NM						
K_g (L mol^{-1})	$4.68.10^5$	$3.74.10^5$	$2.99.10^5$	$2.38.10^5$	$2.00.10^5$	$1.56.10^5$
ΔG (kJ mol^{-1})	-32.35	-32.33	-32.29	-32.22	-32.28	-32.12
$\Delta H°$ (kJ mol^{-1})	-34.69	-	-	-	-	-
$\Delta S°$ (J K^{-1} mol^{-1})	-7.81	-	-	-	-	-
R^2_{adj}	0.9983					

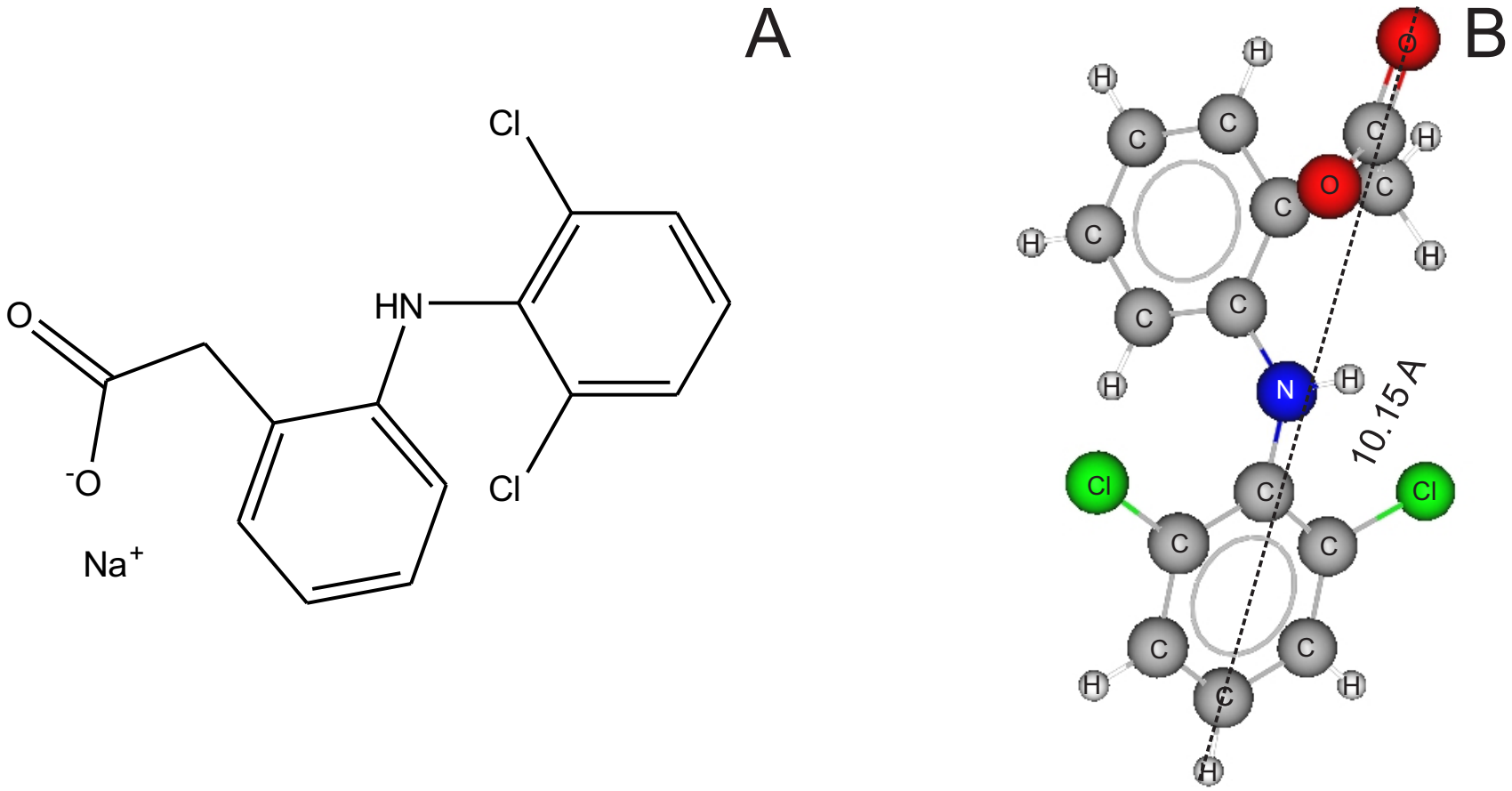

Supplementary Fig 1: (A) Structural formula of DCF; (B) Optimized three-dimensional structural formula of DCF. The dimensions of the chemical molecule was calculated using MarvinSketch version 14.9.22.0 Van der Waals surface area = 359.64 A^2 (pH 4.0-14.0); Polar surface area 52.16 A^2 (pH 4.0-14.0); Dipole Moment 19.21 Debye.

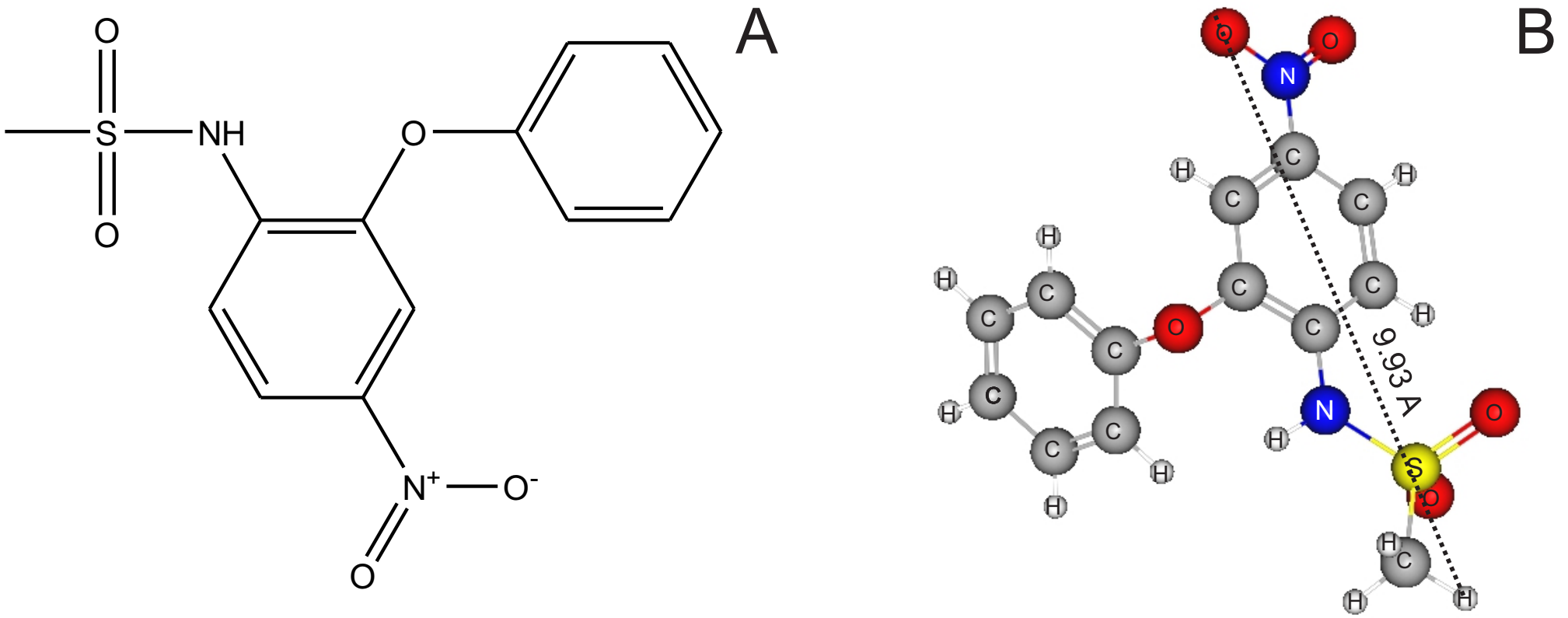

Supplementary Fig 2: (A) Structural formula of NM; (B) Optimized three-dimensional structural formula of NM. The dimensions of the chemical molecule was calculated using MarvinSketch version 14.9.22.0 Van der Waals surface area = 406.46 A^2 (pH 7.0-14.0); Polar surface area 104.12 A^2 (pH 7.0-14.0); Dipole Moment 19.21 Debye.

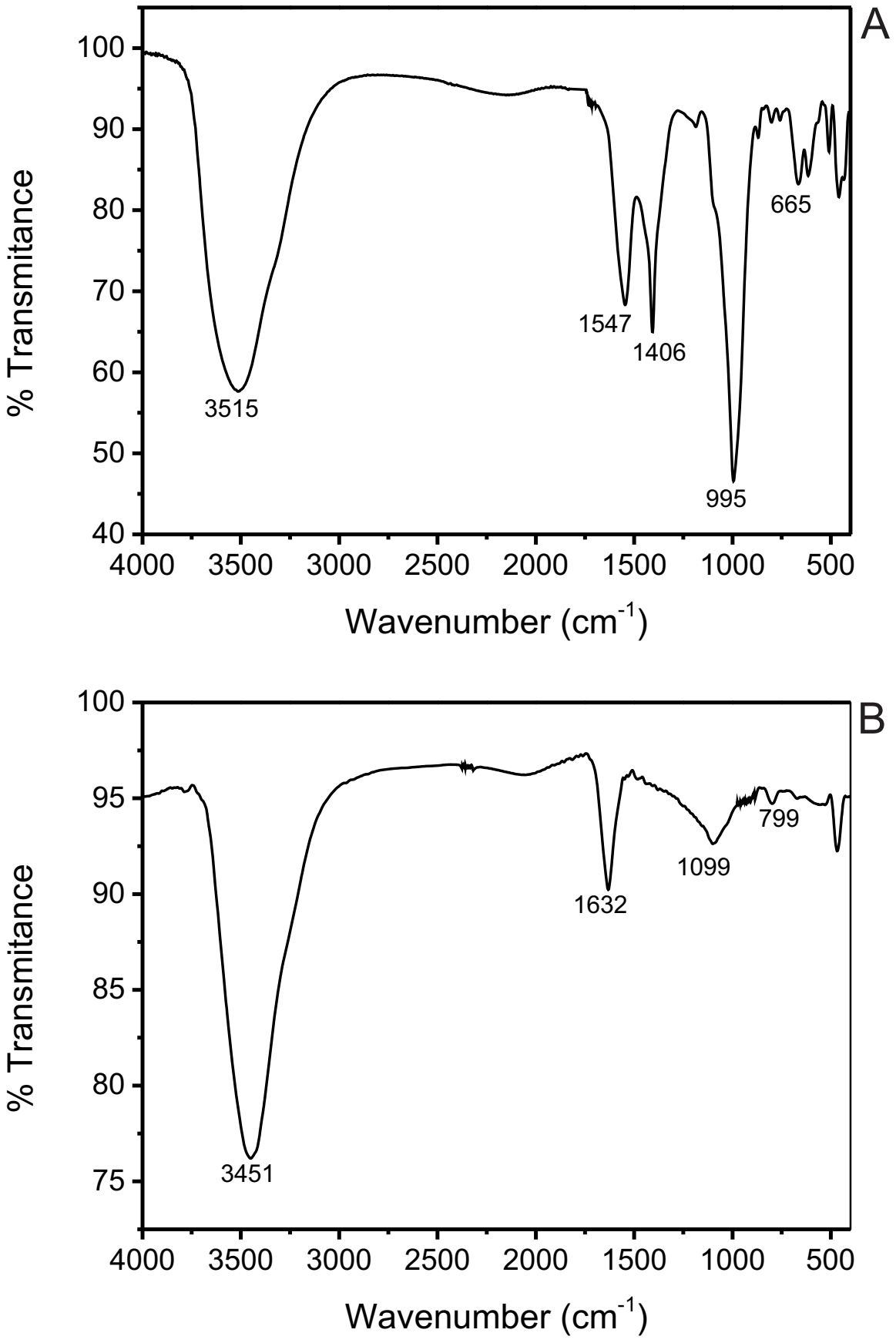

Supplementary Fig 3: FTIR of: A) CSC-1.0 and B) MWCS-1.0. The numbers are expressed in cm^{-1}.

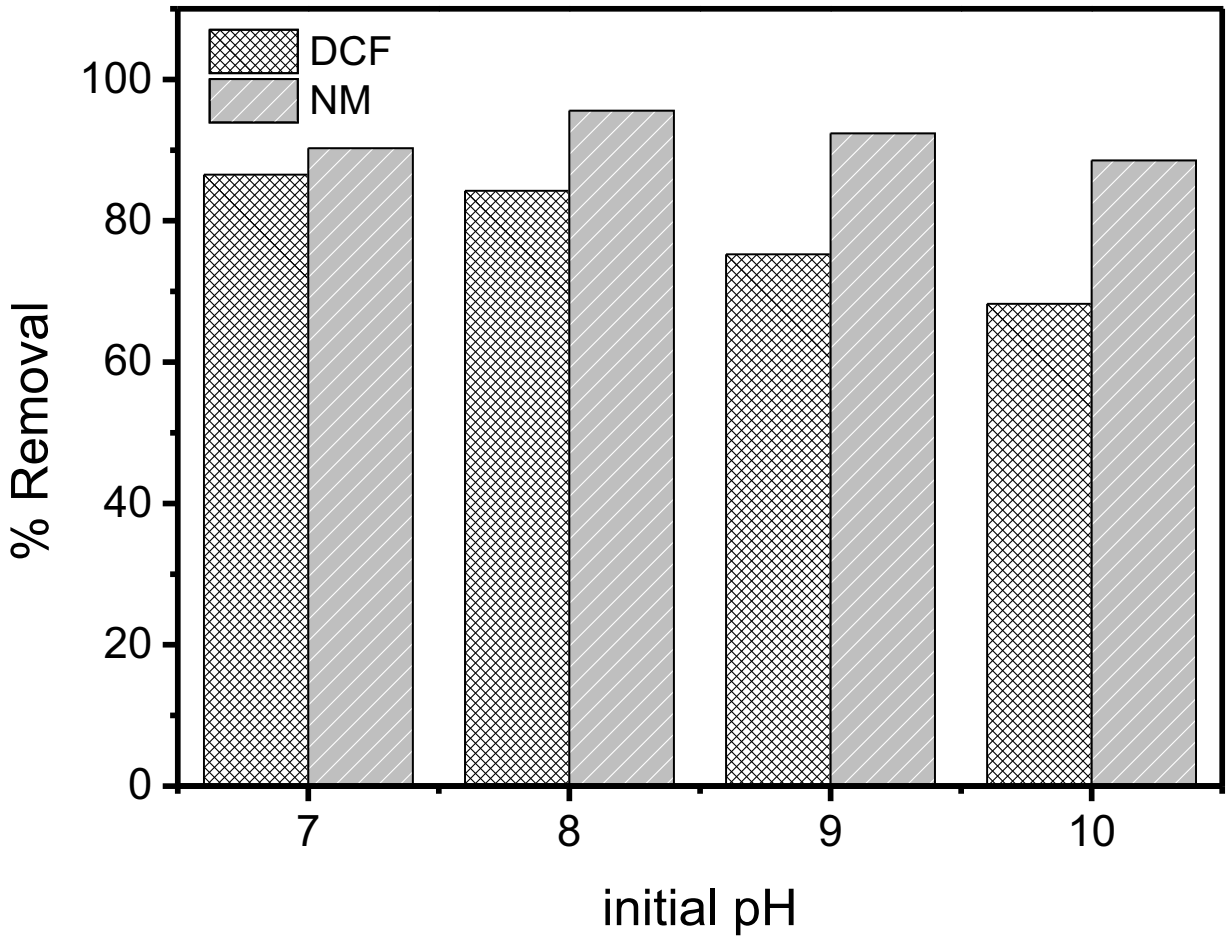

Supplementary Fig 4. Dependence of pH on the sorption capacity of DCF and NM pharmaceuticals on MWCS-1.0 adsorbent. Conditions: temperature, 25°C; adsorbent mass, 50.0 mg; pharmaceutical concentration, 150.0 mg L^{-1}.

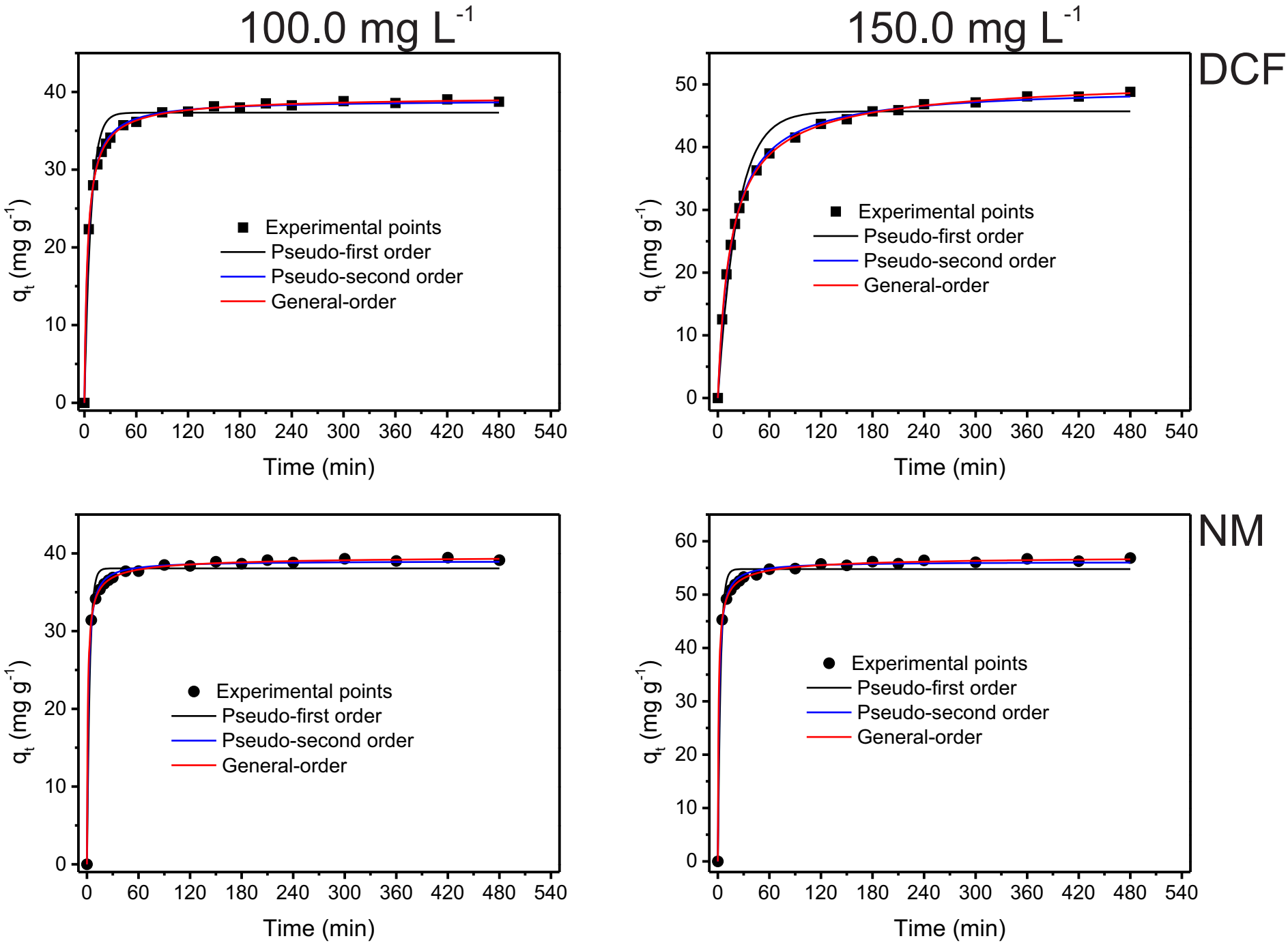

Supplementary Fig 5. Kinetic curves of adsorption of DCF and NM on MWCS-1.0. Conditions: initial pH, 7.0; temperature, 25°C; adsorbent mass, 50.0 mg.

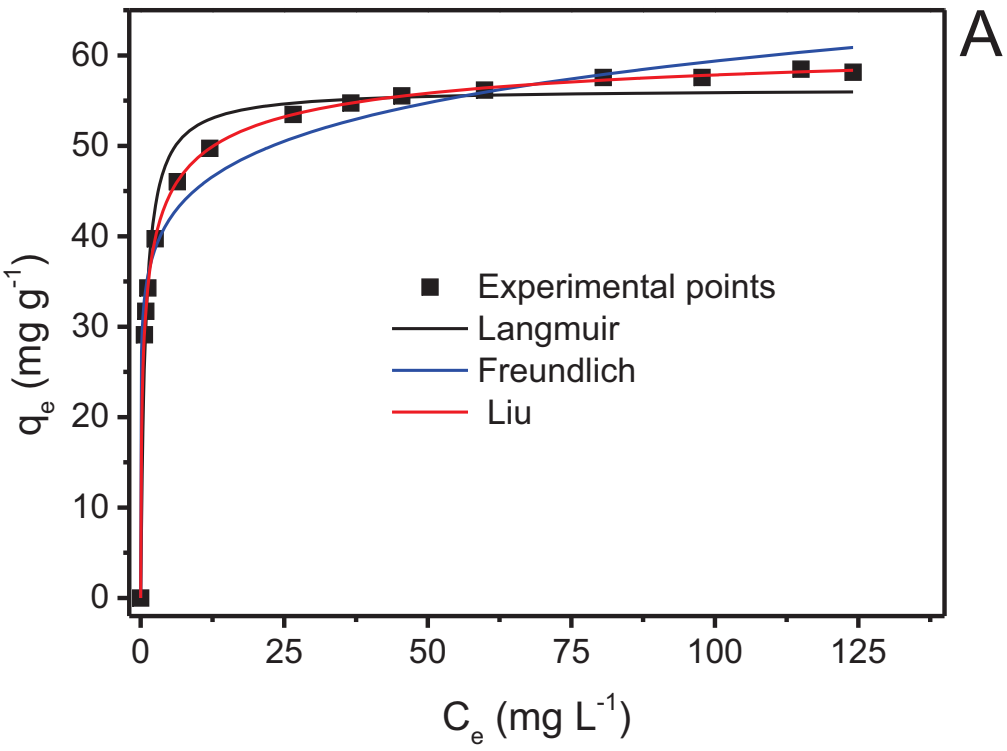

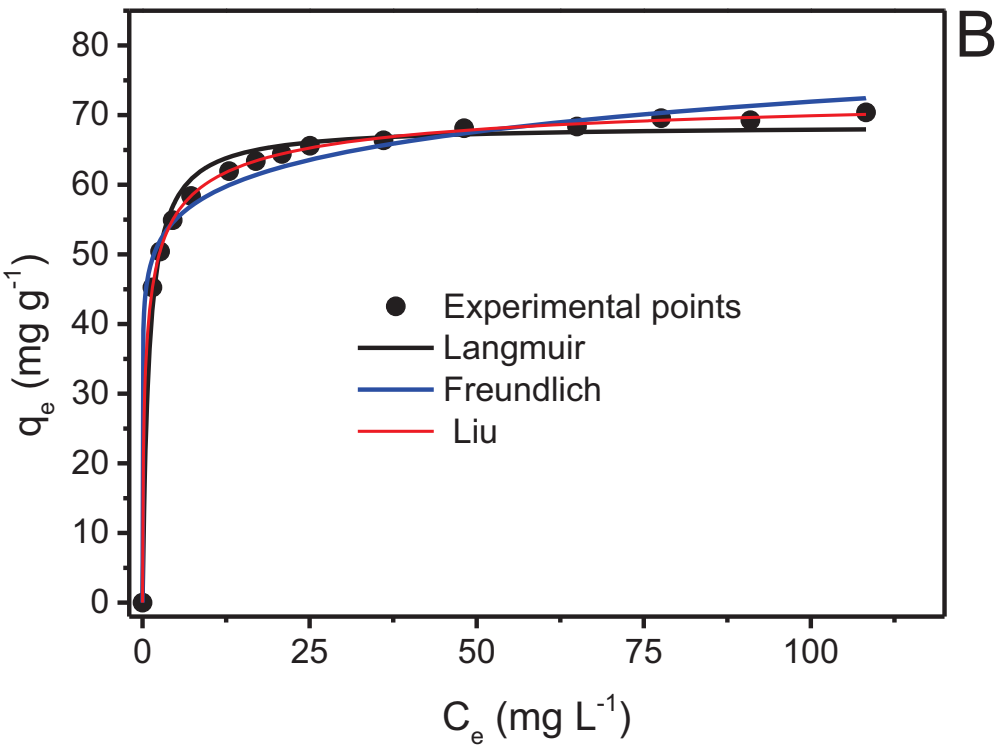

Supplementary Fig. 6. Isothermal curves of **A)** DCF and **B)** NM pharmaceuticals on MWCS at 25°C. Conditions: pH, 7.0 and 8.0 for DCF and NM, respectively; adsorbent mass, 50.0 mg; contact time, 240 min for DCF and 60 min for NM.

APÊNDICE 3

Environ Sci Pollut Res (2017) 24:5918–5932
DOI 10.1007/s11356-016-8304-7

RESEARCH ARTICLE

Efficient removal of amoxicillin and paracetamol from aqueous solutions using magnetic activated carbon

Caroline Saucier[1] · P. Karthickeyan[2] · V. Ranjithkumar[2] · Eder C. Lima[1] · Glaydson S. dos Reis[1,3] · Irineu A. S. de Brum[3]

Received: 30 November 2016 / Accepted: 19 December 2016 / Published online: 7 January 2017

Abstract Activated carbon (AC)/$CoFe_2O_4$ nanocomposites, MAC-1 and MAC-2, were prepared by a simple pyrolytic method using a mixture of iron(III)/cobalt(II) benzoates and iron(III)/cobalt(II) oxalates, respectively, and were used as efficient adsorbents for the removal of amoxicillin (AMX) and paracetamol (PCT) of aqueous effluents. The synthesized nanocomposites were characterized by X-ray diffraction (XRD), Fourier transform infrared spectroscopy (FT-IR), vibrating sample magnetometry (VSM), scanning electron microscopy (SEM), energy dispersive X-ray spectroscopy (EDX) and transmission electron microscopy (TEM). The sizes of cobalt ferrite nanoparticles formed from benzoates of iron(III)/cobalt(II) and oxalates of iron(III)/cobalt(II) precursors were in the ranges of 5–80 and 6–27 nm, respectively. The saturation magnetization (M_s), remanence (M_r) and coercivity (H_c) of the MAC-2 nanocomposites were found to be 3.07 emu g^{-1}, 1.36 emu g^{-1} and 762.49 Oe; for MAC-1, they were 0.2989 emu g^{-1}, 0.0466 emu g^{-1} and 456.82 Oe. The adsorption kinetics and isotherm studies were investigated, and the results showed that the as-prepared nanocomposites MAC-1 and MAC-2 could be utilized as an efficient, magnetically separable adsorbent for environmental cleanup. The maximum sorption capacities obtained were 280.9 and 444.2 mg g^{-1} of AMX for MAC-1 and MAC-2, respectively, and 215.1 and 399.9 mg g^{-1} of PCT using MAC-1 and MAC-2, respectively. Both adsorbents were successfully used for simulated hospital effluents, removing at least 93.00 and 96.77% for MAC-1 and MAC-2, respectively, of a mixture of nine pharmaceuticals with high concentrations of sugars, organic components and saline concentrations.

Keywords Carbon nanocomposites · Magnetic properties · Adsorption · Amoxicillin · Paracetamol

Responsible editor: Guilherme L. Dotto

Electronic supplementary material The online version of this article (doi:10.1007/s11356-016-8304-7) contains supplementary material, which is available to authorized users.

✉ Glaydson S. dos Reis
glaydsonambiental@mail.com; glaydson.simoes@ufrgs.br

[1] Institute of Chemistry, Federal University of Rio Grande do Sul (UFRGS), Porto Alegre, RS, Brazil

[2] Department of Chemistry, Kongunadu Arts and Science College, Coimbatore, Tamil Nadu 641029, India

[3] Department of Metallurgy, Federal University of Rio Grande do Sul (UFRGS), Engineering School, Av. Bento Gonçalves, 9500, Agronomia, Porto Alegre 91501-970, Brazil

Introduction

Nowadays, there is extensive attention around magnetic materials and their potential for many applications such as magnetic sensors, high-density recording media, catalysis (Freitas et al. 2016), the biomedical field (Gao et al. 2006), hydrogen storage (Yildirim and Ciraci 2005), energy storage (Sathiya et al. 2011), flocculation (Chen et al. 2016), coagulation (Santos et al. 2016) and adsorption of hazardous materials (Do et al. 2011; Mehdinia et al. 2015). Nanocomposites consisting of 3D transition metal oxides such as Fe_3O_4 (Ranjithkumar et al. 2014a), α-Fe_2O_3 (Ranjithkumar et al. 2014b), γ-Fe_2O_3 (Singh et al. 2012), MnO_2 (Hu et al. 2011), Mn_3O_4 (Ranjithkumar and Vairam 2012), CoO (Wang et al. 2014), Co_3O_4 (Tang et al. 2016) and NiO (Huang et al. 2007) and mixed metal oxides, $CoFe_2O_4$ (Ai et al. 2011) and $MnFe_2O_4$ (Podder and Majumder 2016), in a variety of structures at nanoscale, and carbon nanomaterials, such as activated carbon (Purkait et al. 2007), carbon nanotubes (Li and Yan

2016) and graphene (Wan et al. 2016), have synthesized successfully and have been investigated for environmental applications such as removal of hazardous chemicals and energy storage in the electrochemical field (Sathiya et al. 2011). Efficiencies of nanocomposite as adsorbents depend on their high surface area, pore volume and the size of their nanometal oxide in their carbon shell (dos Reis et al. 2016a; Gao et al. 2006).

Although the activated carbon may be one of the most commonly used adsorbent for cleaning up polluted effluents, adsorption of organic molecules using powder activated carbon has received less attention, because the separation of organic molecules adsorbed on carbon from an aqueous solution is a time-consuming process. In this connection, magnetic separation is an alternative technique for separating organic compounds adsorbed on magnetic carbon particles from adsorbate solution. Therefore, adsorbent combing nanotechnology and magnetic separation techniques would remove hazardous chemicals from an aqueous solution with good performance (Ai et al. 2011).

Researchers have developed magnetic carbon iron oxide nanoparticles from ferric nitrate in the presence of benzene vapours to improve the stability of nanocomposites. Ranjithkumar and Vairam (2012) and Ranjithkumar et al. (2014a, 2014b) successfully synthesized stable activated carbons embedded with Mn_3O_4, Fe_3O_4 and α-Fe_2O_3 from metal carboxylate by pyrolysis, respectively. Various researchers have developed mixed metal oxide (MMO) such as $MnFe_2O_4$ (Podder and Majumder 2016) and $CoFe_2O_4$ (Sun et al. 2010) for the applications of adsorption and energy storage among ferrites. $CoFe_2O_4$ is an interesting magnetic material due to its moderate saturation magnetization, mechanical hardness and excellent chemical and thermal stabilities (Tan et al. 2007a; Tan et al. 2007b).

All these features could turn magnetic adsorbents in excellent materials for adsorbing drugs in aqueous effluents. The fast growth of pharmaceutical industries led to large discharges of drugs into public waters. One concern with the fate of pharmaceutical compounds in the aquatic environment is enhanced because there is no information about the potential effects of many drugs on a diverse array of living organisms, although they are usually present at very low contents (μg L^{-1} or ng L^{-1}) in public waters (Estévez et al. 2005). The major problems with pharmaceutical wastes are that most drugs are polar substances with reasonable solubility in water Hu and Wang (2016), and usually, they are not completely removed by conventional water treatment plants (Eslami et al. 2016). Therefore, many used drugs have been detected in public waters (Bouabi et al. 2016; Zhang et al. 2016). Taking this into account, adsorption techniques using a suitable adsorbent could be a good option for the removal of pharmaceuticals from aqueous effluents (dos Reis et al. 2016a, 2016b, Rovani et al. 2014).

In this work, the magnetic activated carbon/$CoFe_2O_4$ from various metal carboxylate precursors was prepared and characterized. These magnetic nanoadsorbents were applied to remove pharmaceuticals from aqueous solutions and the results showed to be very efficient for amoxicillin (AMX) and paracetamol (PCT) removal from aqueous solutions.

Materials and methods

Reactants

Powdered activated carbon (AC) (with surface area 893.83 m^2 g^{-1}), iron(III) nitrate. Nonahydrate (99.98%), cobalt(II) nitrate hexahydrate (99.95%), oxalic acid (99.97%) and benzoic acid (99.95%) were purchased from Sigma-Aldrich Chemicals and used as such.

The AXL (99.50%) (see Supplementary Fig. 1) and PCT (99.70%) (see Supplementary Fig. 2) were furnished by MedChemexpress and used without purification.

Synthesis of metal carboxylates

Metal carboxylates, such as iron(III) benzoate, cobalt(II) benzoate, iron(III) oxalate and cobalt(II) oxalate, were prepared by mixing corresponding carboxylic acid with metal salts.

Ferric benzoate was prepared by mixing ferric nitrate (8.08 g in 80 mL of DD water) and benzoic acid solution (7.32 g in 60 mL of hot water) and stirring for 20 min in a magnetic stirrer (Ranjithkumar et al. 2014a). The yellow crystalline powder formed was filtered and dried after washing thoroughly with hot distilled water. The same method was adopted for three other carboxylates, and the details are given in Supplementary Table 1.

Preparation of magnetic activated carbons

The nanocomposites AC/$CoFe_2O_4$, magnetic activated carbon (MAC)-1 and MAC-2, were prepared by immersing 10 g of commercial activated carbon (AC) in a mixture of 50 mL of an aqueous solution of benzoate of cobalt(II)/iron(III) or a mixture of oxalate of cobalt(II)/iron(III), respectively, with constant stirring for 6 h at ambient temperature. The filtered and dried benzoate of cobalt(II)/iron(III) entrapped AC (AC1) and oxalate of cobalt(II)/iron(III) entrapped AC (AC2) were further heated at 600 °C (Ranjithkumar et al. 2014b) and 260 °C (Hermanek et al. 2006) (decomposition temperature of carboxylates), respectively, for 15 min in a muffle furnace to facilitate the insertion of $CoFe_2O_4$ nanoparticles in carbon matrix. The yields of the composites were about 35% (MAC-1) and 45% (MAC-2) after calcination.

Table 1 Chemical composition of simulated hospital effluents

	Concentration (mg L^{-1})	
	Effluent A	Effluent B
Pharmaceuticals		
Paracetamol	25.0	50.0
Amoxicillin	25.0	50.0
Diclofenac	10.0	20.0
Nimesulide	10.0	20.0
Acetyl salicylic acid	10.0	20.0
Sivastatin	10.0	20.0
Captopril	10.0	20.0
Propranolol hydrochloride	10.0	20.0
Enalapril maleate	10.0	20.0
Sugars		
Saccharose	30.0	50.0
Glucose	30.0	50.0
Other organic component		
Urea	20.0	40.0
Citric acid	20.0	40.0
Inorganic components		
Ammonium phosphate	20.0	30.0
Ammonium chloride	20.0	30.0
Sodium sulphate	50.0	70.0
Sodium chloride	50.0	70.0
Sodium carbonate	50.0	70.0
Sodium acetate	20.0	30.0
Magnesium carbonate	50.0	70.0
Potassium nitrate	10.0	20.0
pH	7.0	7.0

Characterization of magnetic activated carbons

Using FT-IR spectra (Thermo Nicolet, Avatar 370), the functional group vibrations of the nanocomposites were recorded. Embedded α-Fe_2O_3 nanoparticles in carbon matrix were identified by Powder XRD with Cu$K\alpha$ radiation (λ = 0.15418 nm) at 40 kV and 40 mA and recorded in the region of 2θ. A field emission scanning electron microscope (JEOL Model JSM—6390LV), an energy dispersive spectrometer (JEOL Model JED—2300) and a transmission electron microscope (TEM; Philips CM-200; operating voltages—20 to 200 kV; resolution—2.4 Ao) were used to confirm the morphology and structure of the magnetic nanocomposite. Magnetic nature of the nanocomposites was measured using a vibrating sample magnetometer (Lakeshore VSM 7410).

Adsorption studies

A 20.00-mL of AMX and PCT solution (70.00–2000.0 mg L^{-1}) was added to 30.0 mg of activated carbon in various 50.0-mL Falcon tubes at different pH values (4.0–10.0) (Prola et al. 2013; Calvete et al. 2010). The mixtures were agitated between 1 and 300 min inside a temperature-regulated shaker (150 rpm) between 25 and 50 °C. To separate the adsorbents from AMX and PCT solutions, the mixtures were centrifuged (10,000 rpm) for 5 min. After the batch adsorption experiment, the unadsorbed AMX and PCT were measured using a T90+ PG Instruments spectrophotometer at a maximum wavelength of 228 and 242.5 nm, respectively. The adsorbed quantity expressed as per unit mass of activated carbon and the percentages of adsorbates removed are given by Eqs. 1 and 2, respectively

$$q = \frac{(C_o - C_f)}{m} \times V \quad (1)$$

$$\%\text{Removal} = 100 \times \frac{(C_o - C_f)}{C_o} \quad (2)$$

q is the amount of AMX or PCT adsorbed by the adsorbent (mg g^{-1}); C_o is the initial adsorbate concentration in contact with the adsorbent (mg L^{-1}); C_f is the adsorbate concentration after the batch adsorption study (mg L^{-1}); m is the mass of adsorbent (g); and V is the volume of the adsorbate solution (L).

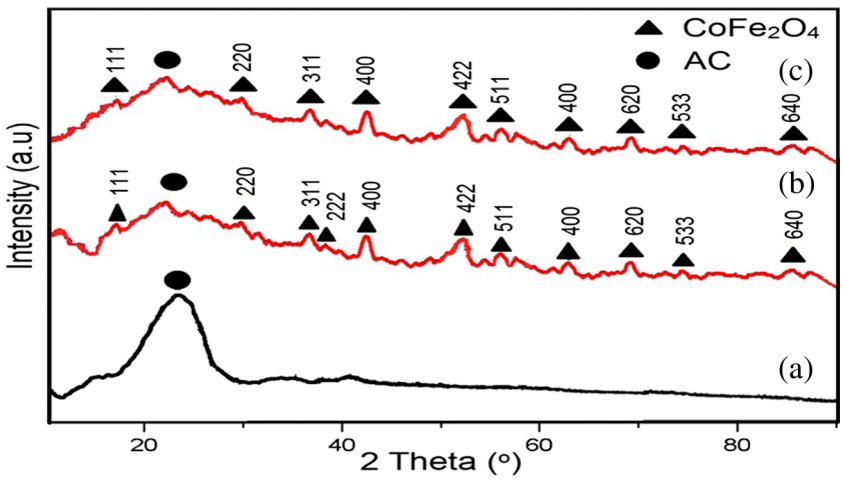

Fig. 1 Powder XRD patterns of *a* AC, *b* MAC-1 and *c* MAC-2

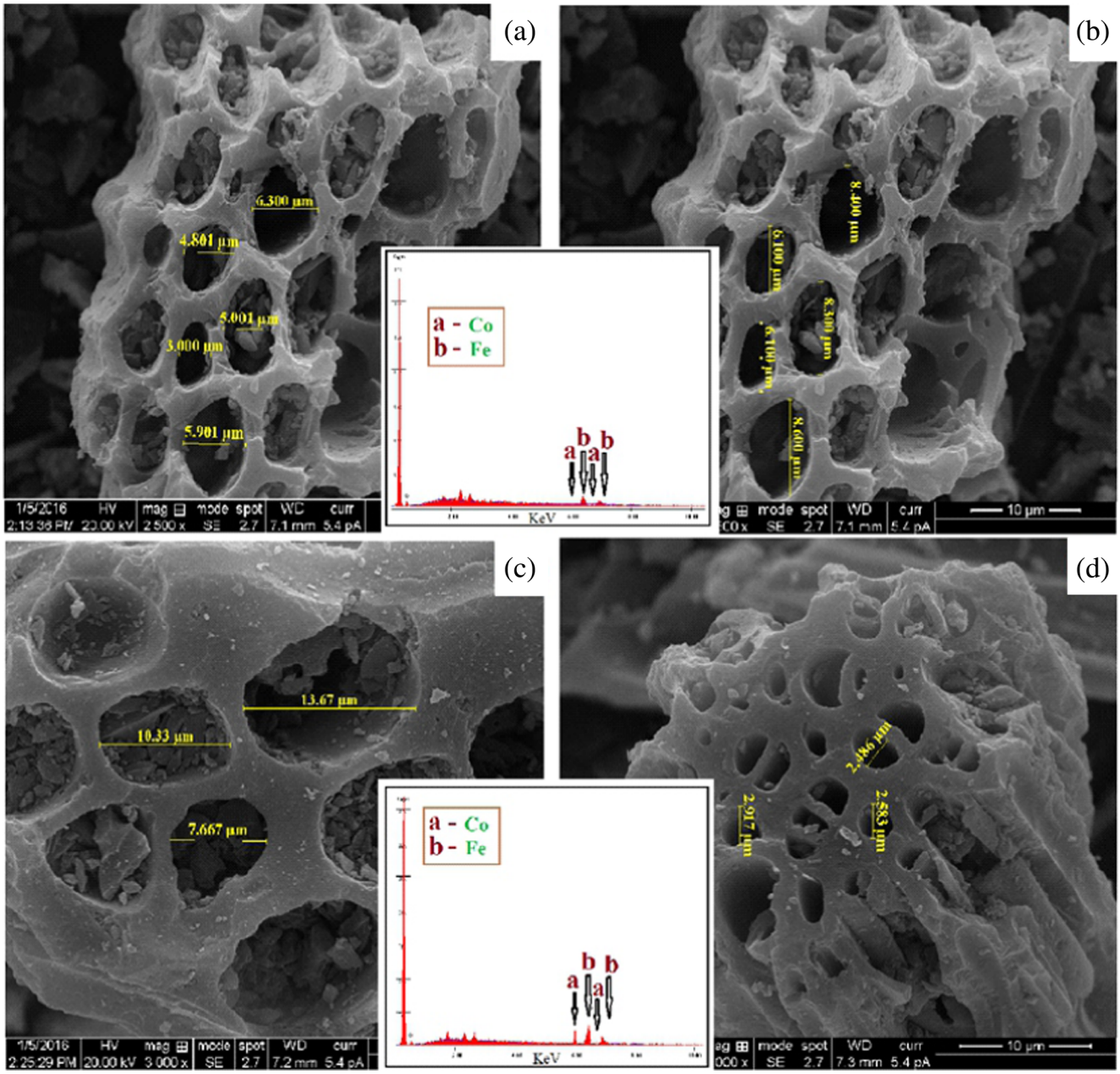

Fig. 2 SEM images of nanocomposites MAC-1 (**a**, **b**) and MAC-2 (**c**, **d**)

Quality control and evaluation of adsorption models

The quality assurance and statistical evaluation of the adsorption process and applied models are shown in supplementary material (Barbosa et al. 2000; Lima et al. 1999, 2002, 2003, 2015; Puchana-Rosero et al. 2016).

Kinetic models

Kinetic data was analysed using pseudo-first-order, pseudo-second-order and general order models (Cardoso et al. 2012). The mathematical relations of pseudo-first-order, pseudo-second-order and general

Table 2 Particle size, pore size and magnetic properties

	MAC-1	MAC-2
Particle size (nm)	5–80	6–27
Porous size (µm) H.L/V.L	3.0–6.3/6.1–8.4	7.0–13.0/2.0–2.9
H_c (Oe)	762.49	456.82
M_r (emu g^{-1})	1.36	0.0466
M_s (emu g^{-1})	3.07	0.2989

order kinetic models are shown in Eqs. 3, 4 and 5, respectively.

$$q_t = q_e \cdot [1 - \exp(-k_1 \times t)] \quad (3)$$

$$q_t = q_e - \frac{q_e}{[k_2(q_e) \times t + 1]} \quad (4)$$

$$q_t = q_e - \frac{q_e}{\left[k_N (q_e)^{n-1} \times t \times (n-1) + 1\right]^{1/1-n}} \quad (5)$$

where t is the contact time (min); q_t and q_e are the amounts of adsorbate adsorbed at time t and at the equilibrium, respectively (mg g^{-1}); k_1 is the pseudo-

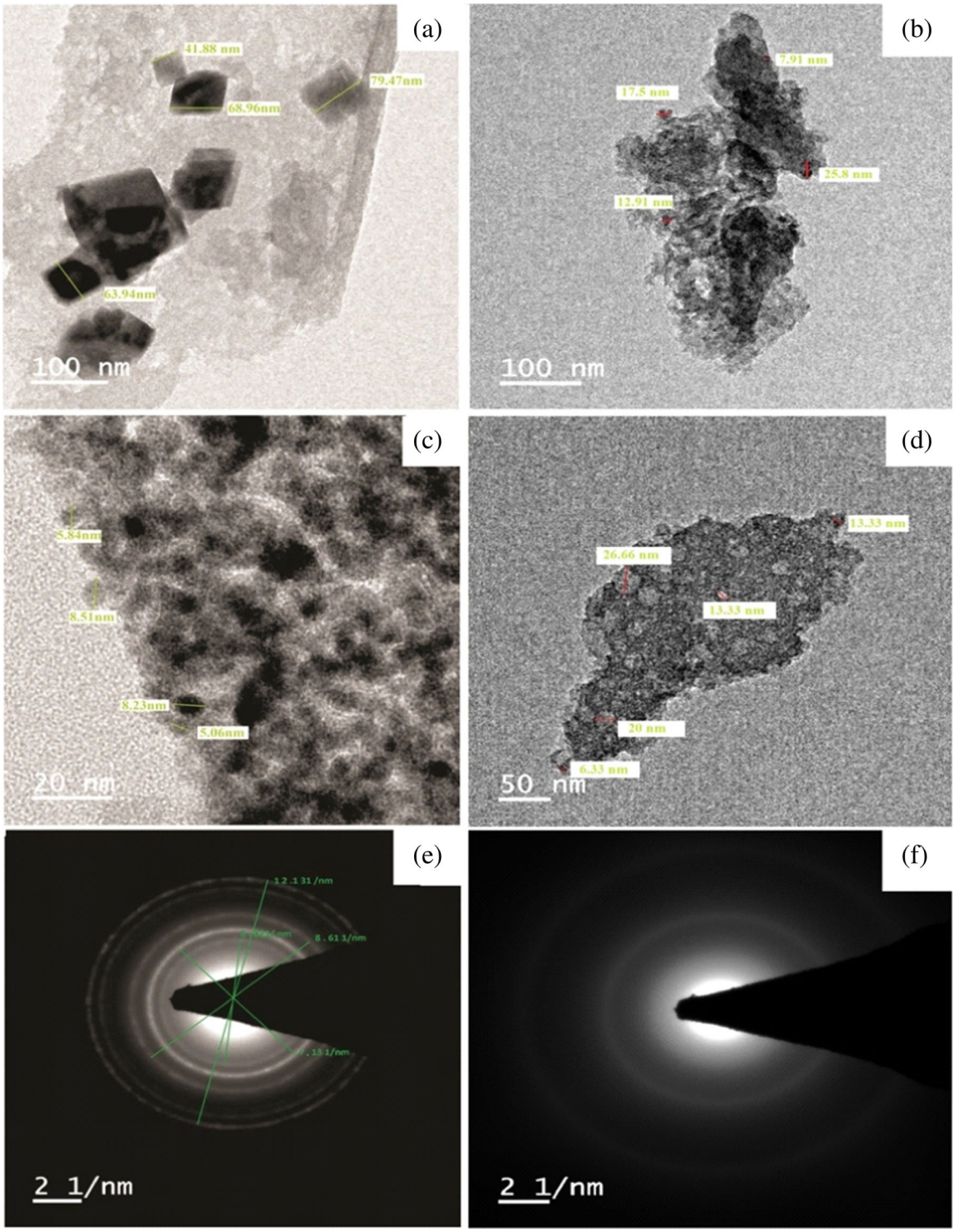

Fig. 3 TEM images of nanocomposites MAC-1 (**a**, **c**, **e**) and MAC-2 (**b**, **d**, **f**)

first-order rate constant (min^{-1}); k_2 is the pseudo-second-order rate constant (g mg^{-1} min^{-1}); k_N is the general order rate constant [h^{-1} (g $mg^{-1})^{n-1}$]; and n is the order of adsorption kinetics (dimensionless).

Equilibrium models

Langmuir, Freundlich and Liu models were employed for analysis of equilibrium data. Equations 6, 7 and 8 show the corresponding Langmuir, Freundlich and Liu models (Cardoso et al. 2012; Calvete et al. 2010; Lima et al. 2015).

$$q_e = \frac{Q_{\max} \times K_L \times C_e}{1 + K_L \times C_e} \quad (6)$$

$$q_e = K_F \times C_e^{1/n_F} \quad (7)$$

$$q_e = \frac{Q_{\max} \times (K_g \times C_e)^{n_L}}{1 + (K_g \times C_e)^{n_L}} \quad (8)$$

where q_e is the adsorbate amount adsorbed at equilibrium (mg g^{-1}); C_e is the adsorbate concentration at equilibrium (mg L^{-1}); $Q_{\max}$ is the maximum sorption capacity of the adsorbent (mg g^{-1}); K_L is the Langmuir equilibrium constant (L mg^{-1}); K_F is the Freundlich equilibrium constant [mg g^{-1}.(mg $L^{-1})^{-1/nF}$]; K_g is the Liu equilibrium constant (L mg^{-1}); and n_F and n_L are the exponents of the Freundlich and Liu models, respectively (n_F and n_L are dimensionless).

Simulated effluents

Two simulated hospital effluents, which consisted of nine pharmaceuticals, two sugars, two organic compounds and eight inorganics usually found in hospital effluents were prepared at pH 5.0. The compositions and concentrations of the components of the effluents are highlighted in Table 1. The purpose of using simulated effluents is to test the sorption capacities of the activated carbons for removal of mixtures of pharmaceutical compounds in a medium that contains high concentrations of salts and organic matter (Saucier et al. 2015a).

Results and discussion

Characterization of magnetic AC/MMOs nanocomposites

FT-IR

FT-IR spectra for the AC, the mixtures of cobalt(II) and iron(III) carboxylates, entrapped carbon (for benzoate AC1 and oxalate AC2) and nanocomposites MAC-1 and MAC-2 are shown in Supplementary Fig. 3a–e, respectively. All the spectra have characteristic peaks in the range of 1500–1570 and 2320–2370 cm^{-1} due to ν_{C-C} in AC and this corroborates that the carbon was not decomposed in the anocomposites MAC-1 and MAC-2 during the thermal decomposition of the carboxylates. The vibrations at 1502 and 1518 cm^{-1}

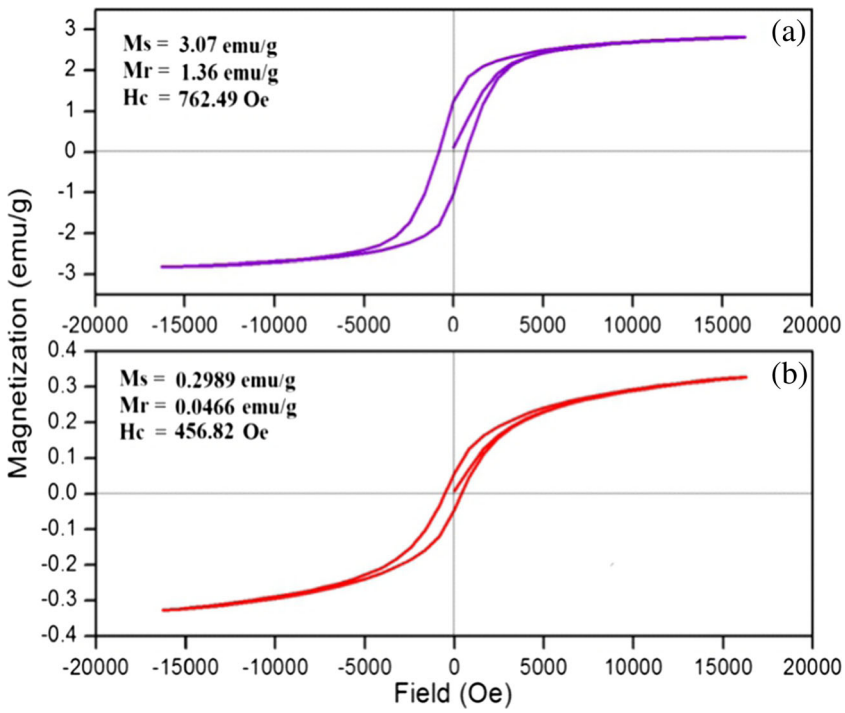

Fig. 4 Magnetization hysteresis loop of nanocomposites MAC-1 (**a**) and MAC-2 (**b**) at room temperature

correspond to asymmetric stretching of $^{a}\nu_{C=O}$, and the vibrations at 1311 and 1372 cm^{-1} are due to symmetric stretching of $^{a}\nu_{C=O}$ in the spectra of AC1 and AC2. The vibrational stretching noticed at 586 and 624 cm^{-1} (AC1) and 659 and 589 cm^{-1} (AC2) in Fig. 1b, c corresponds to ν_{M-O}. These observations indicate that all the metal carboxylates are entrapped by AC. The peak observed at 493 and 592 cm^{-1} in Fig. 1d, e are attributed to ν_{M-O} of $CoFe_2O_4$ in carbon. Moreover, untreated AC and both the nanocomposites (MAC-1 and MAC-2) do not show any carboxylate stretching in their spectra. This reveals that the entrapped metal carboxylates are well decomposed to $CoFe_2O_4$ in carbon shell. These results are similar to other reported values (Ranjithkumar and Vairam 2012).

PXRD

The wide-angle PXRD patterns of AC, MAC-1 and MAC-2 (Fig. 1) indicated activated carbon embedded with a face centred cubic spinal structure (JCPDS no. 22-1086). The medium diffraction peaks in the patterns of all the samples confirmed that the $CoFe_2O_4$ nanoparticles were encapsulated by carbon particles when compared with PXRD patterns of bare $CoFe_2O_4$ nanoparticles. Moreover, the broadness of the peaks of nanocomposites MAC-1 and MAC-2 in Fig. 1 shows that the metal carboxylates are thermally decomposed to nano sizes of cobalt ferrite particles in carbon shell. The rangees of average crystal size calculated according to the Scherrer's formula from the FWHM of the most intense peaks of MAC-1 and MAC-2 were 10–50 and 14–35 nm, respectively, and these values were closely supported with TEM results.

Scanning electron microscopy

SEM images of nanocomposites MAC-1, and MAC-2 are shown in Fig. 2, and their pores sizes are presented in Table 2. Figure 2 shows that white diminutive particles were well diffused in the pores of the carbon shell and were aggregated well because of its paramagnetic nature. From this study, we could not find exact size and shape of the MMO particles in carbon shell, which suggests that the presence of MMOs are in the nanosize range.

TEM

Detailed nanostructure and size investigations by selected area electron diffraction patterns of as-prepared nanocomposites MAC-1 and MAC-2 were conducted by TEM. The TEM images of nanocomposites MAC-1 and MAC-2 at different magnifications are shown in Fig. 3 and reveal that the distributions of nanoparticles are embedded in the carbon matrix. The light coloured region is activated carbon, whereas dark coloured spots indicate the presence of magnetic $CoFe_2O_4$ nanoparticles in the nanocomposites, due to uneven electron penetrability. The size range and shape of embedded $CoFe_2O_4$ nanoparticles are 5–80 nm with spherical and rectangular shapes and 6–27 nm with spherical shapes for MAC-1 and MAC-2, respectively, and this is in good agreement with the PXRD results. SAED pattern of nanocomposites is shown in Fig. 3e, f and confirms that the $CoFe_2O_4$ nanoparticles are highly crystalline for MAC-1 (Tan et al. 2007a; Tan et al. 2007b) and polycrystalline for MAC-2 (Huiqun et al. 2006).

Magnetic measurements

The magnetization measurements for the as-prepared MAC composites were carried out using a vibrating sample magnetometer at room temperature with an applied magnetic field of 15 kOe, which reveals that MAC composites exhibit a clearly hysteretic behaviour. The magnetic hysteresis loops of nanocomposites MAC-1 and MAC-2 are shown in Fig. 4a, b, respectively. Saturation magnetization (M_s), retentivity (M_r) and

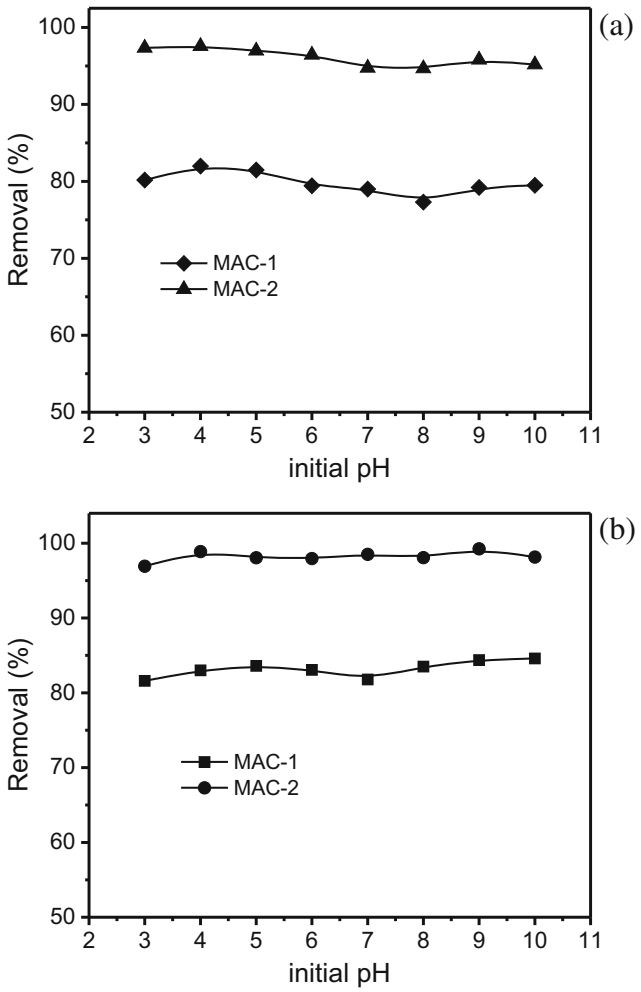

Fig. 5 Effect of initial pH on the adsorption of **a** AMX and **b** PCT. Initial adsorbate concentration was 200 mg L^{-1}, temperature was fixed at 25 °C, adsorbent dosage was 1.50 g L^{-1} and time of contact was fixed at 4 h

coercivity (H_c) of the nanocomposites MAC-1 and MAC-2 are given in Table 2. Magnetic measurement results show that there is a decrease in M_s and an increase in H_c of MAC composites when compared with bare $CoFe_2O_4$ [M_s-94 emu g^{-1} (Huiqun et al. 2006)]. This observation substantiates the fact that the metal oxide is embedded within the activated carbon. Furthermore, the magnetic nature of the nanoparticles is characterized by the ratio of remanence to saturation magnetization (M_r/M_s), and if the ratio is larger than 25%, it clearly indicates that the nanocomposites exhibit ferromagnetic behaviour, whereas, if the ratio is less than 25%, it reveals a formation of super-paramagnetic nature at room temperature. From this fact, MAC-1 and MAC-2 show ferromagnetic and super-paramagnetic behaviour, respectively, substantiating that the M_s value increases with the increase of decomposition temperature of carboxylate causes for increasing the size of MMOs {benzoate (600 °C) and oxalate (260 °C)} (Ehrensberger et al. 1999). These types of MACs have higher energy required for the adsorption process of hazardous chemical removal when compared with pure AC because the toxic chemicals adsorbed by the MACs are separated easily by magnetic separation, the filtration process can be avoided, and time consumption can be reduced.

Average particle size was calculated from Scherrer's formula; porous size (H.L and V.L) of carbon is shown in SEM image; and M_s saturation magnetization, H_c coercivity, M_r Remaan and magnetization were measured at room temperature using vibrating sample magnetometry (VSM).

Effect of pH of adsorbate solution

The pH of the solution is a key factor that could affect the adsorption of a drug on an adsorbent (Arya and Philip 2016; Saucier et al. 2015b; Shan et al. 2016; Zhao et al. 2016). The optimum pH of organics is a function of the chemical nature of adsorbent, and the solubility of the organics also depends on the pH of the solution. In this study, it was observed that for pH values 3–10 (see Fig. 5), the percentage of removal for AMX and PCT was practically constant within this pH interval. For this reason, all the solutions were prepared in pH 7.0, considering that a wastewater contaminated with these pharmaceuticals would need to be neutralized before being

Table 3 Kinetic parameters for adsorption of amoxilicin and paracetamol on magnetic activated carbons (MAC-1 and MAC-2)

	MAC-1		MAC-2		MAC-1		MAC-2	
	Amoxilicin		Amoxicilin		Paracetamol		Paracetamol	
	400 mg L^{-1}	800 mg L^{-1}	400 mg L^{-1}	800 mg L^{-1}	400 mg L^{-1}	800 mg L^{-1}	400 mg L^{-1}	800 mg L^{-1}
Pseudo-first-order								
k_f (min^{-1})	0.1235	0.1238	0.3232	0.3142	0.4062	0.4069	0.5139	0.4973
q_e (mg g^{-1})	153.5	174.5	210.4	254.9	150.1	163.6	198.9	240.5
$t_{1/2}$ (min)	5.613	5.597	2.145	2.206	1.706	1.704	1.349	1.394
$t_{0.95}$ (min)	24.26	24.19	9.270	9.536	7.374	7.363	5.829	6.024
R^2 adjusted	0.9965	0.9961	0.9898	0.9901	0.9999	0.9998	0.9996	0.9999
SD (mg g^{-1})	3.183	3.798	6.082	7.330	0.5083	0.6340	1.066	0.7270
Pseudo-second-order								
k_s (g mg^{-1} min^{-1})	$1.053.10^{-3}$	$9.299.10^{-4}$	0.002320	$1.851.10^{-3}$	0.004454	0.004105	0.004475	0.003515
q_e (mg g^{-1})	165.5	188.1	220.4	267.2	155.7	169.7	206.5	250.0
$t_{1/2}$ (min)	5.736	5.718	1.956	2.022	1.442	1.435	1.082	1.138
$t_{0.95}$ (min)	109.0	108.6	37.16	38.42	27.39	27.27	20.56	21.62
R^2 adjusted	0.9909	0.9913	0.9967	0.9964	0.9749	0.9754	0.9778	0.9768
SD (mg g^{-1})	5.123	5.671	3.481	4.425	6.611	7.107	8.161	10.17
General order								
k_N [min^{-1} (g mg^{-1})$^{n-1}$]	0.02952	0.02630	0.01706	0.01590	0.4213	0.4207	0.4253	0.4753
q_e (mg g^{-1})	156.2	177.7	215.3	260.7	150.0	163.5	199.0	240.5
n	1.309	1.326	1.601	1.586	0.9918	0.9926	1.041	1.009
$t_{1/2}$ (min)	5.494	5.475	2.000	2.066	1.710	1.706	1.333	1.390
$t_{0.95}$ (min)	35.05	35.73	19.54	19.73	7.319	7.313	6.040	6.074
R^2 adjusted	0.9999	0.9999	0.9999	0.9999	0.9999	0.9998	0.9997	0.9999
SD (mg g^{-1})	0.5145	0.5927	0.7197	0.8946	0.5093	0.6505	1.007	0.7422

Adsorbent dosage was fixed at 1.50 g L^{-1}, the initial pH of adsorbate solution was fixed at 7.0 and the temperature was fixed at 25 °C

released to the environment. For the treatment with adsorption, it is not necessary to make any pH adjustments if the solution of the effluent is within pH 3.0–10.0. This result also reveals that the mechanism of adsorption of AMX and PCT onto MAC-1 and MAC-2 should not be electrostatic attraction, since this mechanism is pH dependent as may be observed several times in the literature (Calvete et al. 2010; dos Santos et al. 2015).

Kinetics of adsorption

The kinetic of adsorption of AMX and PCT onto MAC-1 and MAC-2 adsorbents was explored using nonlinear pseudo-first-order, pseudo-second-order and general order kinetic models. The kinetic curves and fitting parameters of the models are shown in Supplementary Figs. 4 and 5 (AMX and PCT, respectively) and Table 3. The fitness of each model is explained using the values of standard deviation of residues (SD). Lower SD value indicates smaller disparity between theoretical and experimental q values. To compare the fitness of each model, the SD of each model was divided by the SD of the minimum value to obtain the SD ratio. For AMX, the general order kinetic model was the best kinetic isotherm model, showing that SD ratio values of pseudo-first-order kinetic models vary from 6.19 to 8.45, while those of pseudo-second-order model vary from 4.84 to 9.96. For PCT, the pseudo-first-order kinetic model presented the lowest SD ratio. For general order kinetic model, the SD ratio ranged from 0.94 to 1.03, and for the pseudo-second-order, the SD ratio ranged from 7.66 to 13.99. Although the pseudo-first-order model was slightly better, the general order kinetic model presented a suitable fitting for the kinetic data. Observing the n exponent of general order for PCT, the n values ranged from 0.9918 to 1.041. Therefore, it is evident that the order of the kinetics of adsorption is very close to pseudo-first-order, being that this kinetic model should explain the kinetics of adsorption for PCT.

The kinetic rate constants of the kinetic models have different units; it is difficult to compare the rates of the kinetics of adsorption of the different activated carbons. The half-life ($t_{1/2}$), which is the time to attain 50% of adsorption capacity at the equilibrium (q_e), was calculated by interpolation of the fitting kinetic curve. Also for AMX, it was observed that $t_{1/2}$ obtained with MAC-1 is about 2.7-fold higher than the $t_{1/2}$

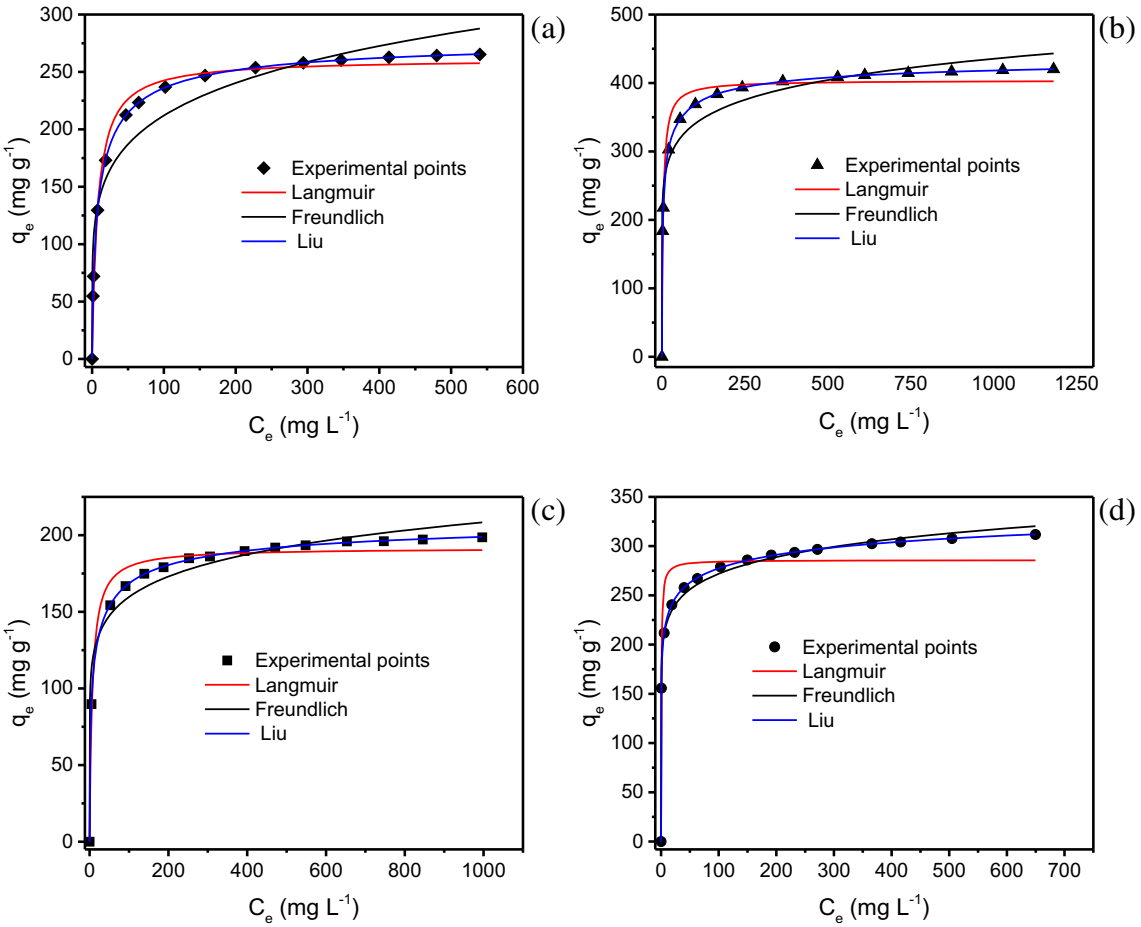

Fig. 6 Isotherms of adsorption of AMX (**a**, MAC-1; **b**, MAC-2) and PCT (**c**, MAC-1; **d**, MAC-2). The time of contact was fixed at 60 and 30 min for AMX and PCT, respectively. Temperature was fixed at 25 °C; adsorbent dosage was 1.50 g L^{-1}; initial pH was fixed at 7.0

obtained with MAC-2, based on the values of the general order kinetic model. For PCT, the $t_{1/2}$ obtained with MAC-1 is only 1.2-fold higher than the $t_{1/2}$ value obtained with MAC-2 (based on pseudo-first-order kinetic model). Therefore, it can be concluded that for AMX, the kinetics of adsorption of these pharmaceutical is faster in MAC-2. For PCT, the differences of kinetics are not so extreme.

In order to determine the time it takes to attain equilibrium, an interpolation was made on the general order and pseudo-first-order kinetic plots for AMX and PCT adsorption, respectively. In this calculation, the value of q_t was 95% of the maximum value of experimental q_e used. This time is defined as $t_{0.95}$. For AMX, the maximum $t_{0.95}$ was 35.73 and 19.73 min using MAC-1 and MAC-2, respectively (values based on general order kinetic model). For PCT, the maximum $t_{0.95}$ values were 7.374 and 6.024 min for MAC-1 and MAC-2, respectively. Based on these values, for further studies, the time of contact for AMX was fixed at 60 min both for

Table 4 Langmuir, Freundlich and Liu isotherm parameters for the adsorption of amoxicillin and paracetamol onto MC-1and MC-2

	AMX											
	MAC-1					MAC-2						
	25 °C	30 °C	35 °C	40 °C	45 °C	50 °C	25 °C	30 °C	35 °C	40 °C	45 °C	50 °C
Langmuir												
Q_{max} (mg g^{-1})	174.8	168.5	213.7	184.4	243.3	261.3	268.1	327.5	365.9	359.0	371.9	403.8
K_L (L mg^{-1})	0.1012	0.1795	0.09475	0.3335	0.1169	0.1296	0.1761	0.08497	0.1179	0.1533	0.2526	0.2631
R^2_{adj}	0.9489	0.9249	0.9765	0.9115	0.9813	0.9882	0.9479	0.9871	0.9954	0.9609	0.9579	0.9744
SD (mg g^{-1})	12.54	13.59	10.36	17.45	10.98	9.608	17.69	12.19	6.999	21.58	23.88	19.12
Freudlich												
K_F(mg g^{-1} (mg L^{-1})$^{-1/nF}$)	62.80	77.67	74.12	87.62	85.51	92.04	134.3	136.8	186.4	169.5	177.1	208.2
n_F	5.876	7.469	5.632	7.590	5.579	5.519	9.411	7.491	9.808	8.472	8.346	9.361
R^2_{adj}	0.9806	0.9894	0.9644	0.9862	0.9499	0.9361	0.9884	0.9396	0.9549	0.9572	0.9643	0.9643
SD (mg g^{-1})	7.734	5.104	12.76	6.895	17.99	22.32	8.351	26.33	21.82	22.58	21.98	22.58
Liu												
Q_{max} (mg g^{-1})	224.0	235.1	245.5	257.5	269.0	280.9	339.4	358.5	378.3	399.2	421.3	444.2
K_g (L mg^{-1})	0.04172	0.05037	0.06185	0.07246	0.08794	0.1053	0.08407	0.1015	0.1227	0.1474	0.1761	0.2142
n_L	0.4467	0.3379	0.5879	0.3158	0.6421	0.7048	0.3400	0.5382	0.7335	0.5031	0.4779	0.5179
R^2_{adj}	0.9998	0.9999	0.9999	0.9999	0.9999	0.9999	0.9999	0.9999	0.9999	0.9999	0.9999	0.9999
SD (mg g^{-1})	0.6939	0.4087	0.4377	0.3080	0.3757	0.3383	0.5244	0.2607	0.3573	0.3327	0.3531	0.2919
	PCT											
	MAC-1					MAC-2						
	25 °C	30 °C	35 °C	40 °C	45 °C	50 °C	25 °C	30 °C	35 °C	40 °C	45 °C	50 °C
Langmuir												
Q_{max} (mg g^{-1})	173.5	130.9	172.4	171.8	150.8	191.6	227.7	251.8	239.2	269.7	283.3	285.8
K_L (L mg^{-1})	0.03788	0.2348	0.07592	0.1011	0.1603	0.1495	0.3146	0.2492	2.549	0.9228	1.954	1.719
R^2_{adj}	0.9986	0.9410	0.9874	0.9814	0.9743	0.9781	0.9306	0.9585	0.9150	0.9144	0.9146	0.9210
SD (mg g^{-1})	1.969	10.13	6.395	7.939	6.407	7.940	17.63	14.47	20.93	24.91	25.12	23.01
Freudlich												
K_F (mg g^{-1} (mg L^{-1})$^{-1/nF}$)	48.07	53.61	55.01	61.02	85.66	93.77	112.8	128.3	137.4	144.3	160.9	285.8
n_F	4.995	6.499	5.326	5.852	11.12	8.648	7.880	8.453	9.586	8.580	9.273	1.719
R^2_{adj}	0.9119	0.9801	0.9434	0.9606	0.9979	0.9729	0.9864	0.9914	0.9916	0.9860	0.9868	0.9937
SD (mg g^{-1})	15.68	5.882	13.54	11.54	1.845	8.830	7.806	6.582	6.572	10.06	9.860	6.496
Liu												
Q_{max} (mg g^{-1})	170.1	177.0	187.7	195.3	204.9	215.1	302.2	322.0	341.9	359.7	378.7	399.9
K_g (L mg^{-1})	0.03858	0.04808	0.06149	0.07720	0.09164	0.1128	0.09690	0.1205	0.1537	0.1940	0.2429	0.3011
n_L	1.122	0.3916	0.6876	0.5512	0.2642	0.5307	0.3593	0.3611	0.2568	0.3086	0.2979	0.2402
R^2_{adj}	0.9997	0.9962	0.9998	0.9999	0.9999	0.9999	0.9999	0.9999	0.9999	0.9999	0.9999	1.0000
SD (mg g^{-1})	0.9648	2.568	0.8959	0.3815	0.4097	0.4594	0.5844	0.4325	0.4574	0.09297	0.4575	0.4819

Adsorbent dosage was fixed at 1.50 g L^{-1}, the initial pH of adsorbate solution was fixed at 7.0 and the temperature was fixed at 25 °C. The time of contact was fixed at 60 and 30 min for AMX and PCT, respectively

adsorbents and for PCT; the time of contact was fixed at 30 min for further experiments. This increase in the time of contact is to guarantee that the equilibrium would be in fact attained.

Equilibrium studies and mechanism of adsorption

The isothermal data were recorded between 25 and 50 °C using the following experimental conditions: contact times between the adsorbate and the adsorbent were fixed at 60.0 and 30 min for AMX and PCT, respectively; the initial pH of the adsorbate solutions were 7.0; and adsorbent dosages used were 1.5 g L^{-1}. Figure 6 shows the adsorption isotherms of AMX and PCT onto MAC-1 and MAC-2 at 25 °C. On the basis of R^2_{adj} and SD values (Lima et al. 2015), the Liu model best describes the equilibrium data of adsorption of AMX and PCT onto two magnetic activated carbon adsorbents at all experimental temperatures (Table 4). For AMX, the SD ratio values of the Langmuir model range from 18.07 to 56.66 (MC-1) and 19.59 to 67.63 (MC-2). The SD ratios of the Freundlich model ranged from 11.15 to 65.98 (MC-1) and 15.92 to 101.0 (MC-2). For PCT, the SD ratio for the Langmuir model ranged from 2.04 to 20.81 (MC-1) and 30.17 to 267.9 (MC-2). For the Freundlich isotherm, the SD ratio ranged from 2.29 to 30.25 (MC-1) and from 13.36 to 108.2 (MC-2). The SD ratio value of Liu isotherm model was 1.0, which signifies that the theoretical equilibrium adsorption capacity predicted by Liu model ($q_{,i,model}$) is closer to the experimental equilibrium adsorption capacity ($q_{,i,-experimental}$) (Prola et al. 2013; Ribas et al. 2014). The R^2_{adj} values equally agree with the SD values—a confirmation that the Liu isotherm model is the best isotherm model for the experimental data.

Analysing the Q_{max} values of the Liu isotherm, it was observed that for AMX, the maximum sorption capacity of MAC-2 was 54.6% higher, on average, than MAC-1, for temperatures from 25 to 50 °C. For PCT, the maximum sorption capacity based on the Liu isotherm was 82.8% for MAC-2 in relation to MAC-1. Therefore, the activated carbon modified with iron oxalate and cobalt oxalate (MAC-2) presented higher sorption capacity than the activated carbon modified with iron benzoate and cobalt benzoate (MAC-1). Decomposition temperature of carboxylates [benzoate/600 °C and oxalate/260 °C] plays a vital role in the alter of

Table 5 Thermodynamic parameters of the adsorption of amoxicillin and paracetamol onto MC-1 and MC-2 magnetic carbon adsorbents

	Temperature (K)					
	298	303	308	313	318	323
AMX–MAC-1						
K_g (L mol^{-1})	1.524×10^4	1.841×10^4	2.260×10^4	2.648×10^4	3.213×10^4	3.848×10^4
$\Delta G°$ (kJ mol^{-1})	−23.86	−24.74	−25.67	−26.50	−27.44	−28.35
$\Delta H°$ (kJ mol^{-1})	29.54	–	–	–	–	–
$\Delta S°$ (J K^{-1} mol^{-1})	179.2	–	–	–	–	–
R^2_{adj}	0.9991	–	–	–	–	–
AMX–MAC-2						
K_g (L mol^{-1})	3.072×10^4	3.710×10^4	4.483×10^4	5.386×10^4	6.435×10^4	7.826×10^4
$\Delta G°$ (kJ mol^{-1})	−25.60	−26.50	−27.43	−28.35	−29.27	−30.26
$\Delta H°$ (kJ mol^{-1})	29.77	–	–	–	–	–
$\Delta S°$ (J K^{-1} mol^{-1})	185.7	–	–	–	–	–
R^2_{adj}	0.9993	–	–	–	–	–
PCT–MAC-1						
K_g (L mol^{-1})	$5.831.10^3$	7.268×10^3	9.296×10^3	1.167×10^4	1.385×10^4	1.705×10^4
$\Delta G°$ (kJ mol^{-1})	−21.48	−22.40	−23.40	−24.37	−25.21	−26.17
$\Delta H°$ (kJ mol^{-1})	34.44	–	–	–	–	–
$\Delta S°$ (J K^{-1} mol^{-1})	187.7	–	–	–	–	–
R^2_{adj}	0.9983	–	–	–	–	–
PCT–MAC-2						
K_g (L mol^{-1})	$1.465.10^4$	1.821×10^4	2.323×10^4	2.933×10^4	3.672×10^4	4.551×10^4
$\Delta G°$ (kJ mol^{-1})	−23.77	−24.71	−25.74	−26.77	−27.79	−28.80
$\Delta H°$ (kJ mol^{-1})	36.61	–	–	–	–	–
$\Delta S°$ (J K^{-1} mol^{-1})	202.5	–	–	–	–	–
R^2_{adj}	0.9995	–	–	–	–	–

the nanosize of the metal oxides in the carbon matrix. Size ranges of the metal oxides in the nanocomposites, MAC-1 and MAC-2, were 5–80 and 6–27 nm, respectively, which are shown in TEM images, and this fact concludes that the nanosize of $CoFe_2O_4$ increases with the increase of decomposition temperature of metal carboxylates. Therefore, the adsorption capacity of MAC-2 is better than that of MAC-1.

Thermodynamic studies and mechanism of adsorption

Calculations from the slope and intercept of the linear plot of Ln(K) versus $1/T$ give $\Delta H°$ and $\Delta S°$ values, respectively, as extensively explained in the literature (Saucier et al. 2015a; dos Santos et al. 2015; Machado et al. 2012; Prola et al. 2013; Ribas et al. 2014). The R^2_{adj} values of the plots are ≥0.99, a measure of the reliability of the $\Delta H°$ and $\Delta S°$ values. Table 5 presents the thermodynamic parameters.

The interactions of adsorbents with the adsorbates can be grouped into two using the magnitude of enthalpy: chemical adsorption and physical adsorption. The enthalpy value of physical adsorption is <40 kJ mol^{-1}. The enthalpy values of adsorption of AMX and PCT onto the MAC-1 and MAC-2 adsorbents match their physical adsorption (Sun and Wang 2010). $\Delta H°$ has positive values, which signifies that the interactions of the adsorbents with AMX and PCT are endothermic. The adsorption of the two adsorbates onto two adsorbents are spontaneous and a favourable process because $\Delta G°$ values are negative. There was an increase in randomness at the solid/liquid interface because $\Delta S°$ has positive values. The molecules of the adsorbates were displaced from the bulk solution when it was adsorbed in the solid phase. Therefore, the entropy of the system increased (Kyzas et al. 2013; Travlou et al. 2013).

Based on the structure of the activated carbons and on the kinetic, equilibrium and thermodynamic data of adsorption, it is possible to propose a mechanism of adsorption of AMX and PCT onto the adsorbents. The interaction of the adsorbates with the magnetic activated carbons should be governed by van der Walls interactions (hydrophobic interactions, π–π stacking), hydrogen bonds and polar interactions of the oxygen and nitrogen groups of the adsorbate with the polar groups of the adsorbents (dos Reis et al. 2016a, 2016b; Gupta and Garg 2015; Kuyumcu et al. 2016; Pezoti et al. 2016; Villaescusa et al. 2011), as depicted in Fig. 7.

Simulated industrial effluents

In order to test the performance of MAC-1 and MAC-2 adsorbents on wastewater treatment, they were applied on two simulated hospital effluents (Table 1). As shown in Fig. 8, the spectra of the simulated effluents before and after treatment with the four activated carbons were recorded from 190 to 600 nm by UV–Vis spectrophotometer. The areas under the absorption bands give the percentages of the mixture of

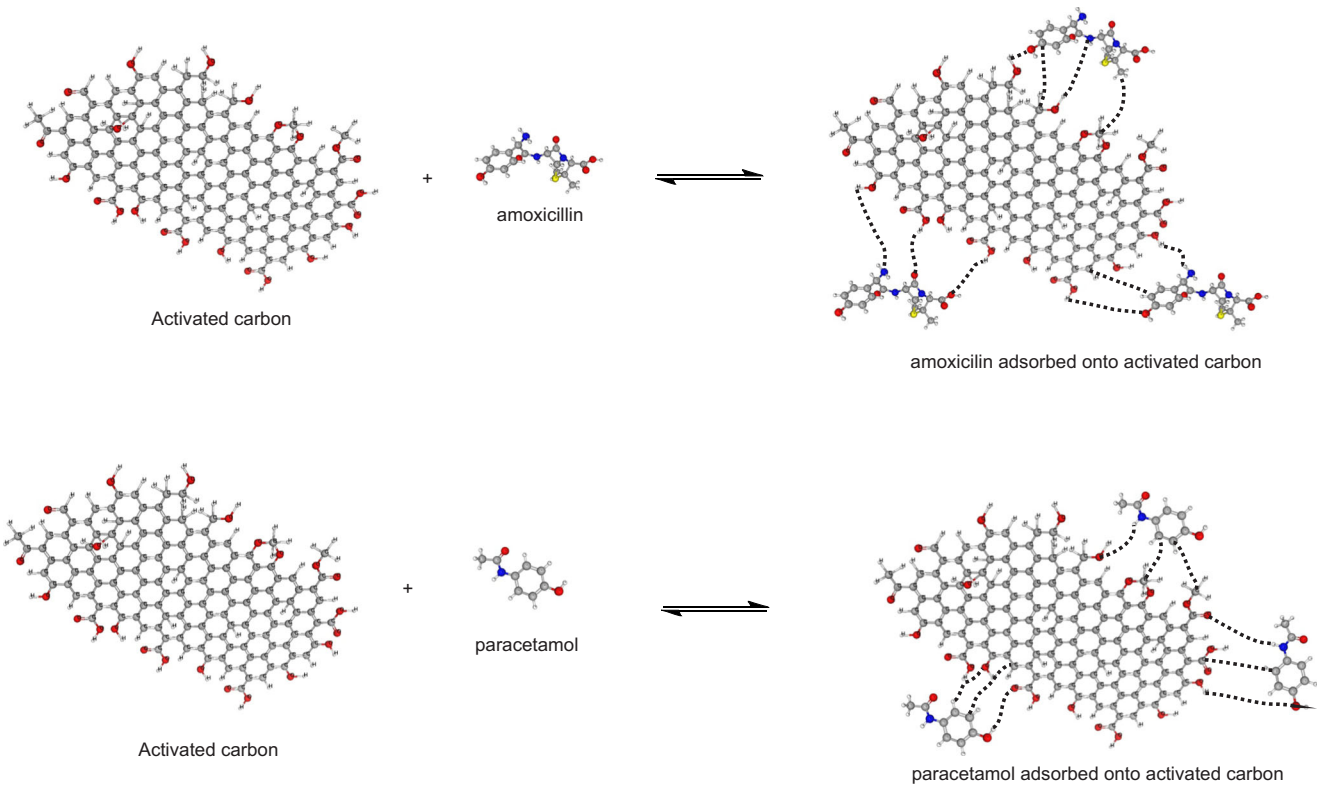

Fig. 7 Mechanism of adsorption of AMX and PCT onto magnetic activated carbon

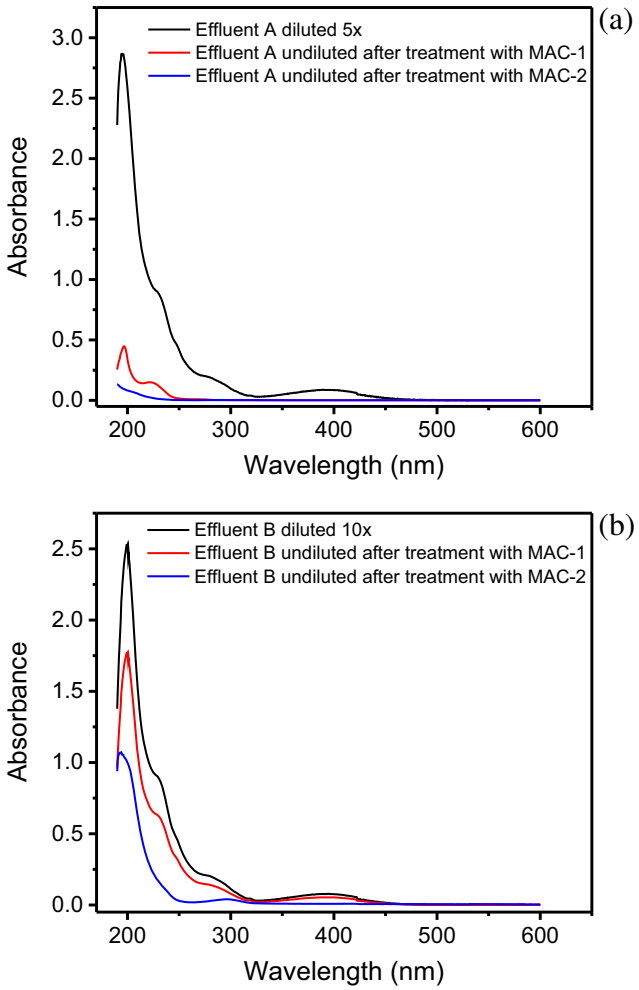

Fig. 8 Simulated effluents. **a** Effluent A. **b** Effluent B. For effluent composition, see Table 2

pharmaceuticals removed from the effluents. MAC-1 removed 97.95% (effluent A) and 93.00% (effluent B), while MAC-2 removed 99.41% (effluent A) and 96.77% (effluents B). The MAC-2 presented a slightly better performance for the treatment of simulated hospital effluents. These results are in agreement with the maximum sorption capacities discussed above.

Conclusion

Activated carbon(AC)/$CoFe_2O_4$ nanocomposites, MAC-1 and MAC-2, were prepared by a simple pyrolytic method using a mixture of benzoates of iron(III)/cobalt(II) and oxalates of iron(III)/cobalt(II), respectively, and they were used as adsorbents for the successful removal of amoxicillin (AMX) and paracetamol (PCT) of aqueous effluents. The synthesized nanocomposites were characterized by Fourier transform infrared spectroscopy (FT-IR), X-ray diffraction (XRD), scanning electron microscopy (SEM), energy dispersive X-ray spectroscopy (EDX), transmission electron microscopy (TEM) and vibrating sample magnetometry (VSM). The kinetics of adsorption was evaluated by using nonlinear pseudo-first-order, pseudo-second-order and general order kinetic models. For amoxicillin, the general order kinetic model was the best model that was adjusted to the experimental data, and for paracetamol, the nonlinear pseudo-first-order was the best fit kinetic model. The equilibrium data were also fit using the nonlinear Langmuir, Freundlich and Liu isotherm models. For both pharmaceuticals using the two adsorbents, the best fitting of the equilibrium data occurred for the Liu isotherm model. The enthalpy, entropy and Gibb's free energy of adsorption were each determined based on Liu isotherms from 298 to 323 K. Based on the structure of the activated carbons and on the kinetic, equilibrium and thermodynamic data of adsorption, it is possible to propose a mechanism of adsorption of AMX and PCT onto the adsorbents. The interaction of the adsorbates with the magnetic activated carbons should be governed by van der Walls interactions (hydrophobic interactions, π–π stacking), hydrogen bonds and polar interactions of the oxygen and nitrogen groups of the adsorbate with the polar groups of the adsorbents. Also, the MAC-1 and MAC-2 magnetic carbons were successfully used as adsorbents for treatment of simulated hospital effluents, removing at least 93.00% (MAC-1) and 96.77% (MAC-2) of a medium containing nine pharmaceuticals, two sugars, two organic substrates and eight inorganic contents that closely simulated hospital effluents.

Acknowledgements The authors thank the National Council for Scientific and Technological Development (CNPq, Brazil) and the Coordination of Improvement of Higher Education Personnel (CAPES, Brazil) for financial support, fellowships, grants and technical support. We also thank Chemaxon for giving an academic research licence for the Marvin Sketch software, version 16.11.1.0, (http://www.chemaxon.com), 2016 used for pharmaceutical physical–chemical properties. We also thank the Centre of Electron Microscopy (CME-UFRGS) for the use of the SEM microscope.

References

Ai L, Li M, Li L (2011) Adsorption of methylene blue from aqueous solution with activated carbon/cobalt ferrite/alginate composite beads: kinetics, isotherms, and thermodynamics. J Chem Eng Data 56:3475–3483

Arya V, Philip L (2016) Adsorption of pharmaceuticals in water using Fe_3O_4 coated polymer clay composite. Micropor Mesopor Mater 232:273–280

Barbosa F Jr, Lima EC, Krug FJ (2000) Determination of arsenic in sediment and soil slurries by electrothermal atomic absorption spectrometry using W-Rh permanent modifier. Analyst 125:2079–2083

Bouabi YE, Farahi A, Labjar N, Hajjaji SE, Bakasse M, Mhammedi MAE (2016) Square wave voltammetric determination of paracetamol at chitosan modified carbon paste electrode: application in natural water samples, commercial tablets and human urines. Mat Sci Eng C 58:70–77

Calvete T, Lima EC, Cardoso NF, Dias SLP, Ribeiro ES (2010) Removal of brilliant green dye from aqueous solutions using home made activated carbons. CLEAN—Soil Air Water 38:521–532

Cardoso NF, Lima EC, Royer B, Bach MV, Dotto GL, Pinto LAA, Calvete T (2012) Comparison of *Spirulina platensis* microalgae and commercial activated carbon as adsorbents for the removal of Reactive Red 120 dye from aqueous effluents. J Hazard Mater 241-242:146–153

Chen Y, Man Luo M, Wangfeng Cai W (2016) Influence of operating parameters on the performance of magnetic seeding flocculation. Environ Sci Pollut Res 23:2873–2881

Do MH, Phan NH, Nguyen TD, Pham TTS, Nguyen VK, Vu TTT, Nguyen TKP (2011) Activated carbon/Fe_3O_4 nanoparticle composite: fabrication, methyl orange removal and regeneration by hydrogen peroxide. Chemosphere 85:1269–1276

dos Reis GS, Sampaio CH, Lima EC, Wilhelm M (2016a) Preparation of novel adsorbents based on combinations of polysiloxanes and sewage sludge to remove pharmaceuticals from aqueous solutions. Colloids Surf A Physicochem Eng Asp 497:304–315

dos Reis GS, Mahbub MKB, Wilhelm M, Lima EC, Sampaio CH, Saucier C, Dias SLP (2016b) Activated carbon from sewage sludge for removal of sodium diclofenac and nimesulide from aqueous solutions. Korean J Chem Eng 33:3149–3161

dos Santos DC, Adebayo MA, Lima EC, Pereira SFP, Cataluña R, Saucier C, Thue PS, Machado FM (2015) Application of carbon composite adsorbents prepared from coffee waste and clay for the removal of reactive dyes from aqueous solutions. J Brazilian Chem Soc 26:924–938

Ehrensberger K, Schmalle H, Oswald H, Reller A (1999) Thermochemical reactivity of transition metal acetates and of a novel DMSO solvate of iron(II) acetate in molecular hydrogen. J Therm Anal Calorim 57:139–149

Eslami A, Asadi A, Meserghani M, Bahrami H (2016) Optimization of sonochemical degradation of amoxicillin by sulfate radicals in aqueous solution using response surface methodology (RSM). J Mol Liq 222:739–744

Estévez MC, Font H, Nichkova M, Salvador JP, Varela B, Baeza FS, Marco MP (2005) Immunochemical determination of pharmaceuticals and personal care products as emerging pollutants. In: Barceló D (ed) Emerging organic pollutants in waste waters and sludge. Springer, Berlin Heidelberg, pp 181–244

Freitas VAA, Maia LA, Belardinelli RE, Ardisson JD, Pereira MC, Oliveira LAC (2016) Magnetic iron species highly dispersed over silica: use as catalysts for removal of pollutants in water. Environ Sci Pollut Res. doi:10.1007/s11356-016-6495-6

Gao C, Li W, Morimoto W, Nagaoka Y, Maekawa T (2006) Magnetic carbon nanotubes: synthesis by electrostatic self-assembly approach and application in biomanipulations. J Phys Chem B 110:7213–7220

Gupta A, Garg A (2015) Utilisation of sewage sludge derived adsorbents for the removal of recalcitrant compounds from wastewater: mechanistic aspects, isotherms, kinetics and thermodynamics. Bioresou Technol 194:214–224

Hermanek M, Zboril R, Mashlan M, Machala L, Schneeweiss O (2006) Thermal behaviour of iron(ii) oxalate dihydrate in the atmosphere of its conversion gases. J Mater Chem 16:1273–1280

Hu D, Wang L (2016) Adsorption of amoxicillin onto quaternized cellulose from flax noil: kinetic, equilibrium and thermodynamic study. J Taiwan Inst Chem Eng 64:227–234

Hu L, Chen W, Xie X, Liu N, Yang Y, Wu H, Yao Y, Pasta M, Alshareef HN, Cui Y (2011) Symmetrical MnO_2-carbon nanotube-textile nanostructures for wearable pseudocapacitors with high mass loading. ACS Nano 5:8904–8913

Huang Q, Wang X, Li J, Dai C, Gamboa S, Sebastian PJ (2007) Nickel hydroxide/activated carbon composite electrodes for electrochemical capacitors. J Power Sources 164:425–429

Huiqun C, Meifang Z, Yaogang Y (2006) Decoration of carbon nanotubes with iron oxide. J Solid State Chem 179:1208–1213

Kuyumcu OK, Bayazit SS, Salam MA (2016) Antibiotic amoxicillin removal from aqueous solution using magnetically modified graphene nanoplatelets. J Ind Eng Chem 36:198–205

Kyzas GZ, Lazaridis NK, Bikiaris DN (2013) Optimization of chitosan and β-cyclodextrin molecularly imprinted polymer synthesis for dye adsorption. Carbohydr Polym 91:198–208

Li H, Yan Q, Hng HH (2016) Nitrogen doped carbon nanotubes encapsulated MnO nanoparticles derived from metal coordination polymer towards high performance lithium-ion battery anodes. Electrochim Acta 187:406–412

Lima EC, Barbosa-Jr F, Krug FJ, Guaita U (1999) Tungsten-rhodium permanent chemical modifier for lead determination in digests of biological materials and sediments by electrothermal atomic absorption spectrometry. J Anal At Spectrom 14:1601–1605

Lima EC, Barbosa RV, Brasil JL, Santos AHDP (2002) Evaluation of different permanent modifiers for the determination of arsenic, cadmium and lead in environmental samples by electrothermal atomic absorption spectrometry. J Anal At Spectrom 17:1523–1529

Lima EC, Brasil JL, Santos AHDP (2003) Evaluation of Rh, Ir, Ru, W-Rh, W-Ir, and W-Ru as permanent modifiers for the determination of lead in ashes, coals sediments, sludges, soils, and freshwaters by electrothermal atomic absorption spectrometry. Anal Chim Acta 484:233–242

Lima EC, Adebayo MA, Machado FM (2015) Chapter 3—kinetic and equilibrium models of adsorption in carbon nanomaterials as adsorbents for environmental and biological applications, Bergmann, CP, Machado FM, editors, Springer 33–69

Machado FM, Bergmann CP, Lima EC, Royer B, de Souza FE, Jauris IM, Calvete T, Fagan SB (2012) Adsorption of Reactive Blue 4 dye from water solutions by carbon nanotubes: experiment and theory. Phys Chem Chem Phys 14:11139–11153

Mehdinia A, Akbari M, Kayyal TB, Azad M (2015) High-efficient mercury removal from environmental water samples using di-thio grafted on magnetic mesoporous silica nanoparticles. Environ Sci Pollut Res 22:2155–2165

Pezoti O, Cazetta AL, Bedin KC, Souza LS, Martins AC, Silva TL, Santos-Jr O-O, Visentainer JV, Almeida VC (2016) NaOH-activated carbon of high surface area produced from guava seeds as a high-efficiency adsorbent for amoxicillin removal: kinetic, isothermand thermodynamic studies. Chem Eng J 288:778–778

Podder MS, Majumder CB (2016) Application of granular activated carbon/$MnFe_2O_4$ composite immobilized on C. glutamicum MTCC 2745 to remove As(III) and As(V): kinetic, mechanistic and thermodynamic studies. Spectrochim Acta Part A Mol Biomol Spectrosc 153:298–314

Prola LDT, Acayanka E, Lima EC, Umpierres CS, Vaghetti JCP, Santos WO, Laminsi S, Njifon PT (2013) Comparison of *Jatropha curcas*-shells in natural form and treated by non-thermal plasma as biosorbents for removal of Reactive Red 120 textile dye from aqueous solution. Ind Crop Prod 46:328–340

Puchana-Rosero MJ, Lima EC, Ortiz-Monsalve S, Mella B, da Costa D, Poll E, Gutterres M (2016) Fungal biomass as biosorbent for the removal of Acid Blue 161 dye in aqueous solution. Environ Sci Pollut Res. doi:10.1007/s11356-016-8153-4

Purkait MK, Maiti A, DasGupta S, De S (2007) Removal of congo red using activated carbon and its regeneration. J Hazard Mater 145: 287–295

Ranjithkumar V, Vairam S (2012) Activated carbon–Mn_3O_4 nanocomposites—synthesis and magnetic studies. Adv Mater Res 584:182–186

Ranjithkumar V, Hazeen AN, Thamilselvan M, Vairam S (2014a) Magnetic activated carbon-Fe_3O_4 nanocomposites—synthesis and applications in the removal of acid yellow dye 17 from water. J Nanosci Nanotechnol 14:4949–4959

Ranjithkumar V, Sangeetha S, Vairam S (2014b) Synthesis of magnetic activated carbon/α-Fe_2O_3 nanocomposite and its application in the removal of acid yellow 17 dye from water. J Hazard Mater 273:127–135

Ribas MC, Adebayo MA, Prola LDT, Lima EC, Cataluña R, Feris LA, Puchana-Rosero MJ, Machado FM, Pavan FA, Calvete T (2014) Comparison of a homemade cocoa shell activated carbon with commercial activated carbon for the removal of reactive violet 5 dye from aqueous solutions. Chem Eng J 248:315–326

Rovani S, Censi MT, Pedrotti-Jr SL, Lima EC, Cataluña R, Fernandes AN (2014) Development of a new adsorbent from agro-industrial waste and its potential use in endocrine disruptor compound removal. J Hazard Mater 271:311–320

Santos TRT, Silva MF, Nishi L, Vieira MAS, Klein MRF, Andrade MB, Vieira MF, Bergamasco R (2016) Development of a magnetic coagulant based on *Moringa oleifera* seed extract for water treatment. Environ Sci Pollut Res 23:7692–7700

Sathiya M, Prakash AS, Ramesha K, Tarascon JM, Shukla AK (2011) V_2O_5-anchored carbon nanotubes for enhanced electrochemical energy storage. J Am Chem Soc 133:16291–16299

Saucier C, Adebayo MA, Lima EC, Cataluña R, Thue PS, Prola LDT, Puchana-Rosero MJ, Machado FM, Pavan FA, Dotto GL (2015a) Microwave-assisted activated carbon from cocoa shell as adsorbent for removal of sodium diclofenac and nimesulide from aqueous effluents. J Hazard Mater 289:18–27

Saucier C, Adebayo MA, Lima EC, Prola LDT, Thue PS, Umpierres CS, Puchana-Rosero MJ, Machado FM (2015b) Comparison of a homemade Bacury shell activated carbon with MWCNT for the removal of Brilliant Blue FCF food dye from aqueous solutions. Clean Air Soil Water 43:1389–1400

Shan D, Deng S, Zhao T, Wang B, Wang Y, Huang J, Yu G, Winglee J, Wiesner MR (2016) Preparation of ultrafine magnetic biochar and activated carbon for pharmaceutical adsorption and subsequent degradation by ball milling. J Hazard Mater 305:156–163

Singh AP, Garg P, Alam F, Singh K, Mathur RB, Tandon RP, Chandra A, Dhawan SK (2012) Phenolic resin-based composite sheets filled with mixtures of reduced graphene oxide, γ-Fe_2O_3 and carbon fibers for excellent electromagnetic interference shielding in the X-band. Carbon 50:3868–3875

Sun CL, Wang CS (2010) Estimation on the intramolecular hydrogen-bonding energies in proteins and peptides by the analytic potential energy function. J Mol Struct 956:38–43

Sun Y, Ji G, Zheng M, Chang X, Zhang Y (2010) Synthesis and magnetic properties of crystalline mesoporous $CoFe_2O_4$ with large specific surface area. J Mater Chem 20:945–952

Tan F, Fan X, Zhang G, Zhang F (2007a) Coating and filling of carbon nanotubes with homogeneous magnetic nanoparticles. Mater Lett 61:1805–1808

Tan IAW, Hameed BH, Ahmad AL (2007b) Equilibrium and kinetic studies on basic dye adsorption by oil palm fibre activated carbon. Chem Eng J 127:111–119

Tang J, Wu S, Wang T, Gong H, Zhang H, Alshehri SM, Ahamad T, Zhou H, Yamauchi Y (2016) Cage-type highly graphitic porous carbon–Co_3O_4 polyhedron as the cathode of lithium–oxygen batteries. ACS Appl Mater Interfaces 8:2796–2804

Travlou NA, Kyzas GZ, Lazaridis NK, Deliyanni EA (2013) Graphite oxide/chitosan composite for reactive dye removal. Chem Eng J 217:256–265

Villaescusa I, Fiol N, Poch J, Bianchi A, Bazzicalupi C (2011) Mechanism of paracetamol removal by vegetable wastes: the contribution of π–π interactions, hydrogen bonding and hydrophobic effect. Desalination 270:135–142

Wan S, Bi H, Sun L (2016) Graphene and carbon-based nanomaterials as highly efficient adsorbents for oils and organic solvents. Nanotechnol Rev 5:3–22

Wang H, Qing C, Guo J, Aref AA, Sun D, Wang B, Tang Y (2014) Highly conductive carbon-CoO hybrid nanostructure arrays with enhanced electrochemical performance for asymmetric supercapacitors. J Mater Chem A 2:11776–11783

Yildirim T, Ciraci S (2005) Titanium-decorated carbon nanotubes as a potential high-capacity hydrogen storage medium. Phys Rev Lett 94:175501

Zhang S, Dong Y, Yang Z, Yang W, Wu J, Dong C (2016) Adsorption of pharmaceuticals on chitosan-based magnetic composite particles with core-brush topology. Chem Eng J 304:325–334

Zhao H, Liu X, Cao Z, Zhan Y, Shi X, Yang Y, Zhou J, Xu J (2016) Adsorption behavior and mechanism of chloramphenicols, sulfonamides, and non-antibiotic pharmaceuticals on multi-walled carbon nanotubes. J Hazard Mater 310:235–245

Quality control and evaluation of adsorption models

To ensure reproducibility, reliability and accuracy of adsorption data, some experiments were carried out three times (Barbosa et al., 2000). Blanks were run in parallel and corrected when necessary (Lima et al., 1999). The solutions of AMX and PCT were stored in the clean glass bottles in a dust-free cupboard (Lima et al., 2002). Prepared standard adsorbate solutions solutions (10.0 – 250.0 mg L^{-1}) were used for calibration in parallel with a blank (Puchana-Rosero et al., 2016).

The linear analytical calibration curve was done on the UV-Win software of the T90+ PG Instruments spectrophotometer. The detection limit of AMX and PCT based on a signal/noise ratio of 3 were 0.080 and 0.070 mg L^{-1}, respectively (Lima et al., 2003).

The fitness of the kinetic and equilibrium data were done using nonlinear methods, which were evaluated using Simplex method, and the Levenberg–Marquardt algorithm using the fitting facilities of the Microcal Origin 2015 software. The suitableness of the kinetic and equilibrium models were evaluated using a determination coefficient (R^2), an adjusted determination coefficient (R^2_{adj}) and the standard deviation of residues (SD) (Lima et al. 2015). Standard deviation of residues measures the differences between the theoretical and experimental amounts of phenol adsorbed. Equations 3, 4 and 5 are the mathematical expressions for respective R^2, R^2_{adj} and SD (Lima et al. 2015).

$$R^2 = \left(\frac{\sum_i^n \left(q_{i,exp} - \bar{q}_{exp} \right)^2 - \sum_i^n \left(q_{i,\,exp} - q_{i,\,model} \right)^2}{\sum_i^n \left(q_{i,exp} - \bar{q}_{exp} \right)^2} \right) \quad (3)$$

$$R^2_{adj} = 1 - \left(1 - R^2\right) . \left(\frac{n-1}{n-p-1} \right) \quad (4)$$

$$SD = \sqrt{\left(\frac{1}{n-p} \right) . \sum_i^n \left(q_{i,\,exp} - q_{i,\,model} \right)^2} \quad (5)$$

In the above equations, $q_{i,\ model}$ is individual theoretical q value predicted by the model; $q_{i,\ exp}$ is individual experimental q value; $\bar{q}_{exp}$ is the average of experimental q values; n is the number of experiments; p is the number of parameters in the fitting model.

Supplementary Table 1. Precursor and amount of precursor for preparation of the iron(III) and cobalt(II) benzoate and oxalate.

Material	Precursor	Amount of precursor (g)
Ferric benzoate	Ferric nitrate & benzoic acid	8.08 & 7.32
Cobalt benzoate	Cobalt nitrate & benzoic acid	5.20 & 4.88
Ferric oxalate	Ferric nitrate & oxalic acid	3.60 & 1.12
Cobalt oxalate	Cobalt nitrate & oxalic acid	2.47 & 1.06

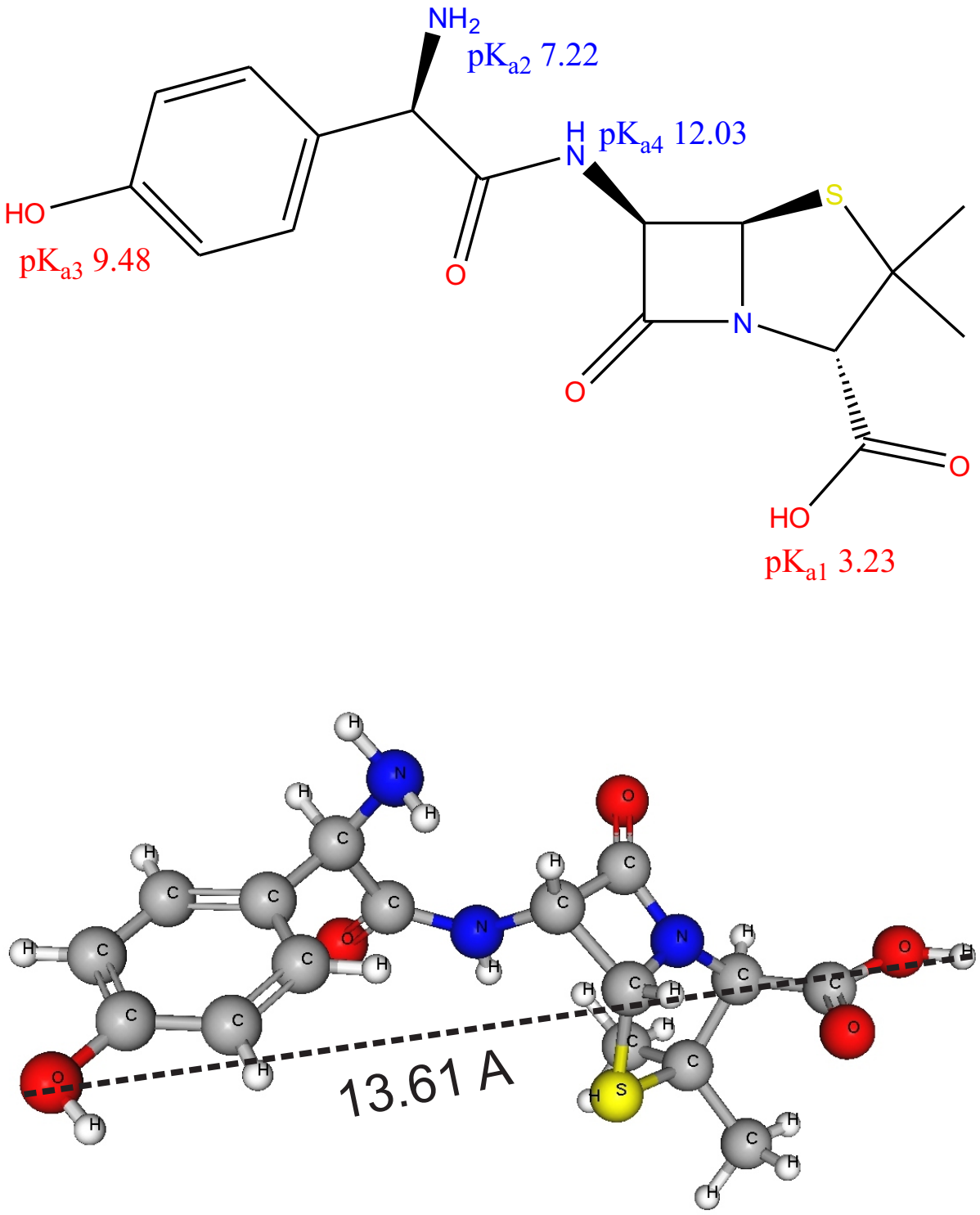

Supplementary Fig 1. A) Structural formula of amoxicillin, pKa values are indicated in the figure; B) Optimized three-dimensional structural formula of amoxicillin. The dimensions of the chemical molecule was calculated using MarvinSketch version 16.6.6.0. van der Waals surface area 476.14 A^2 (pH 7.0); Polar surface area 162.71 A^2 (pH 7.0); Dipole Moment 5.25 Debye; LogP -0.04; Log D -2.31. Hydrophilic-lipophilic balance 19.72

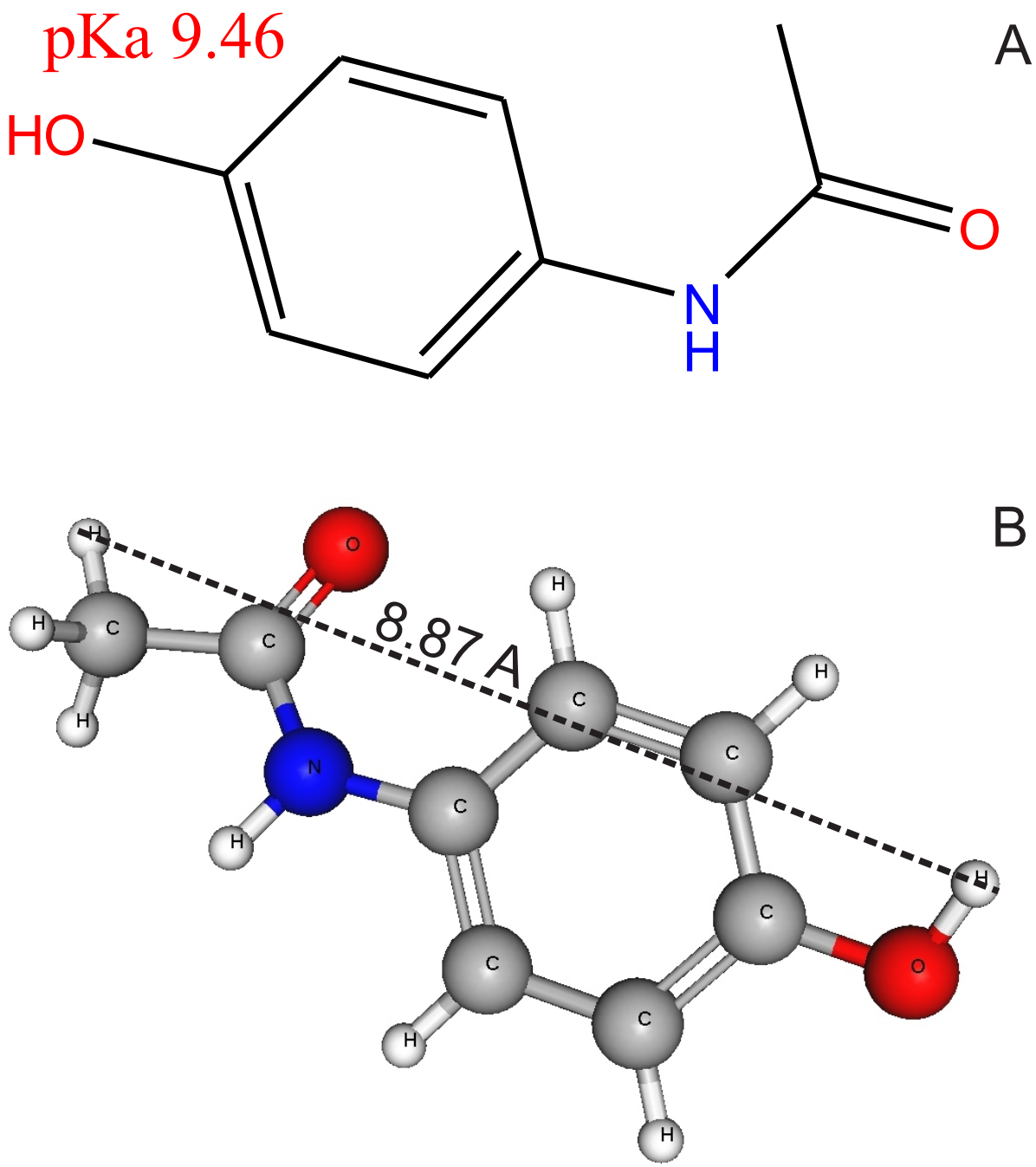

Supplementary Fig 2. A) Structural formula of paracetamol, pKa value is indicated in the figure; B) Optimized three-dimensional structural formula of paracetamol. The dimensions of the chemical molecule was calculated using MarvinSketch version 16.6.6.0. van der Waals surface area A^2 (pH 7.0); Polar surface area 49.33 A^2 (pH 7.0); Dipole Moment 3.60 Debye; LogP 0.91; Log D 0.91; Hydrophilic-lipophilic balance 5.57

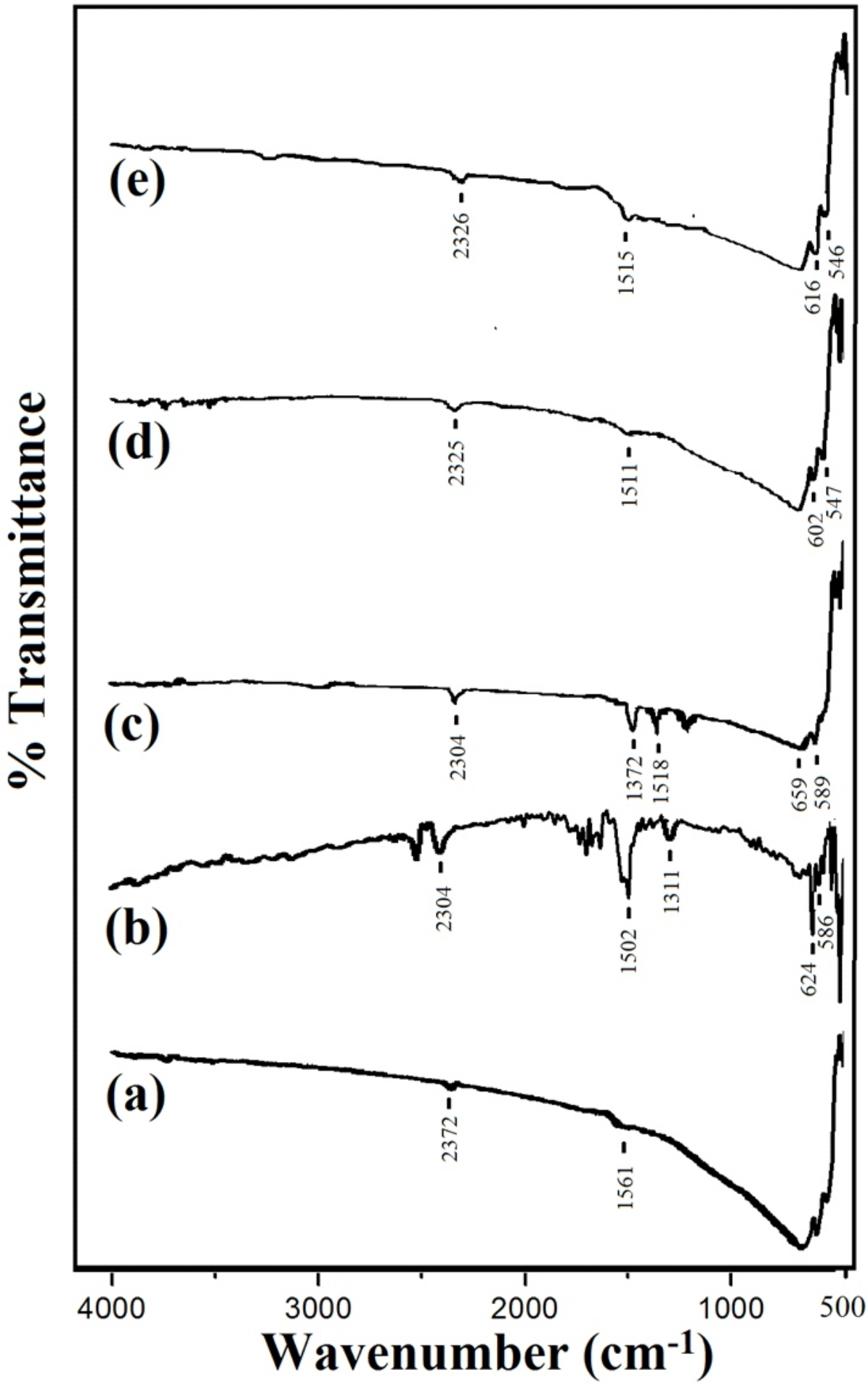

Supplementary Fig. 3. FT-IR spectra of (a) AC (b) AC-1 (c) AC-2 (d) MAC-1 and (e) MAC-2.

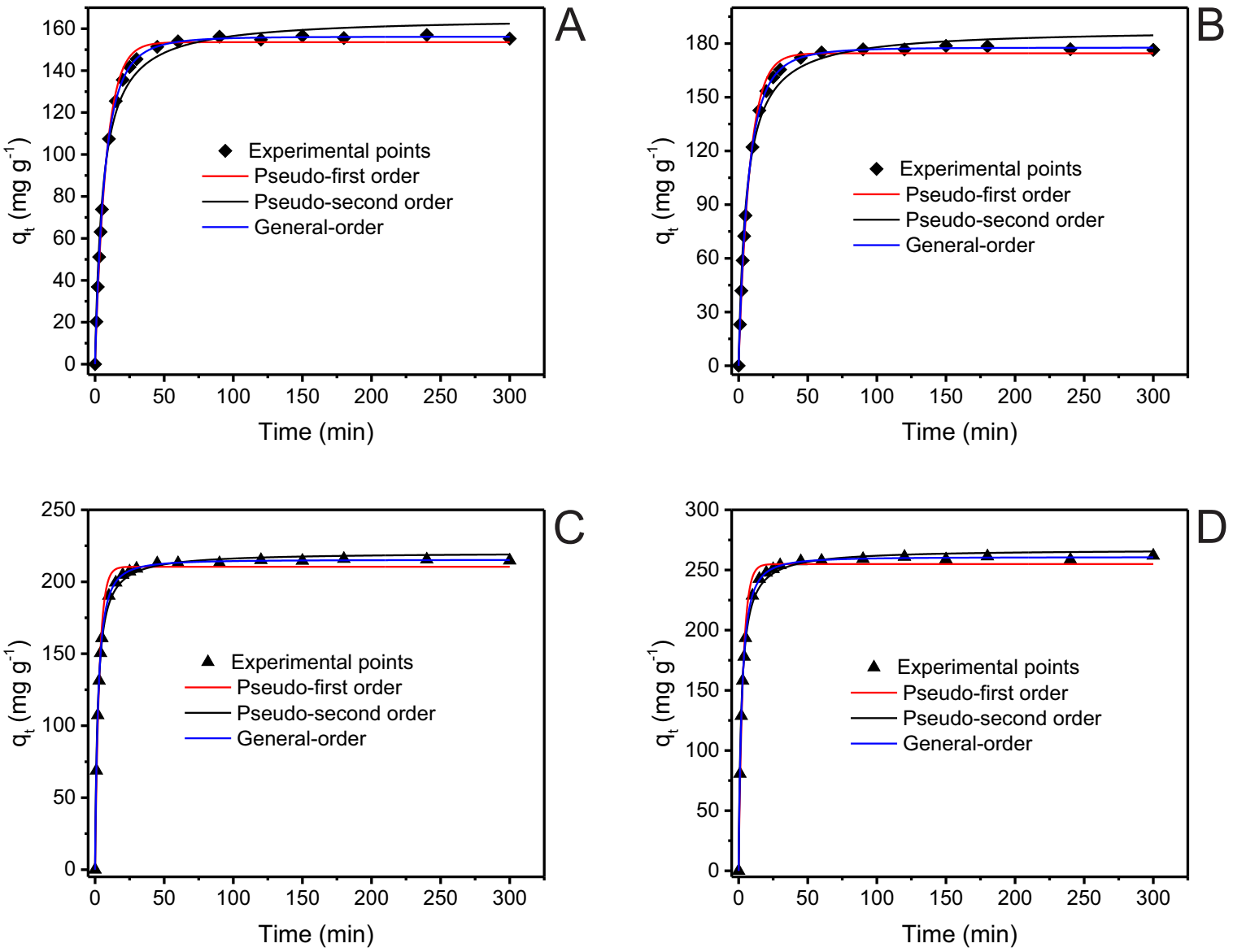

Supplementary Fig 4. Kinetics of adsorption of AMX onto MAC-1 (A, B) and MAC-2 (C,D). Initial AMX concentration 400 mg L^{-1} (A, C) and 800 mg L^{-1}(B, D) Temperature was fixed at 25°C; adsorbent dosage was 1.50 g L^{-1}; initial pH was fixed at 7.0.

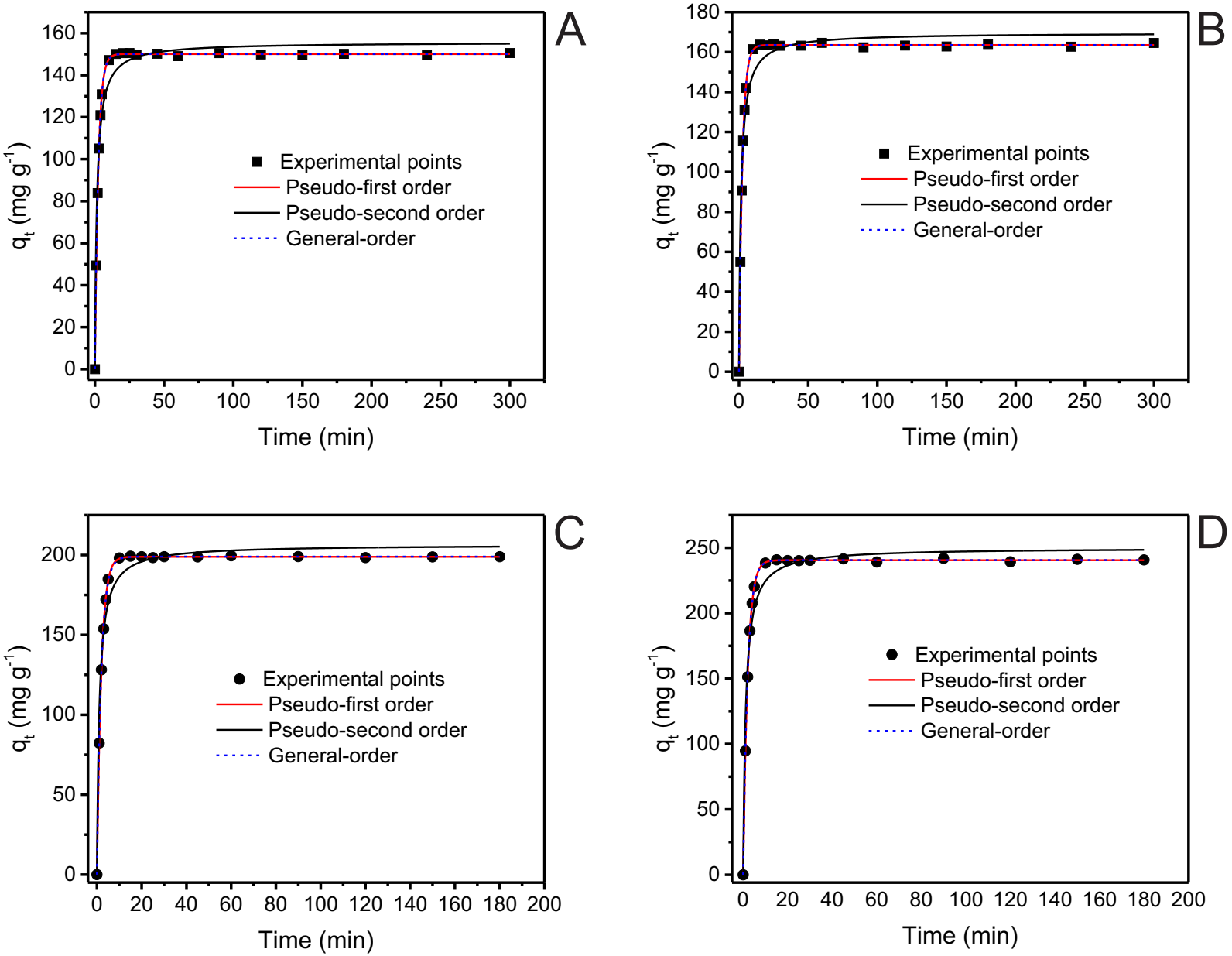

Supplementary Fig 5. Kinetics of adsorption of PCT onto MAC-1 (A, B) and MAC-2 (C,D). Initial PCT concentration 400 mg L^{-1} (A, C) and 800 mg L^{-1}(B, D). Temperature was fixed at 25°C; adsorbent dosage was 1.50 g L^{-1}; initial pH was fixed at 7.0.